Examination of stress and strain in glass structures during pressure treatment using FEM simulation and experimental tests

Dissertation

zur Erlangung des akademischen Grades

Doktoringenieur

(Dr.-Ing.)

von   Christian Gröschl, M.Sc.

geb.   am 09. März 1984 in Freital

genehmigt durch die Fakultät für Maschinenbau

der Otto-von-Guericke-Universität Magdeburg

Gutachter: Prof. Dr.-Ing. Thomas Böllinghaus

                       Prof. Dan Eliezer

                       Dr. rer. nat. Kai Holtappels

Promotionskolloquium am 27. September 2016

I Abstract

Glass is an amorphous material. When compared to steel, both its density and weight is three times lower. Its high theoretical strength makes it stand out as a premier material for a variety of applications. One such application is acting as a pressure resistant vessel for gas storage. Because glass has a high theoretical strength this makes it potentially suitable to withstand much higher pressures than steel or composite vessels. As a result of its brittle character, glass breaks when reaching a critical stress level. Therefore, the stress distribution during pressure load needs to be homogeneous without local stress peaks. At those peaks an initial crack will occur and the material will break.

This PhD thesis is primarily concerned with the determination of the strength of several structures made of single hollow glass fibers during inner pressure treatment. Therefore, different kinds of hollow glass structures with varying parameters of shape and dimension were examined concerning their strength by determining the burst pressure. The burst pressure method was compared to the tensile test method, which poses the common test method for examining the strength of a material. The conclusion reached was that both test methods lead to comparable results and therefore, the burst pressure method poses an adequate tool for examining the strength of a hollow material against inner pressure.

Another tool used in this thesis is the Finite Elements Method (FEM) simulation of internal stress and expansion of glass structures during pressure treatment. FEM was used to validate the burst pressure test results. A few selected material parameters needed to be incorporated, most notably the Young's Modulus. Therefore, the expansion of single glass fibers was measured with light microscope during pressure load. Within the parameters of expansion, wall thickness and applied pressure, the Young's Modulus was calculated with the Barlow's Formula.

According to the results, different two-dimensional models from single fibers to complex structures with up to 1000 single fibers were constructed and simulated with the CFD software Comsol Multiphysics. The expansion as well as the principal stress during pressure load was calculated. Different dimensions as well as different geometries of the glasses were considered to find a structure with the highest possible free volume and at the same time as less stress peaks as possible. This calculation was made in order to determine the best structure for gas storage. For this purpose the calculations were done with different dimensions of round single fibers right up to hexagonal structures consisting of more than one thousand round single fibers, which resulted in constant expansion of the structure. Furthermore, the problem of occurring interspaces between round single fibers, regarding

their burst pressure-decreasing influence, was approached. Closing these interspaces with glass or other materials to avoid unsolicited pressure load led to increased strength of the structure and low storage capacities due to the increased weight and less free inner volume. The behavior of hexagonal fibers was determined as single fiber as well as in bundled condition. The walls between two hexagonal single fibers with applied inner pressure showed homogeneously distributed stress. Merely the outer walls without counter pressure showed high deformation and high structural stress. Based on that knowledge, several structures were modeled varying in different aspects. The fibers with hexagonal shape showed optimal stress distribution and high storage capacities because of high free inner volume, provided that these fibers are surrounded by additional fibers with identical inner pressure. Reducing the wall thickness for even higher free inner volume led to similar distribution but higher stress and expansion. To overcome the problem with the high stress at the outer fibers, the influence of outer fibers with different shape and dimension was simulated as well as the influence of solid glass fibers at the outer layer of the structure. The results showed that a structure with hexagonal thin-walled fibers should be surrounded by round fibers with higher wall thickness. This way the high stress peaks at the outer fibers are lowered.

The examined practical strength of glass is about 100 to 1000 times lower than the theoretical strength. This is caused by defects, which may occur at the glass surface by handling or inside the material by defective production. Since the modeled results are based on the theoretical strength, the optimal wall thickness with a good compromise of strength and free inner volume needs to be found in practical tests. If further handling of the structures is necessary, an outer layer of solid fibers works as a protection layer against damages at the outer hollow glass fibers and increases the strength.

Additionally, the influence of collapsing fibers inside a structure on the remaining system has been modeled as well as the influence of defects like holes or cracks at the surface or manufacturing induced defects inside the material. Any kind of defect leads to areas of high stress, whereby failure occurrence will be encouraged.

In order to approve the theoretical results, the simulated structures were compared to the previously manufactured and tested ones. Due to the burst pressure test results, the tested structures showed low strength compared to the theoretical strength. This was primarily caused by the existence of defects in the material and on the surface of the glass structures. Therefore, the production process needs to be optimized in order to prevent such defects. Furthermore, an additional protection against outer influence like air humidity or the physical contact to other materials is required.

II Zusammenfassung

Glas ist ein amorpher Werkstoff. Im Vergleich zu Stahl beträgt die Dichte und damit auch das Gewicht von Glas etwa 30%. Seine hohe theoretische Festigkeit eröffnet viele Möglichkeiten, Glas als Material für verschiedene Einsatzgebiete zu nutzen. Ein solches mögliches Einsatzgebiet ist die Nutzung als druckfester Gasspeicher. Durch die hohe theoretische Festigkeit könnte ein Gasspeicher aus Glas höherem inneren Druck standhalten als Stahl- oder Kompositbehälter. Glas bricht, wenn ein kritischer Stresswert im Material erreicht wird, was der Tatsache geschuldet ist, dass Glas ein brüchiges Material ist. Deshalb ist es wichtig, dass die im Material auftretende Spannung bei einer inneren Druckbelastung eines solchen Systems möglichst homogen verteilt ist, ohne dass dabei größere Spannungsspitzen auftreten.

Diese Arbeit behandelt in erster Linie die Stabilität verschiedener Glasstrukturen, welche aus einzelnen Hohlglaskapillaren hergestellt sind, gegenüber innerer Druckbelastung. Dafür wurde der Berstdruck von Glasstrukturen mit variierenden Parametern wie Form, Größe oder Anzahl der Kapillaren bei stetig ansteigendem inneren Druck untersucht. Die Ergebnisse der Berstdruckmethode wurde in dieser Arbeit mit Ergebnissen der Zugtestmethode verglichen. Als Resultat lieferten beide Methoden vergleichbare Festigkeitswerte des Materials.

Eine weitere Methode, Materialverhalten bei innerer Druckbelastung zu untersuchen, die in dieser Arbeit angewendet wurde ist die Finite Elemente Methode (FEM). Mit Hilfe dieser Methode wurden Spannungen und Ausdehnung des Materials bei innerer Druckbelastung von verschiedenen Glasstrukturen untersucht. Um die FEM-Simulation durchführen zu können, wurden verschieden Materialkennwerte benötigt, unter anderem der Elastizitätsmodul. Um diesen zu bestimmen wurde die Ausdehnung von Einzelglaskapillaren bei innerer Druckbelastung mit einem Lichtmikroskop gemessen. Mit den Werten der Wandstärke, Ausdehnung, des Durchmessers und des angelegten Drucks konnte der Elastizitätsmodul mit Hilfe der Kesselgleichung errechnet werden.

Die Ergebnisse der FEM-Simulation wurden mit den Berstdruckdaten vergleichbarer Strukturen verglichen. Dafür wurden zweidimensionale Querschnittmodelle von Strukturen aus bis zu 1000 Einzelkapillaren mit Hilfe der Software Comsol Multiphysics erstellt und die auftretende Hauptspannung und Ausdehnung des Materials berechnet.

Sowohl der Einfluss unterschiedlicher Geometrie als auch unterschiedlicher Größe der Einzelkapillaren wurde untersucht, um eine Struktur zu erstellen, die gleichmäßig verteilte Spannung bei Druckbeaufschlagung und gleichzeitig hohes inneres Speichervolumen aufweist, was für den Einsatz als Druckspeicher für Gase unerlässlich ist.

Dafür wurden verschiedene Strukturen aus runden Einzelkapillaren berechnet. Die bei der Bündelung von runden Strukturen auftretenden Zwischenräume stellten allerdings ein großes Problem dar. Daraufhin wurden hexagonale Einzelkapillaren zur Bündelung verwendet, wodurch dieses Problem gelöst werden konnte. Durch das Beseitigen der nicht zur Gasspeicherung nutzbaren Zwischenräume, konnte das innere Speichervolumen deutlich erhöht werden. Weiterhin zeigten hexagonale Einzelkapillaren im gebündelten Zustand gleichmäßige Spannungsverteilung in den inneren Wänden, was einem effizienten Einsatz als Gasspeicher zugutekommt. Auch die Reduzierung der Wandstärke, wodurch das Speichervolumen weiter erhöht werden konnte, führte zu gleichmäßiger Spannungsverteilung in den inneren Materialwänden. Im Gegensatz dazu zeigten die äußeren Wände erhöhte Spannungswerte mit Spannungsspitzen an den Ecken der Kapillaren. Abhilfe konnte durch den Einsatz einer äußeren Kapillarreihe aus Vollglasfasern ohne inneren Zwischenraum geschaffen werden, was allerdings das Speichervolumen reduzierte. Weitere Berechnungen führten zu dem Ergebnis, dass der Einsatz von runden Kapillaren mit etwas höherer Wandstärke zu deutlich reduzierter Spannung im Material führte.

Die in praktischen Versuchen ermittelte Festigkeit von Glas beträgt nur etwa 0,1% bis 1% der theoretischen Festigkeit. Die Ursache für diese Tatsache sind Materialdefekte unterschiedlicher Größe, die sowohl im Material, als auch auf der Oberfläche existieren. Defekte im Material können meistens auf die Produktionsbedingungen zurückgeführt werden, während der Umgang mit den Glasproben nach der Herstellung für Oberflächenschäden verantwortlich ist.

Da die Ergebnisse der FEM-Simulation auf der theoretischen Festigkeit beruhen, kann man damit keine Aussage zum Zeitpunkt des Materialversagens bei stetig ansteigendem inneren Druck treffen. Es ist auch nicht möglich, eine minimale Wandstärke zu berechnen, die eine solche Glasstruktur besitzen muss. Es lässt sich lediglich der Einfluss verschiedener Parameter auf die entstehende Spannung ermitteln und dadurch die optimale Form einer Struktur ermitteln. Es ist wichtig, dass sowohl die Produktionsbedingungen, als auch der Umgang mit solchen Glasproben angepasst werden, sodass keine Materialdefekte entstehen können. Eine nach der Produktion aufgebrachte Schutzschicht auf den Proben könnte diesbezüglich eine deutliche Verbesserung der praktischen Festigkeitswerte mit sich führen.

Um den negativen Einfluss von Defekten zu bestätigen wurde die Spannung von Kapillaren mit kleinen Defekten wie Lufteinschlüssen oder Rissen an der Oberfläche berechnet. Es stellte sich heraus, dass jede Art von Defekten zu Spannungsspitzen im Material führt. Weiterhin wurde der Einfluss von einzelnen versagenden Kapillaren innerhalb einer Struktur auf die auftretende Spannung im System untersucht.

Um die berechneten Ergebnisse zu belegen, wurden die Berstdrücke von vergleichbaren Glasstrukturen ermittelt und mit einander verglichen. Glasstrukturen, die bei der FEM-Simulation geringe Spannungswerte zeigten, besaßen vergleichsweise hohe Berstdrücke, wodurch die berechneten Ergebnisse durch die praktischen Versuche belegt werden konnten.

III Acknowledgments

IV Table of Contents

V Terminology / Shortcuts

Average burst pressure

The average burst pressure is the mean value of minimum and maximum burst pressure. It reflects the pressure range of a test series, but does not reflect the complete range and spread of measured burst pressure. It is suitable to compare different test series to each other based on the average burst pressure value for first evaluation.

Burst pressure

A suitable value to describe the strength of hollow single fibers, structures or multi structures is burst pressure. It is the maximum internal pressure before collapse and is determined by increasing the internal gas pressure with steady rate until fracture.

DOE

The United States Department of Energy is concerned with the policies regarding energy and safety in handling nuclear material of the United States of America.

Cyclic pressure application

Repeated loading and releasing of gas pressure inside a hollow single fiber, structure or multi structure and is characterized as cyclic pressure application. The treatment is done with a given pressure value for a defined number of applications.

Face-to-Face / Edge-to-Edge

On hollow single fibers with hexagonal shape, one differs between the distance of two opposite surfaces (flat-to-flat) or from two opposite edges (edge-to-edge).

FEM

The Finite Elements Method is a numeric evaluation of the material's behavior at varying outer influence like applied tension. For example, the stress and deformation at a defined point of a material at any applied force can be determined analytically. Calculating these values for a large amount of points, which are spread over a surface, leads to a graphically visualization of stress distribution in an entire system.

Free space / free volume

The free space describes the ratio of outer volume and the volume of the glass and is given in %.The free inner volume of a hollow single fiber, structure or multi structure which is available for gas storage is the free space.

Gravimetric energy density

The gravimetric energy density describes the stored energy per kilogram storage system in kWh/kg.

Gravimetric storage capacity (gsc)

The gravimetric storage capacity describes the amount of stored hydrogen in relation to the weight of a storage system in kg H_2/kg. Commonly, the value of gravimetric storage capacity is given in wt%.

Inner diameter (D_i)

D_i describes the inner diameter of a hollow single fiber. On single fibers with a hexagonal shape, one differs between the distance of two opposite surfaces (flat-to-flat) or from two opposite edges (edge-to-edge). Usually, the value is given for flat-to-flat.

Maximum burst pressure

The highest measured burst pressure in one test series and reflects the maximum reachable pressure of a test series.

Minimum burst pressure

The minimum burst pressure is the lowest burst pressure in a test series. Regarding the safety aspect, it is the most expressive value because at pressure application a failure of the system is almost improbable below that specific pressure value.

Multi-structure

Combining several structures leads to multi-structures, which can consist of variable numbers of structures. Multi-structures, made of seven structures, have already proved to be successful.

Outer diameter (D_o)

D_o describes the outer diameter of a hollow single fiber, structure or multi structure. On fibers with a hexagonal outer shape one differs between the distance of two opposite surfaces (flat-to-flat) or from two opposite edges (edge-to-edge). Usually the value is given for the flat-to-flat distance.

Safety factor

In order to run a storage system safely, the maximum pressure which will be allowed for storage has to be smaller than the burst pressure. The safety factor describes the value of that difference. A safety factor of two means that the storage system must withstand a two times higher pressure than the maximum allowed pressure.

Single fiber

A single fiber is a small hollow glass tube which is usually closed at one end and poses the basic element of any glass structure. Single fibers can consist of different kinds of glass materials like borosilicate glass, quartz glass or alumosilicate glass. The shape can differ from round to hexagonal.

Static load

Static load describes a permanent treatment of a hollow single fiber, structure or multi structure with constant given pressure for a defined time period.

Storage pressure

The storage pressure of a storage system describes the maximum internal pressure which is allowed regarding the safety factor. At a safety factor of two the storage pressure is half of the burst pressure.

Stress

Any kind of applied force on a material induces different kinds of internal stress. If the intensity of the induced stress exceeds a critical value the material will break.

Structure

Combinations of assembled single hollow fibers are called structures. They can differ in different parameters like material, amount and dimension of the single fibers. Furthermore, the outer shape may vary; for example, round or hexagonal.

Test series

One test series consists of at least 30 individual tests. This amount of tests is necessary in order to generate a reliable statistic evaluation.

Volumetric energy density

The volumetric energy density describes the stored energy per liter storage system in kWh/l.

Volumetric storage capacity (vsc)

The volumetric storage capacity describes the amount of stored hydrogen in relation to the outer volume of a storage system in kg H_2/l system volume.

WTT Efficiency (well-to-tank)

The well-to-tank efficiency describes the efficiency of an energy carrier like hydrogen regarding its production and transport to the tank [1].

WTW Efficiency (well-to-wheel)

Similar to the WTT efficiency, the well-to-wheel efficiency describes the efficiency of an energy carrier. Compared to the WTT efficiency, the WTW efficiency additionally regards the efficiency of the engine / fuel cell [1].

VI Symbols

Symbol	Description	Unit
σ	Stress	N/mm²
$\sigma_{1,2...,n}$	Principal stresses σ_{Hn} arranged by the algebraic size with $\sigma_1 > \sigma_2 > \sigma_3$….	N/mm²
σ_A	Axial stress	N/mm²
$\sigma_{A,m}$	Mean axial stress	N/mm²
σ_c	Compressive strength	N/mm²
σ_{Co}	cohesion strength	N/mm²
σ_F	Critical stress	N/mm²
σ_{Hn}	Principal stress containing $\sigma_{x,y,z}$ and τ	N/mm²
σ_M	Membrane stress	N/mm²
σ_{max}	Highest occurring principal stress containing σ_x, σ_y, σ_z and τ ($\equiv \sigma_1$)	N/mm²
σ_{min}	Lowest occurring principal stress containing σ_x, σ_y, σ_z and τ ($\equiv \sigma_n$)	N/mm²
σ_P	Stress peaks	N/mm²
σ_R	Radial stress	N/mm²
$\sigma_{R,m}$	Mean radial stress	N/mm²
σ_r	Stress at crack tip	N/mm²
σ_t	Tensile strength / Tensile stress	N/mm²
σ_{th}	Theoretical strength	N/mm²

σ_T	Tangential stress	N/mm²
$\sigma_{T,m}$	Mean tangential stress	N/mm²
σ_{Tor}	Bending stress / Torsion stress	N/mm²
σ_v	Equivalent stress	N/mm²
σ_{vPS}	Equivalent stress at principal stress theory	N/mm²
σ_{vSS}	Equivalent stress at shear stress theory	N/mm²
σ_{vVM}	Equivalent stress at maximum shear strain energy criterion	N/mm²
σ_x	Principal stress acting into x-direction	N/mm²
σ_y	Principal stress acting into y-direction	N/mm²
σ_z	Principal stress acting into z-direction	N/mm²
ε	Strain	-
τ	Shear stress	N/mm²
τ_F	Shear strain stress	N/mm²
γ	Surface energy	J
a	Gravitational acceleration = 9.806	m/s²
A	Area	mm²
A_K	Glued area	mm²
A_p	Load bearing area	mm²
A_σ	Material surface	mm²
c	Fracture length	µm
d	Distance	mm
d_0	Atomic distance	J

D	Elasticity matrix	-
D_i	Inner diameter of hollow glass fiber	mm
da	Current area	mm²
dA	Whole material area	mm²
d_i	Inner diameter of steel pipe	µm
d_n	Coefficient for tensile strength	-
D_o	Outer diameter of glass fiber/structure	mm
E	Young's modulus	MPa
E_i	Young's modulus for component i	MPa
f	Force on current area	N
F	Force	N
F_d	Distributed force	N
l	Length	mm
Δl	Length variation	mm
l_c	Crack length	mm
l_0	Initial length	mm
n	Direction of pressure	-
p	Pressure	N/mm² or MPa
pn	percentage amount of the component	-
R_e	Yield strength	N/mm²
S	Strength	N/mm²
t	Reaction time	s

T	Temperature	°C
T_g	Transformation temperature	°C
T_s	Specific temperature	°C
U	Total energy	J
U_M	Mechanical Energy	J
U_S	Surface energy	J
V	Volume	ml
v	Poisson's ratio	-
z_n	coefficient for compressive strength	-

1 Introduction

Fossil fuels, as resources, are declining while the global energy demand is continuously growing. This asymmetry has resulted in the need for more efficient, environmentally friendly methods of generating and storing energy, i.e., energy carriers.

One of the most promising energy carriers is hydrogen. Its gravimetric energy density is 142 MJ kg^{-1}, which is more than three times higher than that of liquid hydrocarbons, including gasoline (47 MJ kg^{-1}) [1, 2].

However, hydrogen storage poses a big challenge and raises many problems. The small dimension of a hydrogen molecule allows permeation through most common materials whereby a steady hydrogen loss emerges. Furthermore, the low volumetric energy density of hydrogen (11 kJ l^{-1} at standard conditions) [3] necessitates procedures like liquefaction, compression or chemical and physical bonding to a substrate in order to keep hydrogen storage economical.

The U.S. Department of Energy (DOE) annually fixes targets for the volumetric and the gravimetric storage capacity, as these are the two most important values to describe the efficiency of a gas storage system. The gravimetric storage capacity is the ratio of the amount of stored gas compared to the mass of the storage system in g kg^{-1} or wt%. The volumetric storage capacity describes the amount of stored gas compared to the volume of the storage system in g/l. The 2015 target for hydrogen storage systems fixed by the DOE is a volumetric storage capacity of 40 g l^{-1} and a gravimetric storage capacity of 5.5 wt%.

Storing hydrogen in liquid phase at a temperature of T = -253°C leads to 800 times higher energy density [6 - 7]. Keeping hydrogen in liquid phase requires complicated thermal insulation. Nevertheless, a constant amount of hydrogen becomes gaseous and has to be released with a safety valve after reaching about 0.5-0.8 MPa, due to the missing pressure resistance of the storage container [8]. This causes loss of hydrogen, preventing long term storage [10, 11].

The customization of the system to withstand higher pressures up to 30 MPa, called cryo-compressed hydrogen storage, will decrease the hydrogen loss [12, 13]. The high energy effort for compressing and cooling down hydrogen to -253° will decrease the well-to-tank (WTT) efficiency of the system to 41.1%. Nevertheless, cryo-compressed hydrogen storage is the first system that reaches the U.S. DOE's 2015 gravimetric and volumetric storage capacity targets [10].

Another method of hydrogen storage is using metal hydrides. Hydrogen is bound at increased pressure to metal or metal alloy via physical and chemical adsorption. The reaction is exothermic and the emerged heat has to be purged. To release the stored hydrogen, the system needs to be heated up and further heating of energy is necessary. The huge metal amount leads to high costs and high weight; yet, results in low gravimetric storage capacity.

Similar to hydrogen storage in metal hydrides is the storage in metal-organic-framework (MOF) [28 - 49]. Macromolecules composed of metal clusters (e.g. Zn_4O) are affiliated to each other via organic aromatic anions (Linker). The structure is crystalline and shows high porosity, which leads to a specific surface up to 4500 m² g^{-1}. Applying overpressure hydrogen then moves into the pores and couples to the metal cluster's surface. As contrasted with metal hydrides, the bonding of hydrogen to the storage system is physically comparable to London dispersion force. The low bonding energy allows the removal of the hydrogen molecule with slight heating. At a temperature of 77 °C and a pressure of 10 MPa a gravimetric storage capacity of 10 wt% could be reached in laboratory conditions. At room temperature and a pressure of 1 MPa the gravimetric storage capacity is comparably less at 0.3 wt% [48].

Coupled with the comparably low effort, the most prevalent storage system for gases is high pressure storage. Increasing the storage pressure leads to higher volumetric and gravimetric storage capacities. Storage pressures of up to 70 MPa are possibly dependent on the kind of pressure vessels. Higher storage pressures diminish the efficiency of the system [50 - 56]. This is reasoned by the increasing coefficient of compressibility whereby more energy is necessary for compression but the additional amount of stored hydrogen decreases. To reach the energy density of fuel oil a pressure of 350 MPa is required [6].

Pressure vessels are distinguished in four categories. Type I vessel only consists of metal, mostly steel. A storage pressure of up to 20 MPa and high weight causes low gravimetric storage capacities of about 1 wt%. Further development of this vessel leads to Type II vessel. Type II vessel consists of a metal vessel comprised of steel or aluminum and is wrapped with a composite material, mostly glass fiber. The structural stress is managed by both steel and composite in equal shares so the weight of the system could be reduced by using less metal.

Type III pressure vessels are commonly carbon fiber composite vessels with an inlay of steel or aluminum to prevent permeation of gas through the vessel wall. In contrast to Type I and Type II vessels, the structural stress is managed by the composite material only. This construction leads to decreased system weight and higher storage capacities.

The fourth generation of pressure vessels is the Type IV vessel. It consists of a polymer liner which is wrapped with a composite material like carbon fiber or glass fiber that manages the structural stress. The abandonment of any metal material makes Type IV vessels more light weight.

The gravimetric and volumetric storage capacities, as well as the WTT efficiency and the cost of the most common hydrogen storage systems are shown in Table 1 [10].

Table 1: Storage capacities, WTT efficiency and costs of the most common hydrogen storage systems

	gravimetric storage capacity [wt%]	volumetric storage capacity [g l^{-1}]	WTT efficiency [%]	Storage system cost [$ kWh^{-1}]
DOE Target for 2015	**5.5**	**40**	**60**	**2**
liquid	5.6	23.5	22.3	NA
cryo-compressed	9.2	44.7	41.1	12.1
metal hydrides	2.5	25.1	NA	NA
metal-organic-framework	4.1	34.6	41.1	18.1
high pressure 35 MPa	5.5	17.6	56.5	13.4
high pressure 70 Mpa	5.2	26.3	54.2	20.1

Miss DOE Target for 2015	Close to DOE Target for 2015	Comply with DOE Target for 2015

In contrast to carbon fiber, the permeation rate of hydrogen through metal materials is negligible at relevant temperature. Type III vessels were the preferred choice for hydrogen storage because the inner metal layer was necessary to reduce the permeation of hydrogen through the vessel walls. Meanwhile, the permeation rate of Type IV vessels is lower than 1 N cm³ per hour per liter internal volume at 70 MPa [50]. Thus, the safety factors for Type III or Type IV carbon fiber composite vessels, shown in Table 2, are observed, which makes these vessels suitable for high pressure hydrogen storage.

Table 2: Safety factor for the hydrogen permeation rate of Type IV vessels by ISO 15869.3

	H_2 **Permeation Rate**
ISO 15869.3	< 2 N cm³ H_2 / h / L int. Volume (35 MPa) < 2.8 N cm³ H_2 / h / L int. Volume (70 MPa)

In order to deal with the task of developing a lightweight and safe high pressure storage system with high gravimetric and volumetric storage capacities, *C.En Limited* approached the *Federal Institute for Materials Research and Testing (BAM)* with the idea of a new high pressure gas storage system comprised of glass [59 - 65]. The gas is stored in numerous thin hollow glass fibers bundled to multi fibers. These multi fibers consist of thousands of single fibers. Each single fiber poses as an independent pressure vessel. Figure 1 shows a microscopic view of a structure with an outer diameter for every single fiber of 34 µm.
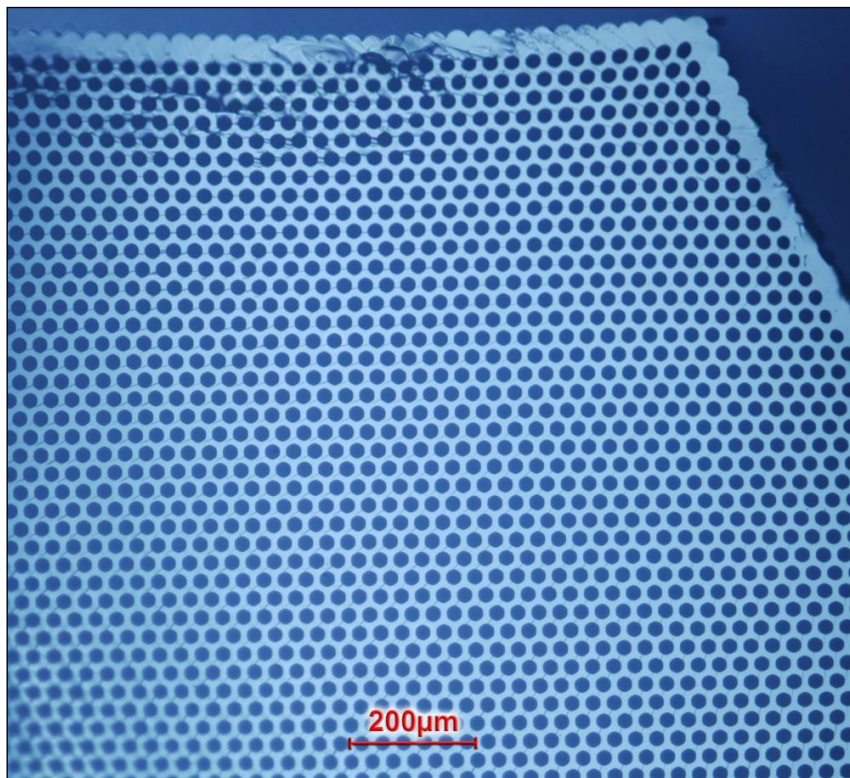
Figure 1: Structure made of 3367 single fibers each with D_o=34µm, solid fibers at the outer surface and an outer diameter of 3.3mm flat-to-flat

Depending on the application and the desired amount of stored hydrogen, a huge amount of multi fibers are combined to form complex structures that are free in shape and volume. One big disadvantage of common high pressure storage systems is the dependency on the shape for optimal force distribution. For example, on edges, a peak of high structural stress will occur. If the stress at this point is too high, the structure will break. To avoid those pressure peaks the common vessels typically have a cylindrical shape. C.En's glass storage system is constructed of thousands of small independent vessel which are not limited by spatial concerns. Therefore, fewer pressure peaks occur, and the outer shape of the system can be adapted to the corresponding application. Figure 2 shows some examples of the bundling of the multi fibers in a typical cylindrical shape (left) or in an unusual triangular structure (right). A further advantage of glass as a storage material is the low permeability of hydrogen through glass at room temperature [66 - 74].
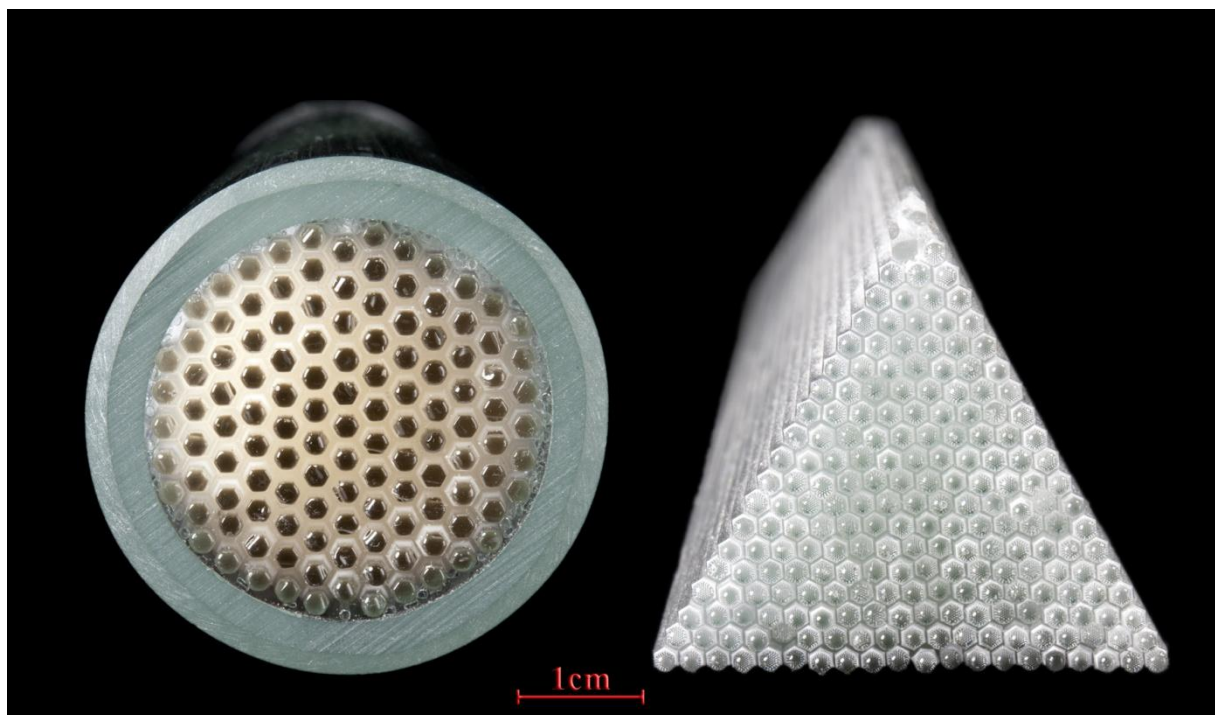
Figure 2: Structures made of borosilicate glass bundled to multi structures with cylindrical shape consisting 202154 single fibers (left) and trigonal shape with 252000 single fibers (right)

2 Motivation

Storage systems for pressurized gases have to be designed in a way so that internal stresses are avoided and stress distribution offers no peaks under increased stress. Basic examinations [96] were carried out with single fibers which showed high pressure resistance. With respect to a final storage system, a numbering up of single fibers is required to achieve acceptable amounts of gas in such systems. In addition to the bundling, the new system offers more freedom with respect to shape and size which then leads to more freedom in design.

The behavior of structures regarding structural stress and strain will differ from single fibers. The process of bundling single fibers, as well as the dimension or shape of the fibers, may have an influence to the structural stress that will occur when applying pressure to the inner surfaces. To determine such values the Finite Elements Method (FEM) is a helpful tool. FEM offers the possibility to simulate the pressure load to the glass structure and calculate and visualize the structural stress distribution and strain. This way the structure can be optimized regarding stress distribution and expansion and the system can be designed theoretically. This approach reduces the amount of necessary test samples and decreases the costs of such studies.

The motivation for this thesis is to use FEM in order to find an optimal way of bundling the single fibers to complex structures. The internal stress has to be well distributed to avoid the initiation of cracks in the glass. At the same time, the inner volume has to be as high as possible for reaching high gravimetric and volumetric storage capacities.

Structures which are comparable with the simulated ones will be produced by *Incom Ltd.* and the burst pressure of these structures will be determined to have a comparison of theoretical and practical results.

3   Fundamentals

In this chapter, some basic properties of glass will be presented. The physical properties, most notably the elasticity and strength of glass, will also be discussed and will include a description of the ability of glass to withstand applied forces like pressure (strength) and to expand at applied force (elasticity). Furthermore, different kinds of defects and their influence to the strength of the material will also be discussed. And finally, the possibility of pre-stressing will be demonstrated for obtaining higher strength of the material.

3.1   Structure Of Glass

The molecular structure of glass is a silicon dioxide network usually in the form of SiO_4 tetrahedrons. Gustav Tammann, one of the first scientists dealing with glass, called glass "the frozen state of a liquid that solidifies without crystallization" [80]. He was concerned with the disordered atomic structure which only has a short-range order and no long-range order. An ordinary crystallization process leads to immediate turning to a stable equilibrium at a specific temperature (T_s). Liquid glass is cooled down rapidly during production process. The transition from liquid to solid state is a steady process as shown in Figure 3 [81].
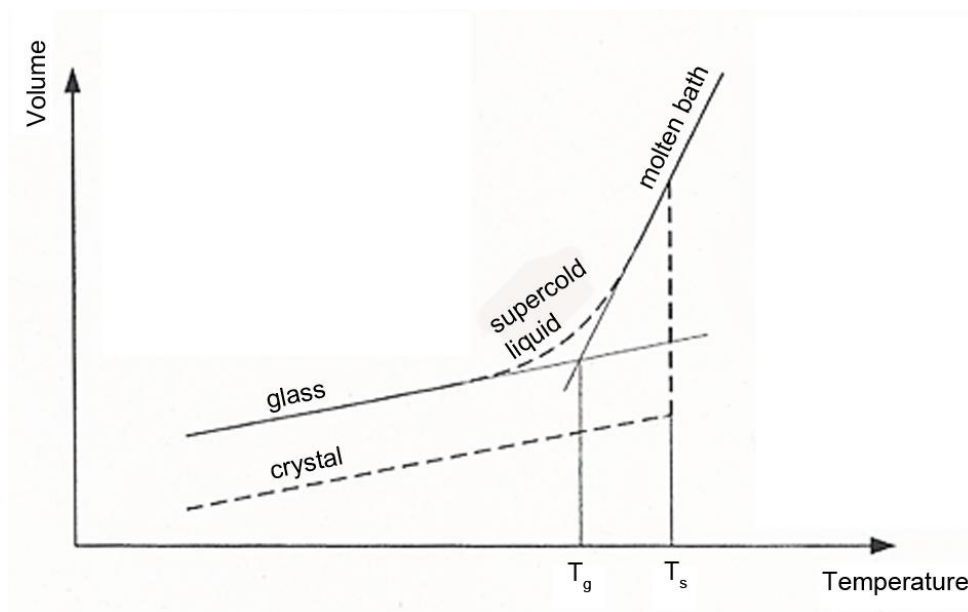

Figure 3: Volume change at the transformation of SiO_2 from liquid to solid state (continuous line) compared to crystallization (dashed line) in dependence of the temperature [81]

The temperature range of becoming solid is called transformation temperature area. In that area glass is a supercold liquid, has a metastable thermodynamic equilibrium and becomes solid while cooling down. Further cooling implements an increasing viscosity until the equilibrium state can no longer be changed. At a minimum viscosity of 10^{13} dPa s, the material is termed glass. The related temperature is the transformation temperature (T_g), which depends on the glass composition. The viscosities of liquefied glass cooling down to a solid state and the corresponding temperatures for Borosilicate glass are listed in Table 3 [81 - 89]. These characteristic points are equal by other glass compositions but the corresponding temperature will differ.

Table 3: Characteristic temperatures and appropriated viscosities of Borosilicate glass during solidification

	Viscosity [dPa s]	**Temperature [°C]**
working point	10^4	1280
softening point	$10^{7.6}$	830
annealing point	10^{13}	570
transformation point	$10^{13.3}$	560
strain point	$10^{14.5}$	530

Due to the fact that glass becomes solid, already before a crystal structure will be constructed, the SiO_2 molecules are not able to form a consistent SiO_4 tetrahedron structure [92, 93]. The molecular structure has voids as exemplary shown in Figure 4.
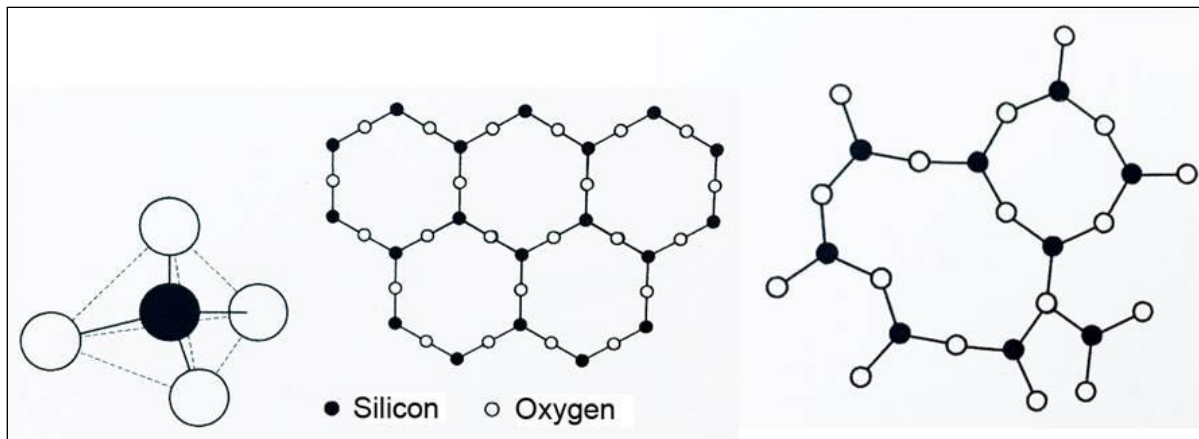
Figure 4: Disordered atomic structure of glass (right) compared to a regular SiO_2 network (left) [94]

The structural strength of glass corresponds to the amount of Si-O-Si bonds. The increased entropy and the resulting faults in the atomic glass structure provide the opportunity to have an influence on the structure and therefore materials properties (see chapter 3.2 "Chemical Resistance" and 3.3 "Physical Properties") by adding specific components. Alkali or alkaline earth ions are able to displace the Si^{4+} ion but cannot bind in a bridged way so the network is opened and the structural strength is weakened. Such ions are called network modifiers. Equation 3-1 displays that process at the example of adding Na^+ in form of Na_2O [95].

$$\equiv\!Si\!-\!O\!-\!Si\!\equiv \;+\; Na\!-\!O\!-\!Na \longrightarrow \;\equiv\!Si\!-\!O\!-\!Na \;+\; Na\!-\!O\!-\!Si\!\equiv \qquad \text{(Eq. 3-1)}$$
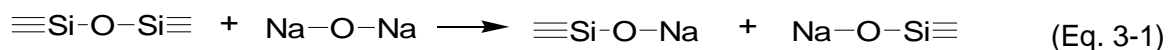
On the contrary, ions like for example Si^{4+}, Ge^{4+} or B^{3+} create new bridged bondings and strengthen the network this way. These ions are called network formers. The third category is called stabilizers. Depending on the concentration, these ions can act as network formers or network modifiers. One of those stabilizers is Al_2O_3. The Al^{3+} ions can replace Si^{4+} ions with terminally bound O^{2-} ions as shown in Figure 5. The O^{2-} ion between two Al^{3+} ions is bridging. The lower positive charge of Al^{3+} compared to Si^{4+} is compensated with remaining alkali ions.
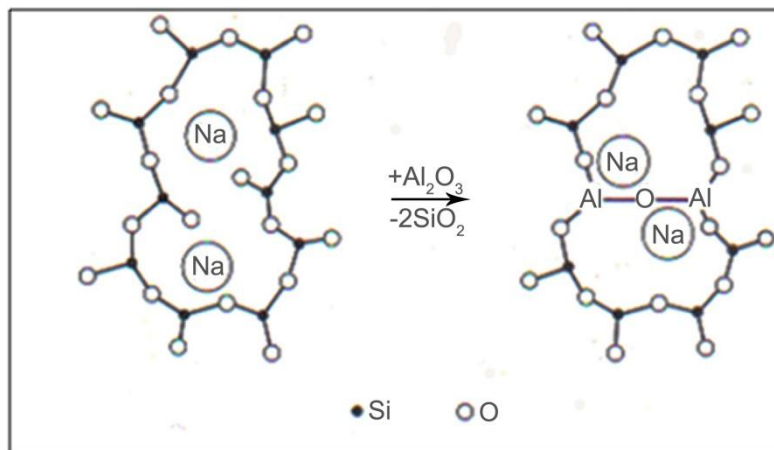
Figure 5: Function of Al_2O_3 as network former in the structure of glass

If Al_2O_3 is added in excessive amount the positive charge cannot be compensated by alkali ions and only three O^{2-} ions will bind. A tetrahedron cannot be formed and Al_2O_3 occurs as network modifier.

The following Table 4 shows a selection of substances and their effect to the glass structure.

Table 4: Substances, which will perform as Network formers, Network modifiers or Stabilizers [169]

Network former	Network modifier	Stabilizer
SiO_2	CaO	Al_2O_3
B_2O_3	K_2O	B_2O_3
P_2O_5	PbO	
GeO_2	Na_2O	
As_2O_3	Li_2O	
As_2O_5	Rb_2O	
Al_2O_3	CsO_2	
	BaO	

The composition of glass has a substantial influence on its physical and chemical properties and can be adjusted according to requirements by adding different components in a controlled way. The chemical composition of four different types of glass are demonstrated in Table 5.

Table 5: Composition of different types of glass [169]

Component	Percentage [mass-%]			
	Quartz glass	**Soda-lime glass**	**Borosilicate glass**	**Aluminosilicate glass**
SiO_2	≥ 99	69 - 74	70 - 87	53 - 60
CaO	-	5 - 12	-	0 - 7
B_2O_3	-	-	7 - 15	0 -8
Na_2O	-	12 - 16	0 - 9	0 - 1
K_2O	-	12 - 16	0 - 9	≤ 0.5
MgO	-	0 - 6	-	0 - 3
Al_2O_3	-	0 - 3	0 - 8	14 - 18
BaO	-	0 - 2	0 - 3	0 - 19

In previous research [96] a series of burst pressure tests with single fibers of quartz glass, borosilicate glass, alumosilicate glass and soda lime glass illustrated borosilicate glass and quartz glass to have the highest burst pressure. Due to the fact that borosilicate glass has a lower transformation temperature the processing of borosilicate glass is much easier and cheaper than that of quartz glass. Although only eight to ten samples were used for every measured value borosilicate glass seems to be a good compromise between strength, effort at production and, costs. The exact composition of the borosilicate glass applied for this thesis has been examined by "Zentrum für Glas- und Umweltanalytik GmbH". The results are displayed in Table 6.

Table 6: Composition of the applied borosilicate glass determined by analysis by "Zentrum für Glas- und Umweltanalytik GmbH" [91]

Molecule	Amount [%]
B_2O_3	11.4
Na_2O	6.65
MgO	0.28
Al_2O_3	6.78
SiO_2	72.00
SO_3	< 0.01
K_2O	2.36
CaO	0.51
TiO_2	0.019
Fe_2O_3	0.025
ZnO	< 0.01
BaO	< 0.01
ZrO_2	0.015

## 3.2 Chemical Resistance Of Glass

The chemical resistance describes the durability of glass with presence of water, acidic or basic solutions or other chemicals and depends primarily on the glass composition [97, 98]. The degeneration of glass caused by chemical reactions is called glass corrosion. Interactions between glass and acidic solutions like HCl, H_2SO_4 or CH_3COOH can lead to ion exchange on the glass surface.

H^+ ions replace the cations like alkaline or alkaline earth ions on the glass surface as shown in the following Equation 3-2.

$$\equiv Si - O - Na \; + \; H_3O^+ \; \rightarrow \; \equiv Si - OH + H_2O + Na^+ \qquad \text{(Eq. 3-2)}$$
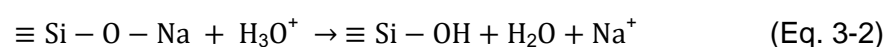
The ion replacement is a non-reversible reaction because the Si-OH groups will start further intramolecular reactions [99]. A 1nm – 1μm thick gelatinous layer of Si-OH and H_2O is

formed on the glass surface. The layer thickness increases with further ion exchange reactions and serves as a protection layer by barring further protons from attacking the glass surface. *I. W. Grebenstschikow* determined the relationship of the increasing layer thickness and a corresponding decreasing amount of attacking protons which finally slows the reaction down. Figure 6 (left) shows the parabolic shape of the graph which visualizes the reaction progress for acidic reaction and is compared to the straight shaped graph of basic reactions (right).
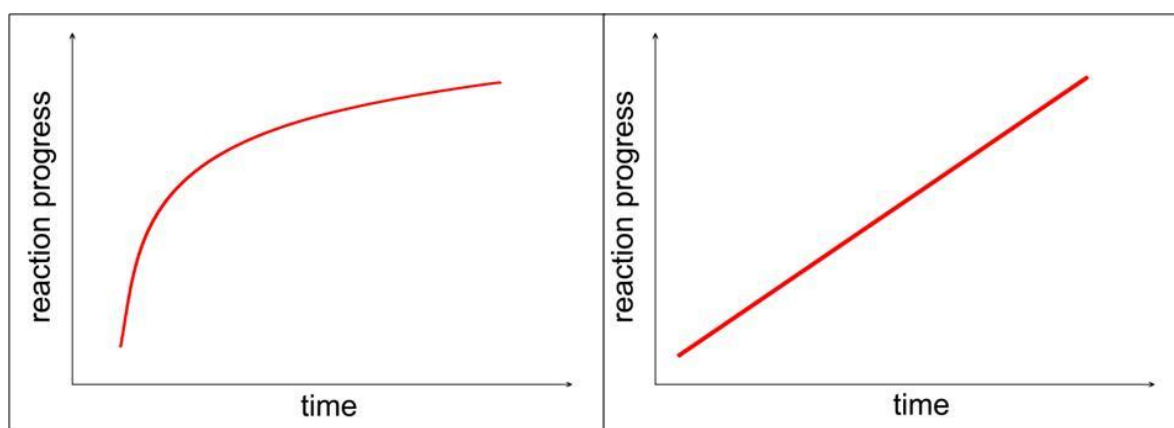

Figure 6: Time dependent reaction progress on the glass surface with acidic solvents (left) and basic solvents (right)

The inhomogeneous formation of the gelatinous layer leads to local centers of high decomposition [99]. Glasses with higher amounts of alkaline or alkaline earth ions are more susceptible to acidic attack than glasses with less cations like quartz glass or borosilicate glass with low amount of B_2O_3 and high amount of SiO_2 [100]. The SiO_2 network is not influenced by acidic solution except by fluoric acid (HF) or phosphoric acid (H_3PO_4) in high concentration [101].

In stark contrast, basic solutions with a pH-value >10 directly influence the SiO_2 network. The hydroxyl ion breaks the Si – O bond, whereby the bridging oxygen ion becomes terminal as demonstrated in Equation 3-3.

$$\equiv Si - O - Si \equiv\ + OH^- \rightarrow\ \equiv Si - O^- +\ \equiv Si - OH \qquad \text{(Eq. 3-3)}$$
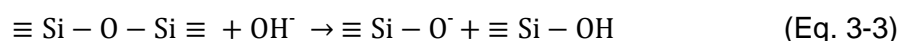
Water is an equilibrium condition of H^+ and OH^- ions. Contact to the glass surface leads to replacement of the cations by protons. Due to that fact, the reaction with water, for examples from air moisture, has the same influence on the glass structure as an acidic reaction. A H_2O molecule delivers a proton to equalize the charge of the terminal oxygen ion by forming a hydroxyl group. As shown in Equation 3-4 a further reaction product is a hydroxyl ion. As a consequence of the acidic reaction, an exposure of hydroxyl ions remains on the glass surface which initiates basic reactions by breaking an additional Si–O bond. Due to that, the chemical impact of water on the glass structure can be described as a combined mechanism of acidic and basic reaction. Zagar and Schillmöller [102] hold ion exchange responsible to be prevalent at low temperatures and short reaction time followed by network dissolution by hydroxyl ions.

$$\equiv Si - O - Na \ + \ H_2O \ \rightarrow \ \equiv Si - OH + Na^+ + \ OH^- \qquad \text{(Eq. 3-4)}$$
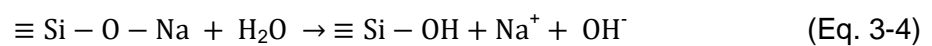
Other network formers like boron or phosphorus ions as well as network modifiers are substituted by basic reactions, too. This way, the glass will be ablated completely. The dissolubility of glass increases with growing pH-value. The reaction speed–time–diagram shows a straight line for basic reaction as shown in Figure 6 (right).

3.3 Physical Properties Of Glass

The physical properties of glass differ regarding to the condition of aggregation liquid or solid. In this chapter, the physical properties of solid glass will be considered [103].

In solid state, glass is a brittle material. Initially, it shows a linear-elastic behavior and follows the Hook's law. There is a constant length variation comparable to most metals. Figure 7 compares the elastic behavior of metal (left picture) and glass (right picture).
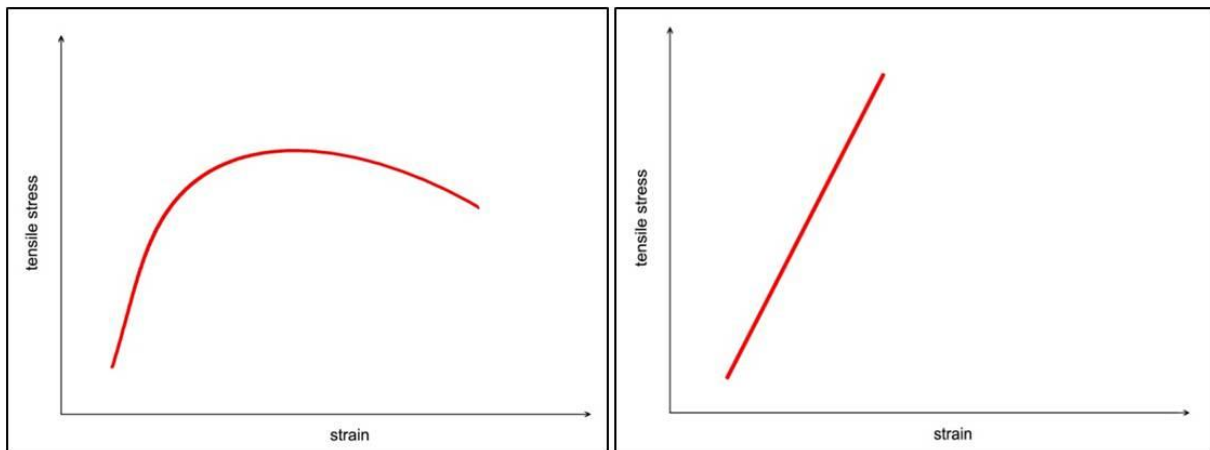
Figure 7: Elastic behavior of steel (left) and glass (right) at applied stress until rupture

If a critical stress is reached, glass cannot emit stored energy in ductile way by plastic deformation like most metals do. Instead, the material breaks. Thus, the stored energy is submitted by creating new surfaces, as well as heat and as kinetic energy.

In the following subchapters, the physical properties elasticity (3.3.1) and strength (3.3.2) are discussed.

3.3.1 Elasticity and Theoretical Young's Modulus Of Glass

For materials with linear-elastic behavior, the relationship of strain and applied stress can be described with the Young's modulus. This material specific parameter represents the elasticity in units of pressure (Pa). It depicts the ability of a material to be able to stand up to deformation when stress is applied; therefore, the relationship of deformation and Young's modulus is inversely proportional. According to Hook's law, the Young's modulus (E) is the quotient of stress (σ) and strain (ε) as visualized in Equation 3-5.

$$E = \frac{\sigma}{\varepsilon}$$

(Eq. 3-5)

Stress can be revealed as force (F) per area (A) and has the units of pressure (Pa).

$$\sigma = \frac{F}{A} \qquad \text{(Eq. 3-6)}$$

Strain is a dimensionless value and is described as length variation (Δl) divided by the initial length (l_0).

$$\varepsilon = \frac{\Delta l}{l_0} \qquad \text{(Eq. 3-7)}$$

Combining Equation 3-5 to 3-7 leads to the Young's modulus shown in the following equation. The Young's modulus is the factor of applied force and initial length divided by the factor of area and length variation.

$$E = \frac{F \cdot l_0}{A \cdot \Delta l} \qquad \text{(Eq. 3-8)}$$

The Young' modulus of glass depends on its composition. Especially CaO and B_2O_3 but also ZnO, BaO. PbO and Al_2O_3 are known to increase the Young's modulus [104]. In contrast, alkaline oxides decrease the Young's modulus.

The Young's modulus of glass with known composition can be calculated. A. Winkelmann and O. Schott [104] determined specific coefficients for the most common components of glass. Therefore, Equation 3-9 with the percentage amount (p_x) and the specific coefficients (E_x) can be used. The component specific coefficients are listed in Table 7 [104]. The amount in the applied borosilicate glass is taken from Table 6 in chapter 3.1 "Structure".

$$E = p_1 \cdot E_1 + p_2 \cdot E_2 + p_3 \cdot E_3 \ldots + p_i \cdot E_i \qquad \text{(Eq. 3-9)}$$

Table 7: Component specific coefficients and amounts for Young's modulus calculation [104]

Compounds	E_i in Glasses without B_2O_3	E_i in Glasses without PbO	E_i in Glasses with B_2O_3 and PbO	Amount in applied borosilicate glass [%]
Na_2O	61	**100**	70	**6.65**
K_2O	40	**70**	30	**2.36**
MgO	-	**40**	30	**0.28**
CaO	70	**70**	-	**0.51**
ZnO	52	**100**	-	**< 0.01**
BaO	-	**70**	30	**< 0.01**
PbO	46	**-**	55	**-**
B_2O_3	-	**60**	25	**11.4**
Al_2O_3	180	**150**	130	**6.78**
SiO_2	70	**70**	70	**72.00**
P_2O_5	-	**-**	70	**-**
As_2O_5	40	**40**	40	**-**

Specific coefficients for SO_3 (< 0.01%), ZrO_2 (0.015%), Fe_2O_3 (0.025%) and TiO_2 (0.019%) are not available. Because of its small amounts in the used glass these components have a negligible influence to the Young's modulus.

Using the coefficients shown in Table 7 and calculating the Young's modulus according to Equation 3-9, results in a theoretical Young's modulus of about $E = 7620$ kg mm^{-2} for the applied borosilicate glass.

According to the relationship which is demonstrated in Equation 3-10 to 3-12 the Young's modulus is about 75000 MPa.

$$1N = 1 \frac{\text{kg m}}{\text{s}^2}$$
(Eq. 3-10)

$$F = m \cdot a \qquad \text{(Eq. 3-11)}$$

The term a is the gravitational acceleration and is defined with the value 9.806 m s^{-2}. Summarizing the acting force per mm² can be determined in the subsequently shown way.

$$F = 7620\,\frac{kg}{mm^2} \cdot 9.806\,\frac{m}{s^2} = 74720\,\frac{kg\,m}{mm^2\,s^2} = 74720\,\frac{N}{mm^2} \qquad \text{(Eq. 3-12)}$$

3.3.2 Strength of Glass

Strength describes the materials resistance of breaking at applied force and is proportionally related to the strength of its chemical bonds. Breaking a material requires work against the cohesive forces of the molecules. Strength can be differentiated in compressive strength and tensile strength. The compressive strength of cubes or cylinders of glass with varying composition and defined dimension is detected by treating the sample with a hydraulic press until it breaks. The compressive strength (σ_c) is the quotient of force (F) and perpendicular to the force running area (A) as displayed in Equation 3-13.

$$\sigma_c = \frac{F}{A} \qquad \text{(Eq. 3-13)}$$

The tensile strength of glass can be determined by pulling glass sticks with varying composition and dimension until rupture. Compared to compressive strength the tensile strength is quite low, but it depends on the glass composition [105 - 109]. Components like CaO, B_2O_3 and BaO as well as PbO and Al_2O_3 were classified as tensile strength increasing components [110].

At the end of the 19th century, A. Winkelmann and O. Schott [110] did research on the strength of glass and specified component-specific coefficients dependent on empirical

values. These coefficients were used to calculate the tensile strength and compressive strength in dependence of the glass composition, which are shown in Table 8 [110].

Table 8: Component specific coefficients and amounts for the calculation of tensile strength and compressive strength

Compounds	coefficient for compressive strength (z)	coefficient for tensile strength (d)	Amount in applied borosilicate glass [%]
Na_2O	0.60	0.02	6.65
K_2O	0.05	0.01	2.36
MgO	1.10	0.01	0.28
CaO	0.20	0.20	0.51
ZnO	0.60	0.15	< 0.01
BaO	0.62	0.05	< 0.01
PbO	0.48	0.025	-
B_2O_3	0.90	0.065	11.4
Al_2O_3	1.0	0.05	6.78
SiO_2	1.23	0.09	72.00
P_2O_5	0.76	0.075	-
As_2O_5	-	0.03	-

The formulas for the calculation of compressive strength (σ_c) and tensile strength (σ_t) are shown in Eq. 3-14 and Eq. 3-15.

$$\sigma_c = p_1 \cdot z_1 + p_2 \cdot z_2 \ldots + p_i \cdot z_i \qquad \text{(Eq. 3-14)}$$

$$\sigma_t = p_1 \cdot d_1 + p_2 \cdot d_2 \ldots + p_i \cdot d_i \qquad \text{(Eq. 3-15)}$$

The terms p_1, p_2... p_i represent the percentage amount of the component, z_i as the corresponding coefficient for compressive strength and d_i for the corresponding coefficient for tensile strength. Inserting the values for the used borosilicate glass results in a tensile strength of σ_t = 7.8 kg mm⁻² which conforms to 76.5 MPa and a compressive strength of σ_c = 110 kg mm⁻² which conforms to 1080 MPa. According to this method, quartz glass (99.99% SiO_2) has a calculated tensile strength σ_t = of 9 kg mm⁻², conforming to 88 MPa and a compressive strength of σ_c = 123 kg mm⁻² or 1206 MPa. Equal to this approach, results of measuring strength are about 0.1% to 1% [111] of the theoretical strength of glass given in literature. Nevertheless, this calculation method is useful as an estimation of changing strength at varying glass composition.

The theoretical strength (σ_{th}) is defined with Equation 3-16 [112] whereby E is the Young's modulus, γ the surface energy and d_0 shows the atomic distance.

$$\sigma_{th} = \sqrt{\frac{E \cdot \gamma}{d_0}}$$

(Eq. 3-16)

According to Equation 3-17 the theoretical strength has a value of about 10% of the Young's modulus [113].

$$\sigma_{th} \approx \frac{E}{10}$$

(Eq. 3-17)

The calculated Young's modulus of the used borosilicate glass is E = 74720 MPa resulting in a theoretical strength of $\sigma_{th} \approx 7472$ MPa which is about 100 times higher than the calculated tensile strength (σ_t = 76.5 MPa) and about six times higher than the compressive strength (σ_c = 1206 MPa) based on empirical values calculated by Winkelmann and Schott [110].

An initial explanation for the difference of theoretical and experimental results was given by Griffith in 1920. He assumed that the reduced measured strength depends on the presence of defects. He declared the highest stress in a material occurs at the tip of a fracture which is demonstrated in Figure 8 schematically.
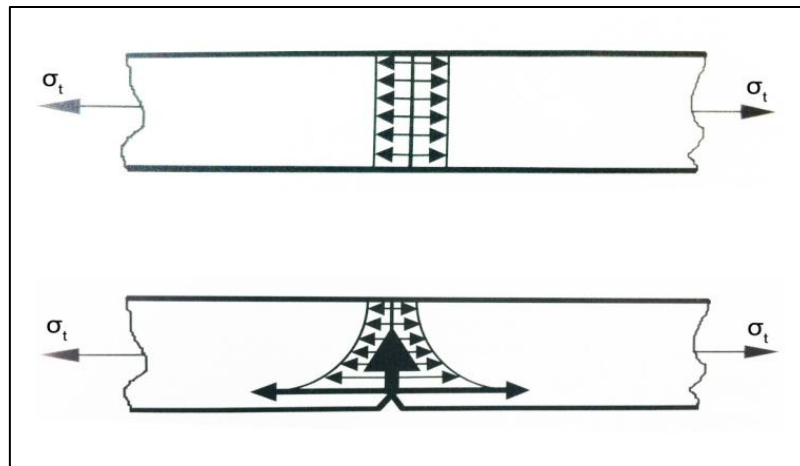
Figure 8: Distribution of stress in a defect free sample (top) and a sample with crack (bottom) at applied tensile stress (σ_t). The arrows display the occurring stress value (size) and direction [116]

Griffith's theory presupposes homogeneous, elastic and isotropic material properties, as well as constant total energy (U) dependent on crack growth. At an existing crack there is equilibrium of surface energy (U_S) and mechanical energy (U_M) including elastic and potential energy. In the case of crack growth, new surfaces are created and thereby the surface energy is increased. The mechanic energy decreases simultaneously to ensure the criterion of constant total energy [118].

$$U = U_M + U_S \qquad \text{(Eq. 3-18)}$$

According to the linear elastic theory, U_M can be represented as a factor of π, the squared fracture length (c^2) and the squared applied stress (σ^2) divided by the Young's modulus in the fracture plain (E).

$$U_M = \frac{\pi \cdot c^2 \cdot \sigma^2}{E} \qquad \text{(Eq. 3-19)}$$

U_S is given by the linear cohesion of surface energy (γ) and the fracture length (c).

$$U_S = 4 \cdot c \cdot \gamma \qquad \text{(Eq. 3-20)}$$

Summarizing Equation 3-18 to 3-20 the energy at constituted fracture length can be expressed as demonstrated in Equation 3-21.

$$U = - \frac{\pi \cdot c^2 \cdot \sigma^2}{E} + 4 \cdot c \cdot \gamma \qquad \text{(Eq. 3-21)}$$

Griffith's theory starts from the premise that the total energy U remains constant at growing fracture.

$$\frac{dU}{dc} = 0 \qquad \text{(Eq. 3-22)}$$

A differentiation of Eq. 3-21, respective to the fracture length (c), leads to Equation 3-23.

$$0 = \frac{-2 \cdot \pi \cdot c \cdot \sigma^2}{E} + 4 \cdot \gamma \qquad \text{(Eq. 3-23)}$$

Converting the equation into the stress (σ) results is the Griffith's flaw which is shown in Equation 3-24.

$$\sigma_F = \sqrt{\frac{2 \cdot E \cdot \gamma}{\pi \cdot c}} \qquad \text{(Eq. 3-24)}$$

The above mentioned equation can be used to calculate the theoretical strength of a material dependent on the fracture length. The term σ_F stands for the critical stress. The equation clarifies that small cracks already decrease the critical stress enormously. If the applied stress (σ) is larger than σ_F, the crack grows incessantly and fracture occurs [118]. Thus, the critical stress is equal to the tensile strength of the material.

In order to find evidence for his theory, Griffith determined the tensile strength of glass fibers with identical shape but different diameter. [120]. He calculated up to 20 times higher strength at decreased sample diameter from 1mm to 3.3µm. He explained this behavior with the lower probability of large cracks at smaller samples. Figure 9 shows the dependence of tensile strength and sample diameter schematically.
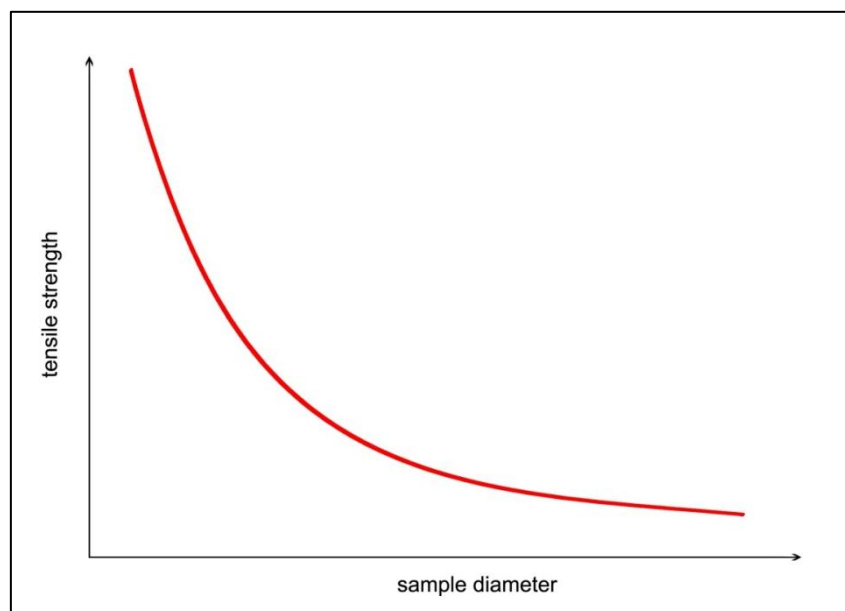
Figure 9: Relationship of tensile strength and sample diameter according to Griffith

Additionally, Griffith tested deliberately damaged glass samples with the result that their tensile strength was increased massively, vis-à-vis their crack size.

Furthermore, he revealed an addiction of the tensile strength to the age of the glass sample. Griffith found an extremely high tensile strength at new glass samples which were prepared a few seconds before strength determination. In contrast to samples prepared a few hours before testing, these new constructed fibers did not show the dependence of the strength on the diameter anymore. To understand the deviating strength of newly prepared glass samples, a look at the glass properties and production is necessary. Directly after

preparation the surface of glass is pristine. Strength affecting defects occur by handling, contact to other surfaces or the influence of moisture. Placing the samples on a table may lead to small scratches. Hence, samples which were tested directly after preparation did not have the chance to get damaged.

In 1955 William H. Otto disproved the relationship of tensile strength and sample diameter [121]. As opposed to Griffith, he had the opportunity to form fibers under controlled constant conditions. He complains against the circumstance that Griffith prepared thinner samples at increased temperature and with faster pulling. Otto repeated Griffith's experiments with samples prepared under identical conditions directly before the tests. The short lifetime of the samples forecloses the presence of large defects comparable to Griffith's results of new prepared samples. He came to the conclusion that all samples showed a comparable strength regardless of their diameter. The temperature of the molten glass showed an influence on the strength of the solid glass. Higher drawing temperature leads to increased strength.

Other scientists approved the non-existent simple relationship of strength and diameter [111], [122], [123], [124]. Nevertheless, Griffith's theory of fewer defects in thinner samples has not been disproved and remains applicable. As proven, there is no direct correlation between strength and sample diameter. Griffith demonstrated that surface defects are the most strength decreasing cause of/for glass samples.

3.3.3 Hydrogen Permeability of Glass

The permeability describes the capability of solid materials to let gases or liquids pass through the material. A high permeability describes a high amount of gaseous or liquid particles passing through the solid material. Due to that, a low permeability is a necessary property of a gas storage system.

Related to its small atomic size, hydrogen shows high permeability through the most solid materials. For reasons of safety, a low permeability is an essential property of a hydrogen storage system. The disordered atomic structure of glass offers large holes in the network, compared to the ordered structure of steel. These holes facilitate the permeation of any kind of atoms or molecules through the network. Depending on the kind of glass, these holes in the structure are filled with different kinds of Kations, whereby the permeability will be influenced.

According to literature, several examinations regarding to the permeability of different kinds of glasses were executed. In 1922 Williams and Ferguson described a permeation of hydrogen through silica glass as exponential function of the temperature with a proportional dependence of the gas pressure [125]. Elsey confirmed a permeation of hydrogen and helium through quartz glass in 1926 [126]. The permeability of glass also depends on the chemical composition of the glass. In 2014 Ried et al. examined the permeability of different kinds of glasses with different measuring methods. Among other methods, they used the vacuum-heat-extraction (VHE). Thereby, a glass fiber with vacuum inside is closed by melting and exposed to hydrogen at increased temperature and pressure. Afterwards, the fibers are exposed to vacuum and heated up continuously. A connected mass spectrometer measures the released substances. Figure 10 demonstrates the amount of released hydrogen during VHE [128]. The red graph displays the amount of released hydrogen from a closed borosilicate glass fiber with vacuum inside. The black graph shows an open fiber for comparison. The open fiber shows the amount of hydrogen, which was adsorbed at the surface. The peak at the red graph at about 650°C demonstrates the hydrogen, which reached into the closed fiber via permeation.
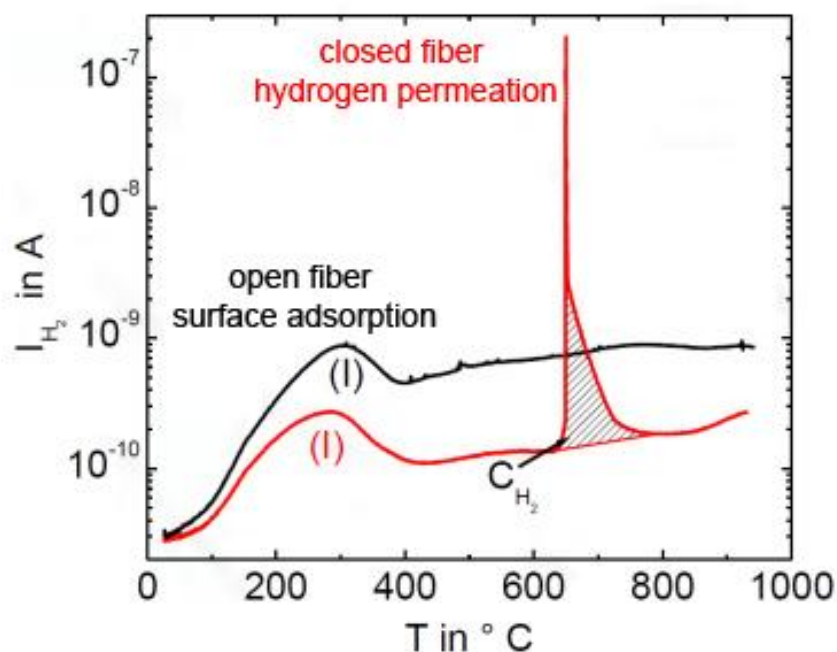
Figure 10: Released hydrogen during vacuum-heat-extraction of a borosilicate glass fiber which was treated with hydrogen at increased pressure and temperature before[128]

They declared a barium-aluminoborosilicate glass to have a three orders of magnitude lower hydrogen permeability at room temperature compared to silica glass and borosilicate glass [129]. Regarding the permeability, they declared this kind of glass to be suitable for long-time hydrogen storage.

3.4 Defects In Glass

Defects are the main reason for the large difference between theoretical and practical strength of glass. Any kind of defect leads to decreased structural strength. There exist different kinds of defects which are presented in this subchapter.

Typical defects may occur during production and are engendered by the liquid state of glass. Typical appearances of this kind of defects are attributed to foreign substances in the molten glass [131].

These so-called stones (Figure 11a) are differentiated into small solid components of completely different material such as metal particles and crystallization products which occur during production process at inconvenient conditions.

Inclusions of corrosion or dissolution products are called knots (Figure 11b). The implemented substance is glass with high viscosity and different properties than the residual glass. This kind of defect is characterized by a commonly round shape.

The aggregate phase of foreign substances is not limited to solid. Gaseous inclusions which could not be removed from liquid glass lead to bubbles in glass after solidification (Figure 11c).

If molten glass components with different properties are joined together but not mixed sufficiently striations may occur (Figure 11d). The results are areas in the glass with varying physical and chemical properties.
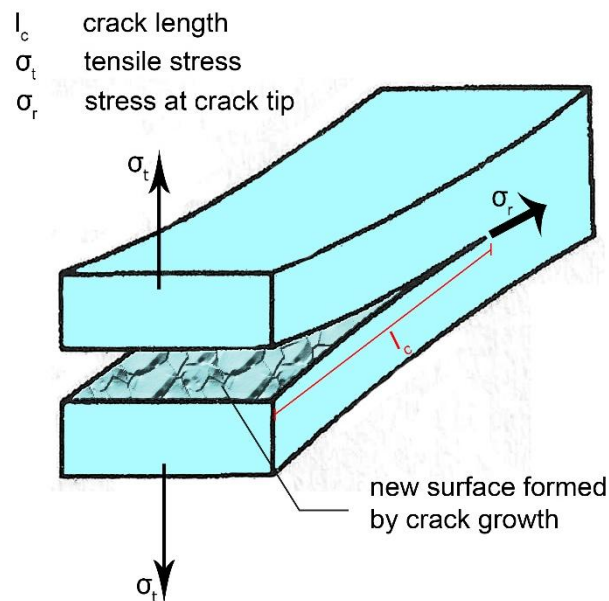
These manufacturing induced volume defects lead to points of increased stress inside the material and decreased strength. Such volume defects often emerge together. For example, bubbles or knots are mostly surrounded by striations as shown in Figure 11, which displays microscopic visualizations of stones, knots, bubbles and striations (from left to right) [132].
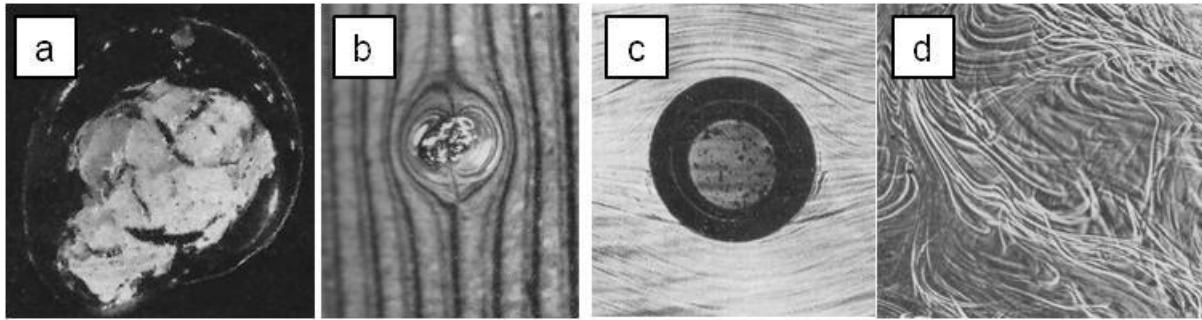
Figure 11: Microscopic visualization of stones (a), knots (b), bubbles (c) and striations (d) [132]

These defects have their origin in the glass production and emerge in the liquid phase of glass during manufacturing process. They typically arise at the surface of the material as well as inside the material. Next up, later produced defects which only occur on the glass surface by physical contact [133] will be discussed. Directly after production the surface of glass is free of scratches or cracks. Such defects are induced by further handling, whereby the surface has contact to other materials. These defects are differentiated in microscale defects and are observable with light microscope and smaller nanoscale defects. They require high-resolution equipment like scanning electron microscope (SEM) for visualization.

The size of a defect can be varied by applying force to the material. Exposing the material to increased tensile stress (σ_t) enlarges the crack (l_c) as shown in Figure 12, and leads to points of high stress (σ_r) at a distance r of the tips of these cracks. Usually, the relation of applied tensile stress and occurring stress at the crack tip is $\sigma_r \gg \sigma_t$.

l_c crack length
σ_t tensile stress
σ_r stress at crack tip

σ_t

σ_r

l_c

new surface formed
by crack growth

σ_t

Figure 12: Occurring stress (σ_r) at crack tip at applied tensile stress (σ_t) incident to increasing crack length (l_c) and newly formed surface [134, 135]

The mechanic energy and therefore the total energy of the material is increased. Compliant with Griffith's condition of existing energy equilibrium at constant total energy, the existing cracks will grow and form new surfaces to transform mechanic energy into surface energy.

According to Griffith's flaw, the strength and the critical stress of the material is reduced at the same time by the expanding crack size. Fracture occurs if the critical stress of the material (σ_F) is exceeded by the applied stress (σ).

Also, in case of applied stress lower than the critical stress ($\sigma < \sigma_F$), the strength of glass may decrease dependent on the ambient conditions. Water, for instance, from air humidity is able to invade into a crack, no matter its size. As previously mentioned, water is able to start chemical reactions with glass ingredients and weaken the structure this way. Thus, the crack grows both in depth and length. This process is called subcritical crack growth. It continues until the critical stress reaches a value below the applied stress and the glass immediately breaks. The reaction rate increases with higher applied stress. This phenomenon is called static fatigue and depends in principal on the presence of water. In the absence of water, like in vacuum, static fatigue will not occur. High temperatures speed up the fatigue, whereas low temperatures like in liquid nitrogen slow the reaction down [136]. The coherence of ambient temperature and material's strength can be confirmed in experimental way. Exemplary results are displayed in chapter 5.7.2 "Influence Of Defects".

Apart from that, the strength of glass can be increased by the influence of water under specific conditions. If no stress is applied, water induced glass corrosion performs a rounding of the crack tip by which the stress at this area is reduced [137]. This behavior was confirmed with FEM simulation and is described in chapter 5.7.2 "Influence Of Defects" in Figure 117 and Figure 118.

3.5 Reduction Of Defects And Internal Stress

Except for the production induced defects like Stones, Knots, Striations and Bubbles, the surface of a glass sample is free of defects like scratches or cracks, directly after production. Any contact of the surface to other materials, even to air moisture, leads to surface defects. In order to restore the defect-free condition, the surface can be approached with different kinds of thermal or chemical treatments.

In order to realize thermal treatment, different strategies exist. At the Flame Polishing method the glass surface is heated up with a flame above T_g. The surface changes to liquid phase. The liquid glass material floats into the cracks and scratches, whereby a new, defect-free surface will be created. This technique affords good handling skills for realizing a consistent heating at the whole surface. The presence of air and gas during that procedure facilitate chemical reactions on the surface of the glass. Furthermore, a rapid temperature alteration leads to additional stress in the material [142, 169].

In order to avoid such strength reducing thermal stress, the Annealing method poses a helpful tool. Thereby, the glass sample will be heated up to the annealing temperature, which depends on the chemical composition of the glass. As discussed in chapter 3.1, the viscosity of the glass has a value of $\eta = 10^{13}$ dPa s at this specific temperature. At this temperature, the material is able to relax thermal stress. Due to the fact, that the annealing temperature is higher than T_g, surface defects will be also healed during that time. Afterwards, a slow and controlled cooling rate is necessary, to avoid further emerging thermal stress. Opposed to this, this method can be also used to create specific areas of stress inside the material. In this case, the method is called tempering and is explained in chapter 3.6 "Pre-stressed Glass" [142, 169].

A chemical method to restore a defect free surface, is the Etching method. Thereby, the outer surface is treated with hydrogen fluoride, which is able to attack the SIO_2 network. In that way, the outer layer of the surface will be removed and a new surface will be created [117, 142, 169].

A preventive method for prohibiting surface defects to be created is the coating of the surface with a protection layer. This protection layer has to be applied directly after the production process of the glass, in order to protect the surface against outer influence. Dependent on the application of the glass, different kinds of coating are available [169].

3.6 Pre-stressed Glass

In glasses with the purpose of withstanding defined load, stress is generated deliberately which acts as an antagonistic force for the expected stress at external force application. External load is compensated appropriately to the intensity of previously generated stress and the strength is increased. Furthermore, a compressive stress on the glass surface causes a closure of small cracks decelerating the infiltration of water, resulting in static fatigue. This technique finds application in miscellaneous industries such as producer for car windows.

There are different approaches to produce stress deliberately in glasses, and it is dependent on material properties such as size, shape and composition. Flat glasses, such as windows, can be pre-stressed thermally [138 - 140]. For obtaining this objective, the glass has to be heated up consistently to a temperature of about 100°C above transformation temperature (T_g). The viscosity at this temperature is about 10^8 dPa s and existing internal stress disappears. Afterwards, the glass surface has to be cooled down rapidly by blowing air or diving into cold liquid. Thus, the material internal temperature differs from the surface temperature by which material intern tensile stress (σ_t) and at the surface compressive stress (σ_c) occurs. Depending on the rate of emitted heat stresses of 120 up to 150 MPa are reached [141]. The upper picture in Figure 13 shows a pre-stressed glass sample at which all surfaces were cooled down equally. The distances from surface to tensile strength area d_1 and d_2 are identical if no external stress (σ) is applied as shown in the bottom picture. In this case the tensile stress area (σ_t) displaces to the surface opposite to the applied stress (σ). The distance from tensile stress area to the surface with external applied stress (d_1) increases, whereas the distance to the opposite surface (d_2) shrinks. If $d_2=0$, the tensile stress area reaches the surface and the sample breaks [142].
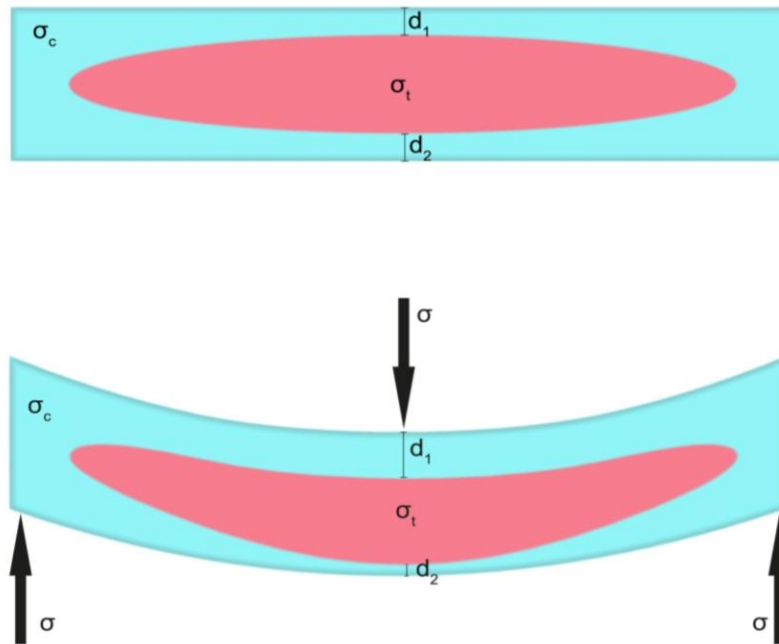
Figure 13: Displacement of tensile stress area (blue) and compressive stress area (red) at applied stress σ [142]

On glasses with smaller dimension containing alkaline ions, surface stress can be afforded by chemical reactions [143]. The glass has to be plunged into a solution with alkaline ions at 50K to 150K below T_g by whereby an ion exchange between the glass surface and the solution occurs. For example, Sodium ions in the glass surface are replaced with Potassium ions. The larger size of Potassium ions leads to compressive stress at the glass surface. In experiments stresses of 400MPa to 500MPa were obtained in this way. According to Fick's law, the amount of exchanged ions and with it the thickness of the produced stress zone is proportionally dependent on $\sqrt{t}$, meaning a two-times higher thickness of the stress zone is obtained by a four-times higher reaction time [144].

3.7 Stress Analysis

The following sub-chapters deal with different kinds of stress in any kind of material as well as the calculation methods of these stresses to determine the best qualified method for strength calculation in glass fibers at applied inner pressure. The investigations of stress distribution can be done for a condition of stationary, alternating or dynamic pressure load

[75]. Depending on the material's properties, there are several strategies to determine a material's internal stress at applied force. During stress analysis, the stress and deformation at a defined point of a material at any applied force will be determined analytically. Calculating these values for a large amount of points spread over a surface leads to a graphic visualization of stress distribution in an entire system. Thus, stress analysis is an adequate way to determine the occurring stress and deformation of a system of any kind of treatment.

Any applied force to a material leads to several kinds of stresses which can be displayed in a Cartesian coordinate system as demonstrated in Figure 14. Thereby, σ_x, σ_y and σ_z are posing the occurring tensile stress to the x-, y- and z-direction of a Cartesian coordinate system. The term τ poses the shear stress. The tensile stresses into x,- y- and z-direction and shear stresses can be combined for obtaining the three principal stresses σ_{H1}, σ_{H2} and σ_{H3} as displayed in the central picture of Figure 14. The right part shows the equivalent stress σ_v which will be affiliated from the principal stresses σ_{H1}, σ_{H2} and σ_{H3}. The equivalent stress σ_v is a scalar value whereby it poses a combined single-axle stress value regarding all occurring tensile stresses and shear stresses [76].
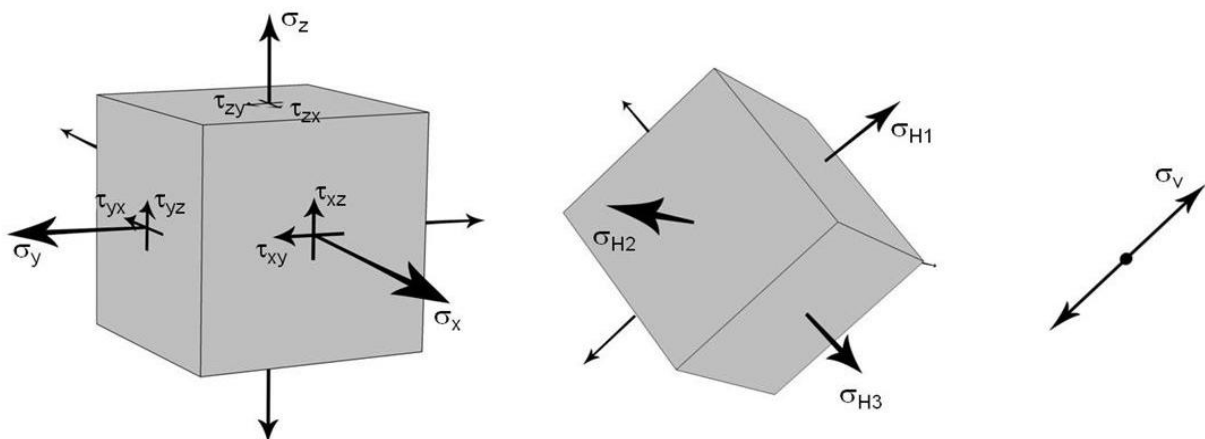
Figure 14: Tensile stresses (σ) and shear stresses (τ) acting into x-, y-, and z-direction (left), combination of these stresses to the principal stresses σ_{H1}, σ_{H2} and σ_{H3} (middle) and the equivalent stress σ_v (right) [76]

To determining the equivalent stress σ_v with one of the subsequent mentioned stress theories, the three principal stresses σ_{H1}, σ_{H2} and σ_{H3} are arranged according to their algebraic size. In the following chapters the term σ_1 is the maximum value of σ_{H1}, σ_{H2} and σ_{H3} ($\equiv \sigma_{max}$), whereas σ_3 describes the lowest value ($\equiv \sigma_{min}$). There exist several strategies to determine the value of equivalent stress σ_v. The choice of the most suitable strategy depends on the material properties and the kind of fracture of the sample. The following subchapters describe the characteristics and the application field of the different stress theories and deal with the question of which of the strategies is the most qualified in determining the stress in hollow glass fibers at inner pressure treatment.

3.7.1 Principal Stress Theory (Rankine)

The principal stress theory was hypothesized by Rankine in 1861 [75 - 78] and holds for brittle materials with low ductility. The brittle fracture grows perpendicular to the highest principle stress. The highest occurring stress and thereby the possible cause of fracture is σ_1 and related to that the equivalent stress σ_v is equal to the first principal stress σ_1 as clarified with Equation 4-1 [76 - 78].

$$\sigma_{v,PS} \equiv \sigma_1 \qquad \text{(Eq. 3-25)}$$

According to the theory, cleavage fracture occurs if the highest principle stress inside the material σ_1 has a higher value than the cohesion strength σ_{Co}. As a result, the premise of failure is complied with only if the highest principal stress σ_1 is equal with the cohesion strength σ_{Co} as subsequently shown in Equation 4-2.

$$\sigma_{1,crit} = \sigma_{Co} \qquad \text{(Eq. 3-26)}$$

In the case of a biaxial stress treatment (plane stress), the equivalent stress σ_v can also be determined from the tensile stresses into x - and y - direction and the shear stresses with Equation 4-3 [76].

$$\sigma_{v,PS} = \sigma_1 = \frac{\sigma_x + \sigma_y}{2} + \sqrt{\left(\frac{\sigma_x - \sigma_y}{2}\right)^2 + \tau_{xy}^2} \quad (>0) \qquad \text{(Eq. 3-27)}$$

3.7.2 Shear Stress Theory (Tresca)

As opposed to the Principal stress theory, the Shear stress theory hypothesized by Tresca in 1868 holds the highest occurring shear stress τ_{max} accountable for the initial fracture of the material [76 - 78]. More precisely, the material fails if τ_{max} reaches the shear stress τ_F so $\tau_{max} = \tau_F$ takes effect. The highest occurring shear stress can be explained with the halved difference of maximum and minimum principle stress.

$$\tau_{max} = \frac{\sigma_1 - \sigma_3}{2} \qquad \text{(Eq. 3-28)}$$

Therefore, the equivalent stress σ_v is the difference of the maximum and the minimum principle stress and equal to the yield strength R_e.

$$\sigma_{v,SS} = R_e = \sigma_{max} - \sigma_{min} = \sigma_1 - \sigma_3 \qquad \text{(Eq. 3-29)}$$

For the case of biaxial stress condition and current principal stresses with different algebraic sign, the equivalent stress σ_v can be determined with Equation 4-6.

$$\sigma_{v,SS} = \sqrt{(\sigma_x - \sigma_y)^2 + 4\tau_{xy}^2} \qquad \text{(Eq. 3-30)}$$

3.7.3 Von Mises Yield Criterion

Similar to the Shear stress theory, the difference of the principal stresses is decisive to determine the equivalent stress σ_v but in this case all principal stresses are considered [76, 79].

$$\sigma_{v,VM} = \frac{1}{\sqrt{2}}\ \sqrt{(\sigma_1 - \sigma_2)^2 + (\sigma_2 - \sigma_3)^2 + (\sigma_3 - \sigma_1)^2} \qquad \text{(Eq. 3-31)}$$

According to von Mises, the material starts yielding after the equivalent stress σ_v exceeds the yield strength R_e. An exceptional issue is the hydrostatic condition in which the three principal stresses have the same value ($\sigma_1 = \sigma_2 = \sigma_3$). In this particular case, cleavage fracture occurs if the stress value exceeds the cohesion strength σ_{Co} of the material. As a matter of principle, the maximum shear strain energy criterion applies for ductile materials like metals of stationary or alternating treatment [76, 79].

3.7.4 Stresses At Inner Pressure Load Of A Pipe

The stress which occurs at inner pressure treatment of a pipe is separated into three principal stresses [75]. The tangential stress σ_T occurs in circumference direction. The axial stress σ_A runs perpendicular to the tangential stress parallel to the surface. The axial stress has the half value of the tangential stress of cylindrical samples. This behavior is discussed in chapter 5.1. The radial stress σ_R occurs in perpendicular direction to the surface. The three stresses are visualized in Figure 15 [75]. The stress which occurs during inner pressure load is a combination of these three stresses.
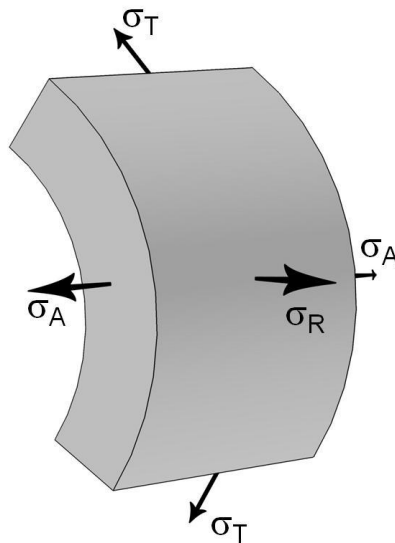
Figure 15: Section of pipeline with the occurring tangential stress σ_T, axial stress σ_A and radial stress σ_R [75]

The represented stresses σ can be determined in accordance with the surface comparison method [75]. The load bearing area is represented by A_p. The term A_σ poses the material surface and p is the applied pressure.

$$p \cdot A_p = \sigma \cdot A_\sigma \qquad \text{(Eq. 3-32)}$$

According to equation 3-32, the mean tangential stress $\sigma_{T,m}$ will be determined by adding the corresponding values into the equation [75].

$$\sigma_{T,m} = p \cdot \frac{A_{p,T}}{A_{\sigma,T}} \qquad \text{(Eq. 3-33)}$$

Analogue, the mean longitudinal stress $\sigma_{A,m}$ is represented as follows [75].

$$\sigma_{A,m} = p \cdot \frac{A_{p,A}}{A_{\sigma,A}} \qquad \text{(Eq. 3-34)}$$

The radial stress σ_R at the inner surface of a pipe is equal to the negative applied pressure p and 0 at the outer surface. Thus, the mean radial stress $\sigma_{R,m}$ is represented by the following Equation [75].

$$\sigma_{R,m} = -\frac{p}{2} \qquad \text{(Eq. 3-35)}$$

As already mentioned, glass is a brittle material. Related to that fact, the material will fail if the highest occurring principal stress has a larger value than the cohesion strength σ_{Co}. In the given case of inner pressure loading of a pipe, the tangential stress is the highest occurring stress. Thus the initial crack occurs in axial direction, perpendicular to the tangential stress direction. Thus, the principle stress theory is the most suitable stress calculation method for applied inner pressure in hollow glass fibers and is used for stress calculation with the finite elements method for this thesis.

3.7.5 Applied Calculation Methods

According to chapter 5.1, the highest occurring stress during pressure treatment in a glass tube is the tangential stress. Due to that fact, two-dimensional profile models of the glass structures were examined. At the inner boundaries of the FEM models an applied pressure is assumed, which acts along the normal of the surface. Pressure is a nonlinear factor because its direction depends on the normal of the surface [174], on which it is acting.

There is a differentiation between the force f, which acts on the current area *da* and the distributed force F_d, which acts on the whole material area *dA*. The force f can be calculated with the following equation [174].

$$f = F_d \, dA \qquad \text{(Eq. 3-36)}$$

If an external pressure *p* is applied, it acts in the current area *da* in the direction *n* according to equation 3-37 [174].

$$f \,=\, p \, n \, da$$ (Eq. 3-37)

The combination of equation 3-36 and 3-37 gives the following equation for the distributed load *Fd*.

$$F_d \,=\, p \, n \, \frac{da}{dA}$$ (Eq. 3-38)

In plane stress condition, which is applicable for the calculations in this thesis, the thickness of a model changes, which is caused by out-of-plane deformation. Therefore, equation 3-38 changes to equation 3-39 [174].

$$F_d \,=\, p \, n \, \frac{da}{dA} \, (1 + \frac{\partial w}{\partial z})$$ (Eq. 3-39)

Glass shows approximately the behavior of a linear elastic material. Furthermore, glass is an isotropic material, related to its amorphous structure. The elasticity matrix for isotropic materials is demonstrated in Equation 3-40 whereby *v* is the Poisson's ratio and *E* is the Young's modulus [174 - 176].

$$D = \frac{E}{(1+v)(1-2v)} \begin{bmatrix} 1-v & v & v & 0 & 0 & 0 \\ v & 1-v & v & 0 & 0 & 0 \\ v & v & 1-v & 0 & 0 & 0 \\ 0 & 0 & 0 & \frac{1-v}{2} & 0 & 0 \\ 0 & 0 & 0 & 0 & \frac{1-v}{2} & 0 \\ 0 & 0 & 0 & 0 & 0 & \frac{1-v}{2} \end{bmatrix} \qquad \text{(Eq. 3-40)}$$

In this thesis, the occurring stress in two-dimensional models is calculated. Therefore, the stress only in x-direction and y-direction has to be considered, what leads to plane stress. Due to the biaxial stress distribution, the elasticity matrix simplified to the subsequently following 3-by-3 matrix [174 - 176].

$$D = \frac{E}{1-v^2} \begin{bmatrix} 1 & v & 0 \\ v & 1 & 0 \\ 0 & 0 & \frac{1-v}{2} \end{bmatrix} \qquad \text{(Eq. 3-41)}$$

The further settings like boundary conditions, approximation type and mesh settings are discussed in chapter 5.6.

4 Experimental

Chapter 4 describes the experimental setup to determine the tensile strength. In this thesis, the tensile strength of the samples is determined by measuring the burst pressure. Furthermore, the preparation of the test samples as well as the procedure of executing burst pressure tests will be explained.

4.1 Requirements Of The Test Facility For Feasibility And Safety

The tests were done in a special safety room at BAM in Berlin, Germany.

There are different directives and regulations for personal and equipment safety while operating installations with compressed flammable gases. The following conditions need to be kept:

The laboratory is split into a testing room where the high pressure equipment is installed and a control room which contains the control and measurement equipment. Both rooms are separated with a 40 cm thick massive wall where all the gas pipelines and electronic wires pass through.

The testing room has a ventilation system and top hung windows which open at low overpressure of 200mbar in case of an explosion to release the pressure into a vertical air tunnel to keep the damages minimized.

The entrance to the testing room is closed with a fire and pressure resistant lockable steel door. During any kind of testing this door has to be closed. Furthermore, a sign is posted that states if tests are running or if safe entry is guaranteed.

The gas cylinders are placed in a ventilated locker in the control room. In case of emergency, the gas supply can be stopped without entering the testing room.

Both rooms are equipped with gas detectors. In case of a leakage, an optical and acoustic signal will be activated. It the ventilation is not switched on, it will be started automatically in case of a gas alert.

All electrical wires are isolated and the entire equipment is grounded.

4.2 Experimental Setup For Burst Pressure Determination

DIN EN ISO 7458 [147] describes the method of testing the pressure resistance of glass containers made for storage of liquids. To determine the pressure resistance of glass fibers with gases inside a test setup optimized for that purpose was constructed. The test setup, shown schematically in Figure 16, has been built of high pressure resistant components from Swagelok.
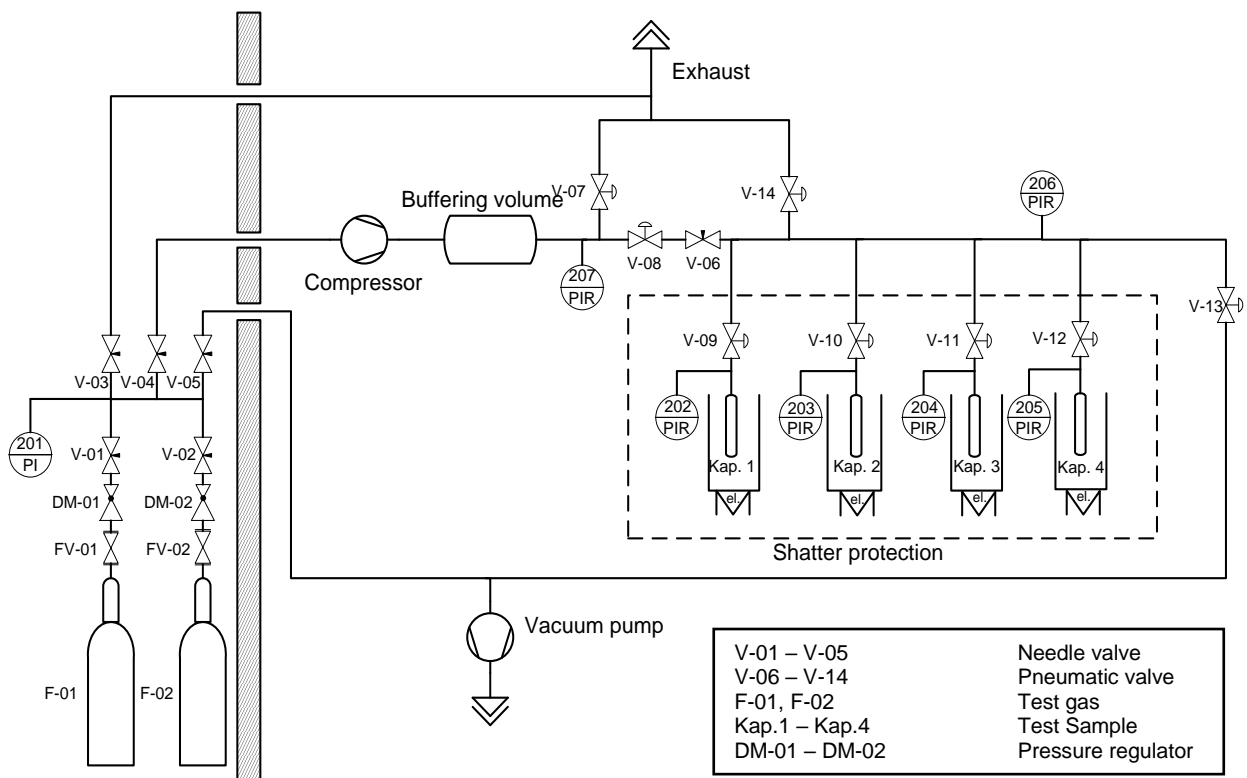
Figure 16: Schematic view of the test setup for high pressure treatment of glass structures constructed according to DIN EN ISO 10628:2000 [148]

An air driven two-stage compressor (Maximator DLE 15-75-2) was used to realize the pressure of 150 MPa. The compressor is not able to create a constant pressure flow due to it design. The pressure increases in batches as shown in Figure 17.
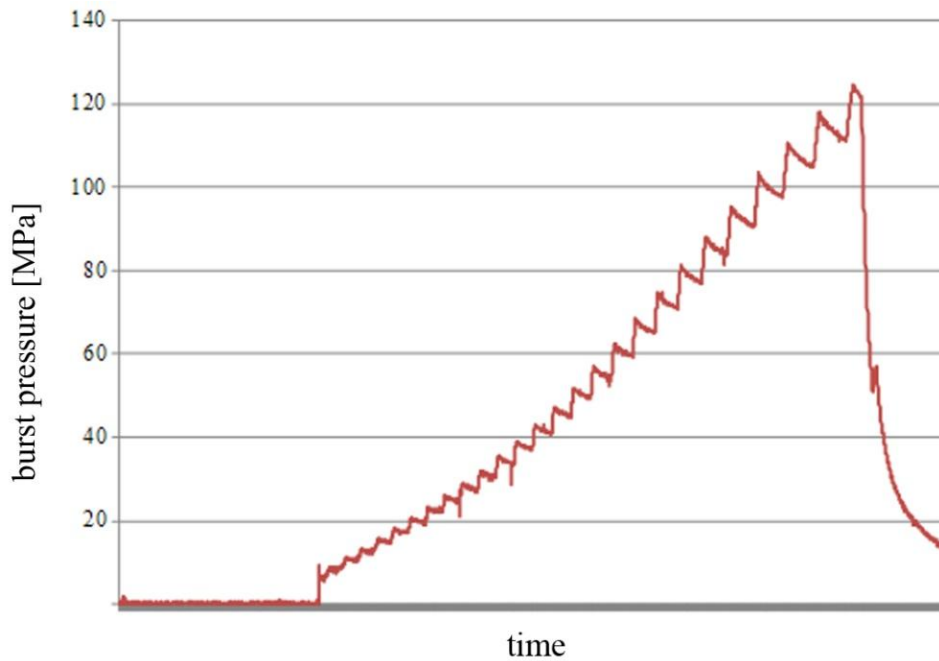
Figure 17: Pressure increase in batches caused by compressor strokes over a period of time

In order to avoid these pressure strokes, a buffering volume V = 80 ml has been installed behind the compressor. Therefore, two high pressure resistant autoclaves were used. Furthermore, a needle valve V-06 between buffering volume and samples effects a profile diminishment resulting in a slow and constant gas flow.

Behind the needle valve there are several connections, each of them closed with a remote controlled pneumatic valve V-09 – V-11. A vacuum pump and an exhaust pipe to the building's ventilation system are plugged to these connections. In addition, four test samples can be connected and tested at the same time.

Pressure sensors (Keller PA 10 and Keller PAA-10) with a measuring range of 0.1-100 MPa are installed to the buffering volume, to the pipeline behind the needle valve and to every sample connection. Pressure interacting with the sensor's membrane changes the electrical resistance. The signal is sent to a transducer and displayed with a digital readout.

The analogue signal of the thermo couples and the transducer is digitalized with a 16-Bit-A/D-Converter (company Jet Systemtechnik GmbH, Typ MCL-USB, 16 channels 16 Bit A/D, sampling frequency 500 kHz), sent to a computer via USB and recorded with BAM developed LabView software. The resolution of the pressure transducers is 10^{-4} bar. Linearity is better than 0.5 % full scale (FS). All pressure-time histories were measured and stored digitally.

The used transducers and pressure sensors with a measuring range of 0.1 – 100 MPa were calibrated before the tests by use of a digital pressure controller, type CPG 2500, WIKA Alexander Wiegand SE & Co. KG. The error of the pressure transducers was smaller than 0.5 % FS.

The tests showed that these sensors work reliably at pressures up to 150 % of their maximum range with acceptable uncertainty of not more than 1%, which makes them applicable at pressures up to 150 MPa. The pressure sensors are connected to the setup with at BAM developed adapters made of CrNiMo-steel 1.4401 (V4A), which is less susceptible against hydrogen embrittlement then CrNi-steel (V2A).

The tests were done at pre-defined temperature to ensure comparable test conditions. For this purpose, every sample is surrounded by an aluminum heating jacket placed on a lifting platform. The current temperature is measured with digital thermometers from the company Greisinger (type GTH 1200 A) with a 1.5 mm coated thermocouples type "K" (NiCr/NiAl) and adjusted automatically in the control room.

When a glass sample bursts, a lot of glass powder accrues. Because of hazard of inhalation, a closable box made of acrylic glass has been built around the setup. A built-in fan transports the released hydrogen out of the box for preventing an explosive atmosphere inside. Glass powder, which accumulates inside the box, is taken out with a vacuum cleaner.

4.3 Sample Preparation

In order to avoid influence of moisture and temperature the glass samples were stored in a dry box with desiccant at 35 °C. The single glass capillaries were glued into 1/16" stainless steel pipes to connect them to the high pressure setup. These pipes were glued into 1/8" stainless steel pipes which were directly connected to the setup. The procedure of connecting multi fibers to the setup is in principal the same. The steel adapters were adjusted to the sample sizes as well as the glued length according to Equation 4-4.

A schematic view of the connection principle is displayed in Figure 18. The term d_i poses the diameter of the open area inside the steel pipe and l demonstrates the length of the glued connection which depends on the diameter of the glass sample, the applied pressure and the strength of the glue as mentioned in Equation 4-1 to 4-4.
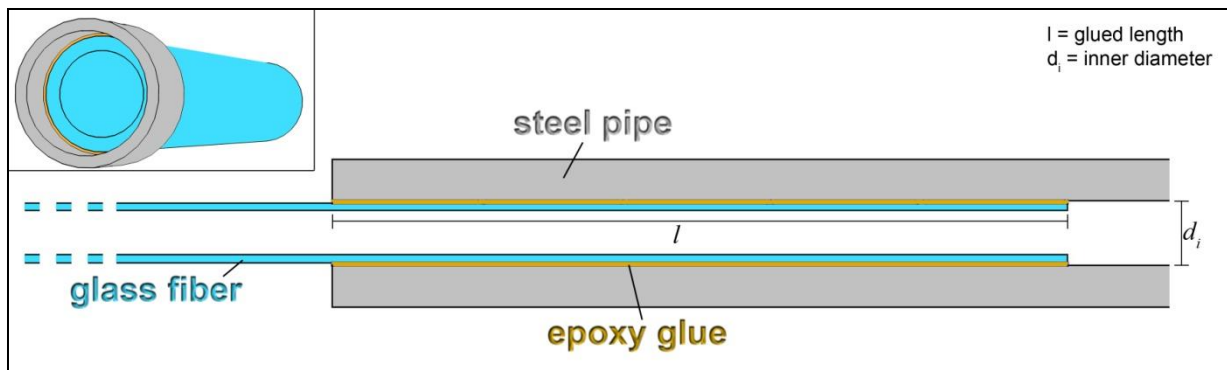
Figure 18: Schematic view of the connection of glass (blue) and metal (grey) with epoxy glue (yellow)

The glue used for that preparation is the epoxy two-component glue "UHU Endfest 300" which is temperature resistant up to 200 °C. The different thermal expansion coefficients of glass, glue and steel lead to leaks at high temperature fluctuation after hardening the glue. To achieve optimal gas tightness the glue was hardened at the same temperature at which the tests were done afterwards. The hardening time of the glue depends on the temperature. At 100 °C the glue becomes solid after 15 minutes, at 25 °C it needs at least 24 hours. The thermal expansion coefficients of the used materials are shown in Table 9.

Table 9: Thermal expansion coefficients of "UHU Endfest 300" epoxy glue [150], borosilicate glass [151, 153] and V4A steel [154]

Thermal Expansion Coefficient		
Borosilicate glass	V4A Steel	"UHU Endfest 300" Epoxy glue
$5.5 - 7 * 10^{-6}$ K^{-1}	$16,5 * 10^{-6}$ K^{-1}	$90 * 10^{-6}$ K^{-1}

The length (l) of the glued connection, which is necessary to avoid that samples are pushed out by pressure due to less adhesion, was calculated in the following way. The values necessary for the calculation are the strength (S) for the glue which is E=18 N mm^{-2} at 40 °C of the used glue (UHU Endfest 300) [150], the inner diameter of the steel pipe (d_i) and the applied pressure (p). The open area of the adapter is calculated according to Equation 5-19 [152].

$$A = \frac{d_i^2}{4} \cdot \pi \qquad \text{(Eq. 4-1)}$$

The applied force on this area is given in Equation 5-20.

$$F = p \cdot A \qquad \text{(Eq. 4-2)}$$

The glued area (A_K) at a length of l=1 mm is determined with the subsequently following Equation 5-21.

$$A_K = \frac{F}{S} \qquad \text{(Eq. 4-3)}$$

Equation 5-22 describes the way to determine the desired length of the glued connection.

$$l = \frac{A_K}{d_i \cdot \pi} \qquad \text{(Eq. 4-4)}$$

The calculation results in a minimum glue length of 1.04 mm to hold a single fiber with an outer diameter of D_o = 400µm in a steel pipe with an inner diameter of d_i = 500µm at an internal pressure of p = 150 MPa. A safety factor of 3 was considered what results in a minimal length of 3.1 mm.

4.4 Procedure Of Determining The Burst Pressure

As a first step to determine the burst pressure of glass samples, the whole test-system was evacuated. The heating devices were activated and the temperature was adjusted. Afterwards, the fiber's surface needed to be examined with light microscope. If no abnormalities, such as defects, have been found the glass samples were connected to the setup and evacuated. Afterwards, the buffering volume was filled with gas by keeping the valve V-4 to the samples closed. After reaching a pressure of about 150 MPa, the pneumatic valve V-4 was opened as well as the valves V-5 to V-8 dependent on which connected sample was tested. The samples were always tested one after another to generate precise pressure-time-histories.

The pressure inside the glass samples was increased continuously with a rate of about 2 MPa s^{-1} until the burst pressure was reached and the sample broke. At this point, the gas flow to the broken sample was interrupted immediately in order to prevent an emerging explosive atmosphere with ambient oxygen. Figure 19 displays the pressure increase during the filling procedure and the point of fiber collapse (burst pressure).
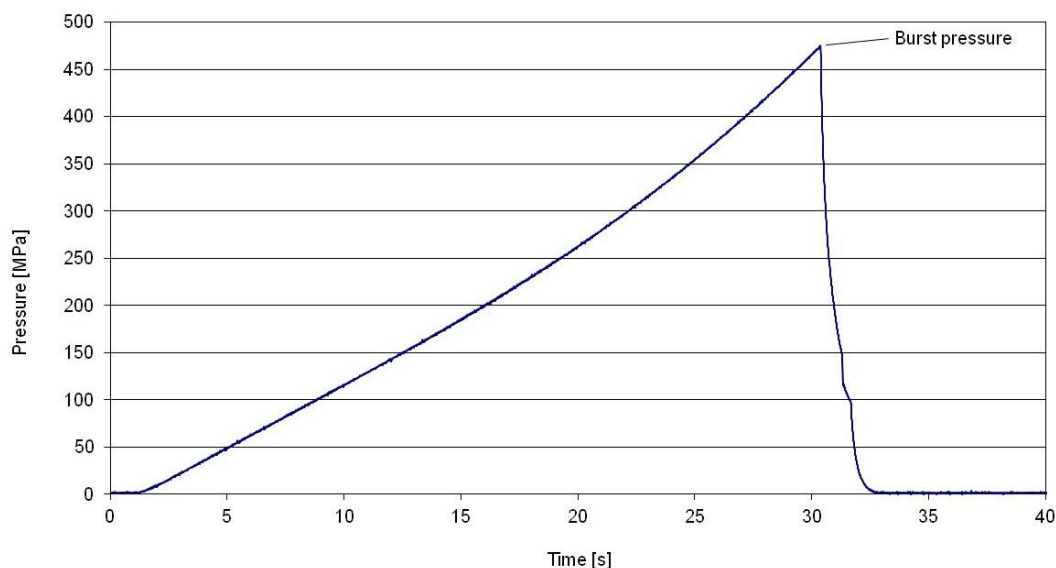
Figure 19: Pressure behavior during filling procedure with visualized burst pressure

5 Results and Discussion

In the course of this chapter, the burst pressure test method is compared to the commonly used tensile test method and the experimental setup of both test methods will be described.

For the calculation of stress and expansion with FEM, the Young' modulus poses a necessary variable. Therefore, the Young's modulus of the used glass material was determined in experimental way. This examination will be discussed in the following sub-chapter 5.2 "Determination Of The Young's Modulus Based On The Expansion".

Furthermore, the following chapter describes the different glass structures, according to their construction, originalities and strength. The production conditions of two different manufacturers will be mentioned. The strength of the structures was determined by examining the burst pressure conformable to chapter 4.4 "Procedure Of Determining The Burst Pressure".

The described glass structures are sorted by the manufacturer and their design elements. For evaluation and comparison, the maximum burst pressure value of a test series is considered because that value is least influenced of material defects and represents the best approximation to the theoretical strength.

Additionally, the following chapter represents the results of calculating stress and expansion of glass structures during internal pressure treatment. Beginning with single fibers, the influence of varying dimension was determined. Next up, different structures consisting of single fibers of varying dimension and shape were constructed virtually and the occurring stress and expansion at applied pressure of 50 N mm^{-2} (MPa) to the inner surface was calculated with the objective to find a structure with well distributed preferably low stress and a minimum expansion. The results are compared with the results of experimentally determined strength of comparable glass structures. The burst pressure of those glass structures was determined, which correlates to the tensile strength, as discussed in chapter 5.1. Additional research deals with the behavior of single fibers as well as structures at stepwise pressure increase and were evaluated in the course of this chapter. Furthermore, a statistical evaluation of the location of the initial break was executed experimentally and afterwards the influence of different kinds of defects was examined.

5.1 Comparison Of Burst Pressure Test Method And Tensile Test Method

There exist a number of test methods to determine the strength of materials. The most common one is the tensile test method where forces are applied to specific samples. These forces differ from those which occur by inside pressure load. In this subchapter the stress σ determined in tensile tests is compared to the stress calculated from burst pressure test results.

Applying internal pressure to hollow glass fibers leads to stress inside the material. The occurring stress inside a cylindrical thin-walled corpus is partitioned in axial (σ_A) and tangential stress (σ_T) as shown in Figure 20.
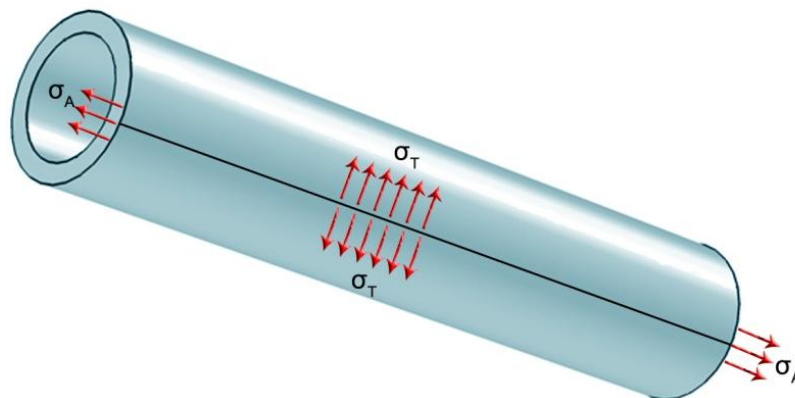
Figure 20: Axial (σ_A) and tangential stress directions (σ_T) at a round hollow fiber

The Barlow's formula describes the internal stress as function of applied pressure (p), outer diameter (D_o) and wall thickness (s) [156, 157]. This formula is valid for thin-walled vessels with an outer-to-inner-diameter-ratio of $D_o / D_i \leq 2.$

$$\sigma_A = \frac{p \cdot D_o}{4 \cdot s}$$
(Eq. 5-1)

$$\sigma_T = \frac{p \cdot D_o}{2 \cdot s} \qquad \text{(Eq. 5-2)}$$

Regarding the difference of Equation 5-1 and Equation 5-2, the relationship of axial (σ_A) and tangential stress (σ_T) can be defined as follows:

$$\sigma_T = 2\,\sigma_A \qquad \text{(Eq. 5-3)}$$

Related to this relationship, the tangential stress is two times higher than the axial stress wherefore the tangential stress will be the critical stress (σ_F) for inside pressure load which leads to fracture.

$$\sigma_F \equiv \sigma_T \qquad \text{(Eq. 5-4)}$$

According to the principal stress theory, the occurring fracture grows perpendicular to the highest principle stress. Hence, the first crack during pressure application occurs parallel to the axial direction as shown in Figure 21 (left). As opposed to this, the initial crack with tensile tension as the only applied force occurs in tangential direction as displayed in the right part of Figure 21.
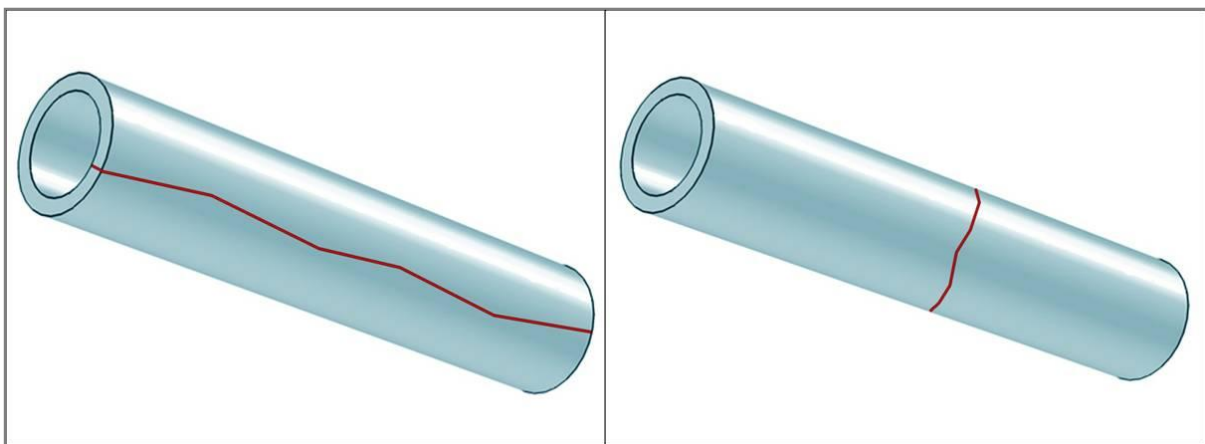
Figure 21: Initial cracks (red liner) in axial direction during pressure load (left) and in tangential direction at tensile test (right)

The common test method to determine a sample's strength is the tensile test method. Therefore, the sample is fixed at the opposite endings. A continuously increasing pulling force is applied until the sample breaks. By dividing the applied force by the cross sectional area of the glass sample the critical stress can be figured out. Opposed to pressure treatment, no tangential stress occurs as shown in Figure 22.
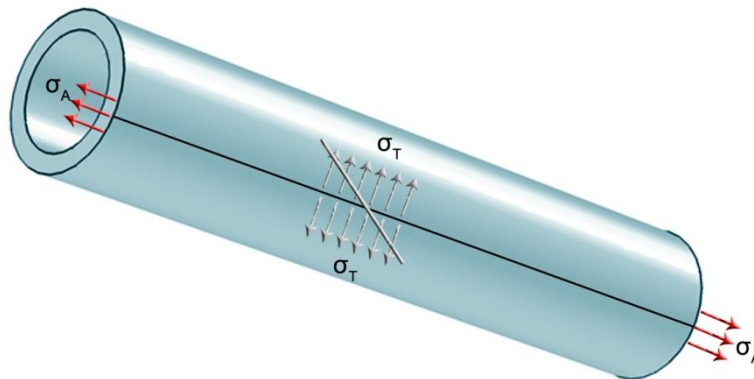
Figure 22: Occurring axial stress (σ_A) at tensile test method without emerging tangential stress (σ_T)

Thus, at tensile test the axial stress is the highest occurring stress which leads to fracture at reaching a critical value. Moreover, the axial stress poses the critical stress as demonstrated in Equation 5-5. Hence, the initial crack occurs in tangential direction as displayed in Figure 21 (right).

$$\sigma_F \equiv \sigma_A \qquad \text{(Eq. 5-5)}$$

For comparison of both testing methods, identical single fibers with an outer diameter of 0.292mm and an inner diameter of 0.267mm were tested using both methods. The tensile test was performed by Air Liquide according to ASTM D 2343-09 [158]. Six samples were tested with tensile test method resulting in an average critical stress of 374MPa. The results are displayed in Table 10 [159].

For calculating the critical stress (σ_T) with the Barlow's formula for tangential stress the average, minimum and maximum burst pressure value of the samples is used. The following Equation 5-6 and Equation 5-7 show the calculation exemplary for the average burst pressure value of p=33.7MPa as well as the outer diameter D_o=0.292mm and the wall thickness s=0.0127mm.

$$\sigma_F = \sigma_T = \frac{p \cdot D_o}{2 \cdot s} \qquad \text{(Eq. 5-6)}$$

$$\sigma_F = \sigma_T = \frac{33.7 \text{ MPa} \cdot 0.292\text{mm}}{2 \cdot 0.0127\text{mm}} = 387.4 \text{ MPa} \qquad \text{(Eq. 5-7)}$$

The average critical stress of 30 test samples tested with burst pressure test method is 387 MPa as also shown in Table 10. As a matter of fact, both test methods lead to comparable average tensile strength values. Also the maximum values are comparable, whereby the comparability of both test methods is proven.

Table 10: Comparison of the determined tensile strength in both methods

Fiber	Inner Diameter [mm]	Outer Diameter [mm]	Free Space [%]	Treatment method	Tensile strength [MPa]		
					Average	Maximum	Minimum
Single EDT-3915	0.267	0.292	83	Internal pressure	387.4	535.9	140.3
Single EDT-3915	0.267	0.292	83	Tensile load	374.4	450.2	303.4

Despite the comparability of burst pressure test and tensile test, both methods show significant differences. The speed of generating stress inside the material can be calculated as described in the following chapters 5.1.1 and 5.1.2.

5.1.1 Velocity Of Stress Generation At Tensile Test Method

According to Hook's law, which was already mentioned in chapter 3.3.1 "Elasticity and Theoretical Young's Modulus", the tension which is applied to a sample at tensile test method can be explained as the factor of Young's Modulus (*E*) and the strain (ε).

$$\text{E} = \frac{\sigma}{\varepsilon} \quad \rightarrow \quad \sigma = \text{E} \cdot \varepsilon \qquad \text{(Eq. 5-8)}$$

According to Equation 3-8, strain is the quotient of length variation (Δl) and initial length (l_0).

During tensile tests a strain rate of 5mm per minute has been chosen which conforms to the ASTM standard to determine the Young's Modulus (ASTM D2343-09 [158]). The length of the tested fibers was 150 mm. Thus, the strain was $\varepsilon = 0.0333$ which corresponds to a strain of 3.3 % per minute. The ASTM standard for tensile tests standardizes a rate of 6.6 % (ASTM D2343-09 [158]). As demonstrated in chapter 3.3.1 "Elasticity and Theoretical Young's Modulus", the calculated Young's Modulus of the tested borosilicate glass based on the composition is about $E = 75000 \, MPa$.

According to Hook's law the applied stress per minute is $\sigma \approx 2500 \, \frac{N}{mm^2}$ at tensile test method.

$$\sigma = \text{E} \cdot \varepsilon \approx 2500 \, \text{MPa} \qquad \text{(Eq. 5-9)}$$

Considering the area which is exposed to that stress, the dimension of the tested fiber needs to be involved into the calculation. The area of the glass which is exposed to the stress is the difference of the area of the whole sample and the area of the free inner space.

$$A_{Glass} = A_{Do} - A_{Di} \qquad \text{(Eq. 5-10)}$$

$$A_{Do} = \frac{\pi}{4} d_o{}^2 = \frac{\pi}{4} 0.292^2 \text{mm}^2 \qquad \text{(Eq. 5-11)}$$

$$A_{Di} = \frac{\pi}{4} d_i{}^2 = \frac{\pi}{4} 0.267^2 \text{mm}^2 \qquad \text{(Eq. 5-12)}$$

$$A_{Glass} = 0.011 \text{ mm}^2 \qquad \text{(Eq. 5-13)}$$

The total force which is applied to the glass sample in one minute can be determined with the Equation 5-14.

$$F = \sigma \cdot A \approx 28 \text{ N} \qquad \text{(Eq. 5-14)}$$

Concerning the small area which is exposed to the applied stress at tensile test method, the total applied force per minute is comparably low.

5.1.2 Velocity Of Stress Generation At Burst Pressure Test Method

In contrast, the stress which the sample is exposed to at burst pressure test method can be calculated as follows. During the test, the pressure increases with an average rate of 2 MPa per second. Therefore the applied pressure per minute is 120 MPa. According to the Barlow's formula the internal stress which occurs at applied pressure in one minute can be determined as follows in Equation 5-15 and 5-16.

$$\sigma = \frac{p \cdot D_o}{2 \cdot s} \qquad \text{(Eq. 5-15)}$$

$$\sigma = \frac{120 \text{ MPa} \cdot 0.292 \text{ mm}}{2 \cdot 0.0125 \text{ mm}} = 1401.6 \text{ MPa} \qquad \text{(Eq. 5-16)}$$

The stress which is generated per minute inside the material is about 1400 MPa. Hereby the speed of generating stress inside the material at burst pressure method is about 30 % lower than at tensile test method. The total force which is applied to the glass in one minute can be determined regarding the area of the inner surface of the fiber which is specified with the following term.

$$A_{\text{Glass}} = 2 \cdot \pi \cdot r \cdot h = 335 \text{ mm}^2 \qquad \text{(Eq. 5-17)}$$

Thereby, r is the inner radius and h is the length of the fiber. The area which is exposed to the applied stress is much larger at burst pressure test method than at tensile test method. With the Equation 5-18 the total force which is applied to the inner surface of the fiber in one minute can be determined.

$$F = \sigma \cdot A \approx 470000 \text{ N} = 470 \text{ kN} \qquad \text{(Eq. 5-18)}$$

Concerning the large area which is exposed to the applied stress at burst pressure test method the total applied force per minute is much higher than at tensile test method.

Nevertheless, the resulting tensile stress of both test methods shows comparable values as already shown in Table 10. Thereby, the speed of generating stress has no influence to the tensile strength of the material.

5.2 Determination Of The Young's Modulus Based On The Expansion

The Young's modulus is one of the necessary values for stress calculation. Hence, the theoretical value based on the composition of the material done in chapter 3.3.1 "Elasticity and Theoretical Young's Modulus was verified by determining the Young's modulus in practical application. Therefore, the expansion of a single fiber with defined dimension has to be examined.

To determine the expansion of a single fiber during pressure load a light microscope was used. The single fiber was placed under the microscope and simultaneously connected to the test setup. The software used (Motic Images Plus 2.0) allows a real-time view and the measurement of dimension of the connected sample. The outer diameter of the connected fiber was determined at atmospheric pressure and directly before bursting. The measured expansion of the fiber was used to determine the Young's module of the material with the Barlow's Formula. Figure 23 displays the outer diameter of a sample before and during pressure load.
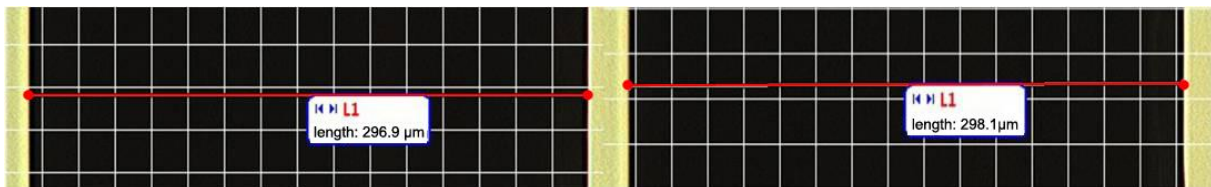
Figure 23: Diameter of a single fiber at atmospheric pressure (left) and at inner pressure of 103 MPa (right)

As already mentioned in Equation 3-5, the Young's modulus describes the relationship of applied stress and strain. The strain of the fiber's outer diameter was calculated according to Equation 3-7. Combining these equations results in the subsequently following relationship.

$$E = \frac{\sigma}{\frac{\Delta l}{l_0}}$$

(Eq. 5-19)

Considering the Barlow's formula the emerging stress can be summarized as described in Equation 5-20.

$$E = \frac{\frac{p \cdot D_o}{2 \cdot s}}{\frac{\Delta l}{l_0}} = \frac{p \cdot D_o \cdot l_o}{2 \cdot s \cdot \Delta l} \qquad \text{(Eq. 5-20)}$$

Because of the examination of the cross sectional area the value of the initial length l_0 conforms to the outer diameter D_o. With $l_0 = D_o$, Eq. 5-20 can be transferred to Eq. 5-21.

$$E = \frac{p \cdot D_o \cdot l_0}{2 \cdot s \cdot \Delta l} = \frac{p \cdot D_o^{\,2}}{2 \cdot s \cdot \Delta l} \qquad \text{(Eq. 5-21)}$$

Table 11 summarizes the results of the measurements. In addition to the expansion at the burst pressure, the table shows the measured outer diameter D_o at ambient condition and the set points for inner and outer diameter. The Young's modulus calculated with the measured values as described above is displayed in the right slot. The average Young's modulus is shown below the table separately.

Table 11: Results of measuring the expansion during pressure load with light microscope and calculated Young's modulus

D_o [mm]	D_i [mm]	Measured D_o start [μm]	Burst pressure [MPa]	Expansion		Young's modulus [MPa]
				[μm]	[%]	
0.40	0.300	401.8	110.0	4.2	1.05	42282.75
0.40	0.300	414.4	102.8	1.9	0.46	92913.54
0.40	0.300	391.3	87.2	1.6	0.41	83448.05
0.40	0.300	411.9	73.3	1.3	0.32	95663.05
0.40	0.300	417.1	93.9	2.2	0.53	74254.59
0.40	0.300	402.5	83.2	1.9	0.47	70941.68
0.40	0.300	393.8	60.6	1.3	0.33	72290.41
0.40	0.300	422.5	50.3	1.2	0.28	74823.87
0.40	0.300	419.4	72.8	1.6	0.38	80032.84
0.35	0.263	295.2	61.9	1.0	0.34	62001.77
0.35	0.263	296.9	103.2	1.2	0.40	87136.44
0.35	0.263	310.4	93.7	1.6	0.52	64855.05
0.35	0.263	291.7	78.8	2.0	0.69	38534.51
0.35	0.263	296.3	97.0	1.3	0.44	75296.09
0.35	0.263	297.6	136.0	1.8	0.60	76915.35

Average Young's modulus [N mm^{-2}]
74930

The value of the average Young's modulus determined by measuring the expansion of glass fibers at pressure treatment is similar to the theoretical value based on the composition of the glass (E_{theor} = 74720 MPa) which was calculated in chapter 3.3.1 "Elasticity and Theoretical Young's Modulus". Hence, that theoretical value was used as parameter for FEM simulation.

5.3 Burst Pressure Test Results of First Hand-Made Glass Structures

The first structures were produced by a German glass fiber manufacturer. The company is specialized in the development of single glass fibers. The production of structures by fusing single hollow glass fibers was a new focus for the company. The multi glass fibers were handmade, whereby the quality of the produced charges differed and made them difficult to compare to each other. Additionally, hand-made production leads to high production time and cost. Hence, especially in the first cases, the amount of comparable test samples was too low for creating a statistical evaluation. Nevertheless, an estimation of the burst pressure value could be done.

5.3.1 Production Process

As basic raw material, single glass tubes with an outer diameter of about 40mm are used. The used material was borosilicate glass. The exact composition is already discussed in chapter 3.1. For constructing multi glass fibers made of fused hollow single glass fibers, the basic glass tubes were drawn to an outer diameter of only a few millimeters. Therefore they needed to be heated up to the material specific transformation temperature. By fastening one end and simultaneous applying a tensile tension at the other end, the tube is stretched. The diameter will be decreased but the ratio of inner and outer diameter keeps nearly constant.

The new smaller glass tubes were arranged and placed inside a large glass tube. That structure was heated up to the transformation temperature and drawn again until the desired outer diameter was reached. For the first structure a constant outer diameter of 4mm was chosen for obtaining comparable results. The drawn structures were cut to a length of 200mm and one end was closed by melting.

5.3.2 Round Structure Made Of Round Hollow Glass Fibers With Interspaces And Outer Glass Shell

The first produced multi glass fibers were labeled A1. The single hollow glass fibers are placed loosely next to each other, as visible in the microscopic view, which is displayed in Figure 24. The entire structure is displayed in the small picture in the upper left corner. The sample has a length of 200mm and an outer diameter D_o=4.15mm. It consists of 370 single hollow glass fibers, each with an inner diameter D_i=0.12mm and an outer diameter D_o=0.15mm. The free inner volume of the hollow glass fibers is 0.84ml. Referring to the structure's volume of 2.70ml, it conforms to 31% free inner volume, while the interspaces are not considered for the calculation. The arrangement of the single fibers is characterized by an unstructured assembly of the single fibers whereby interspaces with varying dimensions occur. Caused by these interspaces, the pressurized gas is also located inside of those interspaces, which potentially has a strength decreasing influence. Hence, the pressure also acts to the surrounding glass shell, whereby it also needs to be pressure resistant.
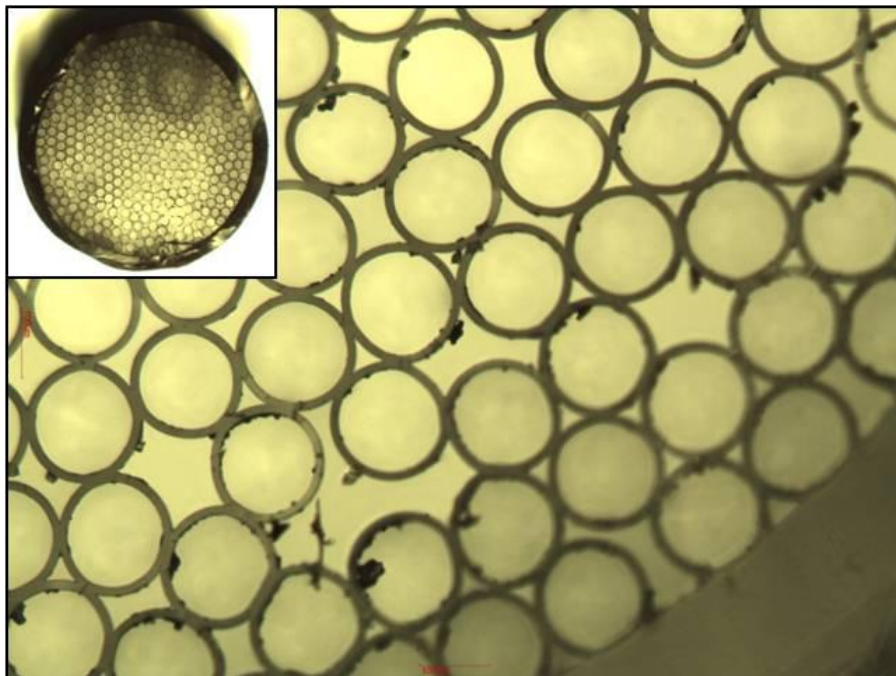
Figure 24: Microscopic view of structure A1 - Round structure with round single hollow glass fibers with interspaces and outer glass shell

Seven samples of this kind were tested for their burst pressure. The results of the burst pressure tests are displayed in Table 12. The maximum value, which is necessary for evaluation and comparison, is marked in red. The burst pressure values vary from 9.4 to 12.7 MPa. All samples broke into thousands of small pieces, and it could not be established if the initial failure occurred at the inner fibers or at the outer shell.

Table 12: Burst pressure test results of structure A1 - Round structure with round single hollow glass fibers with interspaces and outer glass shell

Burst pressure [MPa] of sample 1-7						
10.5	9.4	10.4	10.6	11.1	12.7	10.5

The second kind of multi glass fiber (A2) has a similar structure to the first one and is displayed in Figure 25. The length with 200mm is comparable as well as the outer diameter with D_o=4.15mm. In contrast to structure A1, the single hollow glass fibers have a larger diameter and a relatively smaller wall thickness. Consequentially, the free inner volume of the structure is nearly doubled to 1.61ml. Regarding the structure's volume of 2.69ml, this corresponds to an inner free volume of 60%, if the interspaces are not included in the calculation. Due to the larger single hollow glass fibers the structure contains only 76 fibers. The single fibers are arranged according to the principle of close packing spheres. The interspaced are partially filled with solid glass sticks which do not prevent an invention of the gas into the interspaced. Equally to structure A1, the interspaced lead to the fact that the outer glass shell is exposed to the pressure and thereby needs to be pressure resistant.
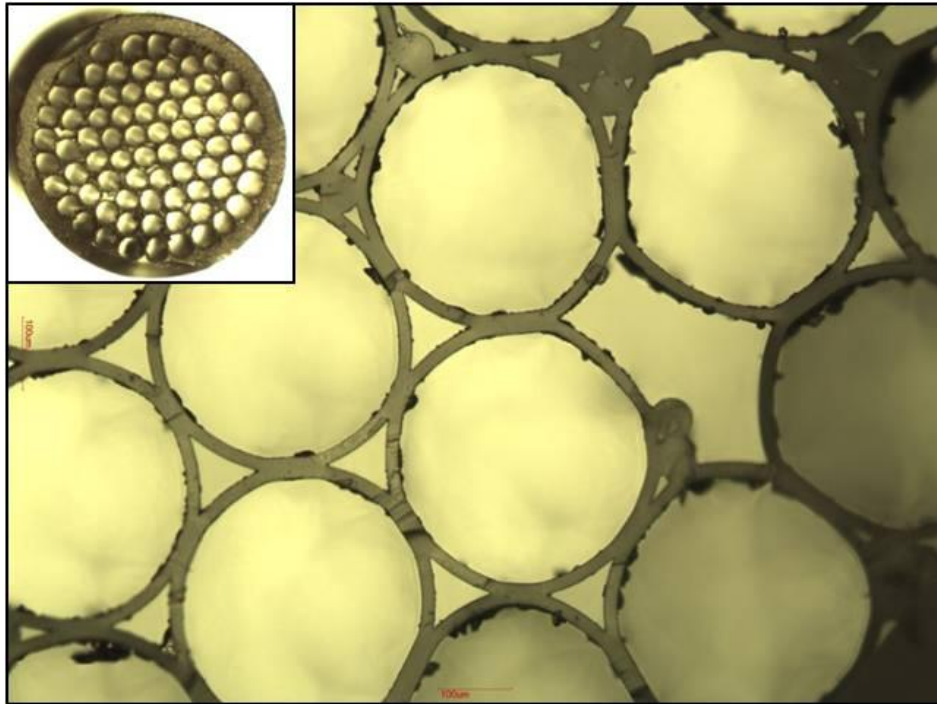
Figure 25: Microscopic view of structure A2 – Thin-walled round structure with large round single hollow glass fibers with interspaces and outer glass shell

The results of six tested A2-structures are displayed in Table 13. The maximum burst pressure value is marked in red. The minimum burst pressure value is 5.1 MPa. The maximum value is 8.8 MPa. Thus, the maximum measured burst pressure value of structure A2 is lower than the minimum measured burst pressure of structure A1 with smaller glass fibers and lower free volume. Nevertheless, the influence of the interspaces cannot be determined.

Table 13: Burst pressure test results of structure A2 – Thin-walled round structure with large round single hollow glass fibers with interspaces and outer glass shell

Burst pressure [MPa] of sample 1-6					
8.8	8.3	8.8	5.1	8.5	7.6

In order to increase the burst pressure the following samples consist of 96 single hollow glass fibers with higher wall thickness. The increased amount of single fibers results in an outer diameter of the structure of D_o=5.77mm. The legth of the samples has been reduced to 100mm. The size of the triangular interspaces between the single fibers is reduced, compared to structure A1 and A2. The outer glass shell is also exposed to the acting pressure and needs to be pressure resistant. The higher wall thickness of the single fibers makes the entire structure larger.. Equal to structure A2, the single fibers are arranged according to the principle of close packing spheres. A microscopic view of the structure is displayed in Figure 26. The small picture in the upper left corner displays the entire structure.
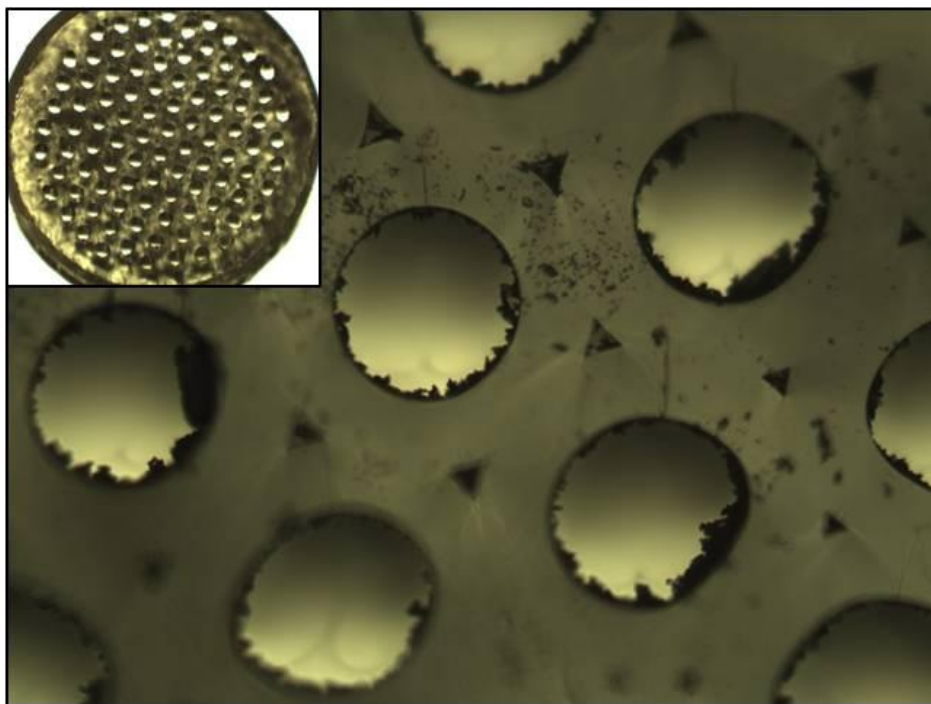
Figure 26: Microscopic view of structure A4 thick – Thick-walled round structure with round single hollow glass fibers with small interspaces and outer glass shell

Three samples of structure A4 thick were tested to determine their burst pressure. The minimum measured burst pressure value is 25.7 MPa and the maximum value is 28.4 MPa. Generally, the burst pressure values are more than two times higher than of structure A1 and more than three times higher than of structure A2.

This trend demonstrates the coherence of the wall thickness of the single hollow glass fibers and the burst pressure value. A relatively higher wall thickness leads to higher burst pressure

values. A further difference of this structure to the previous ones is the smaller size of the interspaces between the single fibers. Furthermore, the length of the structure is halved to 100mm. According to Griffith, the smaller length leads to lower possibility of the presence of strength decreasing defects, which is what leads to statistically higher burst pressure values.

Table 14: Burst pressure test results of structure A4 thick – Thick-walled round structure with round single hollow glass fibers with small interspaces and outer glass shell

Burst pressure [MPa] of sample 1-3		
25.8	28.4	25.7

5.3.3   Round Structures Made Of Round Hollow Glass Fibers Without Interspaces But With Outer Glass Shell

To determine the influence of the interspaces on the strength of the structure, a further structure was produced. The parameters remained the same as at structure A4 thick. The structure also consists of 96 round single hollow glass fibers which are arranged according to the principal of close packing spheres. The only difference was that the structure has been drawn more during the production process. This way, it was possible to disperse the interspaces between the single fibers. That fact implicates the circumstance that the pressure only acts inside the single fibers. The outer glass shell is not directly exposed to the pressure. An additional effect of the extended drawing is a decreased size of the entire structure. The outer diameter is reduced to 4mm. The inner diameter of the single fibers is shrunken with the same ratio. A microscopic view of the structure is displayed in Figure 27. The small picture in the upper left corner displays the entire structure.
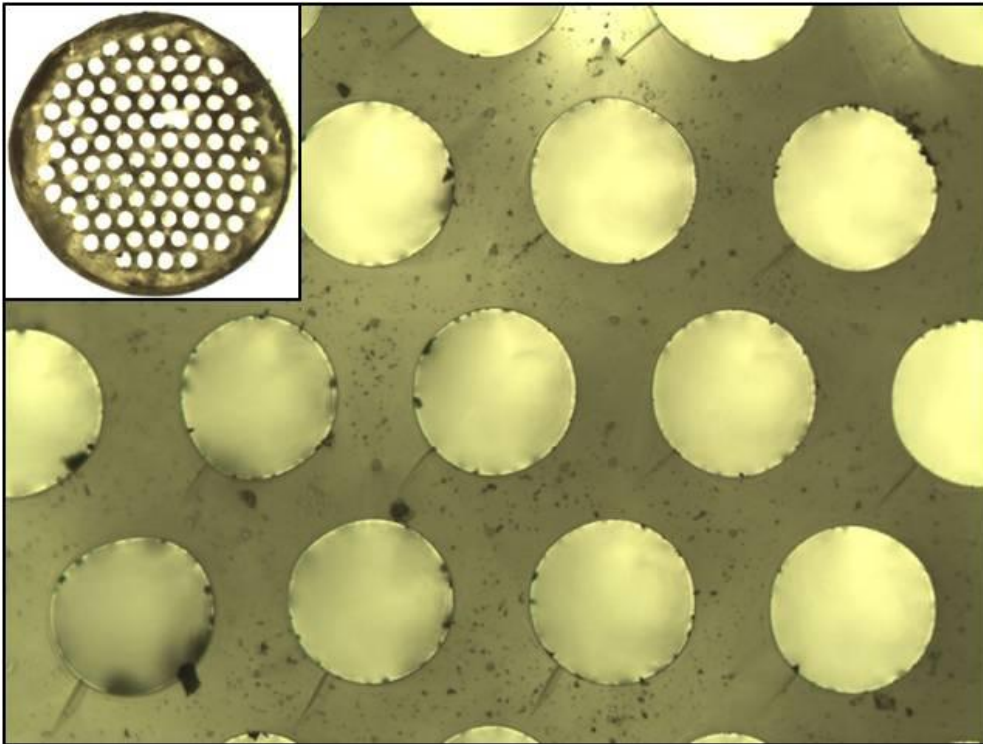
Figure 27: Microscopic view of structure A4 thin – Thick-walled round structure with round single hollow glass fibers without interspaces but with outer glass shell

Five samples were tested concerning their burst pressure. The results are shown in Table 15. The maximum burst pressure value of 56 MPa is marked in red. Compared to structure A4 thick, which is identical, except the additional interspaces and the larger dimension, the highest measured burst pressure value is two times higher at structure A4 thin. The minimum burst pressure is about ten MPa higher than at the previously tested structure.

The increased burst pressure values of structure A4 thin demonstrate the negative influence of interspaces between the single fibers on the strength of the structure. A statement concerning the influence of the decreased dimension of structure A4 thin cannot be given at this time.

Table 15: Burst pressure test results of structure A4 thin – Thick-walled round structure with round single hollow glass fibers without interspaces but with outer glass shell

Burst pressure [MPa] of sample 1-5				
45.1	56.0	40.9	36.4	38.3

In a further production line the interspaces between the single fibers are closed. A structure made of 89 single hollow glass fibers with an outer diameter of D_o=4.1 mm has been produced. A microscopic view of the structure is displayed in Figure 28. The small picture in the upper left corner displays the entire structure. In order to close the interspaces, the structure has been exposed to further heating during the production process. This method leads to a deformation of the single fibers which partially lost their round shape as visualized in Figure 28. Equal to structure A4 thin, the absence of interspaces between the single fibers implicates that the pressure acts only inside the fibers. Compared to structure A4 thin, structure M1 is larger.
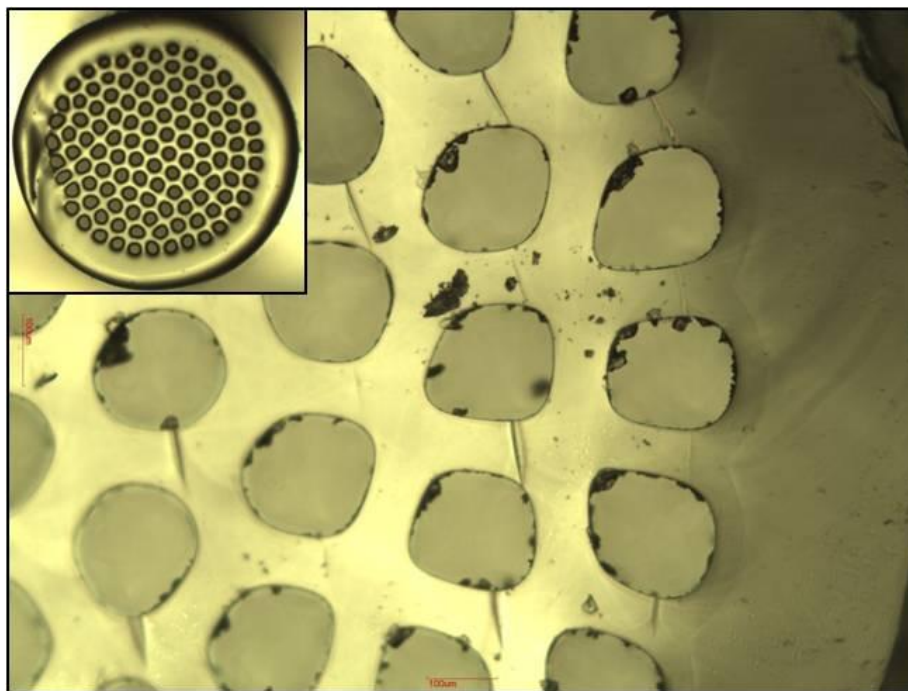
Figure 28: Microscopic view of structure M1 – Thick-walled round structure with round single hollow glass fibers without interspaces but with outer glass shell

Even structure M1 shows a massive appearance, reasoned by the lost storage volume by filling the interspaces. Although the not perfectly round shape of the single fibers, three tested structures of this kind showed high burst pressure values between 69.9 MPa and 87.6 MPa. The maximum measured burst pressure value is marked in red in Table 16.

Table 16: Burst pressure test results of structure M1 – Thick-walled round structures without interspaces but with outer glass shell

Burst pressure [MPa] of sample 1-3		
69.9	87.6	70.6

According to these results, the round shape of the single hollow glass fibers inside a structure seems not to be mandatory for reaching high burst pressure values. In order to obtain high storage capacity values, further bundling tests with hexagonal shaped single hollow glass fibers were examined.

A crucial problem of round single fibers is the wasted storage volume between the single fibers. Interspaces lead to an acting of the pressure between the fibers and to the outer glass shell. Filling the interspaces with glass leads to higher weight and at the same time lower storage volume, whereby the volumetric and gravimetric storage capacity is decreased. This problem is always present if round material needs to be packed closer together. For this purpose, round hollow glass fibers may not be the optimal basic component for reaching an optimal volumetric and gravimetric storage capacity.

5.3.4 Round Structures Made Of Hexagonal Hollow Glass Fibers With Outer Glass Shell

In order to increase the volumetric and gravimetric storage capacity of the glass structures, the shape of the single fibers became hexagonal. In this way the fibers can be arranged in honeycomb structure. In contrast to bundled round single fibers, which are arranged according to the principle of close packing spheres, no interspaces between the fibers occur. The produced structure A3 consists of 76 hexagonal single hollow glass fibers, has a length of 200 mm and an outer diameter of D_o=4.0 mm. A microscopic view of the structure is displayed in Figure 29. The small picture in the upper left corner displays the entire structure. The hexagonal single fibers are surrounded by a round outer glass shell, comparable to the structures with round single fibers. Reasoned by the hexagonal shape of the single fibers, structure A3 shows the highest free inner volume up to this point with a value of 1.61ml. Compared to the volume of the whole structure of 2.51ml, this value corresponds to a free

inner volume of 64%. Due to the fact that no interspaces between the single fibers occur, the pressure only acts to the inner surface of the single fibers.
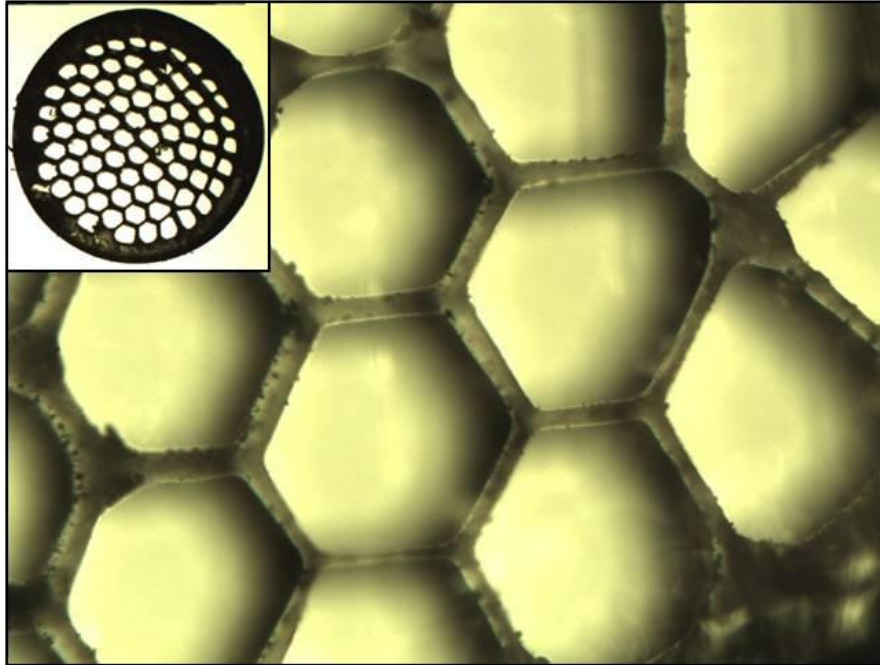
Figure 29: Microscopic view of structure A3 – Thin-walled hexagonal hollow glass structures with outer glass shell

Sixteen samples of structure A3 were tested to determine their burst pressure. The results are displayed in Table 17 and the maximum measured burst pressure value is marked in red. The large range between minimum and maximum burst pressure, which goes from 4.9 MPa to 37.6 MPa, can be explained with the handmade production of the structures. The individual production of any test sample by hand always leads to differences between the samples, which results in varying strength and burst pressure.

Regarding the free inner volume, this structure is most likely comparable to structure A2. The free inner volume of structure A3 is 4% higher than of structure A2. Although the highest measured burst pressure value of structure A3 is about four times higher than the maximum burst pressure value of structure A2, despite the normally more favorable round shaped fibers of structure A2. That result demonstrates the negative influence of acting pressure inside interspaces between the single fibers.

Table 17: Burst pressure test results of structure A3 – Thin-walled hexagonal hollow glass structures with outer glass shell

Burst pressure [MPa] of sample 1 – 16									
5.3	7.5	37.6	7.7	23.7	27.3	15.5	4.9	23.6	5.0
6.9	8.7	26.1	5.8	7.3	22.1				

5.4 Burst Pressure Test Results of Automatically Manufactured Glass Structures

In order to obtain more constant burst pressure values in one test series, another glass structure manufacturer with the option of automated production has been charged with the production of the upcoming structures. As a result of the automated production, the samples of a production line can be made with identical design and quality. Further advantages are variable production conditions like temperature, drawing speed or the possibility to vary the pressure inside the single fibers during the drawing process. In contrast to the previous manufacturer, an outer glass shell is not necessary anymore. This way, additional options for designing a structure will emerge.

First delivered samples (R40), which should demonstrate the possibilities for the design of new glass multi-structures, consist of 122 bundled hexagonal structures, each consisting of 1657 hexagonal single fibers. This way, the multi-structure, which is shown in Figure 30, consists of 202154 single hollow glass fibers, each with an outer diameter of $D_o = 40\mu m$. The 122 hexagonal fibers are surrounded by a massive outer glass shell. The emerging interspaces are filled with larger glass tubes. Consequently, the outer glass shell would be exposed to the inner pressure at pressure treatment. Furthermore, some leaks at the connection of the structures were detected. The outer diameter of the whole structure is 36.3mm and the weight is about 250g. Due to the fact that any structure inside the multi-structure is molten at one end separately, the leaks between them, as well as the larger glass tubes are open at both ends.
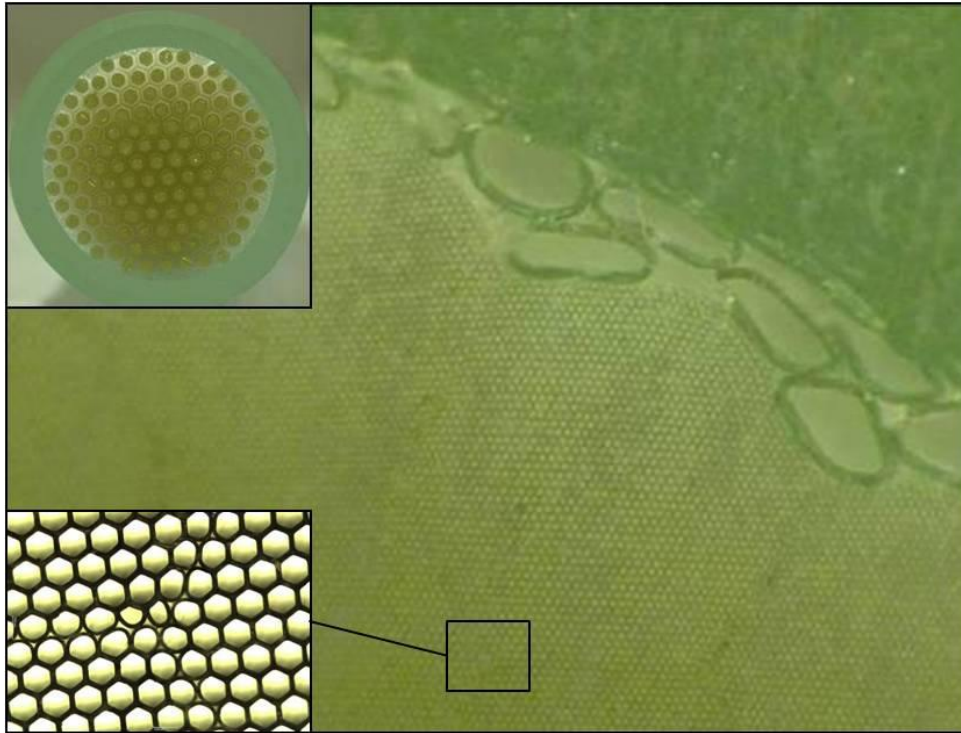
Figure 30: First automatically produced multi-structure fiber R40, containing 202154 hexagonal single fibers in 122 hexagonal structures, surrounded by an outer glass shell

Two samples of multi-structure R40 were examined concerning their burst pressure. To determine the burst pressure of such a structure, all leaks were closed with glue at one end. This way, the structure became gas-tight, but the pressure inside the leaks acts against the connection of the structures. The measured burst pressure values are 4.5 MPa and 5.1 MPa. In contrast to previously tested structures, the large multi-structures did not break into small powdery glass pieces. In both cases the glued end or the outer massive glass shell broke and ripped out several pieces of glass out of the multi-structure.

Table 18: Burst pressure test results of multi-structure R40 – Multi-structure containing 202154 hexagonal single fibers in 122 hexagonal structures, surrounded by an outer glass shell

Burst pressure [MPa] of sample 1 - 2	
4.5	5.1

The second delivered structure is called R100 and was constructed exactly like the first one, except that the outer diameter of the single fibers has been increased to 100µm. Consequently, the amount of single fibers decreased to 271 single fibers per structure. The multi-structure consists of 147 structures, which results in a total number of 39837 single hollow glass fibers in one multi-structure.

Equal to the previously tested comparable structure, existing leaks between the structures had to be closed for burst pressure examination glue for obtaining gas tightness. The measured burst pressure values of two tested samples are 3.0 MPa and 3.2 MPa, as demonstrated in Table 19. The error pattern is comparable to structure R40. Thereby, the structure consisting larger fibers and smaller wall thickness show lower burst pressure values. This behavior is equal to the previously examined hand-made structures.

Table 19: Burst pressure test results of multi-structure R100 – multi-structure containing 39837 hexagonal single fibers in 147 hexagonal structures, surrounded by an outer glass shell

Burst pressure [MPa] of sample 1 – 2	
3.0	3.2

Figure 31 displays several examples of structure R40 and R100 after burst pressure examination. The upper left picture shows the structure virtually in its whole form, only the molten and glued end is broken. The upper right picture shows a completely broken structure. As opposed to the previous tested multi fibers, the fragments of these structures are much larger. The bottom left picture shows the remaining structure inside the adapter. The bottom right picture displays a microscopic view of a structure R100. In this case only the outer glass shell and the larger glass tubes are broken. The inner hexagonal structure of small fibers is still intact.
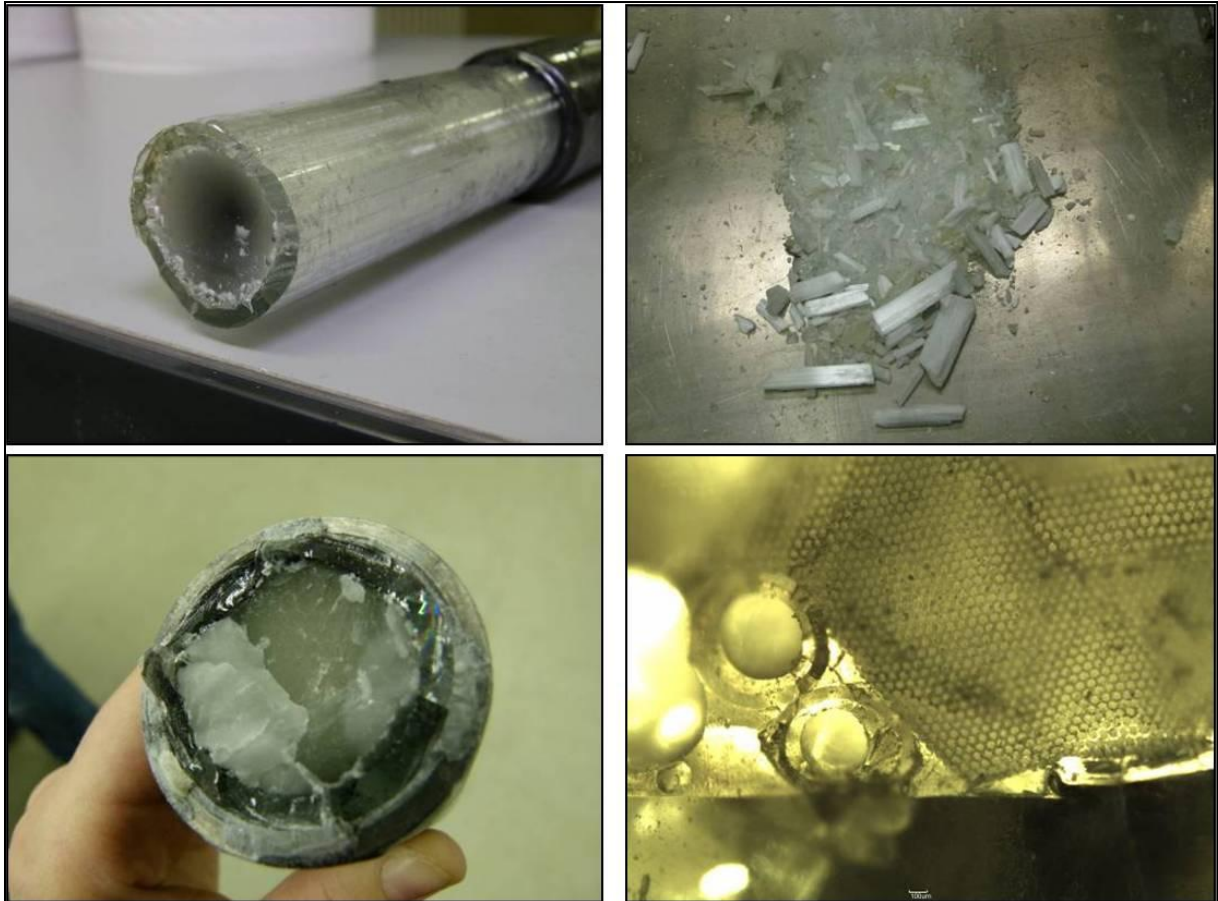
Figure 31: Failure pattern of the multi-structures R40 and R100 – Broken glued end (top left), large broken pieces (top right), after bursting remaining multi-structure in adapter (bottom left) and broken outer glass shell and glass tubes with intact fiber-structure (bottom right)

The next produced multi-structure B100 has a completely different design than all other samples up thus far. The shape has been changed from round to rectangular solid and the fibers of the multi-structure are not surrounded by an outer glass shell. This Multi-structure contains 342002 hexagonal single fibers in 1262 structures, which are bundled to the large rectangular glass block, displayed in Figure 32. The outer diameter of any single fiber is D_o=100µm. The multi-structure has an outer dimension of 80mm by 60mm and a length of 300mm. The weight of the multi-structure is 1270g.
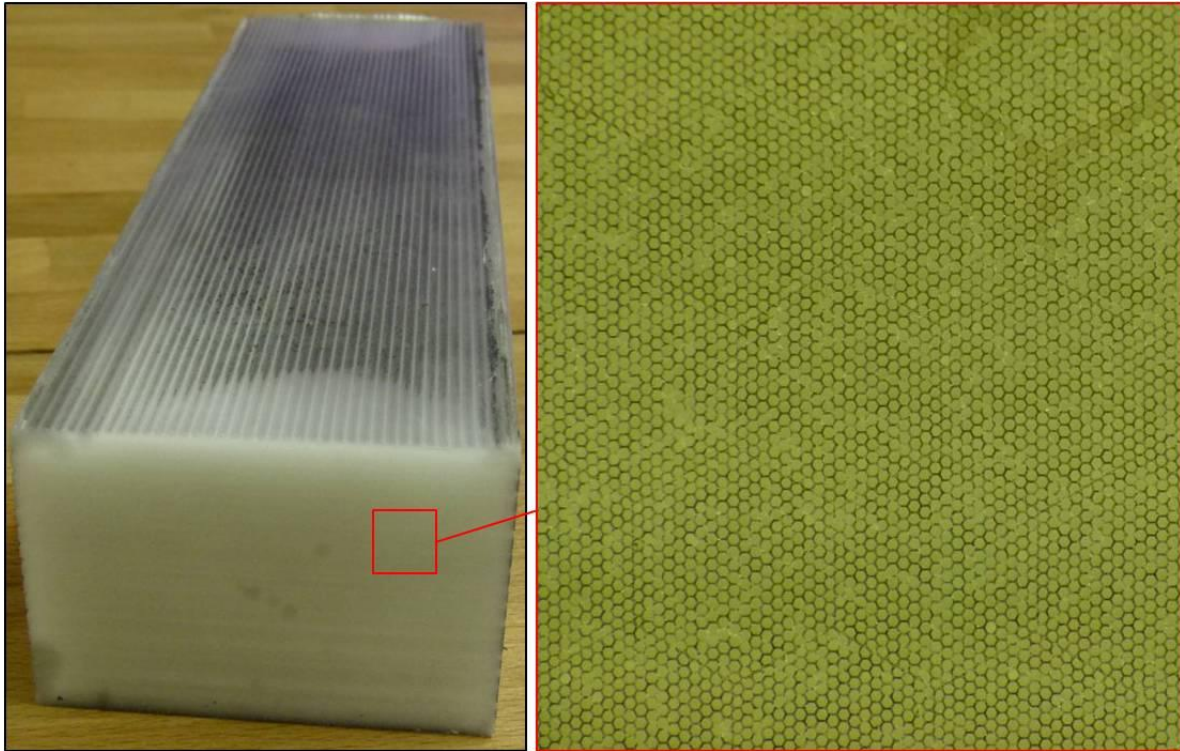
Figure 32: Rectangular solid multi-structure B100, containing 342002 hexagonal single fibers in 1262 structures, without outer glass shell

Similar to multi-structure R40 and R100, there are leaks between the bundled structures of multi-structure B100, which needed to be closed before burst pressure examination. The leaks are visualized with soap-solution in the upper left picture of Figure 33. The end, where the structures were closed by melting, was sealed with glue, comparable to multi-structure R40 and R100 for obtaining gas-tightness.

The missing protection shell also leads to already damaged single fibers at the outer side of the multi-structure. These damages were also closed with glue before pressure treatment.

One sample of multi-structure B100 was available for burst pressure examination. At an inner pressure of 1.95 MPa the molten ends of several structures broke, as illustrated in the upper right picture of Figure 33. The fact that all broken fibers are so close to each other leads to the conclusion that a part the glued end cracked and broke down the multi-fibers.

Following the first point, these damaged multi-fibers were closed with glue at the previously molten end. Additionally, the whole structure has been coated with glue, as demonstrated at the bottom left picture of Figure 33 and afterwards exposed to increasing inner pressure. At an inner pressure of 4 MPa a massive part of the structure including the outer coating broke.

Furthermore, the molten parts of the multi-fibers broke, as shown in the bottom right picture of Figure 33. The burst pressure test results are displayed in Table 20.
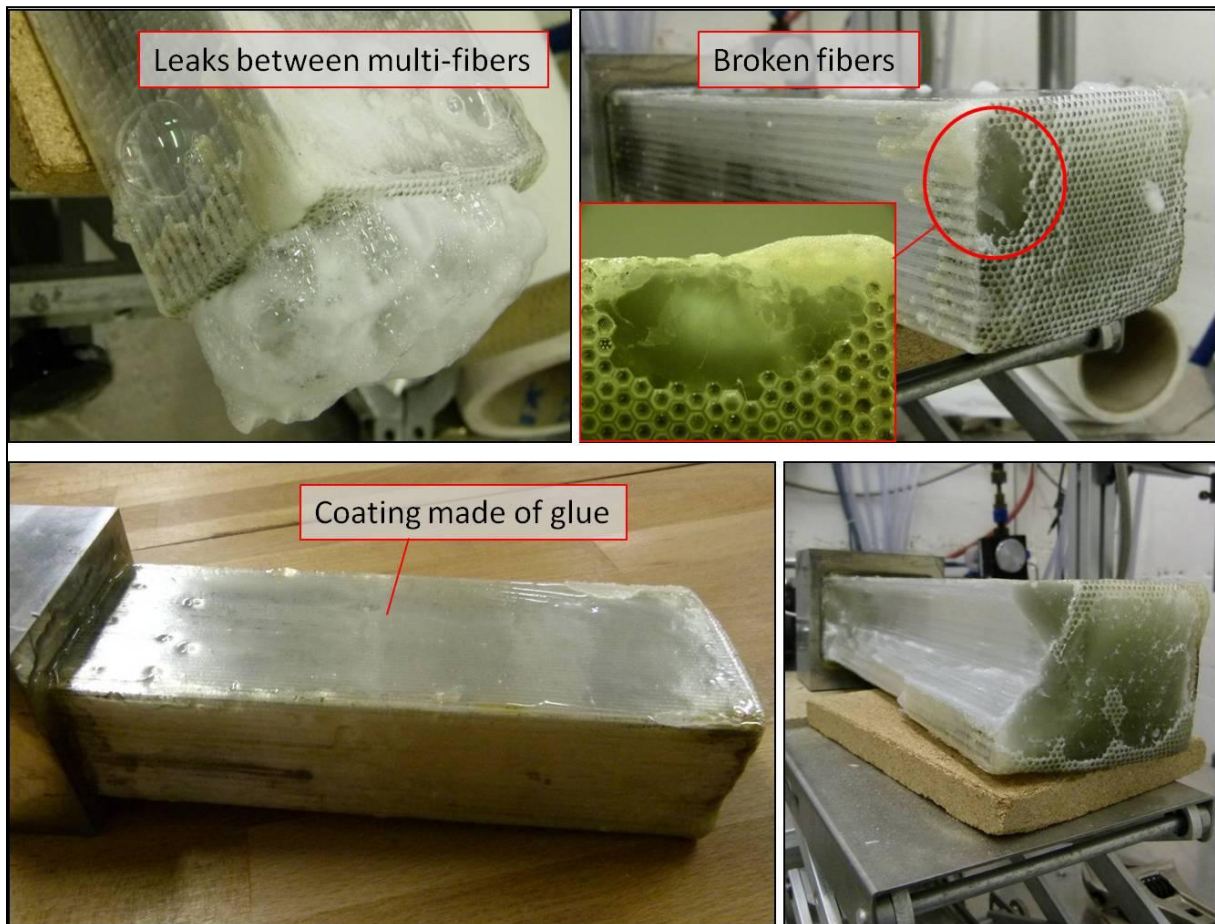
Figure 33: Rectangular solid multi-structure B100 with leaks between the single fibers (upper left picture), broken structures after burst pressure examination (upper right picture), outer protection shell made of glue (bottom left picture) and huge broken part of the multi-structure after second burst pressure test (bottom right picture)

Table 20: Burst pressure test results of multi-structure B100 – Multi-structure containing 342002 hexagonal single fibers in 1262 hexagonal structures, without an outer glass shell

Burst pressure [MPa] of sample 1 - 2	
1.95	4.0
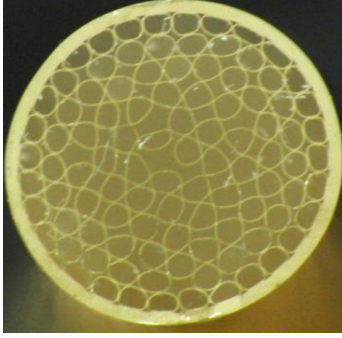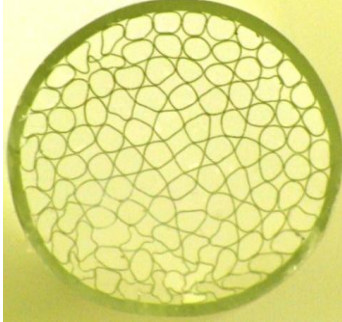
Despite the comparably low burst pressure values of the automatically produced structures R40, R100 and B100, that kind of production offered a lot of new promising possibilities in designing complex multi-structures or smaller structures. Thereby, the next step was the construction of different structures, which should be comparable to the previously tested hand-made samples.

The first trials of automatically produced structures result in four different kinds of structures, which are displayed in Table 21, beside their examined burst pressure values. The maximum burst pressure values of a test series are marked in red.

Sample 1, 2 and 3 were constructed by loosely packing thin-walled single fibers into a large glass shell before drawing. This results in randomly ordered single fibers inside the structure and large interspaces between them. The pressure load on the outer glass shell results in low maximum burst pressure values of 8.3 MPa of sample 1, 3.0 MPa of sample 2 and 7.1 MPa of sample 3.

In the case of sample 4, a vacuum has been applied inside the interspaces during the drawing process with the effect that the interspaces were closed. Furthermore, the shape of the basically round glass tubes changed during the drawing process to hexagonal single fibers. The massive outer glass shell also changed its shape, as demonstrated in the corresponding picture in Table 21. Due to the fact that round shaped pressure vessels facilitate a homogeneous stress distribution, the shape of sample 4 is unsuitable for withstanding high inner pressure. This result is proven by the low measured maximum burst pressure value of 3.9 MPa, despite the closed interspaces between the single fibers.

Table 21: Burst pressure test results of the first automatically produced structures

Sample No.		Burst pressure [MPa]					
1		8.3	3.9				
2		1.7	2.6	3.0			
3		1.2	7.1	3.5	1.0	0.7	
4		3.2	2.8	3.5	3.1	3.9	3.7

For constructing further test samples, smaller single fibers were packed closer to prevent occurring interspaces between the single fibers, comparable to structure A4thin. The resulting structures and their measured burst pressure values are discussed in the following sub-chapters.

5.4.1 Round Structures Made Of Round Hollow Glass Fibers Without Interspaces And With Outer Glass Shell

The automatically produced structure 399-3313-Acontains nearly round single hollow glass fibers and is surrounded by a massive outer glass shell, as displayed in Figure 34,. It has an outer diameter of D_o=3mm and an length of 200 mm. There are no interspaces between the single fibers, whereby the pressure only acts inside the single fibers and not directly on the outer glass shell. The imperfectly round shape of the single fibers and the massive outer glass shell allows for the comparison of the hand-made structure M1, which showed the highest measured burst pressure values, thus far. Compared to structure M1, structure 399-3313-A contains more smaller, single fibers. Equal to the previously produced samples, one end is closed by melting.
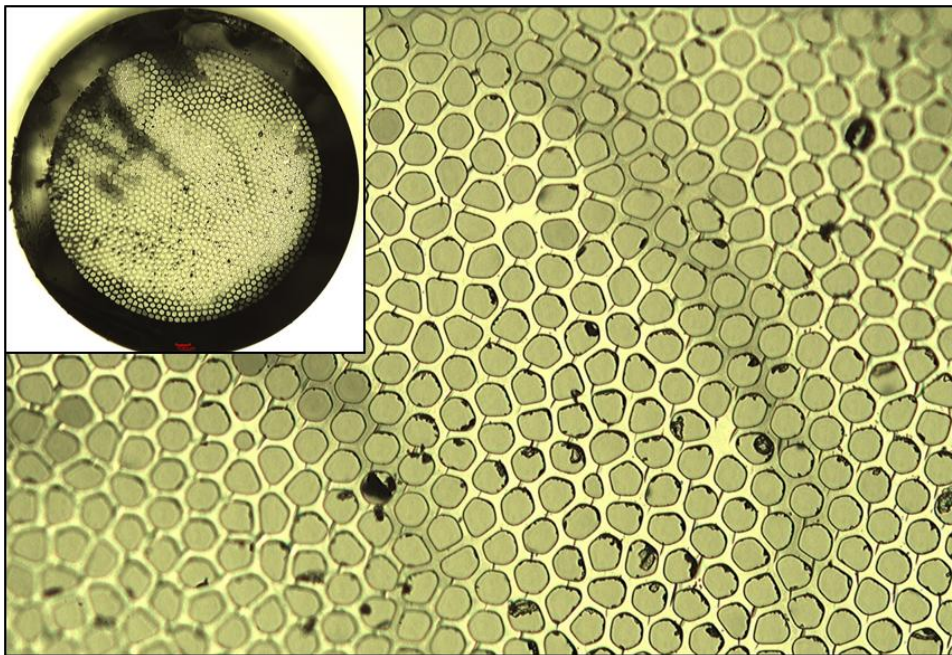
Figure 34: Microscopic view of structure 399-3313-A – Nearly round single fibers without interspaces and with massive outer glass shell

The burst pressure value of 30 samples of structure 399-3313-A was determined and is shown in Table 22. The lowest measured burst pressure is 27.3 MPa. The maximum burst pressure value of the test series is 89.8 MPa and marked in red. This structure shows the highest measured burst pressure value, thus far.

Table 22: Burst pressure test results of structure 399-3313-A - Nearly round single fibers without interspaces and with massive outer glass shell

Burst pressure [MPa] of sample 1-30									
50.9	71.5	82.4	27.3	43.7	51.6	62.9	73.2	44.9	44.0
39.4	67.8	59.3	29.1	42.3	40.8	31.3	60.4	89.8	56.0
76.5	82.4	59.6	52.9	36.3	56.8	70.1	65.6	41.2	34.4

5.4.2 Hexagonal Structures Made Of Hexagonal Hollow Glass Fibers Without Outer Glass Shell

The next step was a more consistent configuration of the single fibers inside the structure. The following produced structure 3574a consists of 3367 hexagonal shaped single fibers, each with an inner diameter of D_i= 37µm. The structure has an outer diameter of D_o=2.9mm and a length of 200mm. One end is closed by melting. The hexagonal shape of the single fibers leads to the absence of any kind of interspaces between the single fibers. The walls between the single fibers are thicker than most of the previously tested structures but, in contrast, there is no outer glass shell surrounding the single fibers. Due to this fact, the structure has an increased inner free volume for gas storage of 60%. Furthermore, the outer shape of the structure could change to hexagonal. Beside the lower weight and higher volumetric and gravimetric storage capacities, the hexagonal outer shape allows further bundling of the structure to multi-structures, comparable to the structures R40, R100 and B100. A further effect of the nonexistent outer glass shell is that merely the single fibers pose the applied inner pressure.
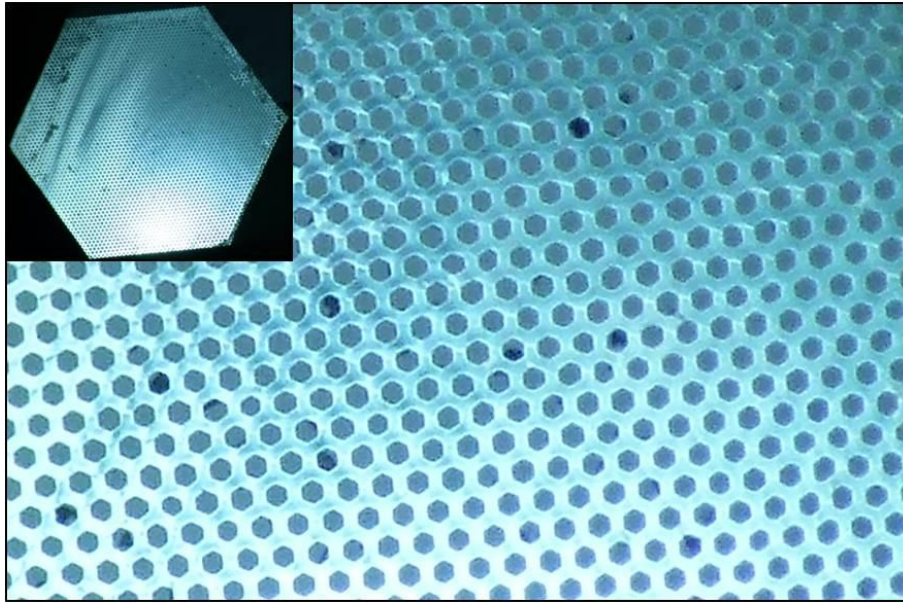
Figure 35: Microscopic view of structure 3574a – Hexagonal single fibers without outer glass shell

30 samples of structure 3574a were tested concerning their burst pressure. The results are displayed in Table 23 and the maximum measured burst pressure value is marked in red. Due to the fact that the hexagonal shape of the single fibers is not optimal for stress distribution during pressure treatment, and that there is no outer glass shell surrounding the single fibers, the highest measured burst pressure value of 50.3 MPa is lower than of comparable massive structures with round shaped single fibers or a massive outer glass shell like structure 399-3313-A. The lowest measured burst pressure value is 27.8 MPa.

Table 23: Burst pressure test results of structure 3574a – Hexagonal single fibers without outer glass shell

Burst pressure [MPa] of sample 1-30									
27.8	40.6	37.7	50.3	29.8	43.8	40.2	38.8	41.7	30.4
32.6	29.9	38.7	38.8	35.2	46.7	39.4	47.8	35.3	37.8
28.5	39.1	35.9	28.7	30.9	49.2	48.1	39.4	28.3	49.8

5.4.3 Round Structures Made Of Hexagonal Hollow Glass Fibers With Outer Glass Shell

Surrounding hexagonal single fibers with an outer glass shell results in the following round-shaped structure 399-3312-A, which is shown in Figure 36. The structure has an outer diameter of D_o=2.9mm and a length of 200mm. Equal to the previously produced structures, one end is closed by melting. Although the single fiber walls are thinner than at structure 3574a, the thick walled outer glass shell makes the multi-structure large. The hexagonal single fibers in combination with the massive outer glass shell allows for a comparison with hand-made structure A3.
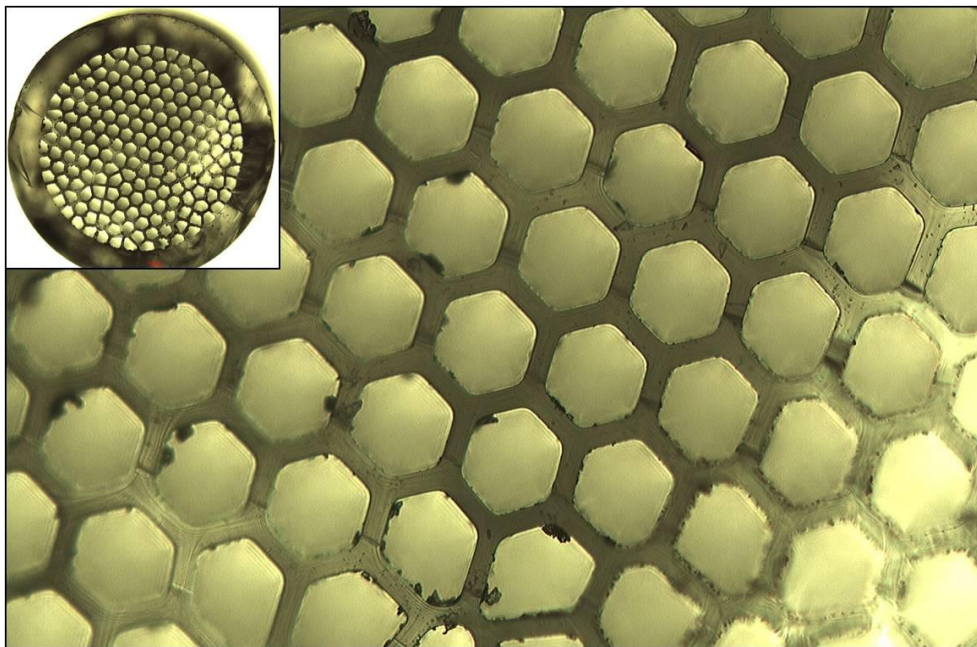
Figure 36: Microscopic view of structure 399-3312-A - Hexagonal single fibers with outer glass shell

Despite the similarities with structure A3, the maximum measured burst pressure value is about three times higher at the automatically produced structure 399-3312-A. The burst pressure test results of seven tested samples of structure 399-3312-A are shown in Table 24. The maximum measured burst pressure value of 98.6 MPa is marked in red. These are the highest measured burst pressure values up to this point, despite the comparably low wall thickness of the single fibers and their hexagonal shape. The lowest measured burst pressure value is 51.

Table 24: Burst pressure test results of structure 399-3312-A - Hexagonal single fibers with outer glass shell

Burst pressure [MPa] of sample 1-7						
51.0	87.7	82.2	98.6	92.6	52.9	76.4

In a further production line structure 399-3314-A with a thinner outer glass shell was produced. The outer glass shell shows an imperfectly round shape and the shape of the single fibers is mainly pentagonal. The structure has an outer diameter of about D_o=2.9mm and a length of 200mm. It consists of 90 single fibers, each with an inner diameter of about 270µm and an outer diameter of about 340µm. The small wall thickness results in a free inner storage volume of 60%.
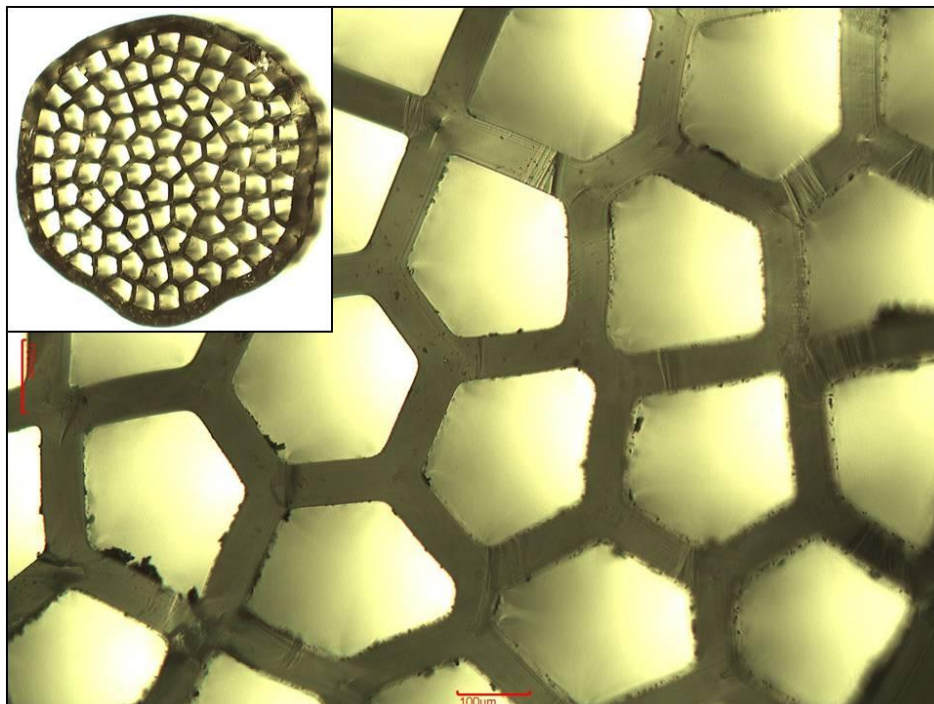
Figure 37: Microscopic view of structure 399-3314-A - Polygonal single fibers with outer glass shell

33 samples of structure 399-3314-A were tested concerning their burst pressure. The results are displayed in Table 23 and the maximum measured burst pressure value is marked in red. Compared to structure 399-3312-A, the highest measured burst pressure value is with 27.6 MPa about four times smaller. This may be reasoned by the larger size of the single fibers, as well as the thinner outer glass shell and the different shape of the single fibers and the outer shell.

Table 25: Burst pressure test results of structure 399-3314-A - Polygonal single fibers with outer glass shell

Burst pressure [MPa] of sample 1-33									
4.9	24.8	23.9	22.4	6.8	27.6	25.4	23.9	25.9	26.4
25.2	14.1	25.1	25.6	18.5	23.5	23.5	24.6	26.0	25.8
25.5	25.7	18.2	19.3	25.0	22.4	24.4	24.3	11.4	24.7
25.2	23.7	22.7							

5.4.4 Hexagonal Structures Made Of Thin-Walled Hexagonal Hollow Glass Fibers Without Outer Glass Shell

In a further step, the free inner volume of the structure has been increased by using thin-walled hexagonal single fibers for creating structure 399-3315-A, which is shown in Figure 38. The abandonment of an outer glass shell allows a hexagonal outer shape of the structure, which has an outer diameter of D_o=2.9mm and a length of 200mm. It consists of 469 hexagonal single fibers with an inner diameter of 100µm flat-to-flat and an outer diameter of 125µm flat-to-flat, which are ordered in honeycomb way. The free inner volume of the structure conforms to 64% of the structure's outer volume. One end of the structure is closed by melting, equal to the previously produced structures.
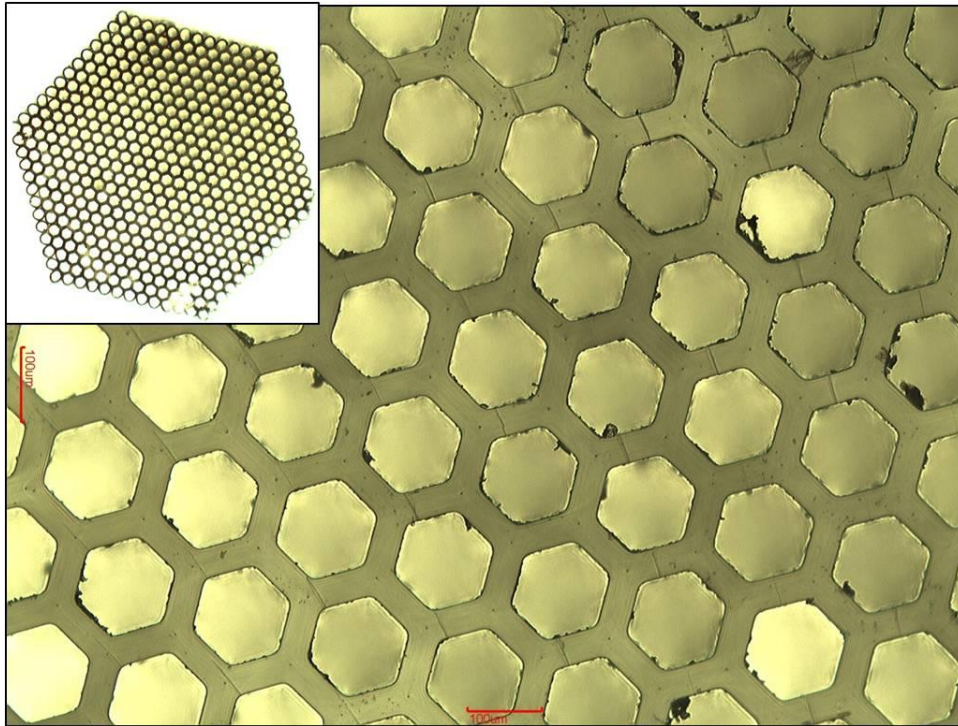
Figure 38: Microscopic view of structure 399-3315-A – Hexagonal single fibers without outer glass shell

Eight samples of structure 399-3315-A were tested concerning their burst pressure. The results are shown in Table 26 and the highest measured burst pressure value of 34.6MPa is marked in red. The lowest measured burst pressure value is 21.9MPa, whereby the difference of minimum and maximum measured burst pressure value is comparably low.

Table 26: Burst pressure test results of structure 399-3315-A – Hexagonal single fibers without outer glass shell

Burst pressure [MPa] of sample 1-8							
24.4	21.9	24.6	34.6	23.0	26.3	23.1	23.9

5.4.5 Hexagonal Structures Made Of Hexagonal Single Hollow Glass Fibers And Solid Fibers At The Outer Corners Of The Structure

In order to obtain high volumetric and gravimetric storage capacities, the massive outer glass shell is obstructive. Furthermore, the resulting round outer shape of the structure prevents effective further bundling to multi-structures.

Nevertheless, the outer glass shell poses an effective protection against damage during transportation and handling. At test series with samples without outer glass shell, a high number of damaged samples was observable, as shown in Figure 39. Especially the single fibers at the outer corners were frequently damaged.
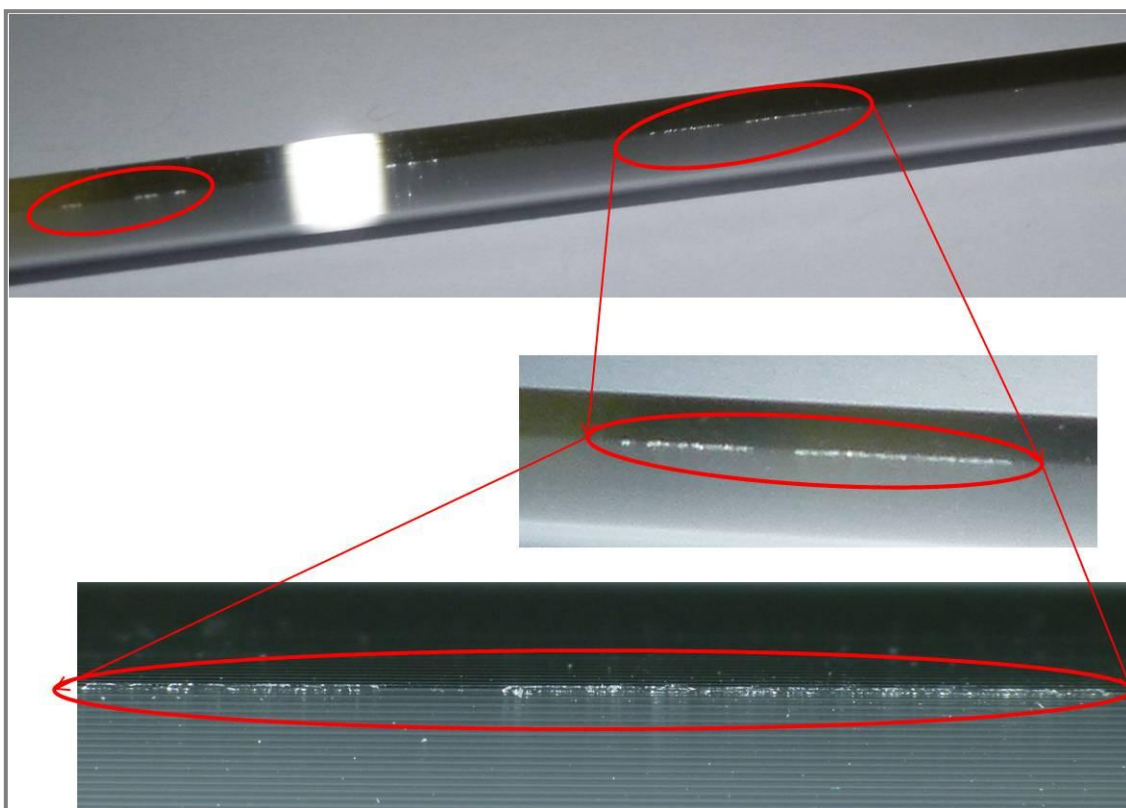
Figure 39: Broken fibers at the corners of the structures after delivery

For protecting these outer single fibers against damage, different structures were produced with solid fibers instead of hollow glass fibers at the outer corners different amounts of solid fibers were tested, from one single solid fiber to eleven solid glass fibers at the corner. Afterwards the burst pressure value of these test series was determined.

Structure 3837 replaces the single fiber at the outer corners with solid material, whereby the amount of damaged samples could be reduced, as demonstrated in Figure 40. The structure has an outer diameter of D_o=3.3mm flat-to-flat. To determine the influence of the length of the structures on the burst pressure, test samples with 200mm length and 300mm were tested. The structure consists of 3361 single hollow glass fibers with nearly hexagonal shape and six round solid fibers at the corners. The fibers are ordered in honeycomb way and one end of the structure is closed by melting. The free inner volume for gas storage is 48% of the volume of the whole structure.
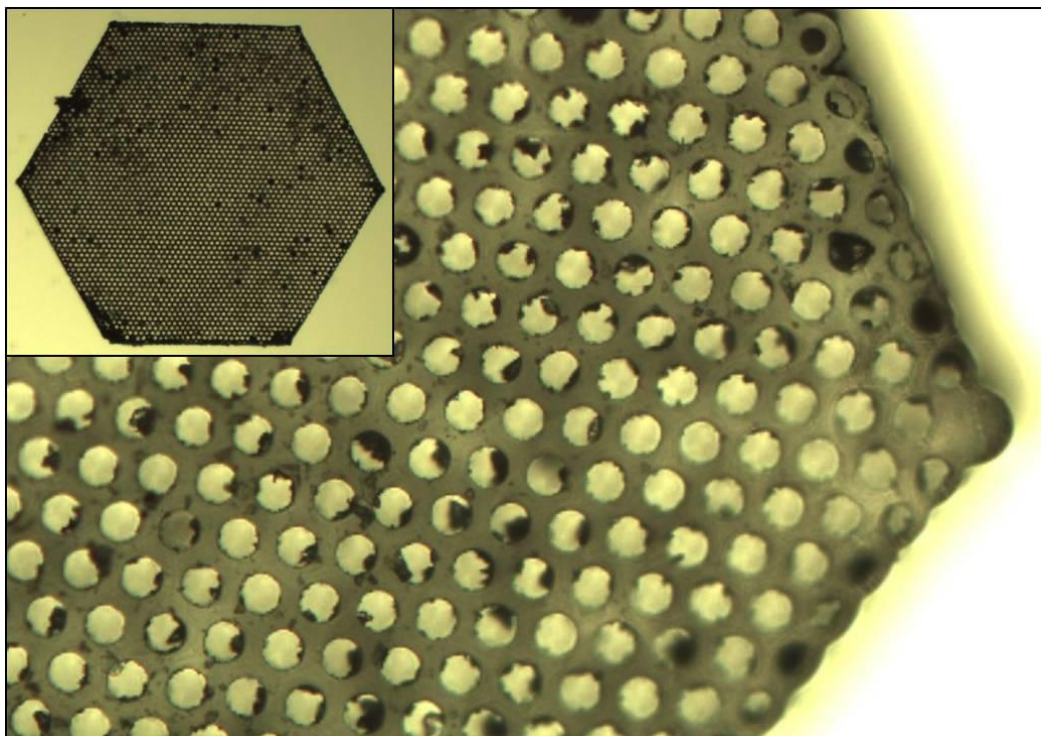
Figure 40: Microscopic view of structure 3837 – Hexagonal single fibers with one solid fiber at each outer corner of the structure

30 samples of structure 3837 with a length of 200mm and 30 samples with a length of 300mm were undergone some burst pressure tests. The results are shown in Table 27 and Table 28. The highest measured burst pressure values are marked in red. Thereby, structure 3837 with a length of 200mm shows with 89.1 MPa the highest measured burst pressure value of all tested samples without outer glass shell, up to this point. The maximum burst pressure value of the test series with a length of 300mm is with 77.0MPa lower than of the shorter samples. Also the minimum burst pressure value at the 300mm samples is with 11.1MPa about three times lower than at the 200mm samples.

Table 27: Burst pressure test results of structure 3837 200 – Hexagonal single fibers with one solid fiber at each outer corner of the structure and a length of 200mm

Burst pressure [MPa] of sample 1-30									
75.9	81.0	49.9	58.0	73.4	81.0	75.5	54.6	56.1	86.6
66.6	52.4	75.2	57.0	88.3	89.1	60.6	50.9	60.5	71.2
59.0	67.1	36.1	79.2	62.0	76.4	51.7	70.0	51.4	73.9

Table 28: Burst pressure test results of structure 3837 300 – Hexagonal single fibers with one solid fiber at each outer corner of the structure and a length of 300mm

Burst pressure [MPa] of sample 1-30									
51.5	77.0	57.3	63.6	11.1	55.8	36.4	62.7	62.0	36.8
49.7	57.9	61.1	67.5	57.5	69.1	66.0	42.4	64.8	63.7
72.6	46.7	43.6	65.8	73.7	36.7	44.3	43.4	51.4	57.4

A further test series deals with identical structures to 3837, but with eleven solid fibers at each outer corner for increasing the protection of the hollow glass fibers. The corresponding structure 3843 is demonstrated in Figure 41 and also produced in 200mm and 300mm length. The outer diameter of the structure is D_o=3.3mm. Due to the fact that 60 additional single fibers are replaced by solid fibers, the structure consists of 3301hexagonal single hollow glass fibers. The reduced amount of hollow glass fibers reduces the free inner volume to 46%. One end of the structure is closed by melting. The better protection by the solid fibers at the corners results in a smaller amount of samples which were damaged during transportation.
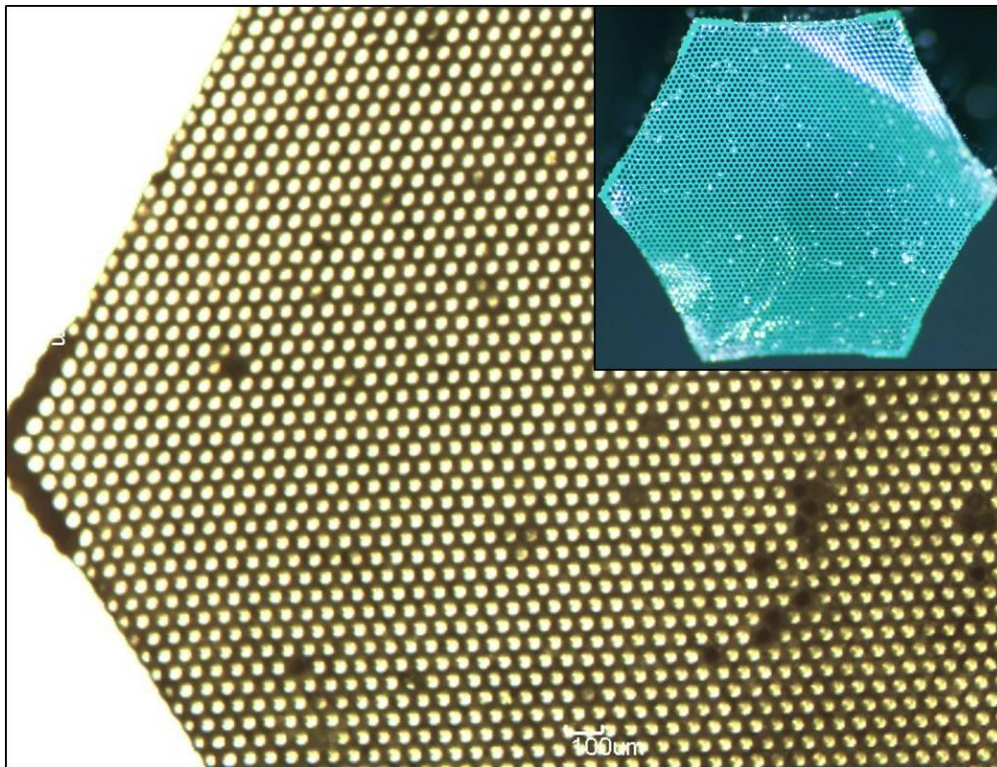
Figure 41: Microscopic view of structure 3843 - Hexagonal single fibers with eleven solid fibers at each outer corner of the structure

30 samples of structure 3843 with a length of 200mm (Table 29) and 32 samples with a length of 300mm (Table 30) were tested concerning their burst pressure value. The highest burst pressure value of 77.0 MPa has been determined at a sample with a length of 300mm. The other samples of the same test series show much lower burst pressure values of maximal 47.8MPa. Thus, the average burst pressure value of this test series is 37.1MPa, about 50% lower than the maximum value. The maximum value at the shorter samples is 51.9MPa. The difference of minimum and maximum burst pressure value is much smaller in this test series. Due to that fact, the average burst pressure value of all tested samples of the test series is with 40.1 MPa higher than the 300mm samples, despite the lower maximum value.

Despite the higher protection of the hollow glass fibers by using eleven solid fibers at each corner of the structure, the maximum, as well as the average burst pressure value is lower than structure 3837. Possibly the larger amount of solid fibers prevents a consistent strain of the structure, whereby higher stress inside the material may occur. Further examinations concerning stress and strain in the material by using FEM simulation will be discussed in chapter 5.6 "Results Of Stress And Expansion Modeling Using FEM".

Table 29: Burst pressure test results of structure 3843 200 - Hexagonal single fibers with eleven solid fibers at each outer corner of the structure and a length of 200mm

Burst pressure [MPa] of sample 1-30									
45.8	38.5	33.5	35.0	40.8	48.3	30.9	37.8	38.2	45.7
31.2	44.7	40.7	40.8	51.9	34.8	50.8	40.6	43.2	38.1
38.9	35.8	31.6	42.7	40.8	37.9	32.0	48.5	38.8	44.5

Table 30: Burst pressure test results of structure 3843 300 - Hexagonal single fibers with eleven solid fibers at each outer corner of the structure and a length of 300mm

Burst pressure [MPa] of sample 1-32									
35.7	33.9	47.3	43.5	30.9	38.9	36.5	36.5	27.6	38.0
34.8	32.8	40.0	37.3	70.8	32.7	29.7	36.5	32.8	36.9
29.8	40.4	47.8	38.4	36.5	33.6	35.4	41.3	35.9	27.1
35.5	32.0								

The test series of structure 3837 and structure 3843 gives some indication of the influence of solid fibers at the outer corners of the structure. The usage of eleven solid fibers has a negative influence on the burst pressure in comparison to the test series with only one solid fiber per corner, which showed the highest measured burst pressure values at samples without outer glass shell, thus far.

Additionally, the comparison of identical samples with varying length demonstrate a degradation of the burst pressure values with increasing length. A possible reason for that phenomenon can be given by Griffith's theory of lower probability of strength decreasing defects in smaller samples, which has been discussed in chapter 3.3.2 "Strength of Glass".

5.4.6 Hexagonal Structures Made Of Hexagonal Single Hollow Glass Fibers And Solid Fibers As Outer Fiber Layer

For a full protection of the outer hollow glass fibers, different test series with samples were examined where all outer single hollow glass fibers were replaced by solid fibers. These test series with varying properties of the samples are discussed in this subchapter. Thus, varying lengths of the samples will be regarded in addition to other properties such as varying wall thickness of the single fibers or the difference of closing one end of the structure by melting or with glue.

The first structure with an outer layer of solid single glass fibers is called 3575a and is equal to the previously tested structure 3574a, with the only difference that the outer fiber row is completely made of solid fibers. Regarding the solid single fibers, which replace hollow glass fibers, the structure consists of 3169 single hollow glass fibers, each with an inner diameter of 33µm. It has a length of 200mm and is closed by melting at one end. The outer diameter of the structure in D_o=2.9mm flat-to-flat. The free inner volume conforms to 42%. A microscopic view is demonstrated in the large picture of Figure 42, the small picture in the upper left corner shows the entire structure.
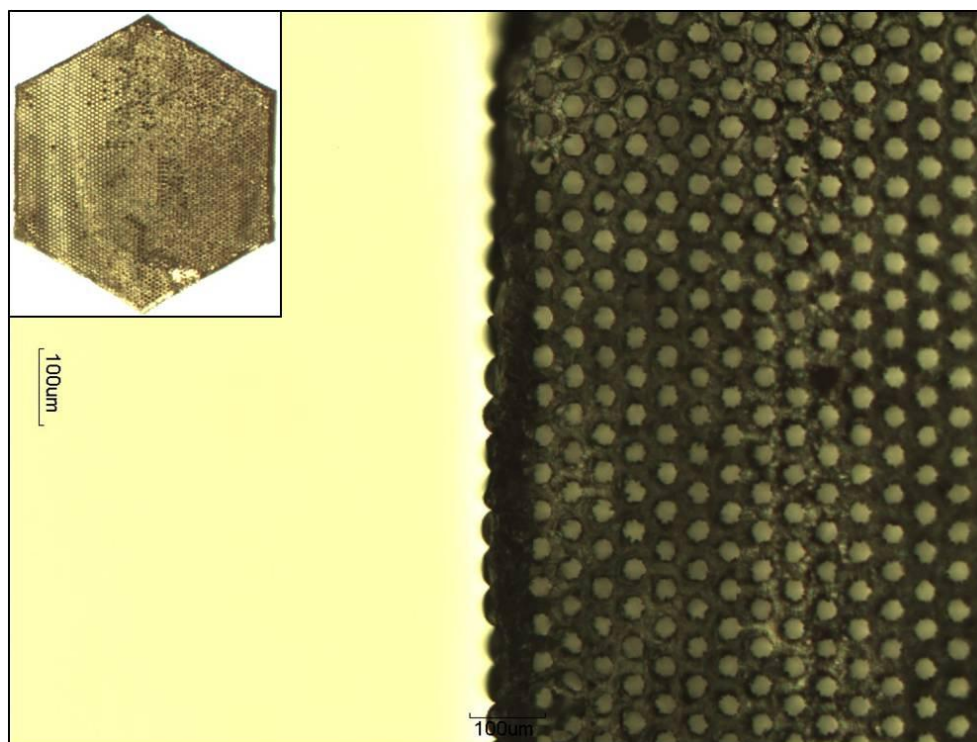
Figure 42: Microscopic view of structure 3575a - Hexagonal single fibers with solid fibers as outer fiber layer

30 samples of structure 3575a were tested concerning their burst pressure. The results are shown in Table 31 and the maximum measured burst pressure value of 53.7MPa is marked in red. The highest measured burst pressure value is comparable to the value of 3574a (50.3MPa), whereby an influence of the outer solid fibers on the burst pressure value is not noticeable. Also the distribution of the burst pressure values of one test series is comparable at both structures. The average burst pressure of structure 3534a is 38.0MPa and the value of 3575 is 38.7MPa.

Table 31: Burst pressure test results of structure 3575a - Hexagonal single fibers with solid fibers as outer fiber layer

| Burst pressure [MPa] of sample 1-30									
31.7	31.5	40.6	39.7	35.5	37.1	40.8	39.8	29.8	37.0
41.8	37.6	37.9	43.4	39.3	46.6	53.7	36.2	29.3	41.9
35.5	38.2	35.3	41.6	46.6	40.1	39.0	38.9	34.5	41.1

A further production line with identical parameters to structure 3575 yields structure 3624-6, which is shown in Figure 43. This test series is the first one in a number of test series with stepwise changing parameters. In this way, the influence of parameters like the single fiber size, the outer diameter of the whole structure, as well as the length or the kind of closing the end of the structure on the burst pressure has to be examined. Structure 3624-6 consists of 3169 single hollow glass fibers surrounded from 198 solid glass fibers. The hollow glass fibers have an inner diameter of 33µm. The produced samples have an outer diameter of D_o=2.9mm flat-to-flat and a length of 200mm. The free inner volume conforms to 45% of the complete volume of the structure. Equal to the previously produced structures, one end of structure 3624-6 is closed by melting directly after production.
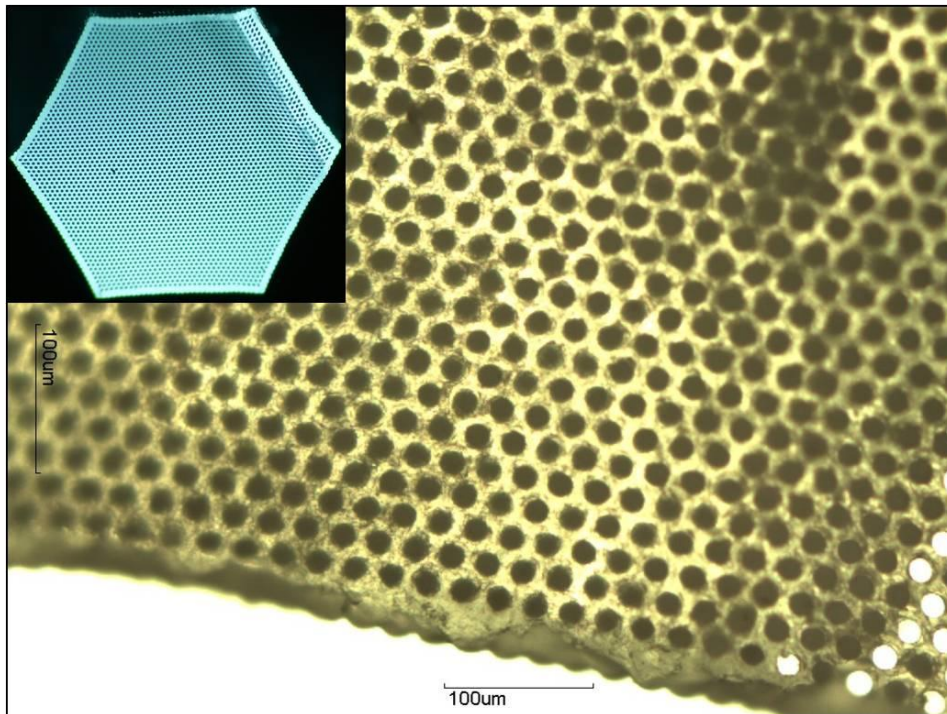
Figure 43: Microscopic view of structure 3624 6 – Thick-walled hexagonal single fibers with solid fibers as outer fiber layer

Thirty-one samples of structure 3624 6 were examined concerning their burst pressure. The results are shown in Table 32 and the highest measured value (75.9MPa) is marked in red. Compared to structure 3575 with identical parameters, the maximum burst pressure of structure 3624 6 is about 50% higher. Also the average value of all burst pressure values of the test series could be increased from 38.7MPa (3575) to 51.8MPa (3624 6).

Table 32: Burst pressure test results of structure 3624 6 – Thick-walled hexagonal single fibers with solid fibers as outer fiber layer

Burst pressure [MPa] of sample 1-31									
51.4	42.7	41.7	68.6	49.7	42.3	66.1	66.9	75.9	69.0
37.5	41.3	39.3	32.2	47.9	49.5	61.9	63.0	50.0	63.9
50.3	56.8	40.8	62.4	53.7	49.3	41.5	45.2	45.0	51.2
50.0									

In the following test series, the inner diameter of the single hollow glass fibers has been increased to 39µm and the wall thickness between these fibers has been reduced. Due to that fact, the free inner volume of structure 3624 7 could be increased to 60%. The amount of 3169 hollow glass fibers as well as the outer diameter of the structure of D_o=2.9mm and the length of 200mm is equal to structure 3624 6. A microscopic view of structure 3624 7 as well at a view of the whole structure is shown in Figure 44. The first test series of this structure has a molten end, comparable to the other produced samples up to this point.
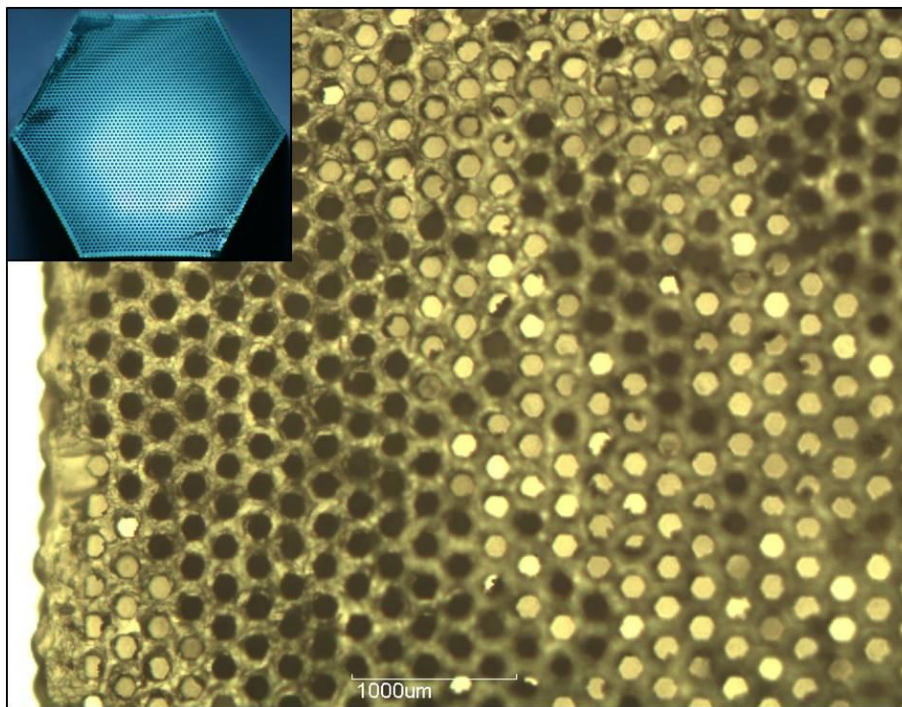
Figure 44: Microscopic view of structure 3624-7 – Hexagonal single fibers with more coalesced solid fibers as outer fiber layer

The highest measured burst pressure value of a test series of 31 samples of structure 3624 7 is 38.4MPa. All burst pressure values of the test series are shown in Table 33 and the maximum value is marked in red. The higher inner diameter of the single fibers and the corresponding higher free space result in a 50% lower maximum burst pressure value, compared to structure 3624 6 with only 45% free inner volume.

Table 33: Burst pressure test results of structure 3624 7 – Hexagonal single fibers with more coalesced solid fibers as outer fiber layer

Burst pressure [MPa] of sample 1-31									
25.6	19.9	18.8	18.6	23.5	26.7	20.4	24.3	13.6	18.6
16.3	26.6	25.3	28.3	27.2	30.2	37.5	25.6	27.7	31.2
22.4	38.4	34.3	35.0	29.2	29.4	24.8	35.5	30.5	33.0
33.3									

The following test series deal with samples of structure 3624 7, which were not closed by melting at one end. Therefore, samples with an original length of 300mm were cut to 200mm and 100mm. One end was closed with epoxy glue afterwards. These samples are labeled as 3624 A. 14 samples with a length of 200mm and 11 samples with a length of 100mmas well as 31 samples with the original length of 300mm were tested concerning their burst pressure value. The burst pressure values of the 300mm samples are shown in Table 34. The highest measured value of 39.5MPa is marked in red. The results of the 200mm samples are shown in Table 35 and the results of the shorter samples are displayed in Table 36. Similar to previously prepared tests with varying sample length, the highest measured value of the shorter 100mm samples is slightly higher than of the 200mm structures. In comparison to the samples with a length of 300mm the maximum burst pressure value is slightly decreased. A possible explanation of that fact is the manual cutting procedure. During this procedure, further defects could occur, whereby the burst pressure will be decreased. Compared to structure 3624 7 with molten end, the maximum burst pressure values of samples with glued end are nearly identical. Due to that fact, the influence of the kind of closing the end of the structure is negligible.

Table 34: Burst pressure test results of structure 3624 A 300 – Hexagonal single fibers with more coalesced solid fibers as outer fiber layer and a length of 300mm

Burst pressure [MPa] of sample 1-31									
29.3	22.9	32.4	28.8	29.1	29.9	30.2	27.8	23.0	27.7
31.9	36.6	27.3	26.8	28.5	39.5	31.6	24.4	28.1	14.6
18.7	29.1	37.7	18.3	24.5	28.9	30.1	29.7	28.0	33.1
33.9									

Table 35: Burst pressure test results of structure 3624 A 200 – Hexagonal single fibers with more coalesced solid fibers as outer fiber layer and a length of 200mm

Burst pressure [MPa] of sample 1-14									
31.5	34.7	36.7	30.8	36.6	29.0	27.7	37.0	34.0	31.3
34.6	33.1	31.9	24.5						

Table 36: Burst pressure test results of structure 3624 A 100 – Hexagonal single fibers with more coalesced solid fibers as outer fiber layer and a length of 100mm

Burst pressure [MPa] of sample 1-11									
29.5	30.0	17.1	19.6	23.9	25.6	27.4	30.5	18.3	37.2
38.1									

In a further test series, the wall thickness between the single hollow glass fibers has been increased. The inner diameter of the single fibers kept constant at 39µm, as well as the amount of 3169 single hollow glass fibers, surrounded from 198 solid fibers. Due to these properties, the outer diameter of the resulting structure 3624 8 has been increased from 2.9mm to 3.3mm. A microscopic view of the structure, as well as a view of the whole structure is displayed in Figure 45. The additional material results in a decreased free inner storage volume of 45%.
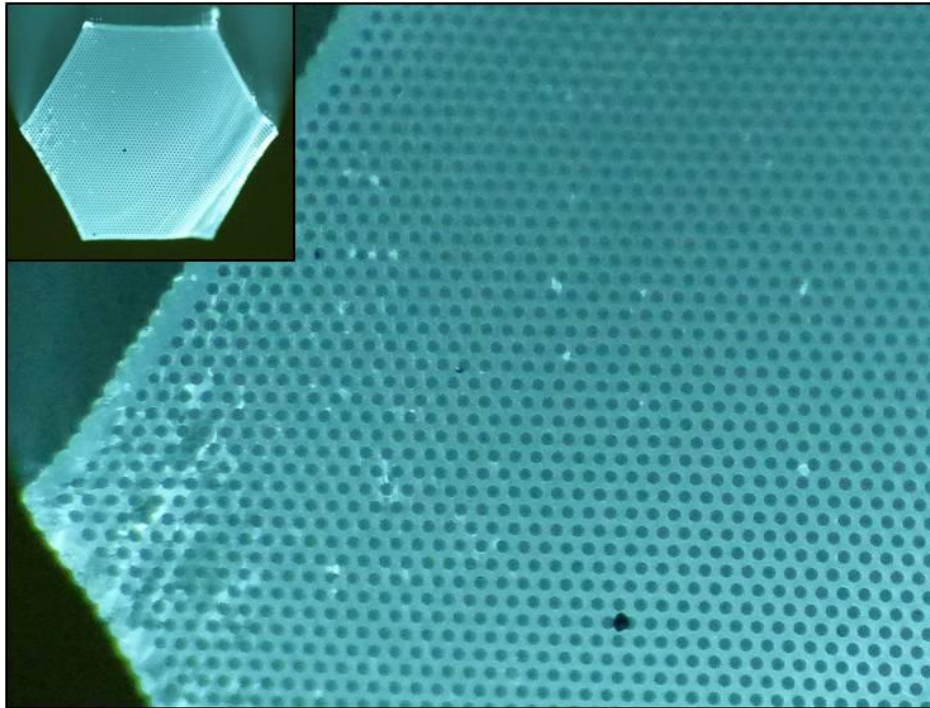
Figure 45: Microscopic view of structure 3624 8 – Hexagonal single fibers with solid fibers as outer fiber layer

The burst pressure of 27 samples of structure 3624 8 was examined and the results are displayed in Table 37. The highest measured burst pressure value is marked in red. Although the higher outer diameter of the structure, the maximum burst pressure value is comparable to structure 3624 6, which also has a free inner volume of 45%. Compared to structure 3624 7 with 60% free volume, the maximum burst pressure value is nearly doubled.

Table 37: Burst pressure test results of structure 3624 8 – Hexagonal single fibers with solid fibers as outer fiber layer

Burst pressure [MPa] of sample 1-27									
48.9	46.7	37.0	71.1	27.6	48.0	46.3	40.6	51.8	51.0
41.7	49.7	54.7	51.4	45.8	48.9	68.6	54.6	49.6	29.3
57.8	43.0	57.8	54.5	24.9	48.1	59.6			

A further production line of the same fiber showed single hollow glass fibers with varying inner diameter from 29µm to 39µm. As visible in the microscopic picture of structure 3624 9, , there is no continual arrangement of larger and smaller single fibers inside the structure but a random order of the differently dimensioned single fibers, as illustrated in Figure 46. The amount of 3169 single hollow glass fibers, as well as the 198 surrounding solid fibers and the outer diameter of the structure of D_o=3.3mm flat-to-flat is equal to structure 3624 8. Due to the presence of smaller single fibers as the only change in comparison to structure 3624 8, the free inner volume of the structure 3624 9 has to be lower than 45%. An exact value is not available. The structure 3624 9 has been produced in a length of 200mm and 300mm. One end has been closed by melting directly after production.
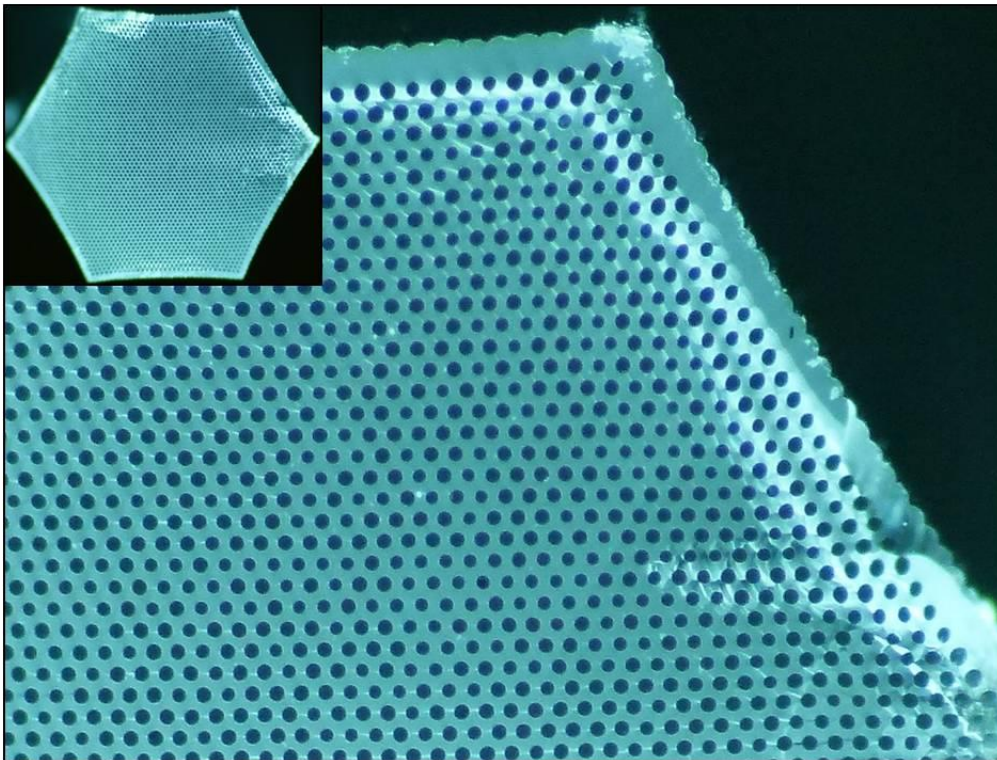
Figure 46: Microscopic view of structure 3624 9 – Thick-walled hexagonal single fibers with solid fibers as outer fiber layer

The results of 30 samples of structure 3624 9 with a length of 200mm, which were tested to determine their burst pressure, are displayed in Table 40. The results of 31 samples with a length of 300mm are shown in Table 41. In both cases the maximum burst pressure value is marked in red. The highest measured burst pressure value of the shorter samples is 46 MPa higher than at the comparable structure 3624 8, which is related to the smaller single fibers and the corresponding lower free inner volume. The maximum burst pressure value of 117.1 MPa is the highest measured burst pressure value of all structures, up to this point. The maximum burst pressure value of the 300mm samples is with 88.7MPa lower than at the shorter samples, but still the highest measured value of all tested samples with a length of 300mm. Related to the given free inner volume of 45%, this structure 3624 9 poses the best gravimetric storage capacity of all tested structures, up to this point. Due to the fact that the free inner volume seems to be lower than declared by the manufacturer, a validated statement concerning the storage capacity cannot be given.

Table 38: Burst pressure test results of structure 3624 9 200 – Hexagonal single fibers with solid fibers as outer fiber layer and a length of 200mm

Burst pressure [MPa] of sample 1-30									
66.0	46.2	80.7	43.8	91.1	51.9	66.6	44.2	117.1	66.0
86.9	103.6	63.9	109.2	99.7	51.6	62.6	63.2	95.1	54.5
92.6	66.2	42.7	42.4	109.4	42.6	47.3	39.3	68.0	50.1

Table 39: Burst pressure test results of structure 3624 9 300 – Hexagonal single fibers with solid fibers as outer fiber layer and a length of 300mm

Burst pressure [MPa] of sample 1-31									
40.8	41.9	62.7	59.6	55.2	55.3	72.2	61.3	76.9	48.1
68.9	70.9	36.1	78.5	44.0	46.7	47.4	77.1	41.2	51.6
37.5	38.1	39.9	37.5	76.7	88.0	59.1	41.8	43.0	63.7
88.7									

The samples of the following test series 3624 10 showed several kinds of defects on the surface of the structures. The structure has the same properties as structure 3624 8. It consists of 3169 single hollow glass fibers with an inner diameter of 39μm, surrounded from 198 solid fibers. The outer diameter of the structure is D_o=3.3mm. Resulting from these properties, the free inner volume corresponds to 45% of the volume of the whole structure. The samples have been produced in a length of 300mm and 600mm. Figure 47 shows a microscopic view of scratches in the left picture and broken out parts in the right picture, whereby the solid fibers, as well as several layers of hollows glass fibers behind them are damaged.
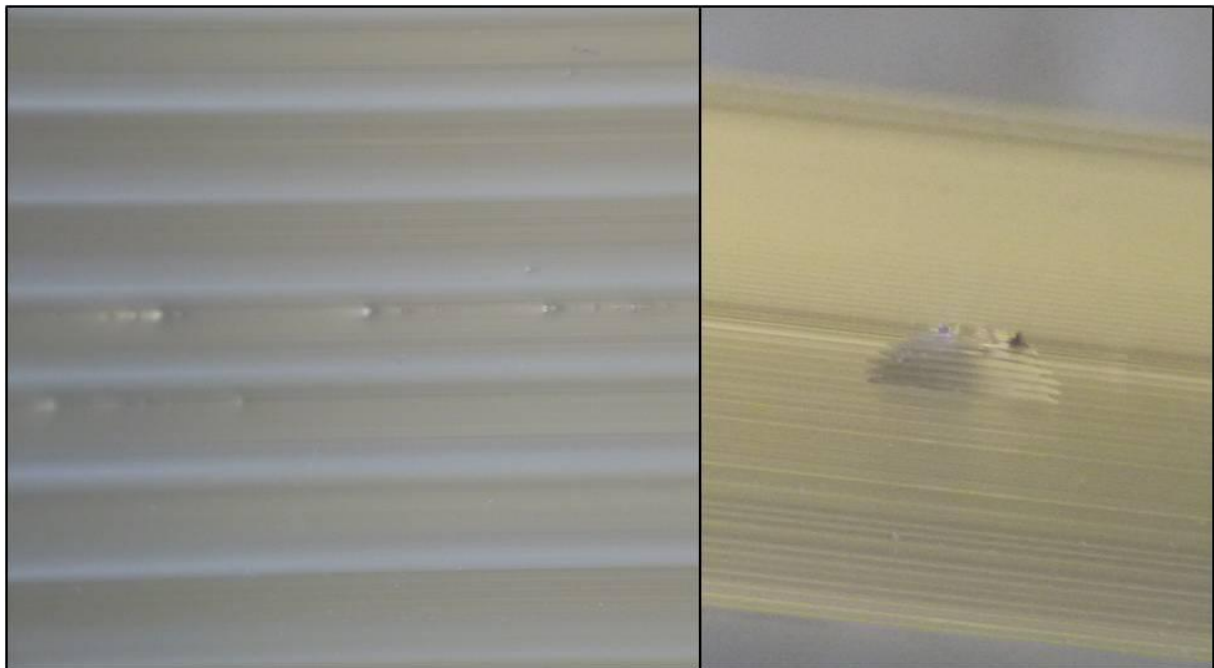
Figure 47: Microscopic view of the surface of structure 3624 10 – Defects on the surface (left) and damaged fibers (right)

29 samples of structure 3624 10 with a length of 300mm and 30 samples with a length of 600mm were tested concerning their burst pressure. Therefore, the damages at the surface were closed with epoxy glue for obtaining gas tightness. The results of the shorter samples are displayed in Table 40 and the results of the larger samples are shown in Table 41. The highest measured burst pressure values are marked in red. The maximum burst pressure value of the shorter samples is with 48.6MPa slightly higher than the maximum value of the

samples with a length of 600mm (44.2MPa). Compared to structure 3624 8, which has the same properties, the maximum burst pressure value is more than 20MPa lower at structure 3624 10. One explanation for this behavior is the higher length of the samples of structure 3624 10, but the defects are supposed to be the primary cause for the decreased burst pressure.

Table 40: Burst pressure test results of structure 3624 10 12" – Hexagonal single fibers with solid fibers as outer fiber layer

Burst pressure [MPa] of sample 1-29									
40.1	35.5	35.3	29.9	39.8	43.0	42.5	40.7	37.6	32.6
38.8	36.2	48.6	35.0	30.9	38.1	34.0	39.1	38.1	39.0
32.8	34.0	37.8	27.6	37.9	45.9	38.8	31.6	42.6	

Table 41: Burst pressure test results of structure 3624 10 24" – Hexagonal single fibers with solid fibers as outer fiber layer

Burst pressure [MPa] of sample 1-30									
37.8	31.4	29.2	35.1	34.2	26.4	37.5	32.7	43.2	25.6
32.2	36.7	42.9	38.4	36.3	36.5	36.9	24.7	25.0	44.2
38.6	26.4	34.7	38.5	42.0	32.1	37.8	23.6	23.5	34.1

For several other tests, which are not considered in this thesis, nine further production lines of sample 3624 8 have been produced over a time period of about one year. In order to ensure a constant quality of the different production lines, a burst pressure test series of every production line has been examined. Equal to structure 3624 8, the samples consist of 3169 single hollow glass fibers, which are surrounded from 198 solid fibers. The outer diameter of the samples is Do=3.3µm and the length is constant 300mm. The free inner volume is 45% of the whole structure's volume. The production lines are labeled as 3859 1 to 3859 9 and the burst pressure test results are displayed in Table 42. The highest measured burst pressure value of every production line is marked in red. The maximum burst pressure value of the production lines vary from 66.9MPa to 83.6 MPa. These values are comparable to the maximum burst pressure value of structure 3624 8 and demonstrate a constant quality as well as a good reproducibility of the samples.

Table 42: Burst pressure test results of 9 different production lines of structure 3859 - Hexagonal single fibers with solid fibers as outer fiber layer

Burst pressure [MPa] of production line 1									
43.5	71.5	36.8	42.8	64.4	59.3	56.4	56.1	61.1	32.4
47.9	29.7	29.3	34.2	54.6	35.2	65.4	74.6	62.5	44.9
79.2	43.8	61.2	55.0	63.2	39.2	38.1			
Burst pressure [MPa] of production line 2									
37.6	48.8	47.0	53.4	52.1	67.4	47.6	64.2	63.8	43.4
Burst pressure [MPa] of production line 3									
49.8	59.2	54.3	49.7	46.8	68.3	67.0	65.6	58.4	36.1
Burst pressure [MPa] of production line 4									
36.3	68.9	55.0	47.8	61.5	56.5	50.9	42.3	49.6	57.4
45.8	61.7	46.6	57.1						
Burst pressure [MPa] of production line 5									
54.3	49.5	63.9	51.3	46.8	59.2	57.2	66.9	63.2	60.2
59.8	51.2	58.6	49.0						
Burst pressure [MPa] of production line 6									
33.9	79.5	53.6	33.0	59.1	63.9	43.9	34.4	53.8	49.0
57.1	56.6								
Burst pressure [MPa] of production line 7									
63.2	38.0	48.0	52.6	53.3	42.5	64.6	80.6	69.6	35.7
83.6	56.2	42.1							
Burst pressure [MPa] of production line 8									
51.2	33.4	39.9	34.8	47.5	47.2	36.9	37.3	41.6	63.4
53.8	64.7	62.5	63.8	60.1	33.1	58.1	56.0	58.4	65.3
68.2	61.6	52.6	45.2	38.7	65.3	68.2	61.6	52.6	45.2
38.7									
Burst pressure [MPa] of production line 9									
54.2	36.4	40.6	55.0	31.9	29.2	75.0	71.2	47.6	29.9
61.9	44.7	14.4	59.3	72.0	40.5	68.8	76.5	59.4	65.4
66.0	52.1	44.7	63.3	43.4	77.0	71.1	68.6	44.9	61.0
58.4									

In order to generate a structure with possibly high gravimetric and volumetric storage capacity, the wall thickness between the single fibers has been reduced at structure 3576a. 1387 single hollow glass fibers with hexagonal shape are surrounded from round solid fibers. The inner diameter of the single hollow glass fibers is 39µm. At a length of 200mm the produced samples are closed by melting, directly after production. The lower wall thickness and the lower amount of fibers results in a lower outer diameter of the structure of $D_o=1.5$mm. The reduced amount of glass material results in an increased free volume. About 80% of the volume of the whole structure are free storage volume. As visible in the microscopic view in Figure 48, the low wall thickness results in emerging interspaces between the single fibers. Related to the small wall thickness of the single fibers, the interspaces were not closed during the drawing process. As already mentioned, these interspaces have a negative influence on the burst pressure value of a sample because the applied pressure acts against the connection of the single fibers.
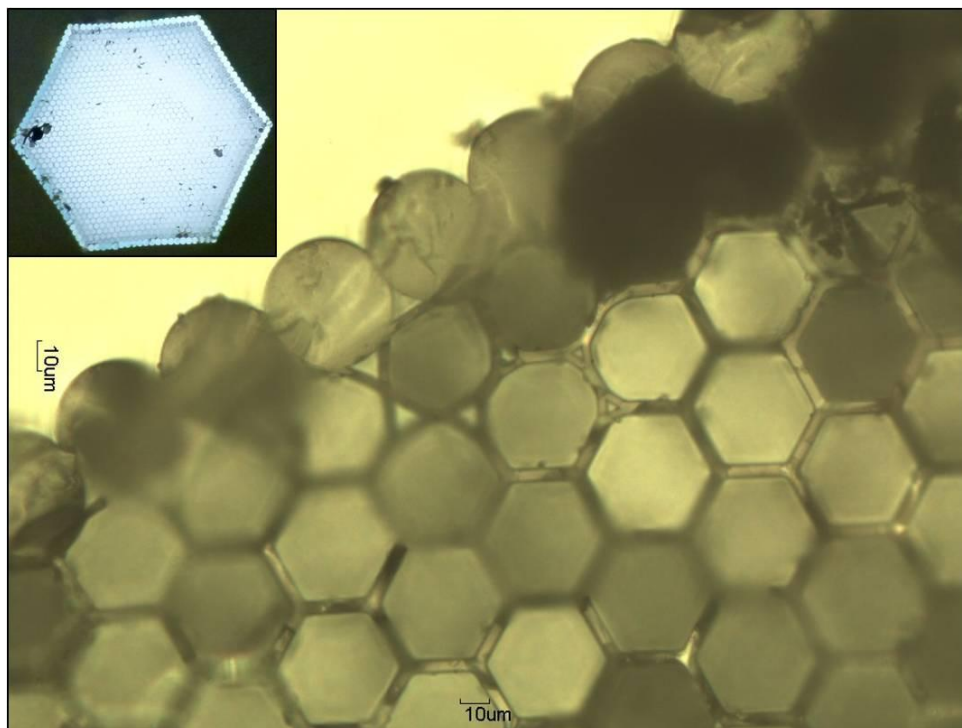
Figure 48: Microscopic view of structure 3576a – Thin-walled hexagonal single fibers with solid fibers as outer fiber layer

The highest measured burst pressure value of a test series consisting 32 samples of structure 3576, is 11.3 MPa. Compared to the previously tested samples, this maximum burst pressure value is comparably low. One reason will be the increased free inner volume of the structure. Another important, strength-reducing fact pose the interspaces between the single fibers.

Table 43: Burst pressure test results of structure 3576a – Thin-walled hexagonal single fibers with solid fibers as outer fiber layer

Burst pressure [MPa] of sample 1-32									
8.6	10.6	10.0	11.2	8.9	5.6	6.6	4.2	10.7	3.2
9.0	10.6	11.3	2.9	9.7	7.6	8.8	11.1	9.3	5.3
5.0	4.1	2.5	11.0	7.0	9.0	8.3	7.2	8.7	10.4
9.6	8.0								

5.4.7 Hexagonal Structures Made Of Hexagonal Single Hollow Glass Fibers Surrounded From Round Hollow Glass Fibers

The following production lines deal with the task of increasing the free inner volume by replacing the solid outer single fibers with thick-walled round hollow glass fibers.

The first produced structure of this kind has similar properties to structure 3576a. It is labeled as structure 3577a and consists of 1387 hexagonal single hollow glass fibers, each with an inner diameter of 37 µm. The length of the produced samples is 200mm and the outer diameter is 1.5mm. One end is closed by melting. The solid outer fiber layer of structure 3576a has been replaced with round, thick-walled hollow glass fibers. Due to the fact that the outer fiber layer poses additional volume for gas storage, the free inner volume of the structure is increased to more than 80%. An exact value is not available. Equal to structure 3576, interspaces between the single fibers occur, especially between the hexagonal and the outer round fibers.
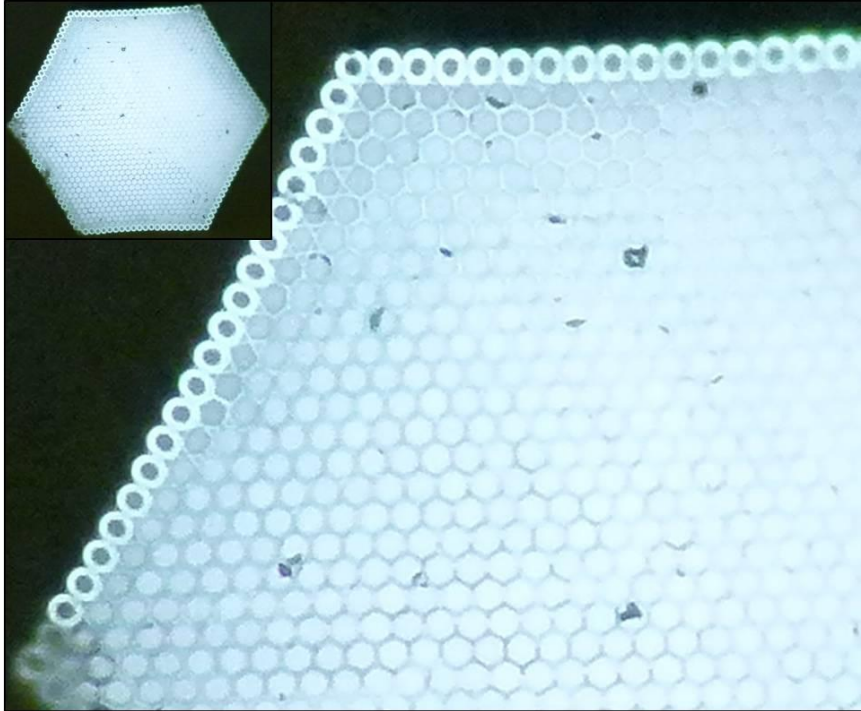
Figure 49: Microscopic view of structure 3577a – Thin-walled hexagonal single fibers surrounded by round single hollow glass fibers

The highest measured burst pressure value of 31 tested samples of structure 3577a is 10.3MPa. The results are shown in Table 44 and the highest measured burst pressure value is marked in red. Equal to structure 3576a, the high free inner volume, as well as the interspaces between the single fibers have a burst pressure decreasing influence on the structure.

Table 44: Burst pressure test results of structure 3577a – Thin-walled hexagonal single fibers surrounded by round single hollow glass fibers

Burst pressure [MPa] of sample 1-31									
1.5	1.6	1.5	1.4	3.5	3.4	1.6	2.1	6.0	1.9
2.3	1.2	2.2	1.4	1.4	1.8	1.7	1.4	9.2	1.5
2.3	7.0	1.2	5.2	3.8	10.3	3.7	4.4	10.1	1.8
6.5									

Structure 399-3316-A is a further structure of hexagonal single hollow glass fibers, which are surrounded from round hollow glass fibers. Compared to the previously tested structures of this kind, the wall thickness between the single fibers has been increased. The inner hollow glass fibers have an inner diameter of 39µm and an outer diameter of 50µm. The structure consists of altogether 3367 single fibers and has an outer diameter of 3.3mm. The length of the produced samples is 200mm. At one end, the samples are closed by melting. The structure has a free inner volume of 64% and is shown in Figure 50. Comparable to structure 3577, there are infrequent interspaced between the hexagonal single fibers and the round outer single fibers.
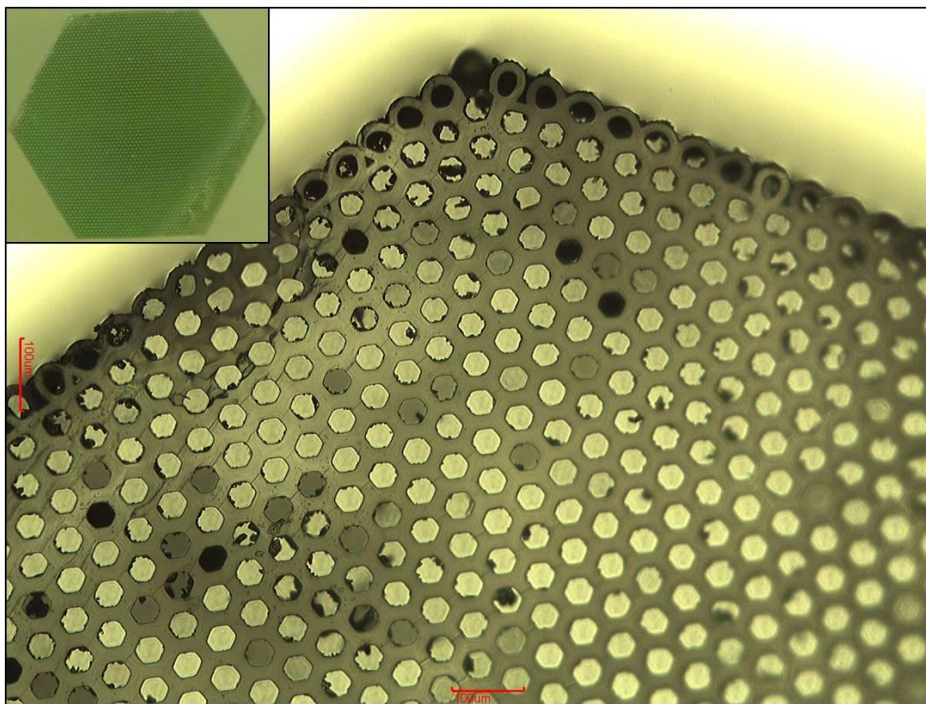
Figure 50: Microscopic view of structure 399-3316-A – Hexagonal single fibers surrounded by round single hollow glass fibers

The highest measured burst pressure value of 30 tested samples of structure 399-3316-A is 71.9 MPa. All measured burst pressure values are displayed in Table 45 and the maximum value is marked in red. Although the free inner volume is only about 20% lower than at structure 3577 and that there are still interspaces between the single fibers, the maximum burst pressure value is about seven times higher. In comparison to structure 3577, the interspaces are less frequented and to a lesser extent. Due to the fact that only a small amount of the samples was randomly examined with microscope, the samples with the high

burst pressure values may contain a small amount of interspaces. Thereby, structure 399-3316-A poses the best compromise regarding free inner volume and burst pressure value.

Table 45: Burst pressure test results of structure 399-3316-A – Hexagonal single fibers surrounded by round single hollow glass fibers

Burst pressure [MPa] of sample 1-30									
42.5	47.9	33.5	32.0	63.8	36.0	46.5	50.0	55.8	65.1
71.9	35.0	33.0	60.6	35.3	47.8	56.4	46.4	64.7	59.4
44.9	56.0	25.4	46.7	38.0	44.0	53.6	31.9	41.4	41.9

5.4.8 Tapering The Open End Of Structures

In order to increase the storage capacities of a system made of glass structures, reducing the glass material for decreasing the weight of the system is but one of a few possibilities. An additional heavy part of the system is the metal adapter in which the glass structure will be placed. Design related, size and weight of the adapter grows with increasing outer diameter of the glass structure. The principle of connecting the glass structure to the adapter is already discussed in chapter 4.3 "Sample Preparation".

Due to the fact that the ratio of inner and outer diameter of a glass structure keeps constant during the drawing process, the opportunity to taper the open end of a glass structure by heating up and drawing only this part of the structure is available. This way, the dimension of the adapter can be decreased, while most of the glass structure remains in original size. Figure 51 demonstrates a comparison of an ordinary structure, which is connected to a metal adapter (1) and a structure with identical outer diameter, but tapered end (2). The amount of single fibers as well as the dimension of these fibers is identical in both structures. Merely at the tapered end, the outer diameter of the structure is decreased. Comparing the two metal adapters demonstrated the different size and the corresponding lighter weight of the smaller adapter. In this way, the gravimetric and volumetric storage capacities of the storage system will be increased, depending on the amount of used glass structures and adapters.
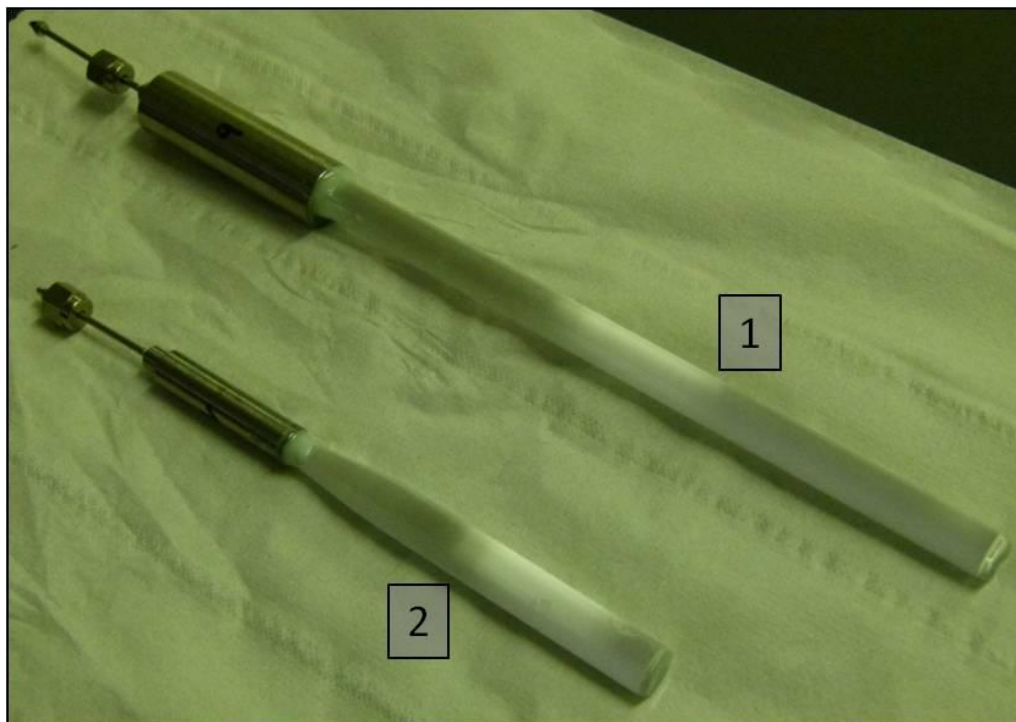
Figure 51: Common multi fiber (1) compared to a multi fiber with tapered end

A produced structure with tapered open end is labeled 3624 T and shown in Figure 52. Except for the tapered end, the properties of the structure are identical to structure 3624 A. It consists of 3169 hexagonal single hollow glass fibers with an inner diameter of 39µm, surrounded from 198 solid fibers. The outer diameter of the structure is 2.9mm flat-to-flat and the length is 200mm. One end is closed by melting. The other end is tapered to a ratio of 33% of the original size. Due to the fact that the ratio of inner and outer diameter keeps constant during the drawing process, the free inner volume keeps at 60%, equal to the identical structure 3624 A without a tapered end.

Figure 52: Structure 3624 T – One end tapered to 33% of the original size

10 samples of structure 3624 T were available for burst pressure tests. The results are shown in Table 46 and the maximum burst pressure value is marked in red. Compared to the maximum burst pressure value of structure 3624 A (37MPa), the tapered structure 3624 T showed an increased maximum burst pressure value of 43.4 MPa. In this case, too, the theory of higher strength of smaller samples, which was postulated by Griffith in 1920 and already discussed in chapter 3.3.2 "Strength of Glass", offers a possible explanation for this behavior. Due to these results, tapering the open end of the glass structures leads to increased storage capacities which is caused by the decreased weight and dimension of the metal adapter, as well as increased strength of the glass structures.

Table 46: Burst pressure test results of Structure 3624 T – One end tapered to 33% of the original size

Burst pressure [MPa] of sample 1-10									
39.5	33.9	22.4	43.4	42.6	34.6	38.6	36.6	34.4	36.6

5.4.9 Multi-Structure Made Of A Number Of Structures

The hexagonal shape of the latest examined structures allows a further bundling to multi-structures. Therefore, a defined number of identical hexagonal structures will be ordered in honeycomb assembly and drawn again. In this way, the single structures will be fused and a complex multi-structure will emerge. An example of such kind of a multi-structure is given in Figure 53. Several kinds of multi-structures with varying parameters were produced, but not tested concerning their burst pressure, up to this point. These multi-structures pose the next step in the evolution of high pressure gas storage system made of hollow glass fibers and need to be examined.
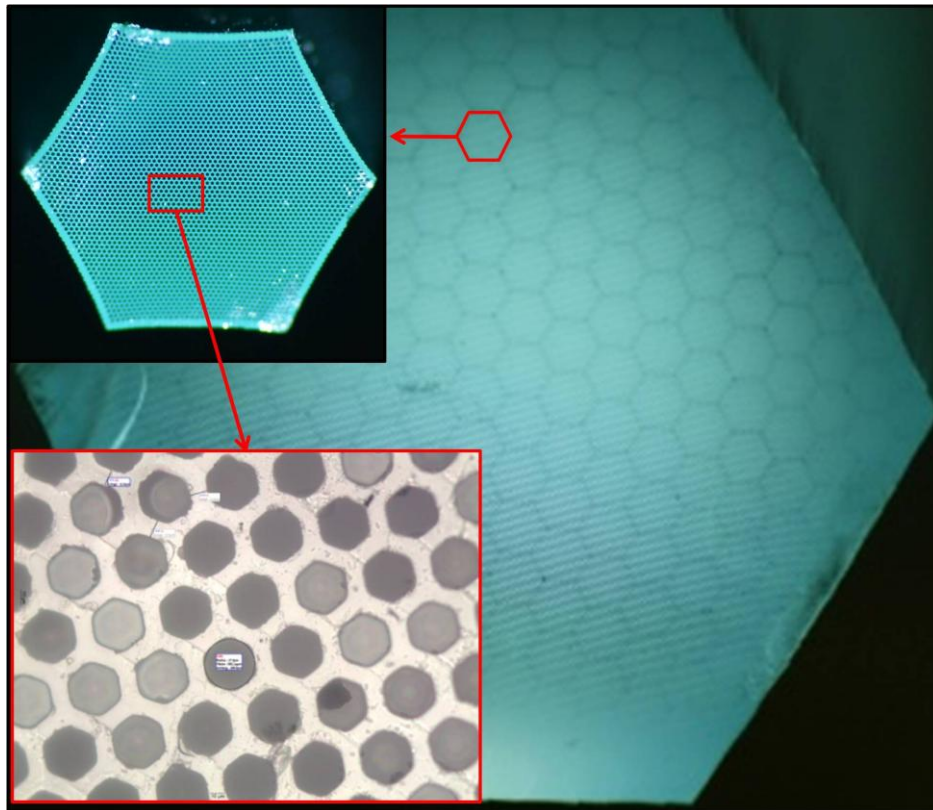
Figure 53: Multi-structure, made of a number of identical structures

5.5 Summary Of Burst Pressure Test Results

The first hand-made structures gave a first impression of the possibility of bundling single fibers to structures. Due to the limited opportunities in hand-made production, the variable properties are reduced to the fiber dimension and the wall thickness. Varying the temperature and speed of drawing leads to differences in the structure like emerging interspaces or the shape of the single fibers. Due to the hand-made production, the reproducibility of the structures posed a problem. Furthermore, an outer glass shell was necessary as related to the production conditions.

The burst pressure tests of the hand-made structures demonstrated the negative influence of interspaces between the single fibers on the burst pressure. Additionally, a higher burst pressure at samples with higher wall thickness and in that regard lower free inner volume show much higher burst pressure values than thin-walled samples. The highest measured burst pressure value of all tested hand-made samples showed the comparably massive structure M1 with 87.6MPa.

The change to automatic production offered a number of further opportunities regarding design and dimension of the produced structures. Furthermore, a reproduction with constant quality became possible.

First test series of samples with varying properties concerned with varying shape of the single fibers inside a structure. The usage of hexagonal single fibers inside a structure leads to different advantages, compared to single fibers with round shape. The honeycomb assembly of the single fibers leads to the absence of interspaces between the single fibers. Furthermore, less glass material is necessary, whereby the weight of the structure will be reduced and the storage capacities are increased.

The absence of an outer massive glass shell leads to decreased weight of the structure. Furthermore, the associated change to hexagonal outer shape of the structures offered additional possibilities like further bundling to multi-structures. For receiving a protection of the single hollow glass fibers against outer influence the effect of solid fibers as outer fiber layer of the structure was examined. Compared to structures without any kind of protection, the amount of already damaged delivered structures could be reduced. The influence of such a solid fiber layer as protection shell on the burst pressure could not be noticed. Due to the fact that the usage of solid fibers instead of hollow glass fibers decreases the free inner volume, an outer layer of solid fibers is an adequate way of protecting the hollow glass fibers, but optimizing the transport for preventing outer damage will be necessary for obtaining higher storage capacities. The influence of replacing the solid fibers with thick-walled round hollow glass fibers could be demonstrated with structure 399-3316-A. Although the comparably high free inner volume of 64%, the structure shows a high maximum burst pressure value of 71.9MPa.

Another way to decrease the weight of the storage system is by tapering the open end of the glass structure. This way the adapters can be smaller. Furthermore, a burst pressure test series offered increased maximum burst pressure values at tapered samples, compared to a similar, but not tapered structure.

Figure 54 demonstrates the comparison of the measured maximum burst pressure values (blue points) of all tested samples and the corresponding gravimetric storage capacities for these values (red points). Related to these graphs, structure 3624-9 poses the highest burst pressure values, as well as the highest gravimetric storage capacity. Due to the fact that the free inner volume is necessary for the calculation of the gsc value, and that this value of the structure seems to be smaller than the given value of 45%, the gravimetric storage capacity of structure 3624-9 is invalid. Disregarding this value, the structure with the highest gravimetric storage capacity is 399-3316-A, although the maximum burst pressure value of

this structure is lower than many other structures. Responsible for the high gsc value is the high free inner volume of that structure. A further conspicuity are the values of the tapered structure 3624T. Although the comparably low burst pressure value, the gravimetric storage capacity of that structure is comparable to other structures with higher burst pressure values and identical free volume. This is caused by the reduced weight of the structure by tapering one end.
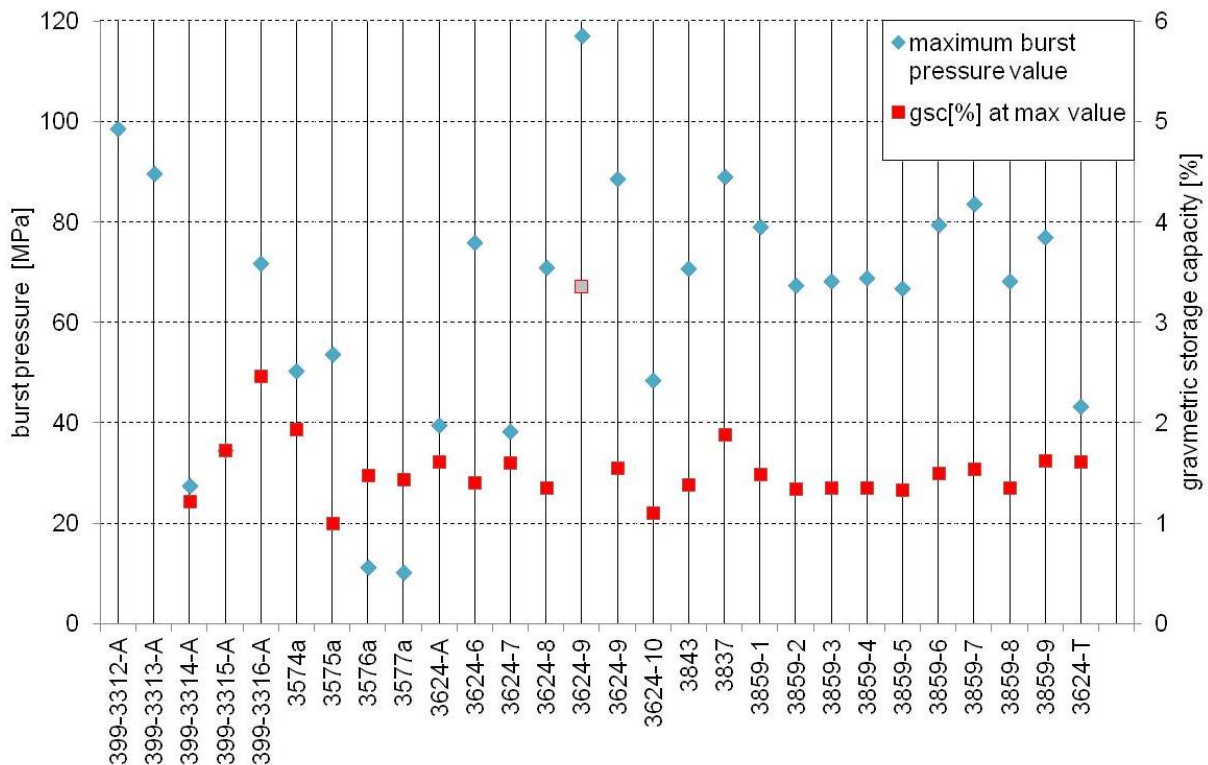
Figure 54: Comparison of the measured maximum burst pressure values of all tested samples and the corresponding gravimetric storage capacities for these values

The possibility of bundling hexagonal structures to multi-structures was examined and first samples were produced. Up to this point, the burst pressure value of such multi-structures was not determined.

Several test series with visible defects on the outer surface of the glass structures, demonstrated the negative influence of such defects on the burst pressure value, compared to identical samples without defects.

With regard to the experimental results, one of the most influencing parameters for burst pressure is the free inner volume of a structure. A higher free volume leads to smaller burst pressure values. The following Figure 55 demonstrated the dependence of the burst pressure value on the free inner volume. For the purpose of demonstrating the dependence, structures 3624-6, 3624-7, 3624-8 and 3624-9 are compared to each other. The only difference of these structures is the free inner volume.

As demonstrated in Figure 55, the burst pressure value shows a decreasing trend at increasing free inner volume although more than three values at the abscissa are necessary for a validated statement, the trend of the graph shows an exponential decrease.
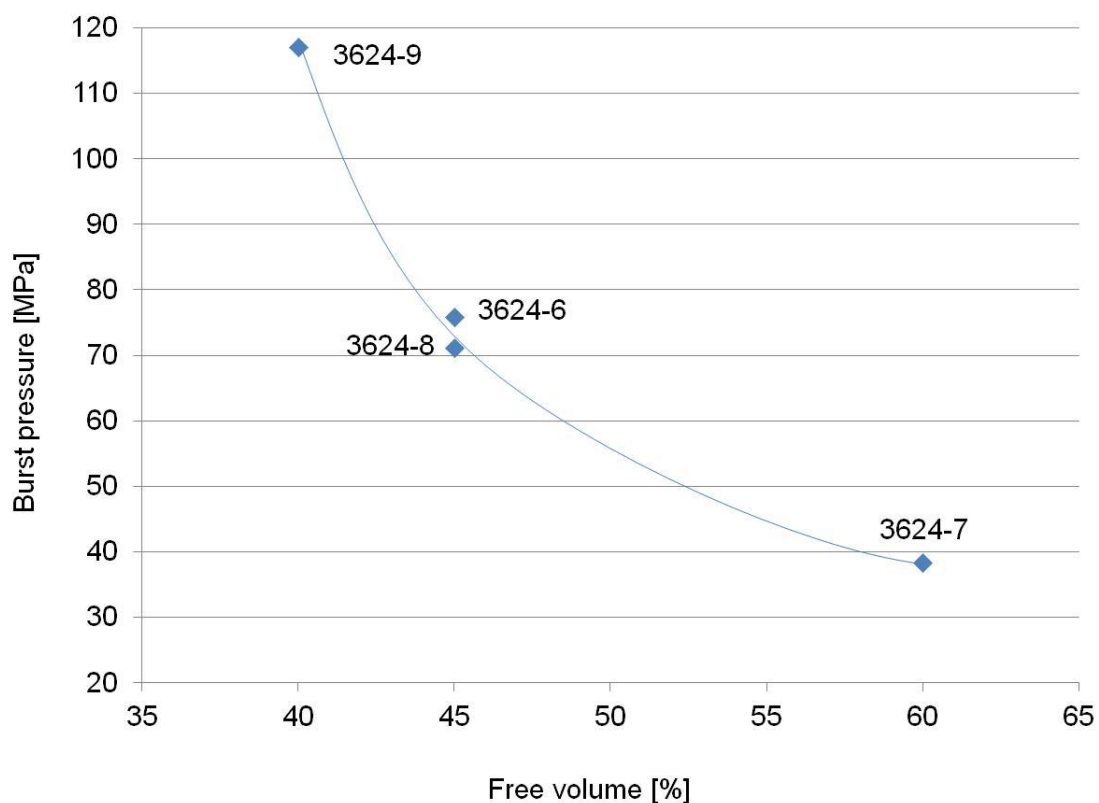
Figure 55: Dependence of burst pressure value on free inner volume, demonstrated by comparing the maximum burst pressure values of the structures 3624-6, 3624-7, 3624-8 and 3624-9

The burst pressure examination poses a helpful tool for comparing the strength of different structures. The samples are destroyed during the test procedure, making this kind of

examination is quite expensive. Furthermore, there is always an influence of additional parameters like defects or small variations between the tested samples of one test series. Because of these variations the experimental evaluation is not an adequate tool to determine the exact influence of varying parameters like the shape or the amount of the single fibers, an outer glass shell or the existence of solid fibers, the free inner volume or several kinds of defects. In contrast to this, numerical simulation with the finite elements method poses a helpful tool for solving that problem and is used for further examination in the following chapter.

5.6 Results Of Stress And Expansion Modeling Using FEM

For the FEM calculation the software Comsol Multiphysics 4.1 with the module "Structural Mechanics" was used. The material model silica glass was chosen and the material properties were adjusted to the material properties of borosilicate glass which were given by the manufacturer or determined in this thesis. The desired material properties of borosilicate glass for the calculations are the Young's modulus which was specified with 75000 N mm^{-2} in chapter 3.3.1 and chapter 5.2 and the Poisson's ratio which is given as 0.2 [162]. During pressure treatment, the occuring stress in axial direction only depends on the area of glass which is exposed to the tensile stress. Contrary to this, the tangential stress is influenced by the shape and dimension of the glass fibers. According to Barlow's formula, the tangential stress is the highest occurring stress in a tube during inner pressure treatment. The tangential stress is biaxial, as already mentioned in chapter 5.1. Due to that fact, the stress distribution in x-direction and y-direction needs to be determined. Thus, two-dimensional profile models of several types of glass fibers and structures were built. For the inner boundaries a pressure was applied. The used mesh is a triangular mesh with varying size between 0.02 µm and 10 µm, dependent on the size of the structure. At directly compared structures the mesh size was constant. The 2D approximation type was plane stress. According to chapter 5.3.1, the glass structures are fused by melting during production process. After this procedure the glass structure is one body with no deviating contact areas between the single fibers. According to this procedure, structure models were built by fusing single fibers without separate contact areas. Just like real glass structures, they behave like one body at the contact area. Afterwards one triangular mesh was placed on the whole model.

Unless otherwise stated, the FEM calculations were done at constant applied pressure of 50 MPa to obtain comparable results. The international accepted limit for hydrogen storage is 70

MPa. Due to the fact that the distribution of the stress is equal at 50 MPa and 70 MPa, the results of the simulation are valid for any storage pressure. Merely the overall value of the stress and expansion will be increased at higher applied inner pressure. According to the conclusion in chapter 3.7 "Stress Analysis", the principal stress theory takes place, therefore, the principal stresses were calculated and the first principal stress, which has the highest value, is shown as result. Furthermore, the expansion of the material was determined. The simulation assumes defect free material whereby the results should be comparable to the theoretical strength of glass. A stationary condition of stress treatment was considered for the simulation.

5.6.1 Comparison Of Different Basic Materials Regarding Stress And Expansion At Pressure Treatment

In a first step, three different commercial available glass materials were compared to each other. The internal stress and expansion of three single fibers made of borosilicate glass, quartz glass and alumosilicate glass were simulated for an applied pressure of 50 MPa. Therefore, the material parameters for the Young's modulus and the Poisson's ratio were changed according to the values which were given by the glass manufacturer [162 - 164].

Each sample has an outer diameter of 400μm and an inner diameter of 300μm. Although the difference of the values between the three materials is quite marginal, alumosilicate glass is the material with the lowest occuring internal stress as well as the lowest expansion. In stark contrast, borosilicate glass is exposed to the highest stress and expansion. Quartz glass shows values between borosilicate glass and alumosilicate glass. Thus the maximum stress values vary from a minimum value of 178.99 MPa to a maximum value of 179.09 MPa. The variation of the expansion values is similar low with an only 0.06 μm higher maximum value at borosilicate glass compared to the minimum value at alumosilicate glass. Figure 56 demonstrates the results of the FEM simulation. Summarizing, the occurring stress and expansion of the three glass materials at an applied pressure of 50MPa are nearly identical.

Material		
Borosilicate glass	Quartz glass	Alumosilicate glass
Outer/Inner Diameter [µm]		
400 / 300	400 / 300	400 / 300
Maximum stress [MPa]		
179.07	179.03	178.99
Minimum stress [MPa]		
128.91	128.88	128.85
Expansion [µm] / [%]		
0.74 / 0.19	0.68 / 0.17	0.60 / 0.15
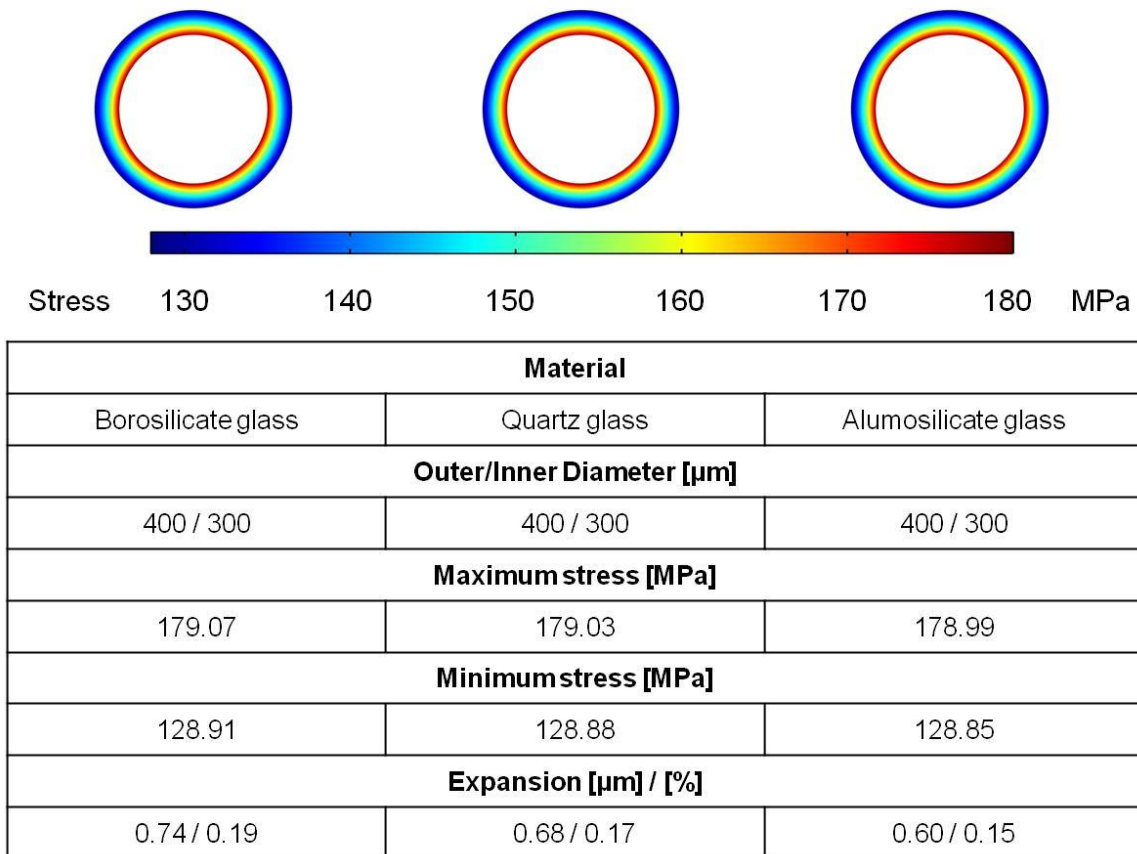
Figure 56: Comparison of Borosilicate glass, Quartz glass and Alumosilicate glass regarding the occurring first principal stress and expansion with 50 MPa applied inner pressure

Previous research [96], validated by the experimental results of R. Meyer [169], turned fibers made of borosilicate glass 3.3 [160 - 162] with an outer diameter (D_o) of 400µm, an inner diameter (D_i) of 300µm and a length of 20cm out to be the most qualified fibers for gas storage in practical experiments because of its high burst pressures. Related to that fact, the inner pressure in hollow glass fibers made of borosilicate glass must be higher for reaching the critical stress of the material, whereby borosilicate glass shows the highest critical stress value and therefore the highest strength of the tested materials.

Admittedly, only eight to ten samples were tested for every measuring value which is not enough for a qualified statistical evaluation. These examinations were repeated and confirmed by R. Meyer [169]. According to these results, borosilicate glass was chosen as basic material to do further research on the influence of fiber dimension or of varying ambient conditions like temperature and humidity during pressure treatment [168, 169]. Hence, borosilicate glass was chosen as material for the FEM calculation in this thesis.

5.6.2 Behavior Of Round Single Fibers At Inner Pressure Treatment

Beginning with the previously mentioned borosilicate glass fiber, a comparable two-dimensional model was created. Simulating applied pressure of 50 MPa to the inner surface of that single fiber with an outer diameter D_o=400 µm and an inner diameter D_i=300 µm made of borosilicate glass results in a homogeneous stress distribution as displayed in Figure 57 (left). The stress intensity decreases from the inner to the outer surface from 179 MPa to 129 MPa. Expectably, the occurring stress is well distributed without any peaks of high stress. The occurring stress is converted to mechanical energy. The result is a deformation of the cylinder in terms of displacement (strain). The highest value at the inner surface is 0.38µm decreasing to the outer surface to 0.34µm. That circumstance leads to a shrinking wall thickness of 0.04µm (≈10%). The total expansion of the cylinder corresponds to the double strain of the outer surface (0.345 · 2) and amounts with 0.69µm about 0.17% of the cylinders outer diameter.
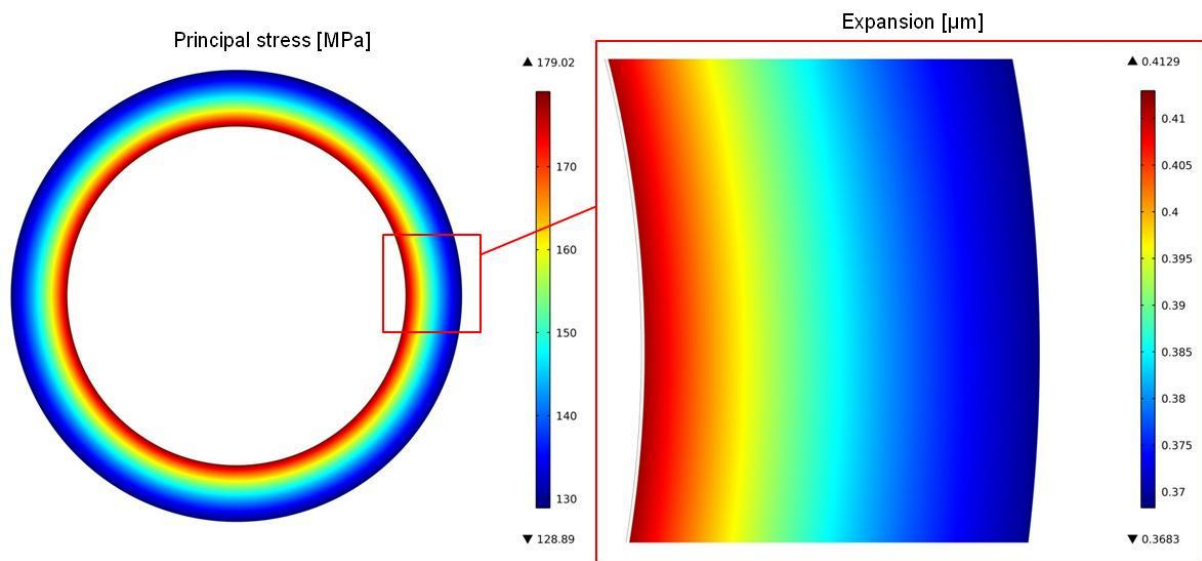
Figure 57: Calculated first principal stress in MPa (left) and expansion in µm (right) at a single fiber made of borosilicate glass with an outer diameter D_o=400µm and an inner diameter D_i=300µm with 50 MPa applied inner pressure

Regarding stress and expansion during step wise pressure increase results in the following Figure 58 within which the minimum and the maximum stress in MPa as well as the expansion in μm are displayed. The left table column displays these values for an applied pressure at the inner surface of 5 MPa. Going on to the right the applied pressure is increased stepwise by 10 MPa up to 45 MPa in the right table column. The pictures above the columns visualize the calculated stress in the fiber at the respective applied pressure. The minimum and the maximum stress as well as the expansion grow linear to the increased pressure. A nine times higher stress leads to nine times higher values of minimum and maximum stress as well as expansion.
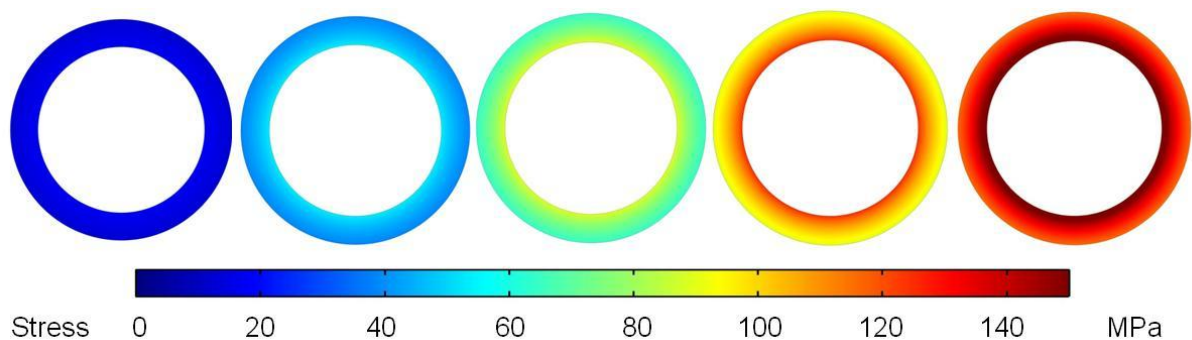
Pressure inside [MPa]				
5	15	25	35	45
Minimum stress [MPa]				
13	39	64	90	116
Maximum stress [MPa]				
18	54	89	125	161
Expansion [μm]				
0.08	0.23	0.38	0.53	0.68

Figure 58: Increase of first principal stress and expansion during continuous pressure increase at a round single fiber made of borosilicate glass with D_o=400μm and D_i=300μm

The result of plotting the calculated values for stress and expansion against the applied pressure is illustrated in Figure 59. The diagram displays the internal stress at the primary ordinate (left) and the expansion at the secondary ordinate (right). The abscissa shows the

applied pressure in MPa. The minimum and maximum stress (red and green graph) as well as the expansion (blue graph) of the fiber is linear dependent on the applied pressure. The higher the applied pressure the higher is the difference between minimum and maximum internal stress. This behavior is typical for materials with linear-elastic behavior.
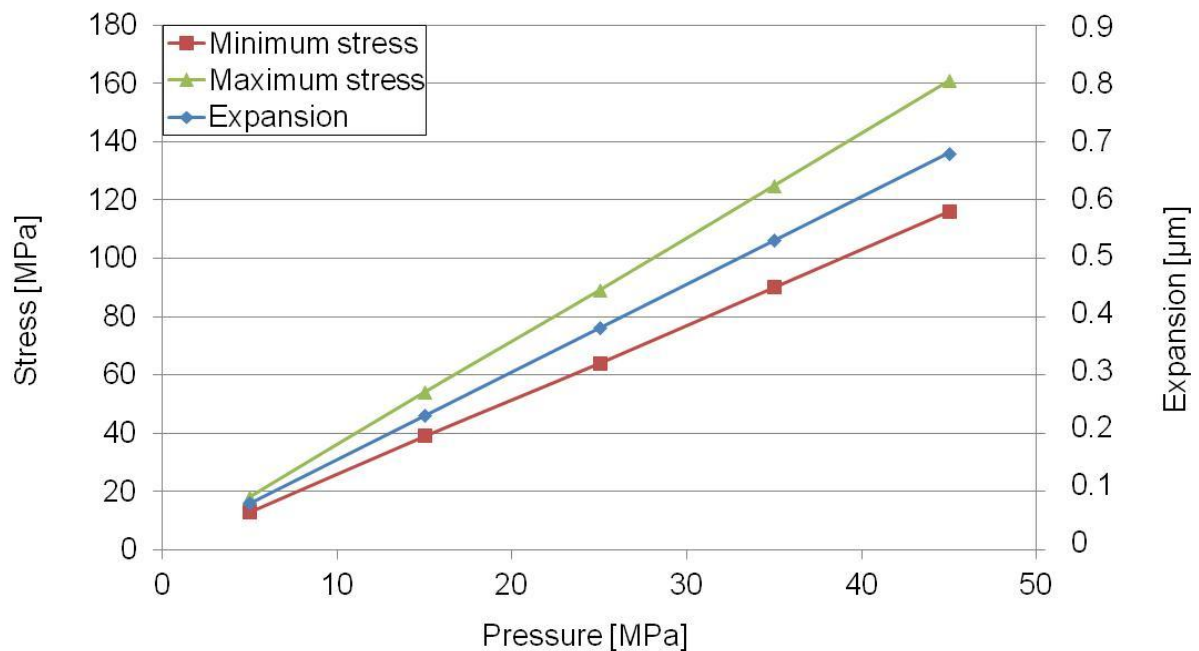
Figure 59: Dependence of minimum and maximum first principal stress (red and green graph) as well as expansion (blue graph) on the applied pressure at round single fibers made of borosilicate glass with D_o=400µm and D_i=300µm with 50 MPa applied inner pressure

5.6.3 Influence Of Varying Wall Thickness At Constant D_i On The Strength Of Single Fibers

Regarding the influence of the wall thickness, the simulation has been repeated for samples with varying dimension. In the first step, the inner diameter has been fixed to 250µm. The wall thickness varies stepwise from 5µm from the left column to 75µm at the right column of the table in Figure 60. The diagrams above the columns visualize the calculated stress in MPa which occurs at the respective applied pressure. According to the results of FEM

simulation, a higher wall thickness leads to less occurring internal stress and lower expansion. The occurring maximum stress of a sample with 5 µm wall thickness is about ten times higher than that of a sample with 75 µm. The maximum stress is more than 10 times higher of the thin-walled sample. Independent from the wall thickness, the difference between minimum and maximum stress is constant about 50 MPa.

Outer diameter [µm]				
260	280	320	360	400
Inner diameter [µm]				
250	250	250	250	250
Wall thickness [µm]				
5	15	35	55	75
Maximum stress [MPa]				
1298	446	207	143	114
Minimum stress [Mpa]				
1247	395	157	93	64
Expansion [µm] / [%]				
4.28 / 1.65	1.46 / 0.52	0.66 / 0.21	0.44 / 0.12	0.34 / 0.085
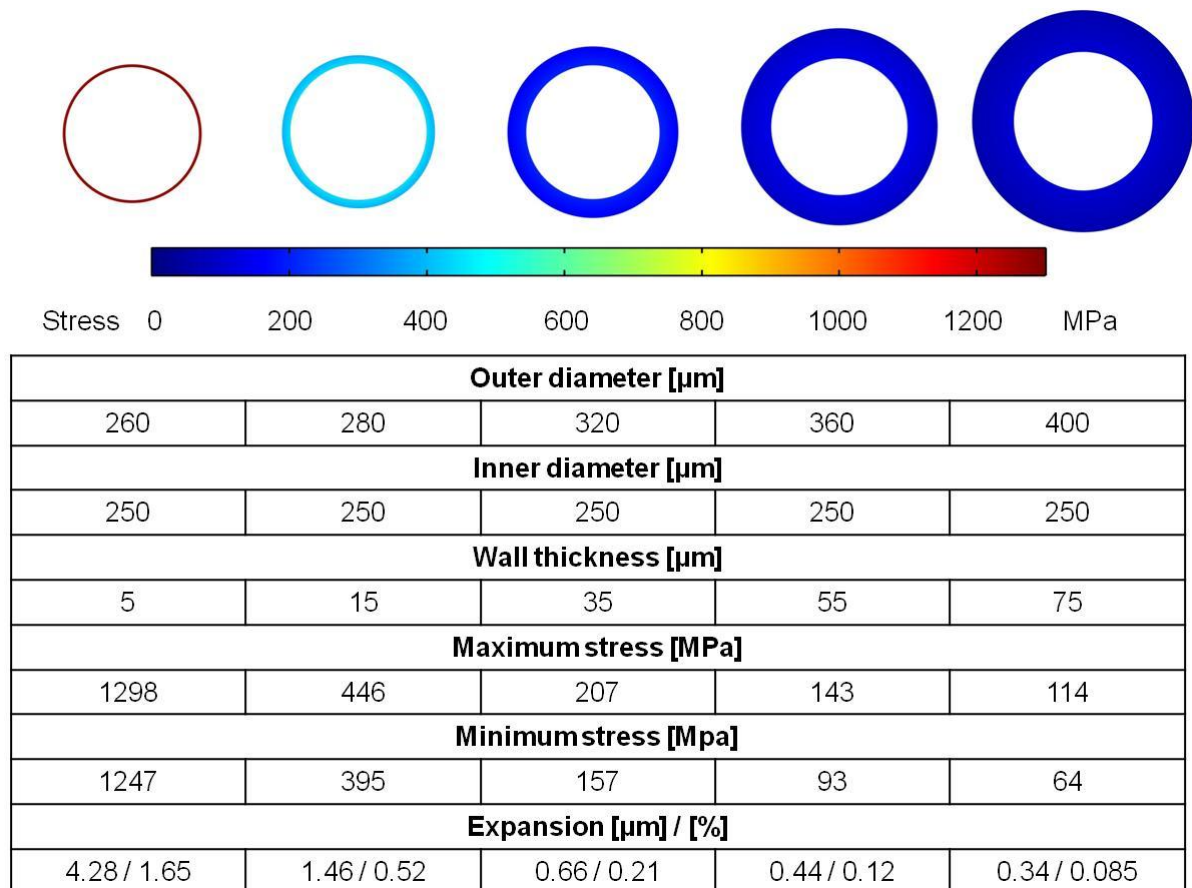
Figure 60: Influence of varying wall thickness at constant inner diameter on the occurring first principal stress and expansion at a round single fiber made of borosilicate glass with 50 MPa applied inner pressure

Plotting the minimum and maximum stress against the sample's wall thickness as shown in Figure 61 leads to an exponential decrease of the occurring stress when constantly decreasing the wall thickness at constant inner diameter. The difference between minimum and maximum stress keeps constant at about 50MPa as already mentioned, despite the higher stress value of the samples with lower wall thickness. According to the decreased stress values, the increased wall thickness leads to lower expansion of the sample's

diameter. Like the stress value, the expansion decreases exponentially at constant increased wall thickness. Thereby, a direct correlation of stress and expansion values is observable.

According to this behavior, the wall thickness of a single fiber used for high pressure gas storage should not exceed a defined value; in the given case about 20 µm. Otherwise, the exponential increasing internal stress prevents high storage pressures.
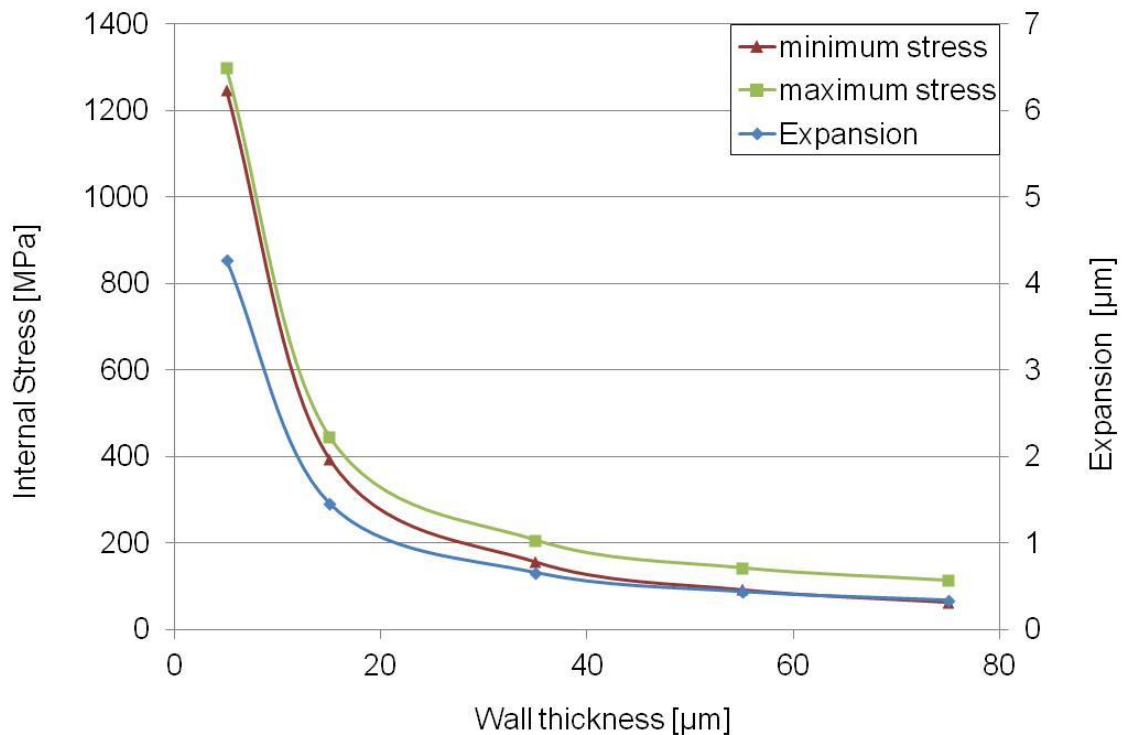

Figure 61: Dependence of minimum and maximum first principal stress (red and green graph) as well as expansion (blue graph) on the wall thickness at round single fibers made of borosilicate glass with constant inner diameter D_i with 50 MPa applied inner pressure

The decreasing strength of fibers with lower wall thickness caused by higher internal stress values could be confirmed in experimental tests which were executed and discussed in the PhD thesis of R. Meyer [169]. Hence, the burst pressures of single fibers with identical inner diameter D_i=267µm but varying wall thickness was determined. According to Barlow's formula, the critical stress of a sample can be determined with the burst pressure. Thereby, it is an adequate instrument to compare the strength of different samples as already shown in Table 10 in chapter 5.1.

Table 47 displays the results of the burst pressure tests of five different kinds of single fibers with varying wall thickness but constant inner diameter. As displayed in Table 47 and Figure 62, the burst pressure increases at higher wall thickness. Due to the fact, that the samples of test series 5 did not break at an inner pressure of 150 MPa, the real burst pressure and thereby the critical stress is potentially higher than shown in Table 47 and Figure 62. The lower burst pressure of thinner walled samples demonstrates that the critical stress at which the sample breaks is reached at lower applied pressure compared to samples with higher wall thickness. Additionally, the critical stress has been calculated with the Barlow's formula (Equation 5-2) and is also shown in Table 47. Despite the varying wall thickness, the critical stress, at which the sample broke, alternates between 350MPa and 450MPa. The critical stress value 289 MPa at test series 5 is not significant, because the samples did not break at an inner pressure of 150MPa, which poses the maximum reachable pressure of the test setup.

Table 47: Burst pressure of single fibers with varying wall thickness but fixed inner diameter of 267µm

Test series No.	1	2	3	4	5
Inner diameter [µm]	267	267	267	267	267
Outer diameter [µm]	302	323	336	420	555
Wall thickness [µm]	17.4	28.0	34.7	76.4	144.0
Maximum burst pressure [MPa]	46.6	78.3	71.6	131.2	150.0*
Critical stress [MPa]	404	452	347	361	289*

* Sample did not break at an inner pressure of 150MPa (maximum of test setup)
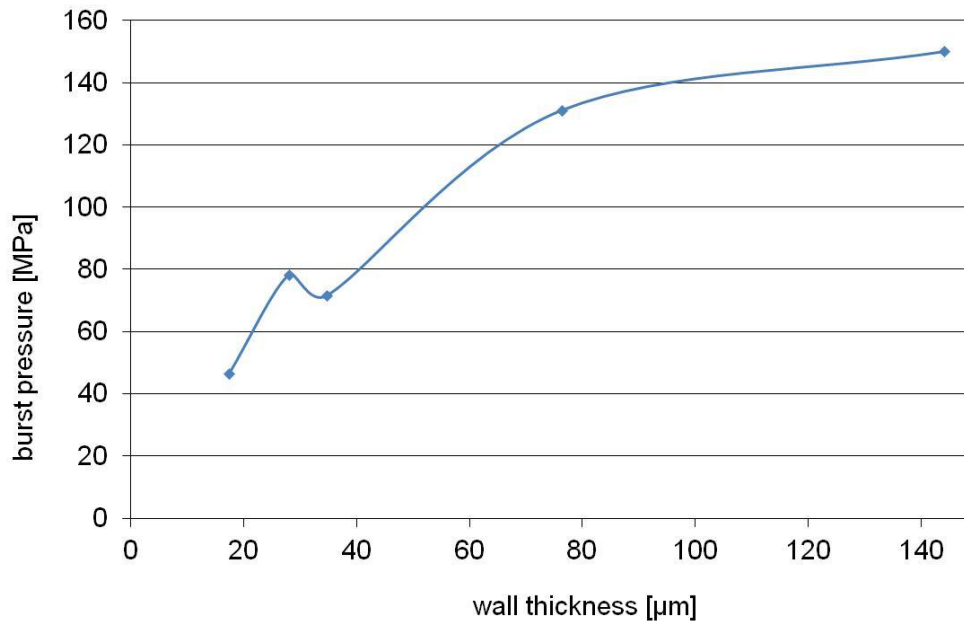
Figure 62: Dependence of measured burst pressure on the wall thickness at round single fibers with constant inner diameter made of borosilicate glass with 50 MPa applied inner pressure

Up until this point, the Griffith theory of increasing strength at decreasing sample diameter does not apply for the given case of fixed inner diameter. With constant inner diameter, hollow fibers with applied inner pressure show decreasing strength with decreasing outer diameter.

5.6.4 Influence Of Varying Sample Size At Constant Ratio Of D_i And D_o On The Strength Of Single Fibers

Further examination deals with shrinking outer diameter and inner diameter at a constant ratio. A FEM simulation was executed for three samples which were scaled-down to 10% of the initial sample size in each step from the left column to the right column of the table displayed in Figure 63. The pictures above the columns demonstrate the internal stress in MPa calculated with FEM simulation. The ratio of outer diameter and inner diameter kept constant. The occurring stress as well as the total expansion does not change when varying the sample's dimension at fixed inner and outer diameter ratio. According to that calculation,

the size of a fiber does not have an influence on its strength provided that the ratio of inner to outer diameter (D_i/D_o ratio) keeps constant.
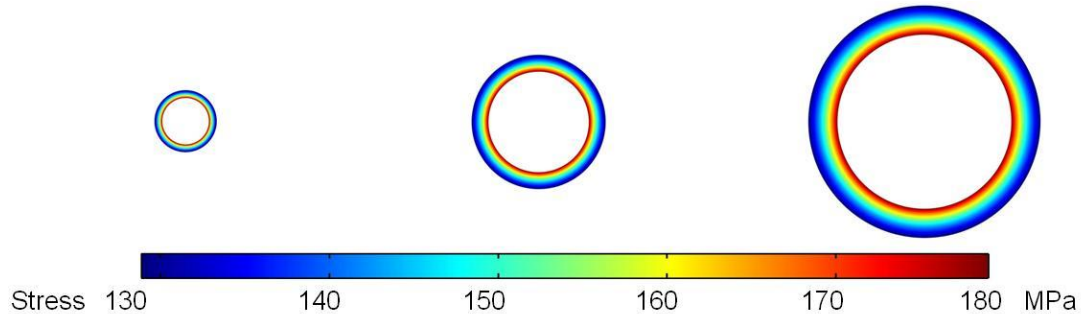
Outer diameter [µm]		
4	40	400
Inner diameter [µm]		
3	30	300
Free space [%]		
64	64	64
Maximum stress [MPa]		
179	179	179
Minimum stress [Mpa]		
129	129	129
Expansion [µm] / [%]		
0.0034 / 0.09	0.034 / 0.09	0.34 / 0.09

Figure 63: Influence of varying sample size at fixed D_i/D_o ratio on occurring first principal stress and expansion at round single fibers made of borosilicate glass with 50 MPa applied inner pressure

The calculation of the internal stress as function of the applied pressure is subsequently demonstrated. As demonstrated in Figure 20 in chapter 5.1, the tangential stress (σ_T) is the highest occurring stress during pressure treatment, therefore the Barlow's formula for tangential stress is used.

$$\sigma_T = \frac{p \cdot D_o}{2 \cdot s}$$
(Eq. 5-22)

Inserting the values for applied pressure (p), outer diameter (D_o) and wall thickness (s) for each of the three single fibers results in identical values for internal stress as shown below in Equation 6-2 to 6-4.

Single fiber D_o = 4µm; D_i = 3µm

$$\sigma_{T1} = \frac{50\text{MPa} \cdot 4\mu m}{2 \cdot 0.5\mu m} = 200\text{MPa} \qquad \text{(Eq. 5-23)}$$

Single fiber D_o = 40µm; D_i = 30µm

$$\sigma_{T2} = \frac{50\text{MPa} \cdot 40\mu m}{2 \cdot 5\mu m} = 200\text{MPa} \qquad \text{(Eq. 5-24)}$$

Single fiber D_o = 400µm; D_i = 300µm

$$\sigma_{T3} = \frac{50\text{MPa} \cdot 400\mu m}{2 \cdot 50\mu m} = 200\text{MPa} \qquad \text{(Eq. 5-25)}$$

Calculating the internal stress with the Barlow's Formula confirms the results of FEM simulation. The internal stress is equal to 200MPa for all three samples at pressure treatment with identical pressure (p = 50MPa).

Contrary to this, practical tests show different behavior. Three burst pressure test series of single fibers with varying dimension but constant Di/Do ratio were performed and published by R. Meyer [169]. The burst pressure values are summarized in Table 48, as well as the critical stress. Figure 64 demonstrates, that the test samples with smaller D_o/D_i-ratio and thereby less glass material related to the free inner volume, show consistently lower burst pressure values. In opposition to the theoretical results of FEM simulation, all three test

series showed increasing burst pressure values at decreasing sample size. Also the critical stress increases with decreasing wall thickness.

The yellow-marked third fiber with a D_o/D_i-ratio of 1.33 in Table 48 has with an inner diameter of 300µm and an outer diameter of 400µm the same dimension as the simulated single fiber. The with FEM simulation calculated stress at an inner pressure of 50MPa is 179.02MPa. As already mentioned, the stress inside the material increases in straight way with increasing applied pressure, whereby an interpolation of the stress is possible. The maximum measured burst pressure value of the tested sample is 124.5MPa. After interpolation, the theoretical stress inside the material will be 445.8MPa. According to the test results, the critical stress at the burst pressure of the sample was 498MPa. The similarity of these two values demonstrates, that the calculated stress values by using FEM simulation correspond to the real stress value, determined in experimental studies.

Table 48: Burst pressure and correlating critical stress value of single fibers with varying dimension but fixed D_i/D_o ratio [169]

	Outer diameter D_o [mm]	Inner Diameter D_i [mm]	D_o / D_i	Wall thickness [µm]	Maximum burst pressure [MPa]	Critical stress (tangential) [MPa]
$D_o / D_i = 1.15$	0.30	0.26	1.14	18.50	71.10	576
	0.35	0.30	1.16	23.50	72.50	540
	0.60	0.52	1.15	40.00	46.40	348
	0.65	0.56	1.15	43.50	111.20	831
	0.86	0.75	1.15	57.50	40.70	304
	1.00	0.87	1.15	66.50	41.40	311
	2.00	1.73	1.16	135.00	29.50	219
	3.75	3.25	1.15	250.00	20.80	156
$D_o / D_i = 1.25$	0.15	0.12	1.25	15.00	91.50	458
	0.20	0.16	1.25	20.00	88.30	442
	0.25	0.20	1.25	25.00	104.90	525
	0.30	0.24	1.25	30.00	112.30	562
	0.37	0.30	1.25	37.00	100.40	502
	0.50	0.40	1.25	50.00	101.20	506
	0.75	0.60	1.25	75.30	64.20	320
	0.95	0.76	1.25	95.00	64.30	322
	1.50	1.20	1.25	150.00	52.10	261
$D_o / D_i = 1.33$	0.30	0.23	1.33	37.50	107.60	430
	0.35	0.26	1.33	43.50	119.60	481
	0.40	0.30	1.33	50.00	124.50	498
	0.45	0.34	1.33	56.00	132.50	532
	0.75	0.56	1.33	93.50	97.70	392
	1.40	1.05	1.33	175.00	69.60	278
	1.65	1.24	1.33	207.00	60.10	240
	2.30	1.73	1.33	287.50	52.90	212

As explained in chapter "Terminology", the free space value explains the inner-to-outer-diameter-ratio, while the wall thickness is set by the inner and outer diameter. Therefore, the wall thickness is an adequate value to describe the dimension of a sample in case of constant free space.

Figure 64 displays the coherence of burst pressure and wall thickness graphically. A free space value of 75% correlates to a D_i/D_o ratio of 1.15, 64% free space correlates to a D_i/D_o ratio of 1.25 and 56% free space correlates to a D_i/D_o ratio of 1.33. In each case, the graphs show a maximum burst pressure of a wall thickness of about 40-50µm. At samples with lower wall thickness, defects caused by shipping and handling may have larger influence and lower

the strength appreciable whereby samples with lower wall thickness than 50 µm show lower burst pressures. At the same time, these samples show higher deviation of the average burst pressure. The higher deviation suggests the presence of further influences, such as defects compared to the samples with higher wall thickness and lower spreading burst pressure values.
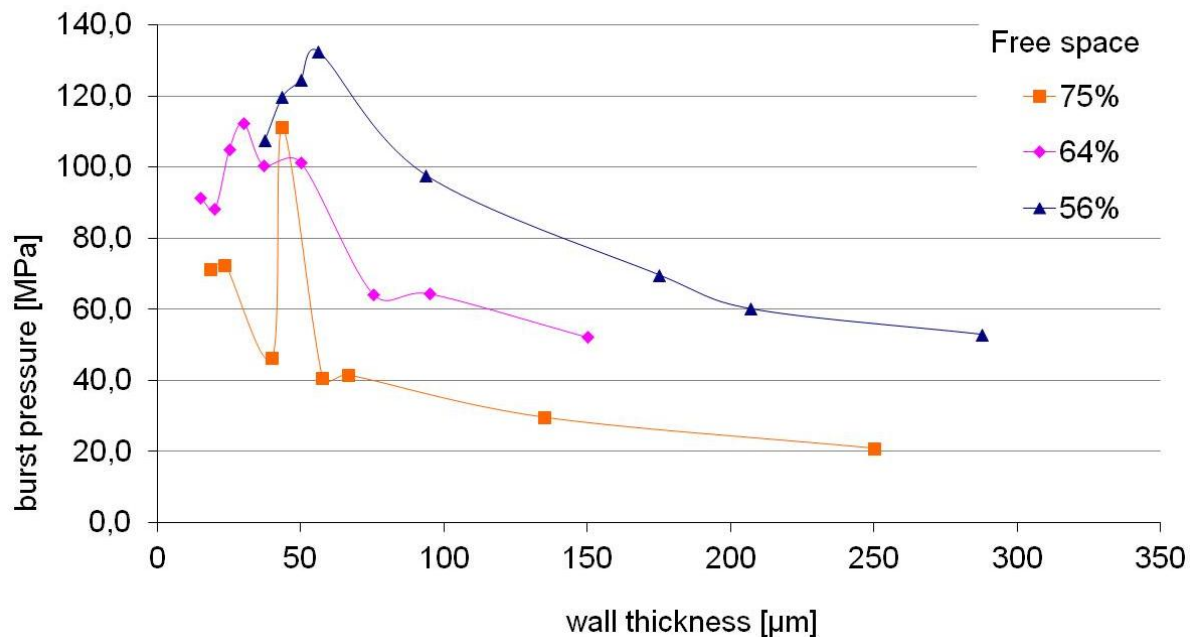
Figure 64: Dependence of burst pressure on wall thickness at round single fibers with fixed ratio of inner and outer diameter [169]

For a wall thickness higher than 50µm, the results fully correspond to the Griffith theory of increasing strength at decreasing sample size. That circumstance can be explained with the existence of defects. In larger samples, the possibility of large strength-influencing defects is higher and therefore, the statistical strength will be lower. Precisely because the FEM simulation neglects the possibility of defects, the Griffith's theory of increasing strength with decreasing wall thickness cannot be approved by FEM simulation.

In summary, the former results show that fibers with higher free space show lower strength. Related to the target of reaching possibly high storage capacities, a compromise between possibly high free space ratio and sufficiently high burst pressure value needs to be determined. According to the large difference of theoretical and practical strength of glass, FEM simulation is not suitable for that purpose.

On the other hand, samples with smaller dimension show higher strength at constant free space and therefore they are able to withstand higher inner pressure. The fibers need to be as small as possible, in order to increase the gravimetric storage capacity. Due to the fact that this phenomenon depends on randomly emerging defects, this relationship cannot be explained with FEM simulation because the material is assumed to be defect free.

5.6.5 Combination Of Materials With Varying Young's Modulus To A Single Fiber

Further examinations dealing with the influence of combining fibers with different properties were examined. Two fibers with different Young's modulus of 73100 MPa and 67100 MPa were combined. A fiber is placed inside a second, larger fiber. The outer diameter of the inner fiber is equal to the inner diameter of the larger outer fiber, whereby the combination of both fibers yield a single fiber made of two different materials. The overall size of the combined structure is D_o=400µm and D_i=300µm, equally to the basic single fiber examined in chapter 5.6.2 "Behavior Of Round Single Fibers At Inner Pressure Treatment". Fibers made of different glasses show varying stress distribution as shown in Figure 65. Using a glass with higher Young's modulus as inner fiber leads to higher stress of the inner surface than of a conventional fiber comprised of one kind of glass. The higher Young's modulus leads to lower expansion which results in reduced stress on the inner surface of the outer fiber. Thus, the total stress occurring at the outer fiber is lowered compared to a fiber made from one material. The expansion is about 0.71 µm which corresponds to 0.178% of the outer diameter.

In Figure 66 the position of the two fibers was changed so the inner fiber shows lower Young's modulus and thereby higher expansion at constant pressure. Since the expansion of the inner fiber is inhibited by the outer fiber the maximum stress at the inner surface is lowered. On the other hand, the increased pressure on the inner surface of the outer fiber leads to slightly increased stress of the outer surface of the fiber. Thereby, the expansion slightly increased and shows a value of 0.717 µm which corresponds to 0.179 % of the outer diameter.
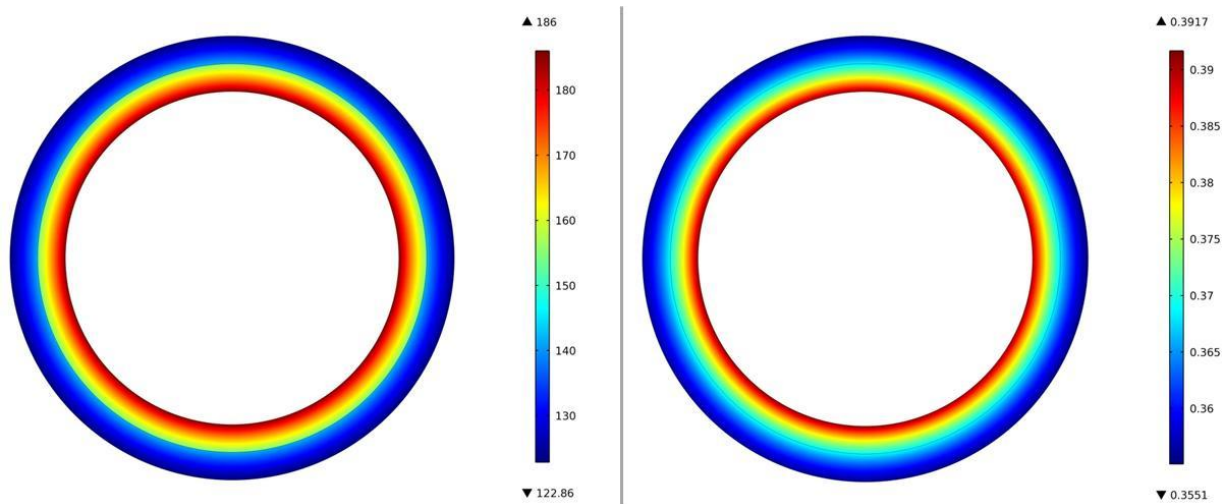
Figure 65: Occurring first principal stress in MPa (left) and expansion in µm (right) at a round single fiber with D_o=400µm and D_i=300µm constructed by plugging a fiber with higher Young's modulus as inner fiber with 50 MPa applied inner pressure
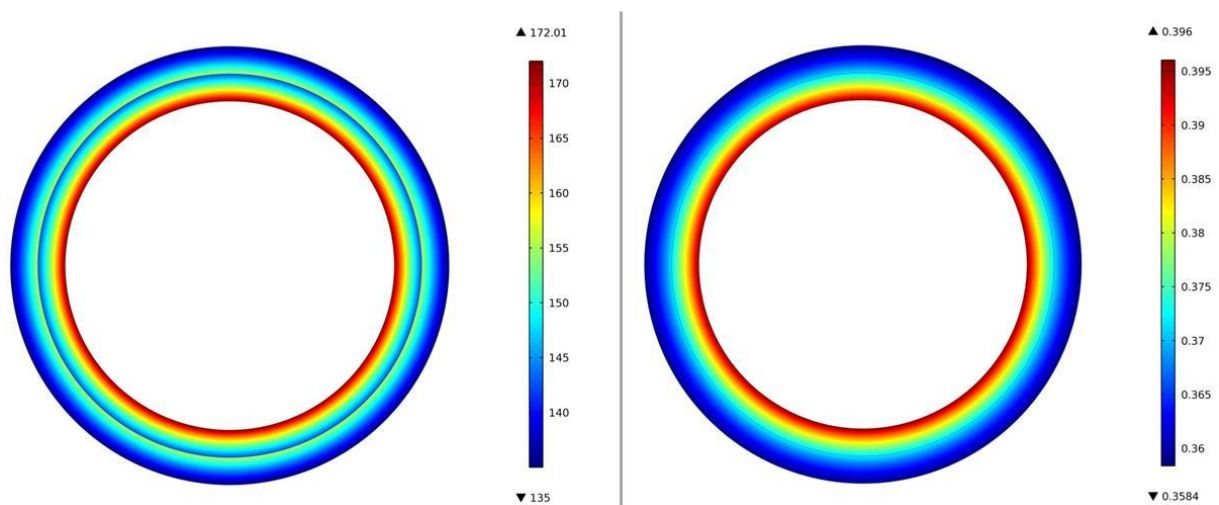
Figure 66: Occurring first principal stress in MPa (left) and expansion in µm (right) at a round single fiber with D_o=400µm and D_i=300µm constructed by plugging a fiber with lower Young's modulus as inner fiber with 50 MPa applied inner pressure.

In order to determine the influence of mixed-material single fibers, several test series were examined with single fibers by R. Meyer [169], which consist of different materials. Primarily, the used materials differentiate in the coefficient of thermal expansion (CTE). The

composition and the Young's modulus of C1S-glass is not available, but will differ from the Young's modulus of C5-glass (utterance of the manufacturer). The CTE of the used C5-glass is with $5.5K^{-1}10^{-6}$ higher than the CTE of C1S-glass with $4.65K^{-1}10^{-6}$. Table 49 shows the results, as well as the calculates critical stress at the highest measured burst pressure. The first called material in column "material" is the outer material of the sample and the second one poses the inner material. Due to these test results, the samples with the C1S-glass as inner material show a decreased critical stress than all other material combinations. Thereby, the combination of different materials in one single fiber may have an influence of the strength of the single fiber. Caused by missing information about composition and Young's modulus of C1S-glass, an direct comparison to the results of FEM simulation cannot be done.

Table 49: Burst pressure test results and critical stress of single fibers made of mixed material

material	OD [µm]	ID [µm]	Wall thickness [µm]	FS [%]	Max. burst pressure [MPa]	Critical stress [MPa]
C5	222	178	22	64	99.8	504
C5	207	178	15	73.6	60.5	417
C5–C5	203	178	13	76.6	62.6	489
C5-C5	305	267	19	76.6	52	417
C5-C5	400	356	22	79	45.9	417
C5-C1S	203	164	20	65	62	315
C5-C1S	381	308	37	65	50.5	260
C1S-C5	203	163	22	60	96.2	444
C1S-C5	305	248	36	60	87.4	370
C1S-C5	394	309	47	60	84.8	355

5.6.6 Round Single Fibers Bundled To Hexagonal Structures

In order to increase the free volume for gas storage, the single fibers need to be bundled to complex structures. Due to the expansion of the single fibers, bundling leads to further problems like increased stress values at the connection points of the fibers. The subsequently following sub-chapters discuss the influence of varying shape, dimension and amount of single fibers on the occurring stress and expansion in a structure.

The stress and expansion was calculated for a structure built of 19 borosilicate glass single fibers with D_i=300µm and D_o=400µm by packing single fibers according to the principle of close-packing of spheres, which results in a hexagonal structure. The pressure was supposed to act only at the inner surfaces and not at the emerged interspaces between the fibers. As opposed to single fibers, areas of increased stress (stress peaks) occur at the connection points of the fibers, whereby crack growth will be supported in this area. This is reasoned by the expansion of every single fiber. At the connection points the fibers are prevented from consistently expanding. The stress distribution and the expansion are shown in Figure 67. The left picture shows the whole structure and the right picture offers an enlarged view to the most significant part.
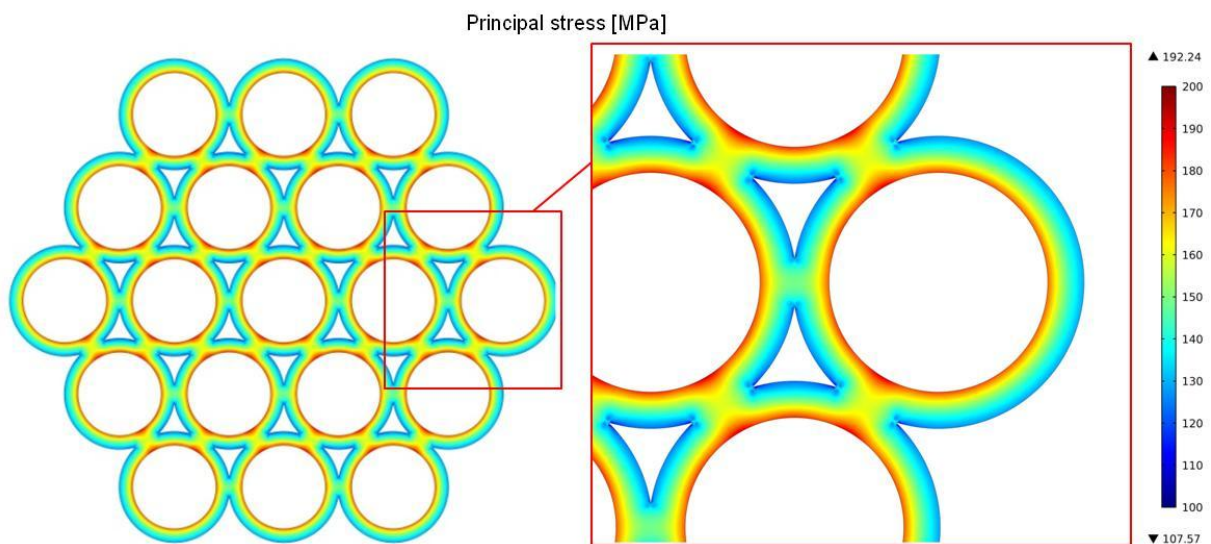
Figure 67: Occurring first principal stress in a structure made of 19 round single fibers with D_o=400µm and D_i=300µm bundled according to the principle of close packing spheres with 50 MPa applied inner pressure

The expansion is displayed in the left picture of Figure 68, whereby the expansion of the fibers figures up from the center fiber to the outer ones. The right picture of Figure 68 demonstrates an enlarged view. The black line shows the position of the outer fiber without pressure load as comparison to the expanded wall at 50 MPa. The total expansion of the structure is about 3.6 µm. If the outer diameter is about 2000µm from edge to edge, the expansion is about 0.18%. This correlates to the value of single fibers of the same dimension (chapter 5.6.2). The increased expansion from the center of the structure to the outer side is caused by the fact that the expansion is visualized as displacement. Thereby, the expansion of the center fiber displaces the neighbored ones. These fibers will also expand whereby the displacement of the fibers in the third row is even higher.
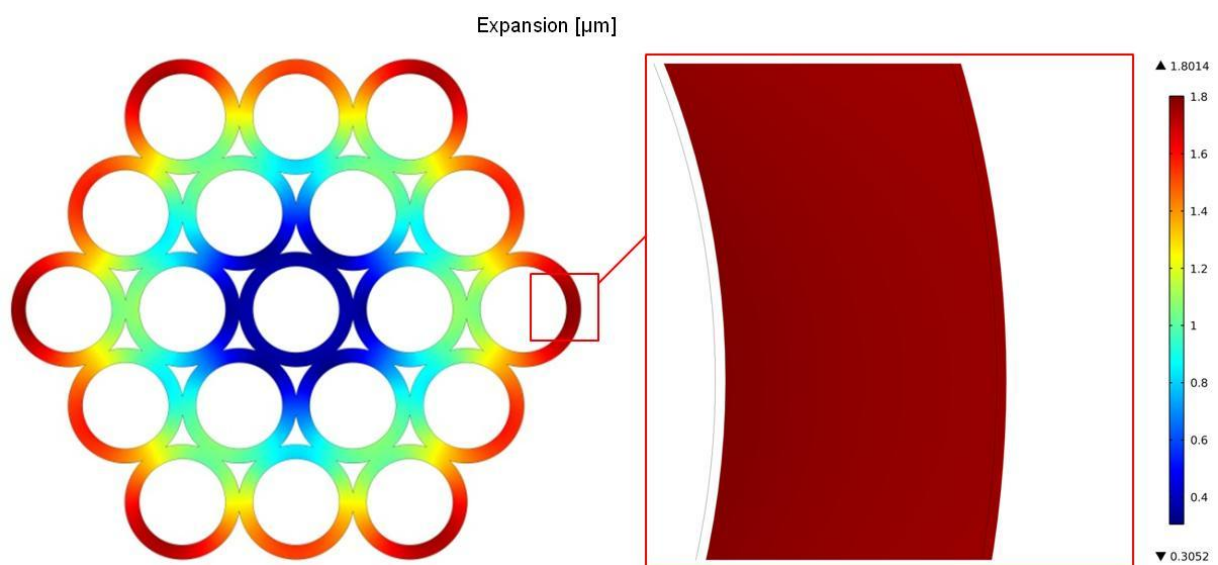
Figure 68: Occurring expansion in a structure made of 19 round single fibers with D_o=400µm and D_i=300µm bundled according to the principle of close packing spheres with 50 MPa applied inner pressure

Increasing the pressure inside the structure continuously shows a similar behavior to that of the single fiber (chapter 5.6.2). The table in Figure 69 displays the minimum and maximum internal stress as well as the expansion. The left column displays these values for an applied pressure at the inner surface of 5 MPa. Ongoing to the right, the applied pressure is increased stepwise by 10 MPa up to 45 MPa in the right column. The pictures above the columns visualize the calculated stress in the structure at the applied pressure. As illustrated in Figure 69 the minimum and maximum stress, as well as the expansion raise continuously

at a constant rate. The minimum pressure increases from 11 MPa to 97 MPa. The maximum stress increases from 19 MPa to 173 MPa. Consequently, a nine times higher applied pressure leads to nine times higher minimum and maximum stress values. Also the value of expansion is nine times higher at 45 MPa applied pressure.
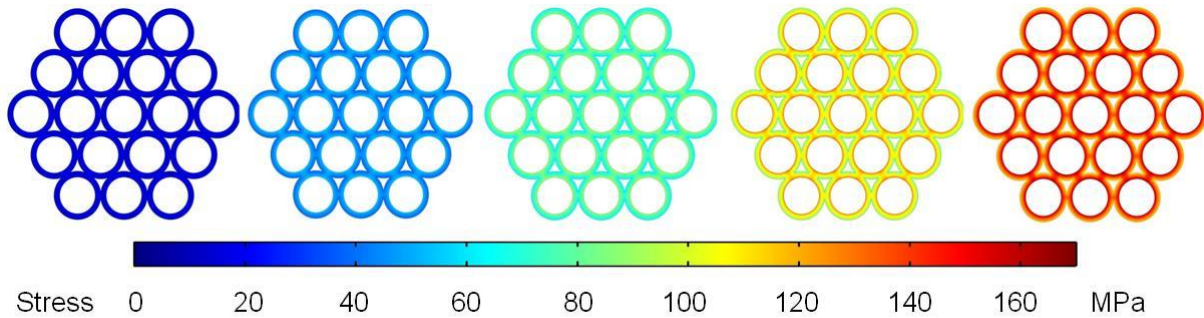
Pressure inside [MPa]				
5	15	25	35	45
Minimum stress [MPa]				
11	28	54	75	97
Maximum stress [MPa]				
19	64	96	134	173
Expansion [µm]				
0.36	1.06	1.78	2.52	3.24

Figure 69: Behavior of first principal stress and expansion during continuous pressure increase at a structure made of 19 round single fibers made of borosilicate glass with D_o=400µm and D_i=300µm

Figure 70 demonstrates the modeling results graphically. The diagram displays the occurring stress in MPa at the primary ordinate (left) and the expansion in µm at the secondary ordinate (right). The abscissa shows the applied pressure in MPa. The graphs of the minimum and maximum stress (red and green graph) plotted against the applied pressure show a straight trend. Equally to the single fiber (chapter 5.6.2) the difference between minimum and maximum stress increases with higher applied pressure. That is related to the fact that the maximum stress is constantly about two times higher than the minimum stress.

The blue graph, which shows the expansion of the structure against the applied pressure, also shows a straight course.
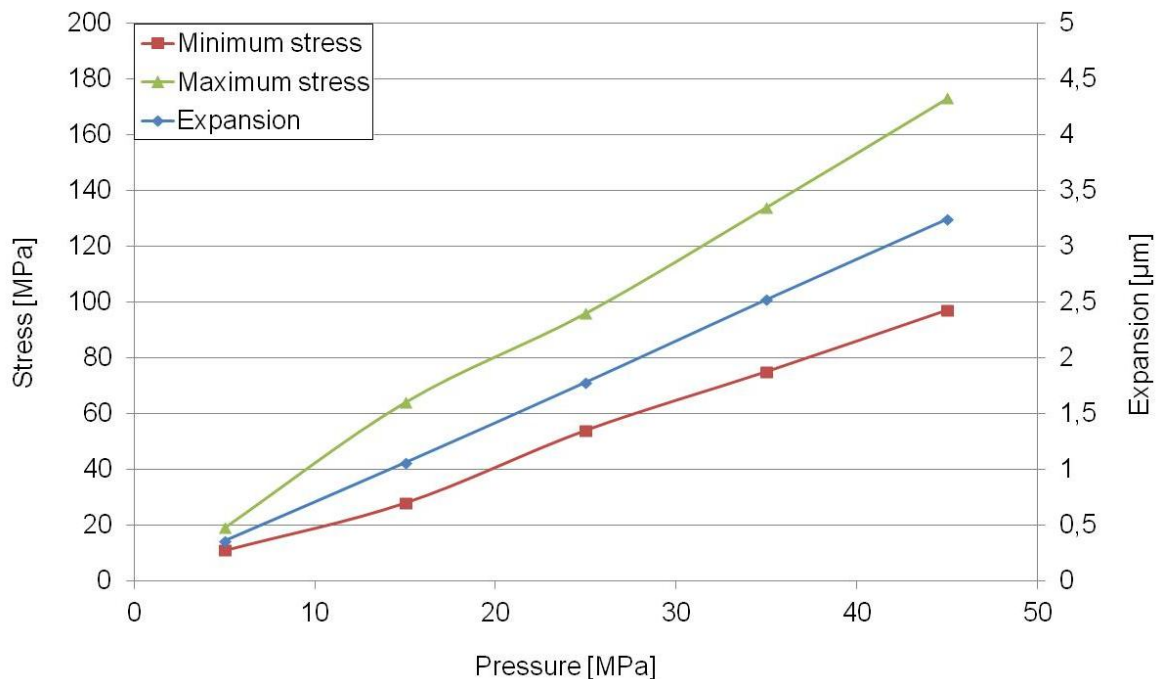
Figure 70: Dependence of occurring minimum and maximum first principal stress (red and green graph) as well as expansion (blue graph) on the applied pressure at a structure made of round single fibers with D_o=400µm and D_i=300µm

So far, the structure of 19 bundled fibers shows similar behavior to that of a single fiber. A more precise examination of stress and expansion value in relation to the structure size considers the construction of larger models. Structures of 19, 61 and 127 single fibers (each having the dimension of D_o=400µm and D_i=300µm) have been simulated and compared to a single fiber with the same dimension. The fibers were bundled according to the principle of close-packing of spheres and the results are displayed in Figure 71. From the left to the right column the amount of single fibers has been increased stepwise. In the first step, 19 fibers were bundled to form a hexagonal structure, as previously discussed. With every further step two rows of fibers were added. The resulting structures consist of 61 fibers in the third column and 127 fibers at the fourth column. The structures and the occurring stress of applied pressure of 50 MPa are shown above the associated column of the table.

The value of occurring minimum as well as maximum stress are nearly constant of any sample, independent of the amount of fibers. The maximum stress value of 192 MPa still occurs at the connection points of the fibers. The remaining stress at the inner surface of the fibers is constantly 179MPa. This value is equal to the stress at the inner surface of the single fiber. The total expansion of the structures is about 0.18% of the outer diameter. The expansion of a single fiber with equal dimension is about 0.17% of its outer diameter.

That demonstrates that building large structures by bundling round single fibers according to the principle of close-packing of spheres leads to constant internal stress and expansion independent on the amount of bundled fibers. Due to this results, the simulation of structures with 19 single fibers is also convincing for structures, which are made of a larger number of single fibers.
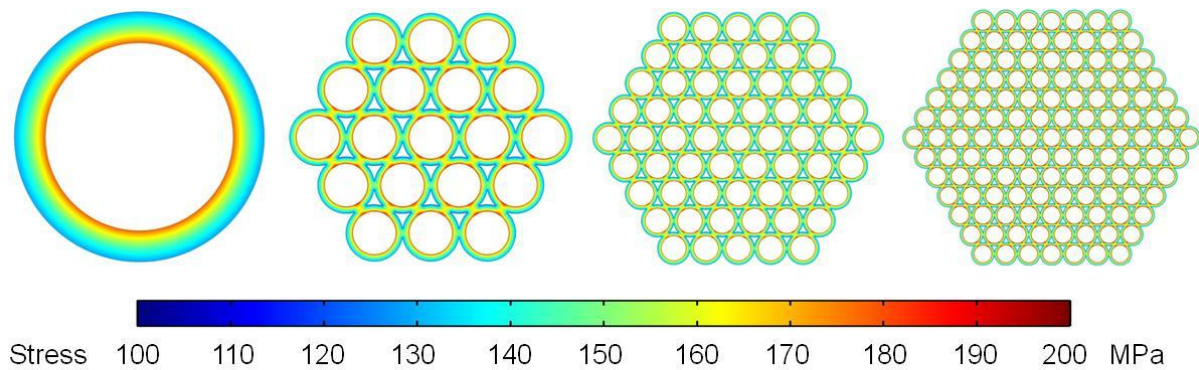
Amount of single fibers			
1	19	61	127
Minimum stress [MPa]			
129	108	108	102
Maximum stress [MPa]			
179	192	192	192
Expansion [µm] / [%]			
0.68 / 0.17	3.6 / 0.18	6.4 / 0.18	9.28 / 0.18

Figure 71: Influence of increasing amount of round single fibers with D_o=400µm and D_i=300µm on the occurring first principal stress and expansion of a structure bundled according to the principle of closed packing spheres with 50 MPa applied inner pressure

The diagram, which is displayed in Figure 72, plots the occurring stress in MPa (primary ordinate, left) and the expansion in µm (secondary ordinate, right) against the amount of fibers in a structure. The lower red line shows the minimum stress and the upper green line displays the maximum stress in MPa. The minimum and maximum stress keeps nearly constant of the bundled structures. Merely the single fiber shows lower maximum but higher minimum stress. The expansion in µm which is visualized by the blue graph grows with increased sample size. As already mentioned, this behavior leads to constant total expansion in % independent of the amount of fibers in the structure.
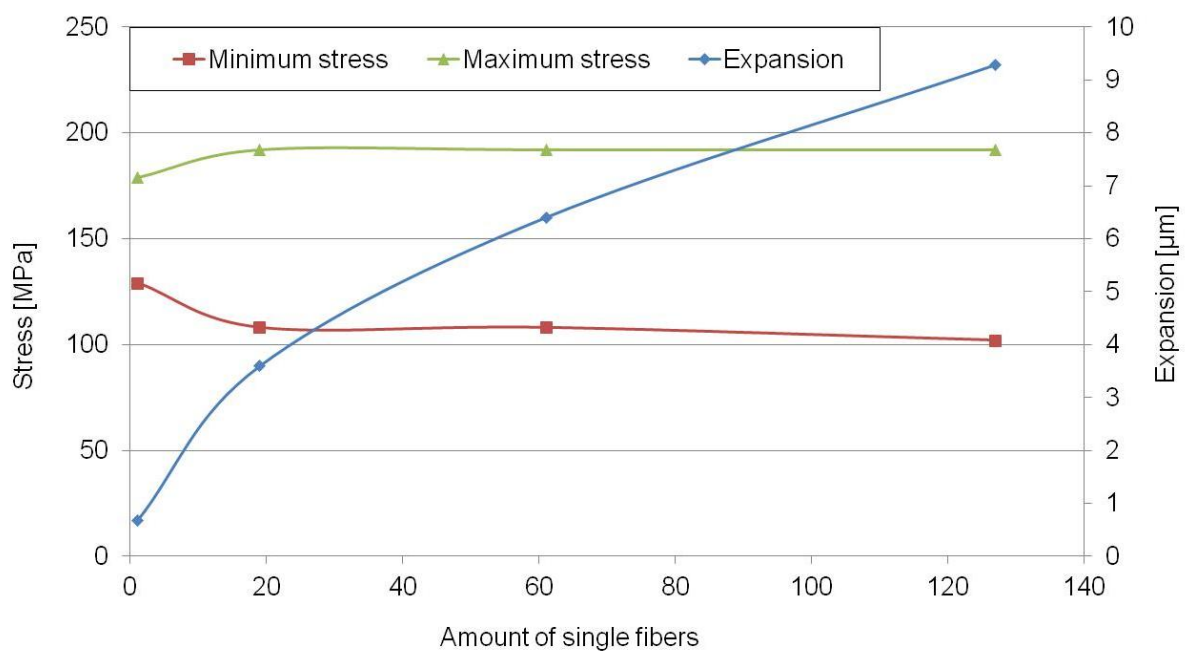
Figure 72: Dependence of minimum and maximum first principal stress as well as expansion on the amount of single fibers in a structure made of round single fibers with D_o=400µm and D_i=300µm with 50 MPa applied inner pressure

In practical application it is not possible to avoid pressure load inside the interspaces between the single fibers when connecting them as described in chapter 4 "Experimental". The pressure inside the interspaces works against the connection of the fibers which leads to areas of increased stress inside the material as shown in Figure 73 (left). The maximum stress is with 864MPa more than 4 times higher than without applied pressure inside the interspaces (192MPa). The maximum expansion is about 4.2µm, which conforms to 0.21% of

the structures outer diameter of about 2000µm and is almost equal to the strain of 0.18% that occurs in the same structure without loaded interspaces.

Furthermore, the unsolicited pressure inside the interspaces leads to additional deformation which is exaggeratedly displayed in Figure 73 (right), the visualized expansion is multiplied by 100. If the fibers are assumed to expand without breaking, they lose their round shape and approach to the hexagonal shape. This imbalanced deformation, visualized by arrows in Figure 73 (right), causes additional areas of increased stress at the inner surface of the fibers, noticeable at the red areas on the inner surface of the fibers of about 400MPa. Furthermore, the occurring negative stress indicates the presence of compressive stress. The inner surface of the interspaces will be compressed, which is caused by the bending deformation the material.
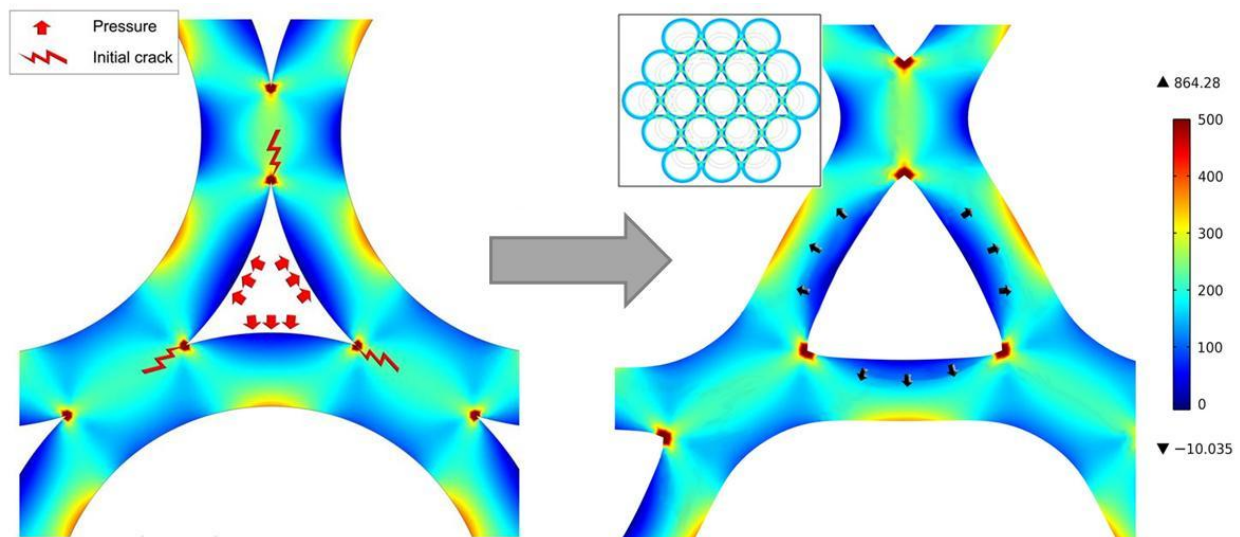
Figure 73: Effect of applied pressure (50 MPa) inside the interspaces between round single fibers on the first principal stress with visualized areas of the initial crack (left) and exaggerated displayed deformation (right) including the whole entire structure

Results of experimental tests confirmed the low strength compared to single fibers. Several analogue samples with an outer diameter D_o=4.15mm were examined and their burst pressure was determined. The results are already discussed in chapter 5.3.2 "Round Structure Made Of Round Hollow Glass Fibers With Interspaces And Outer Glass Shell". The highest reached burst pressure values of the tested structures A1 and A2 were constantly is a range of about 10 MPa. The highest measured values are 12.7MPa at structure A1 and

8.8MPa at structure A2. Microscopic pictures of two examples with related highest measured burst pressure values are presented in Figure 74. The small pictures in the upper left corners show the entire structure whereby the large pictures show an enlarged view of the connection points of the fibers. Conditioned by the manufacturing process, the fibers were placed in a glass tube to avoid leaking gas through the interspaces. A further problem of this construction is the automatically applied pressure to the outer protection shell through the interspaces, whereby the principle of a multi vessel storage system is no longer given.
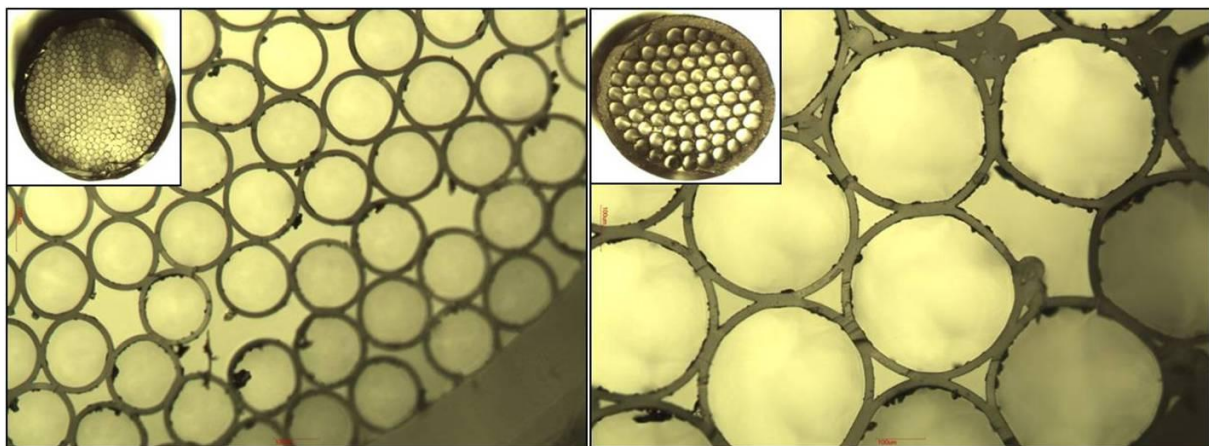
Maximum burst pressure value [MPa]	Maximum burst pressure value [MPa]
12.7	8.8

Figure 74: Microscopic view of structure made of bundled round single fibers and open interspaces (A1 left), respectively partially filled interspaces (A2 right) and the correlating the maximum burst pressure value

5.6.7 Round Single Fibers Bundled To Hexagonal Structures With Closed Interspaces

As interspaces between single fibers in complex structures seems to be problematic, structures without voids were modeled. For that purpose the 19-fiber-structure shown in Figure 67 was used with the same specification, but the interspaces were filled with the same glass the fibers are made of. In real production process, small solid glass fibers were placed inside the interspaces during production process. While drawing the structures these glass sticks molt and closed the interspaces. The left picture of Figure 75 shows the whole structure and the right picture offers an enlarged view of the most significant part. The

maximum stress value is about 204MPa and conforms to the structure with open interspaces but pressure load only inside the fibers, as already mentioned in

Figure 67 (192MPa). Equal to that structure, the maximum stress is located at the connection points of the single fibers.
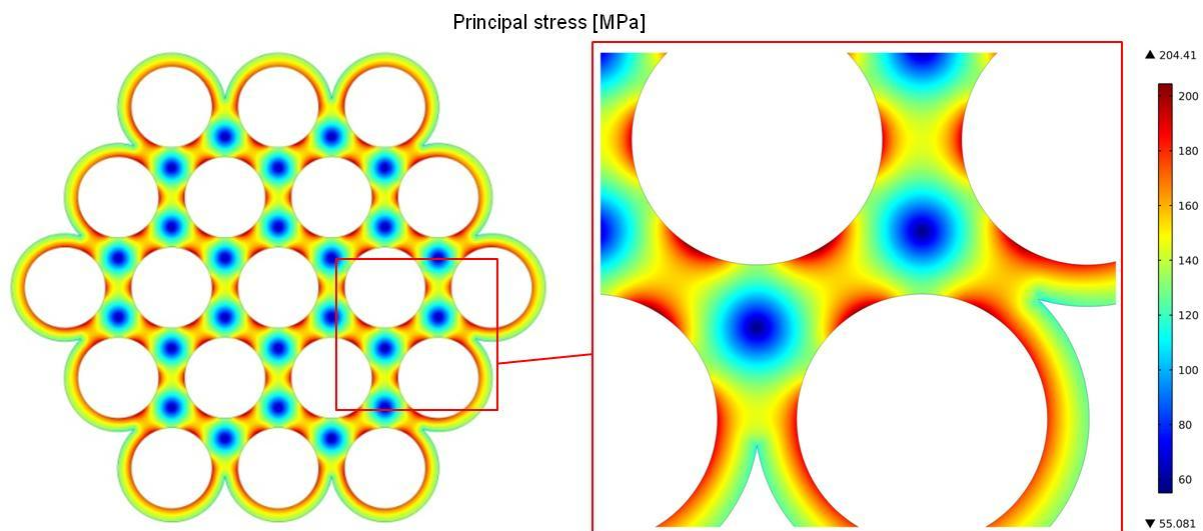
Figure 75: Occurring first principal stress [MPa] in a structure made of 19 round single fibers with D_o=400µm and D_i=300µm bundled according to the principle of close packing spheres and closed interspaces with 50 MPa applied inner pressure

A further property, which is not influenced by filling the interspaces, is the total expansion which is displayed in Figure 76. Similar to the 19-fiber-structure with interspaces, (Figure 67), the expansion increases from the center of the structure to the outer side because the expansion is visualized as displacement. The expansion of the structure is about 3.34µm, which results in a total expansion of 0.17%. This value is equal to the total expansion of the comparable structure with open interspaces.
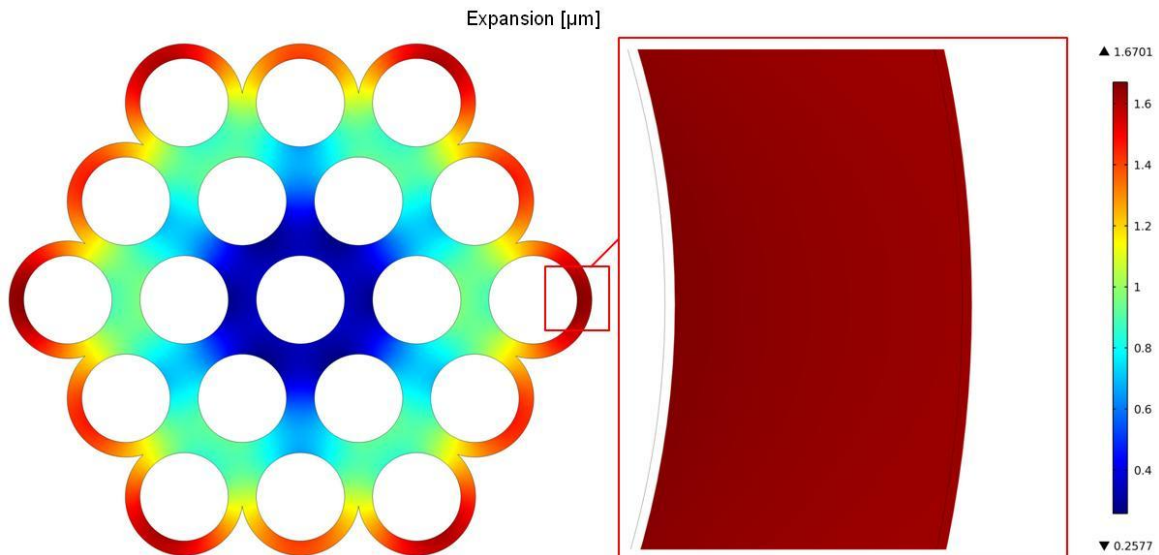
Expansion [µm]

Figure 76: Occurring expansion [µm] in a structure made of 19 round single fibers with D_o=400µm and D_i=300µm bundled according to the principle of close packing spheres and closed interspaces with 50 MPa applied inner pressure

The filling of the interspaces with glass is a plausible method for guaranteeing the pressure to be applied only inside the single fibers. The additional glass has a positive influence to the strength by decreasing the occurring stress during pressure load.

Subsequently, an outer shell made of the same glass such as the fibers was added as shown in Figure 77 (left). The outer fibers are assumed to be protected against defects on the outer surface caused by handling or the influence of moisture. During the manufacturing process, the structure was placed inside a glass tube and the interspaces were filled with glass. The resulting massive appealing structure shows in total a well distributed stress with the only maximum stress peaks of 194 MPa at the six fibers which represent the corners of the hexagonal inner structure. Furthermore, the stress at the connection points of the single fibers is reduced to about 100 MPa up to 150 MPa. This implies a shift of the maximum stress areas from the connection points of the fibers to the outer corners of the structure caused by the outer glass shell. The total expansion of the structure is about 0.09% of the outer diameter and shown in Figure 77 (right). Thus, the expansion is nearly halved by the outer glass shell.
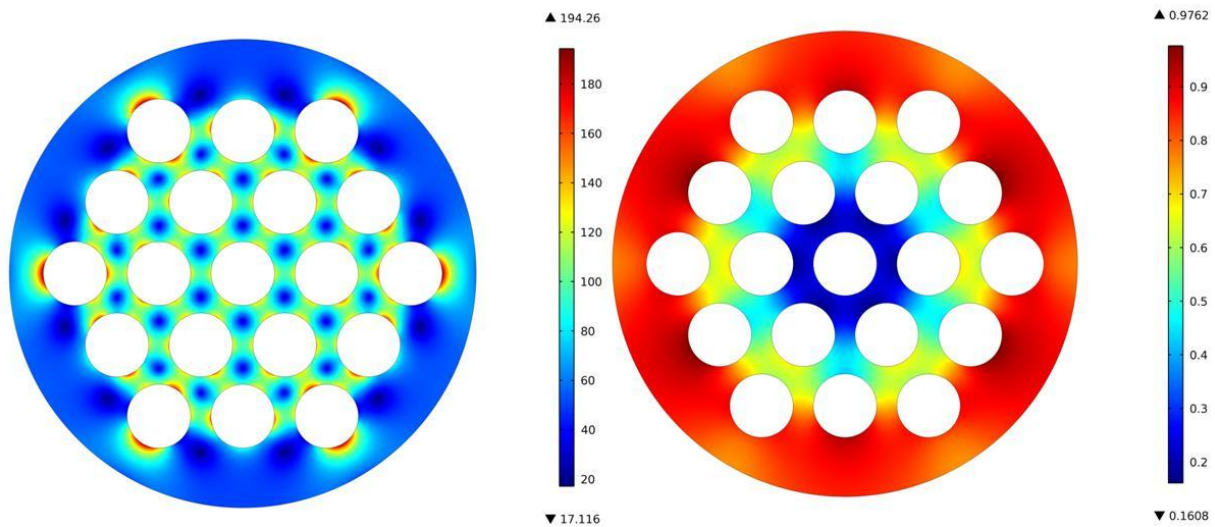
Figure 77: Occurring first principal stress (left) and expansion (right) in a structure made of 19 round single fibers with D_o=400µm and D_i=300µm bundled according to the principle of close packing spheres with closed interspaces and an additional outer glass shell with 50 MPa applied inner pressure

Determining the burst pressure of comparable structures in experimental tests leads to high strength resulting in a maximum burst pressures of 56.0 MPa at the tested structure A4 thin, respectively 87.6MPa MPa at structure M1 (chapter 5.3.3). Structure A1 is displayed in microscopic view in Figure 78 with the corresponding maximum burst pressure values of structure A1 and A2. The right picture shows an enlarged section of the structure which is entirely shown on the left picture.
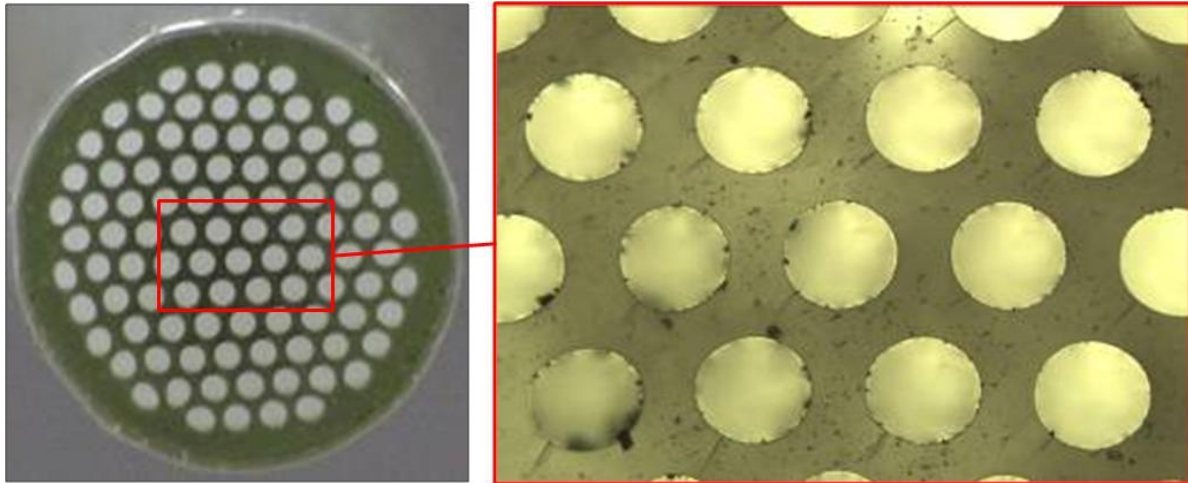
Maximum burst pressure values [MPa]	
Structure A4 thin	Structure M1
56.0	87.6

Figure 78: Microscopic picture of structure A4 thin, made of round single fibers bundled according to the principle of close packing spheres with closed interspaces and an additional outer glass shell and the correlating average burst pressure values of the comparable structures A4 thin and M1

Similar to single fibers with round shape stepwise increase of the applied pressure to such a structure with outer glass shell and closed interspaces demonstrates a linear dependence of minimum and maximum stress as well as expansion from the applied pressure. The calculated results are displayed in Figure 79. Increasing the pressure stepwise by 10 MPa up to 45 MPa, the stress increases at each step constantly about 3 MPa of the minimum stress and about 40 MPa of the maximum stress. Due to this fact, the stress values increase linear to the increasing pressure, similar to the behavior of the corresponding single fiber at stepwise pressure increase. A nine times higher applied pressure leads to about nine times higher values of minimum and maximum stress. The expansion also shows a steady increase.

Pressure inside [MPa]				
5	15	25	35	45
Minimum stress [MPa]				
2	5	9	12	15
Maximum stress [MPa]				
19	58	97	136	175
Expansion [µm]				
0.195	0.58	0.96	1.36	1.76
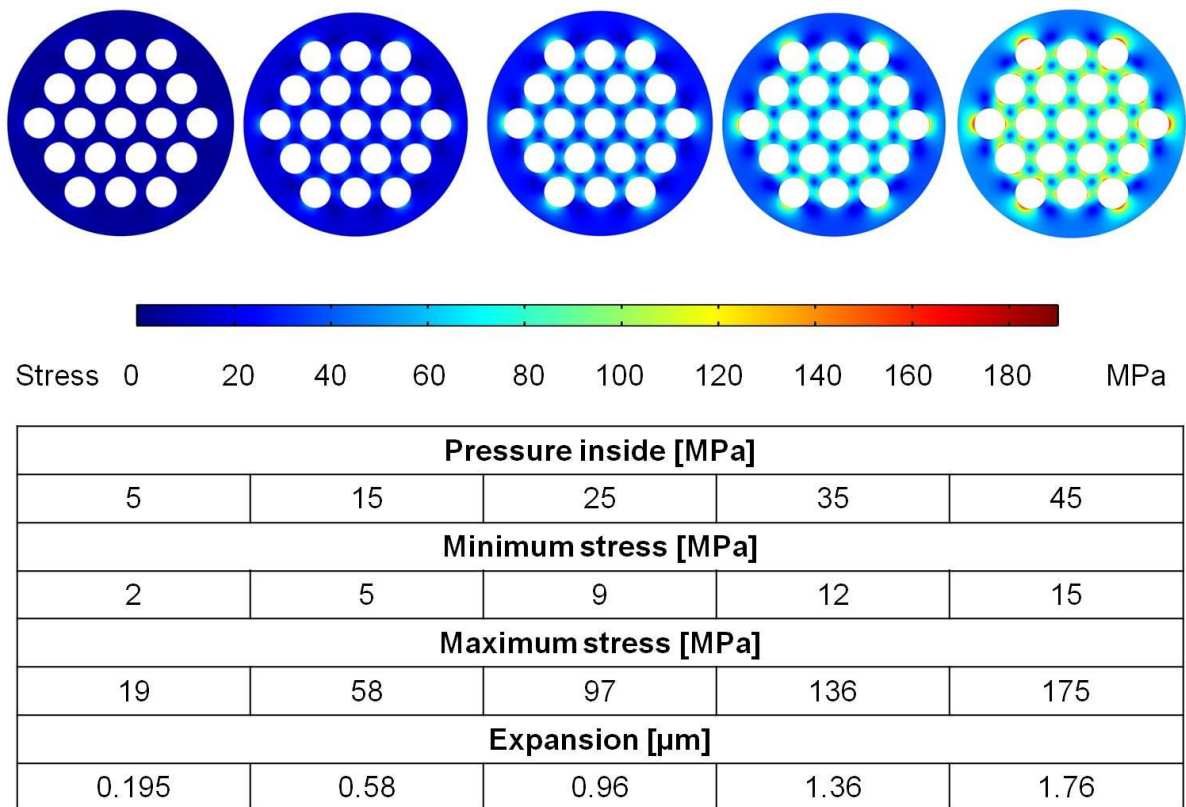
Figure 79: Behavior of first principal stress in MPa and expansion in µm during continuous pressure increase in a structure made of 19 round single fibers with D_o=400µm and D_i=300µm bundled according to the principle of close packing spheres with closed interspaces and an additional outer glass shell

The calculated values for stress and expansion, plotted against the applied pressure, are illustrated in Figure 80. The diagram displays the internal stress in MPa at the primary ordinate (left) and the expansion in µm at the secondary ordinate (right). The abscissa shows the applied pressure in MPa. The minimum and maximum stress (red and green graph) as well as the expansion (blue graph) of the fiber is linear dependent on the applied pressure. Related to that circumstance, the graphs follow a straight trend.
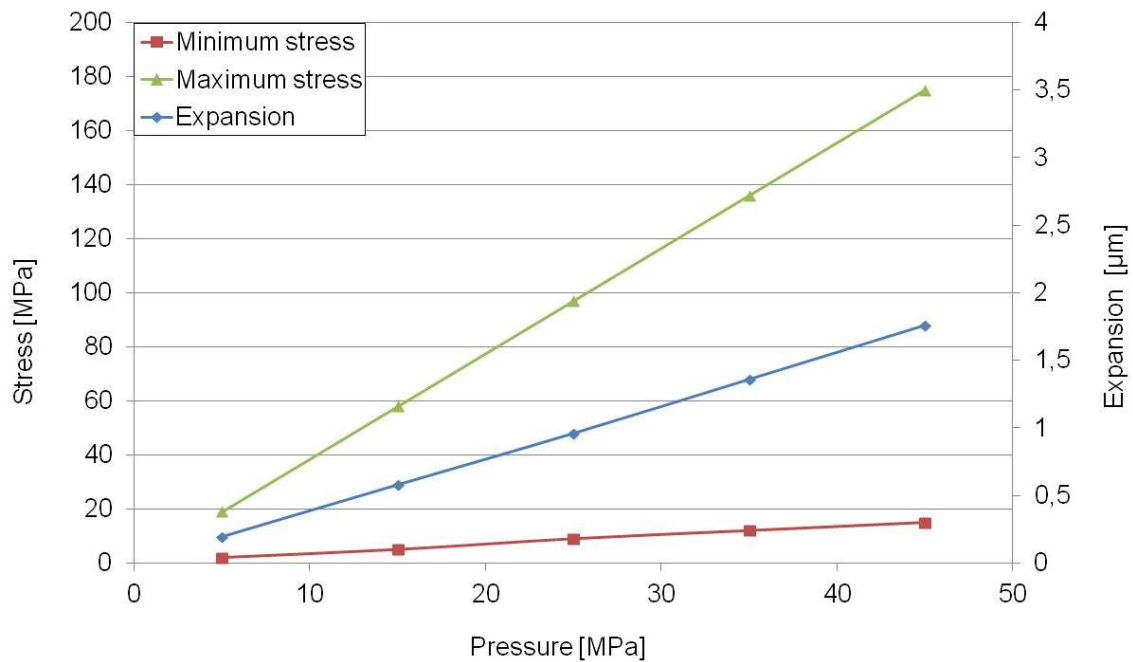
Figure 80: Dependence of minimum and maximum first principal stress as well as expansion of the amount of single fibers in a structure made of 19 round single fibers with D_o=400µm and D_i=300µm with closed interspaces and an additional outer glass shell

The additional material of the filled interspaces and the glass shell leads to higher weight of the structure and a lower percentage of free inner volume, by which the gravimetric and volumetric storage capacities are decreased. By filling the interspaces with lighter material, loss of gravimetric storage capacity will be diminished but the lower volumetric storage capacity keeps constant. Further on, new problems may occur. A differing heat expansion coefficient of the new material could come to diverse expansion of the different materials at temperature fluctuation. In case of lower expansion than the glass leaks may occur and if the expansion of the filling material is higher than of the glass new stress peaks may emerge.

5.6.8 Hexagonal Single Fibers Bundled To Hexagonal Structures

Interspaces will emerge always, when round single fibers are bundled. The same time, the volumetric and gravimetric storage capacities are lowered. In order to deal with this topic the shape of the single fibers was changed to hexagonal. The wall thickness of the modeled fiber is 25 µm. Comparable to the already examined round single fibers the outer diameter

measured from one surface to the opposed surface (flat-to-flat) is 400µm. Compared to the examined round single fibers the inner diameter (flat-to-flat) is increased to 350µm.

Figure 81 shows the peaks of maximum stress of 3300MPa at the corners of single fibers in hexagonal shape. Further areas of increased stress occur in the middle of the straight walls. These stress areas have a value of about 1000MPa and are caused by bending deformation which is displayed in Figure 83.
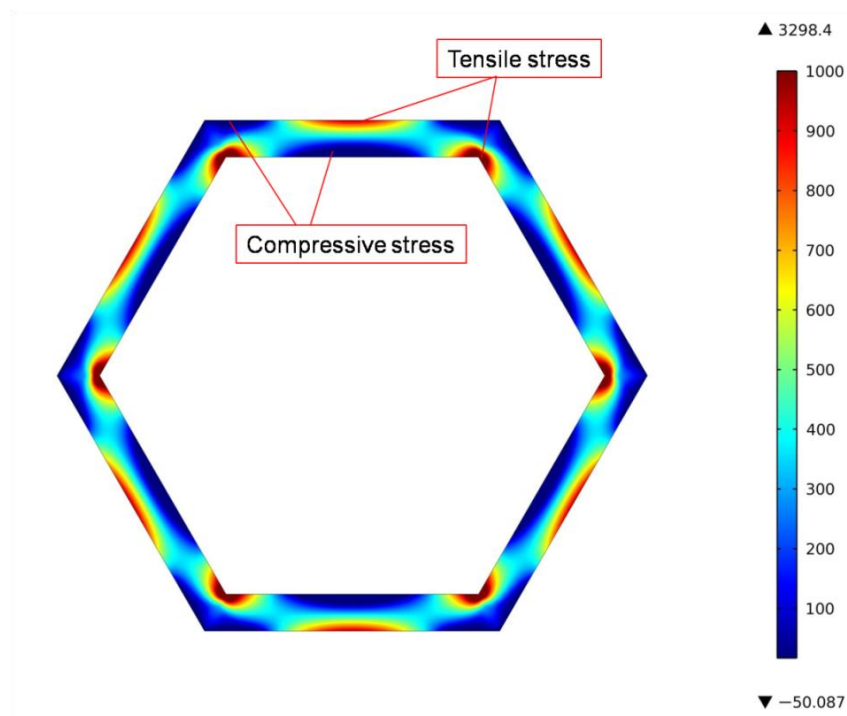
Figure 81: Occurring tensile stress (positive stress values) and compressive stress (negative stress values) in MPa in a single fiber with hexagonal shape with D_o=400µm and D_i=350µm flat-to-flat made of borosilicate glass with 50 MPa applied inner pressure

Furthermore, hexagonal fibers show compressive stress, as demonstrated in Figure 82. The highest compressive stress with a value of about 50 MPa emerges at the inner straight walls. Further compressive stress with a value of about 10 MPa can be found around the outer edges. These surfaces are clinched because of bending deformation. Coherent to this, the opposed surface is exposed to increased tensile stress.
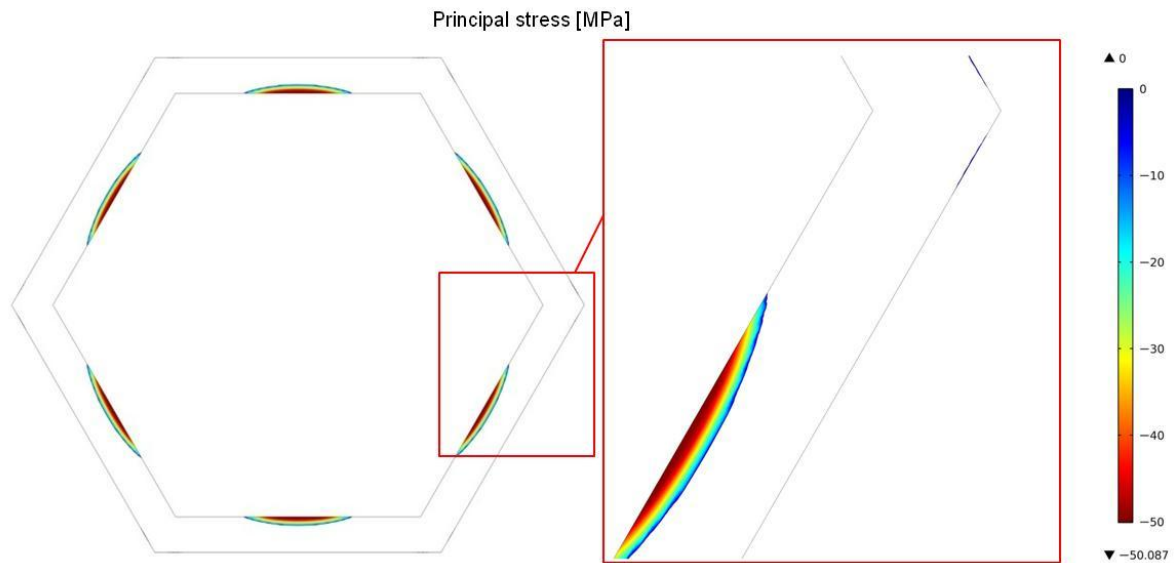
Figure 82: Separately displayed compressive stress in MPa in a single fiber with hexagonal shape with D_o=400µm and D_i=350µm flat-to-flat with 50 MPa applied inner pressure

The expansion at the corners is about 0.6µm whereas its maximum of 2.3µm is in the middle of the straight walls, as illustrated in Figure 83. This imbalanced deformation leads to bending of the straight walls to the outer side and bending stress occurs. This bending stress is characterized by increased tensile stress at the outer surface of the straight walls and compressive stress at the inner surface of these walls. Figure 83 also illustrates the deformation of the material. The position of the material in unloaded condition is visualized by the black lines.
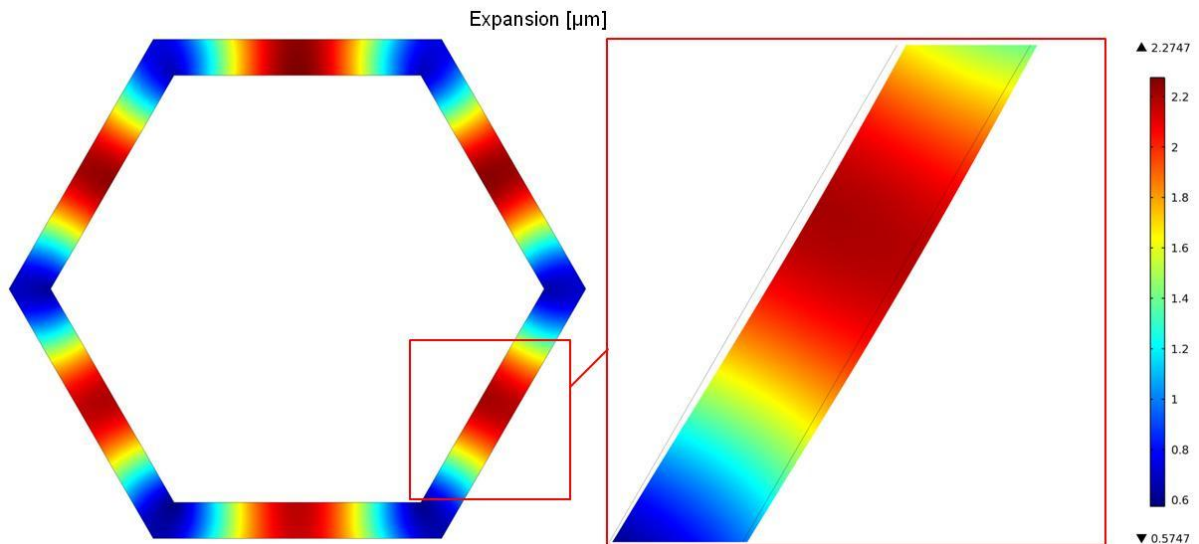
Figure 83: Occurring expansion in µm in a single fiber with hexagonal shape with D_o=400µm and D_i=350µm flat-to-flat with 50 MPa applied inner pressure

Stepwise increase of the pressure up to 45MPa inside the fiber leads to increasing maximum stress as well as expansion as displayed in Figure 84. The minimum and the maximum stress as well as the expansion at the sides and at the edges grow linear to the increased pressure. As result of the bending deformation during pressure load, compressive stress emerges at the outer edges and at the inner straight walls what is described as negative stress in principal stress calculation. The apparently decreasing negative minimum stress at increasing pressure indicates increasing compressive stress at stepwise pressure increase.
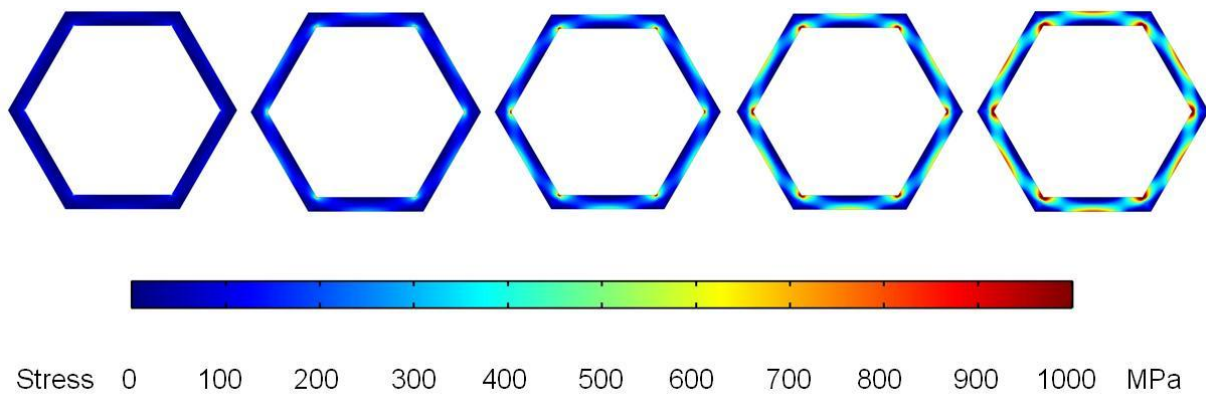
Pressure inside [MPa]				
5	15	25	35	45
Minimum stress [MPa]				
-5	-15	-25	-35	-45
Maximum stress [MPa]				
331	992	1652	2311	2970
Expansion [µm] side / edge				
0.4 / 0.1	1.4 / 0.4	2.3 / 0.7	3.2 / 1.0	4.1 / 1.3

Figure 84: Behavior of first principal stress and expansion during continuous pressure increase at a hexagonal single fiber with D_o=400µm and D_i=350µm flat-to-flat made of borosilicate glass

As visualized by the graph in Figure 85, the compressive stress as well as the tensile stress raises at increased applied pressure with the same rate as the applied pressure. Doubling the pressure results in doubled compressive stress and tensile stress. Thus, the graphs follow a linear trend, comparable to single fibers with round shape. Figure 85 illustrates this behavior with the red and the green graph, visualizing the dependence of the minimum and maximum stress on the applied pressure. The expansion, also displayed in Figure 85, needs to be differentiated to the expansion at the edges (blue graph) on the one hand and the expansion of the straight walls caused by bending deformation (purple graph). The expansion of the straight walls is permanently three to four times higher than at the edges. Nevertheless, both expansion values increase in linear way at constant pressure increase.
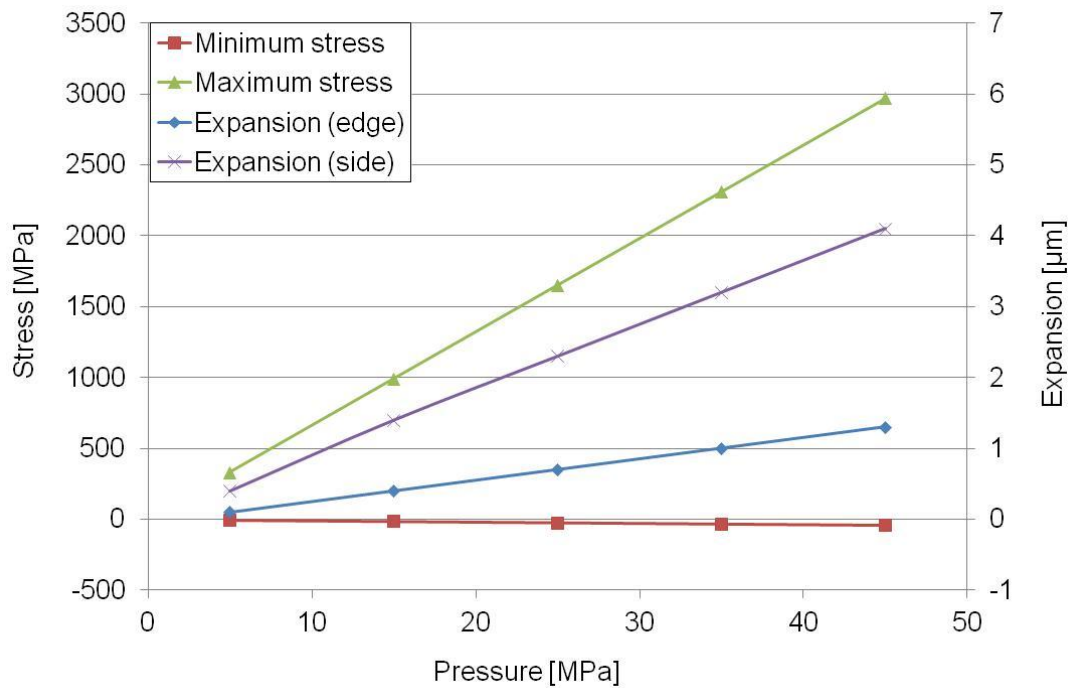
Figure 85: Dependence of minimum and maximum first principal stress as well as expansion on the applied pressure at hexagonal single fiber with D_o=400µm and D_i=350µm flat-to-flat made of borosilicate glass

A completely different behavior is observable after bundling such fibers to structures. The fibers were bundled to honeycomb structure. In this way no volume for gas storage is lost because of interspaces. Equally to the structure with round fibers, 19 fibers have been bundled for modeling. The diameter from one outer surface to the opposite outer surface is D_o=400µm. The wall thickness is halved to 25µm compared to the round single fibers. After bundling, the walls of two neighbored fibers add together to 50µm. The fact that any inner wall has the same pressure on both sides, as displayed by the arrows in Figure 86, inhibits bending of the walls.

At the marked in red outer walls there is no counter pressure. Related to this bending deformation to the outer side occurs what is visualized with the red bent walls.
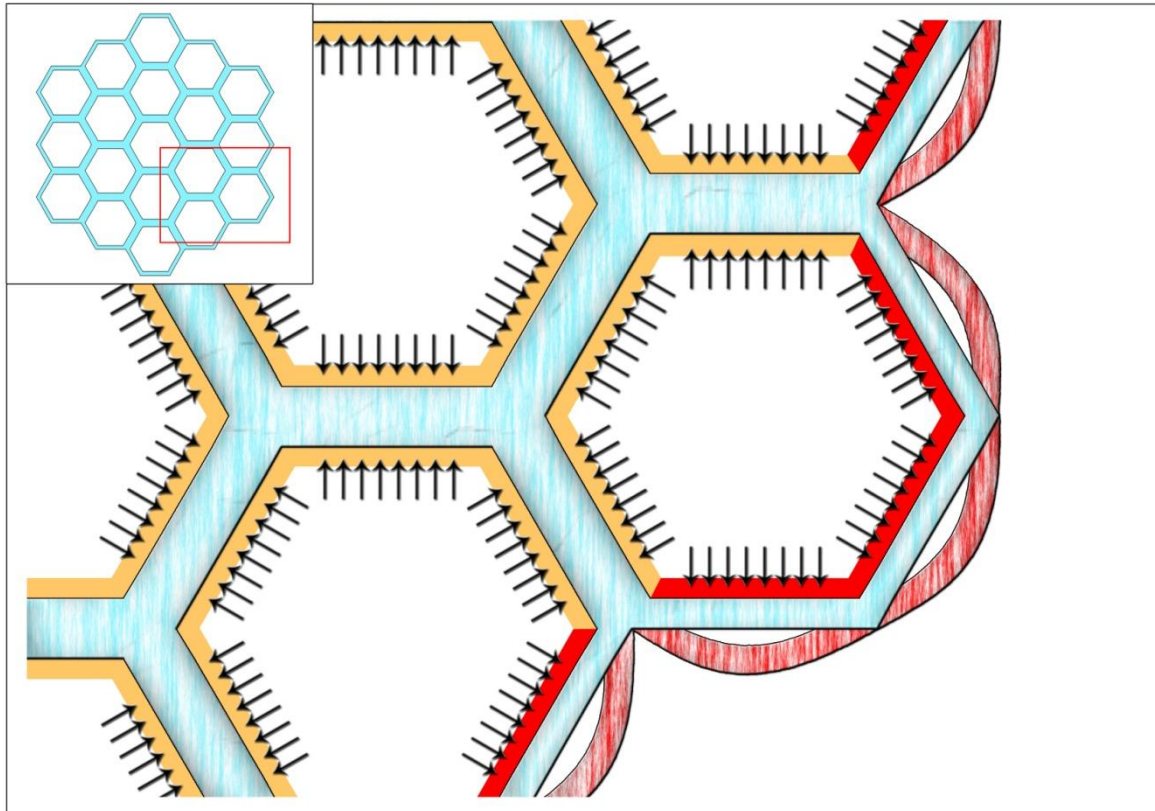
Figure 86: Inner walls with counter pressure (yellow) compared to outer walls without counter pressure (red) and resulting bending deformation (red hatched) at applied inner pressure

According to the deliberations in Figure 86, the stress between the fibers is nearly constant with approximately 300 MPa, which is confirmed by the result of the FEM simulation, displayed in Figure 87. There is no bending deformation at these inner walls. On the contrary, the inner corners of the inner fibers feature approximately 3 times higher stress value of about 800MPa, compared to the same structure made of round fibers. Merely on the outer walls without counter pressure, the stress is uneven distributed. The outer fibers show the same behavior at the outer walls as hexagonal single fibers with same bending deformation and bending stress as shown in Figure 87 and Figure 88. The maximum stress is about 3400 MPa at the inner edges and further stress peaks of about 1000 MPa at the outer straight walls of these outer fibers. At the inner surface of these outer walls the prevalent stress is compressive similar to the hexagonal single fibers.
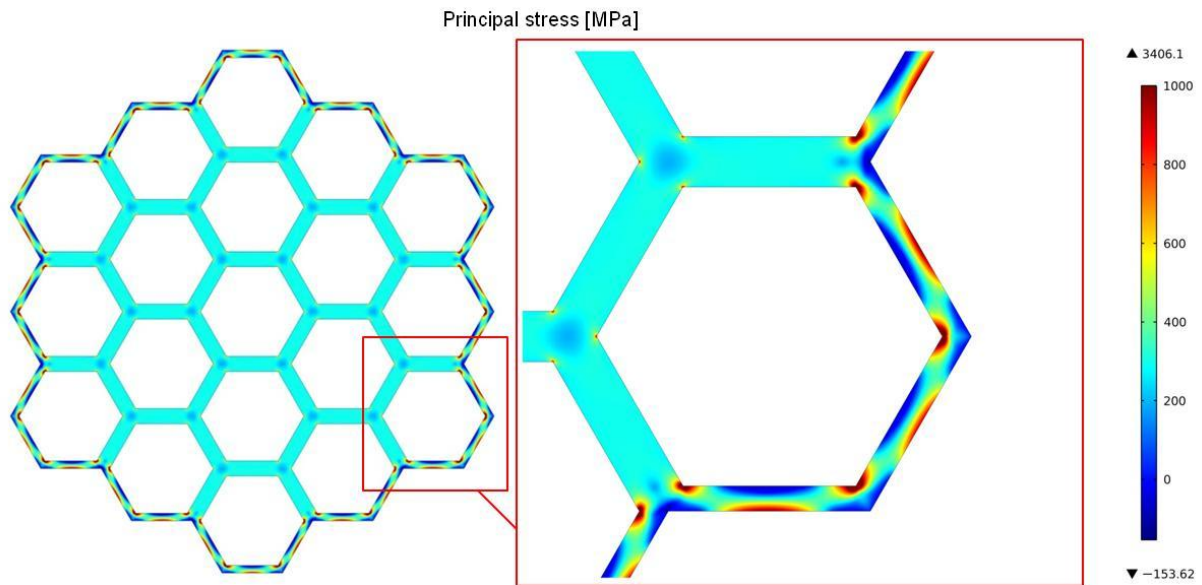
Figure 87: First principal stress in MPa at a structure made of 19 hexagonal fibers with D_o=400µm and D_i=350µm flat-to-flat bundled in honeycomb way with 50 MPa applied inner pressure

Figure 88 visualizes the expansion of the hexagonal structure, made from 19 hexagonal single fibers. Disregarding the bending deformation, the total expansion of the structure is about 6µm, what is about 0.4% of the structure's outer diameter. Similar to the expansion of structures with round fibers, this value of total expansion is the summed expansion of the five single fibers from edge to edge. Every single fiber of the structure shows an expansion of about 1.3 µm at the walls. The result is an increasing expansion from the center of the structure to the outer side.
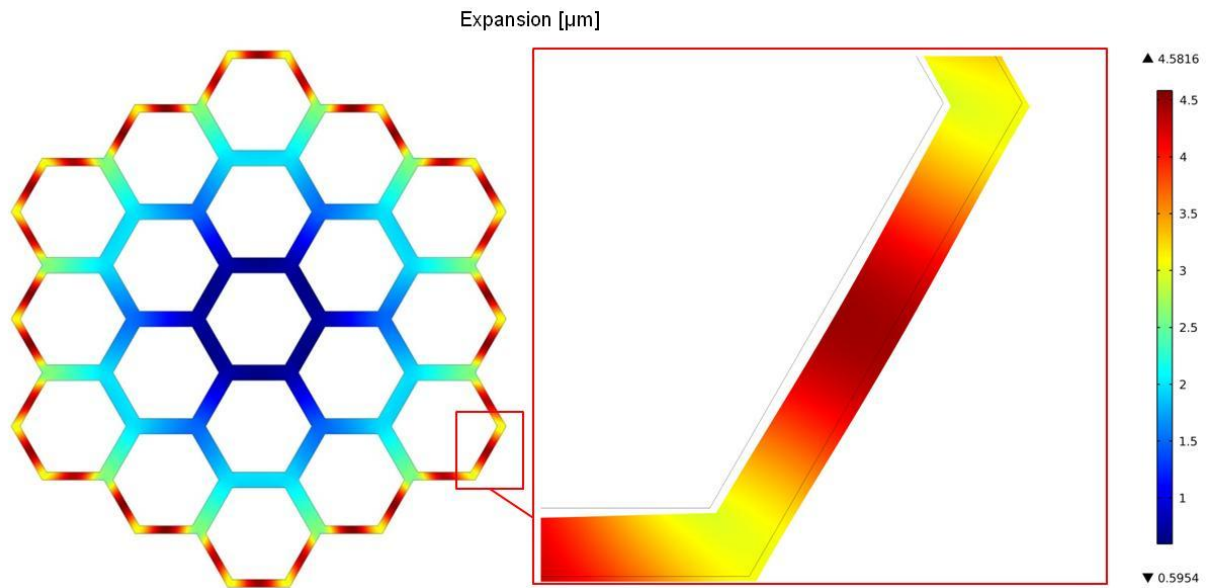
Figure 88: Expansion in µm at a structure made of 19 hexagonal fibers with D_o=400µm and D_i=350µm flat-to-flat bundled in honeycomb way with 50 MPa applied inner pressure

Sizing up the bundled structure continuously, shows up further differences to bundled round fibers as displayed in Figure 89. Therefore, structures of 19, 61 and 127 single fibers, each having the dimension of D_o=400µm (flat-to-flat) and a wall thickness of 25µm, has been simulated and compared to a single fiber with the same dimension. The fibers were bundled in honeycomb way. In contrast to round fibers, the bundled hexagonal fibers show constant stress distribution at the inner walls with low fluctuation. The minimum and maximum stress only dominates at the outer walls without counter pressure at the opposite surface. Increasing the amount of fibers leads to slightly increasing maximum stress values. In contrast to this, the compressive stress, visualized by the minimum stress value is nearly constant despite the growing structure size. Similar to the structure of bundled round fibers the total expansion is about 0.39% and only merely influenced by the structure size.
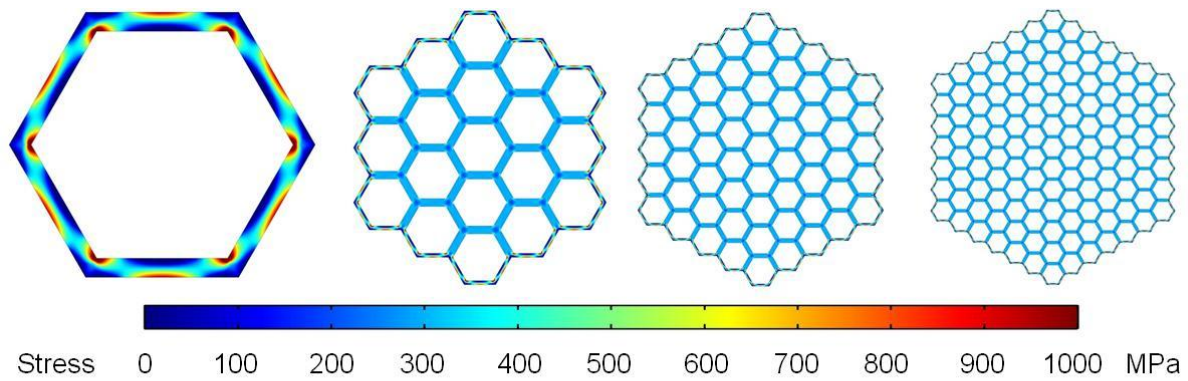
Amount of single fibers			
1	19	61	127
Minimum stress [MPa]			
-50	-154	-151	-162
Maximum stress [MPa]			
3298	3406	3458	3847
Expansion [µm] / [%]			
1.42 / 0.36	6.2 / 0.39	11.0 / 0.39	15.1 / 0.38

Figure 89: Influence of increasing amount of hexagonal single fibers with D_o=400µm and D_i=350µm flat-to-flat on the occurring first principal stress and expansion at a structure bundled in honeycomb way with 50 MPa applied inner pressure

The behavior of internal stress and expansion is graphically visualized in Figure 90. The diagram plots the occurring stress in MPa (primary ordinate, left) and the expansion in µm (secondary ordinate, right) against the amount of fibers in a structure. The lower red line shows the minimum stress in MPa and the upper green line displays the maximum stress in MPa. The general behavior of stress and expansion resembles the behavior when bundling round fibers. The minimum and maximum stress is nearly constant for the bundled structures. Only the single fiber shows higher minimum but lower maximum stress values. The expansion in µm which is visualized by the blue graph grows with increased sample size. This behavior leads to constant total expansion in %, independent of the amount of fibers in the structure.
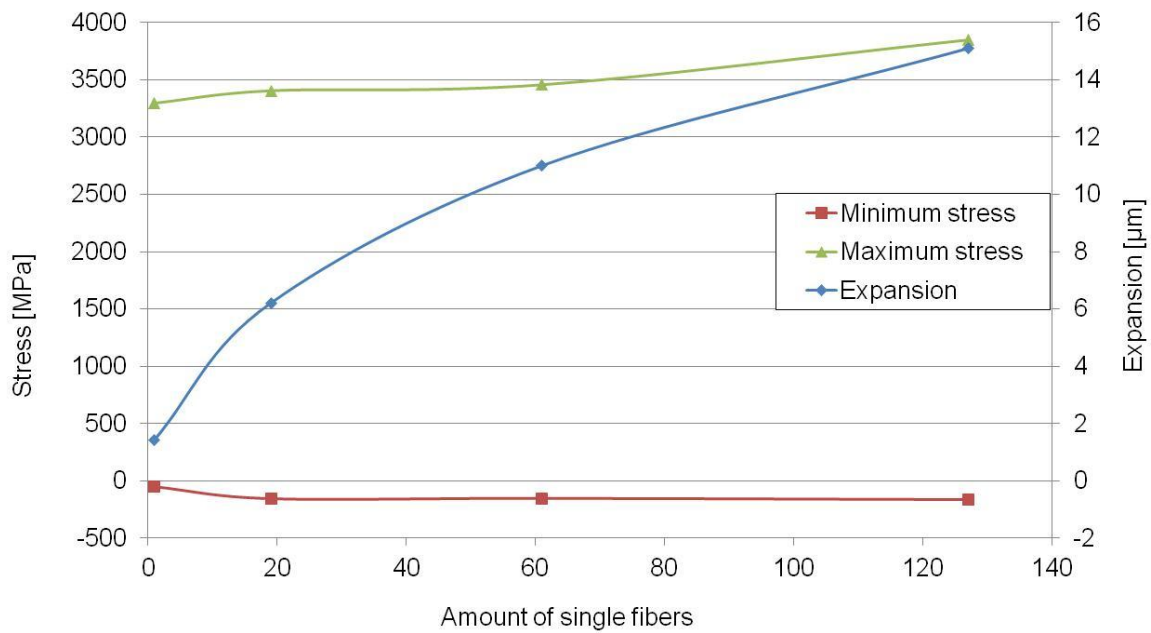
Figure 90: Dependence of minimum and maximum first principal stress as well as expansion on the amount of hexagonal single fibers with D_o=400µm and D_i=350µm flat-to-flat on the occurring stress and expansion at a structure bundled in honeycomb way with 50 MPa applied inner pressure

The comparable structure 399-3315-A was tested concerning its burst pressure and was already discussed in chapter 5.4.4 "Hexagonal Structures Made Of Thin-Walled Hexagonal Hollow Glass Fibers Without Outer Glass Shell". The highest measured burst pressure value of that structure is 34.6 MPa and is shown in Figure 91, as well as a microscopic view of the structure.
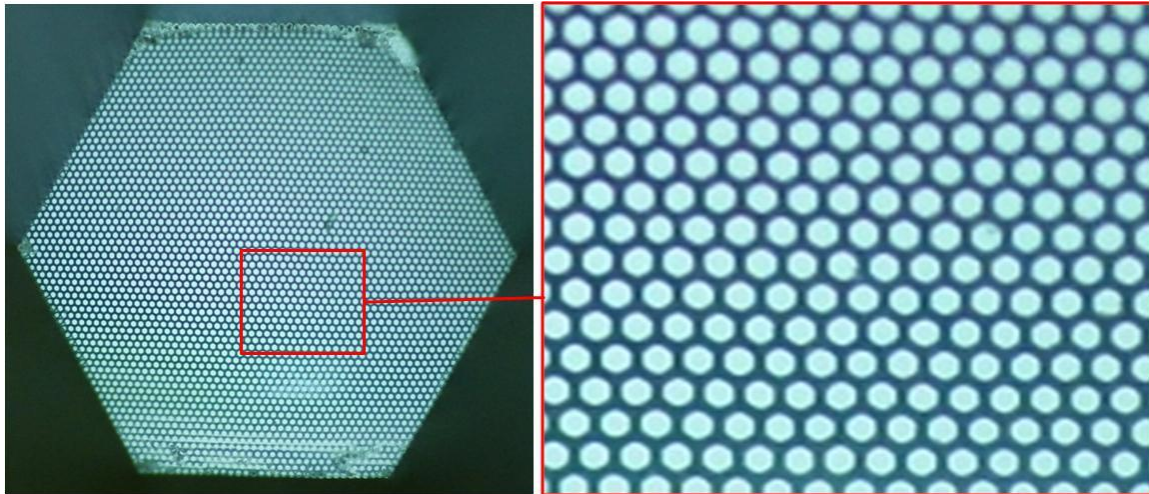
Maximum burst pressure [MPa]
34.6

Figure 91: Microscopic view of a structure made of hexagonal fibers bundled in honeycomb way and rounded inner edges with burst pressure values

Adding an outer shell made of glass, comparable to the 19-fiber structure with hexagonal fibers, leads to reduced stress at the inner as well as to the outer walls, as demonstrated in the left picture of Figure 92. The bending stress at the outer fibers is quartered to 200MPa. The stress at the 50µm thick walls between the fibers is still nearly constant with low fluctuation of about 50MPa. The highest stress of 1141MPa still appears at the corners of the hexagonal fibers. The compressive stress is also reduced to less than 10% compared to the same structure without outer glass shell and shows a maximum value of 12 MPa. Due to the outer glass shell, the expansion is reduced to 3.7µm which corresponds to 0.19% of the structure's outer diameter. Furthermore, the bending deformation at the outer walls of the outer fibers is prevented which coheres with the reduced compressive stress. The expansion is demonstrated in the right picture of Figure 92.
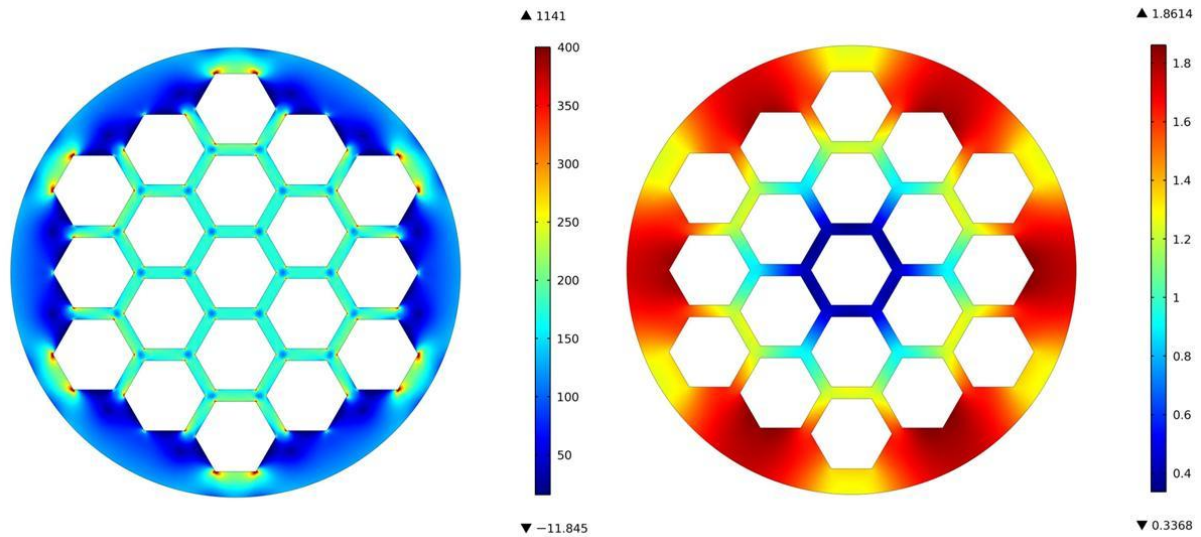
Figure 92: Calculated first principal stress in MPa (left) and expansion in µm (right) at a structure made of hexagonal fibers with an outer diameter D_o=400µm and an inner diameter D_i=350µm flat-to-flat and an additional outer glass shell with 50 MPa applied inner pressure

Figure 93 shows a microscopic picture of structure 399-3312-A with hexagonal fibers and a massive outer glass shell. The entire structure is demonstrated in the left picture and an enlarged view is shown in the right picture, focusing on the outer fibers neighbored to the shell, which show various shape. Although that fact, the structure shows comparable high burst pressures with a maximum value of 98.6 MPa. The results are also displayed in Figure 93. Due to that results, structures consisting single fibers with hexagonal shape and an outer glass shell are also able to withstand high inner pressure.
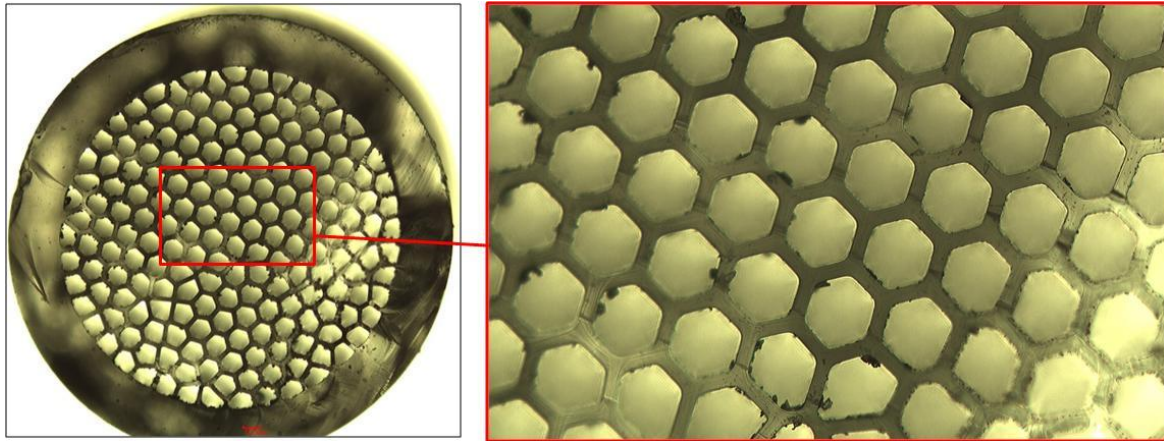
Maximum burst pressure [MPa]
98.6

Figure 93: Microscopic view of structure made of hexagonal fibers and an additional outer glass shell with the determined maximum burst pressure value

5.6.9 Influence Of Varying Free Space On Structures Made Of Hexagonal Single Fibers

In order to reach potentially higher storage capacities, the massive outer glass shell is counterproductive. Beside the additional weight, its round shape interferes further bundling of these structures because of occurring interspaces which are similar to the bundling of round single fibers. For that reason, the thickness of the fiber walls was reduced to 5 µm at the subsequently following simulation (displayed in Figure 94), which results in a wall thickness of 10 µm between the fibers. This change leads to three times higher stress of about 1700MPa between the fibers with homogeneous allocation when compared to the same structure with 50µm wall thickness,. The fact that the outer walls of the outer fibers also shrunk leads to stress peaks up to 47000MPa.
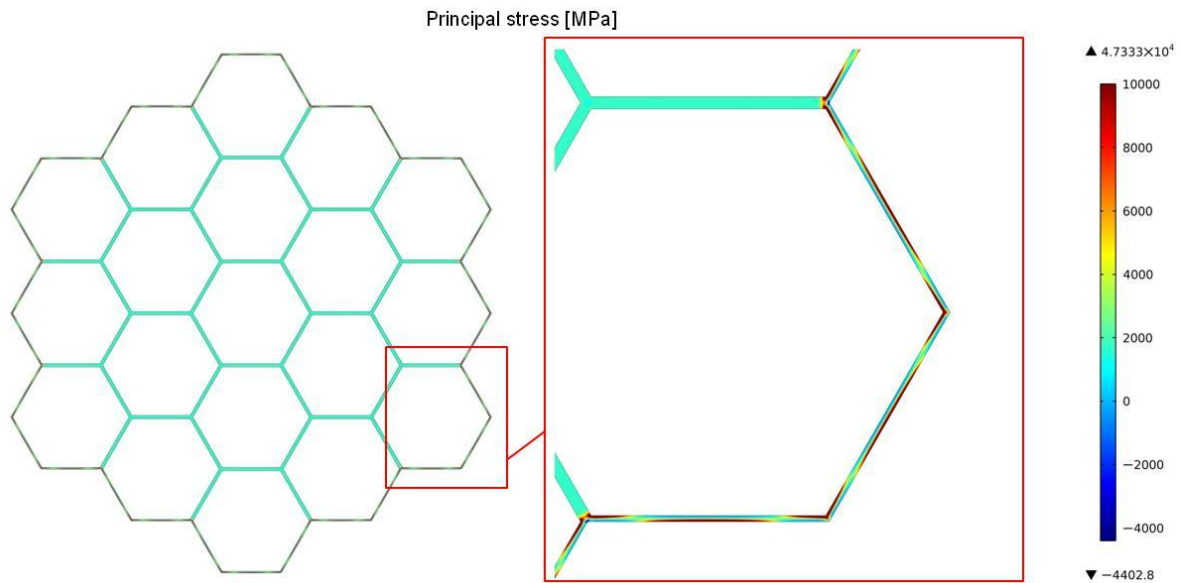
Figure 94: Occurring first principal stress in MPa at a structure made of 19 hexagonal fibers with D_o=400µm and D_i=390µm flat-to-flat bundled in honeycomb way with 50 MPa applied inner pressure

Even with thinner walls the stress between the fibers is well distributed with a value which is below the theoretical strength of glass. Nevertheless, the occurring peaks of high stress at the outer fibers pose a problem which needs to be solved as well as the stress peaks at the corners.

5.6.10 Influence Of Rounding The Inner Edges Of Hexagonal Fibers On Their Strength

Microscopic examinations as shown in Figure 95 of structures with hexagonal fibers reveal a slight rounding of the inner surface at the corners and are observable in the enlarged view in the right picture. This phenomenon is caused by the manufacturing process, and is significantly increased with structures made of fibers with higher wall thickness. Related to the manufacturing process, there is coherence between the wall thickness of the single fibers and the intensity of rounding. Thus, the higher the wall thickness the higher is the intensity of rounding.
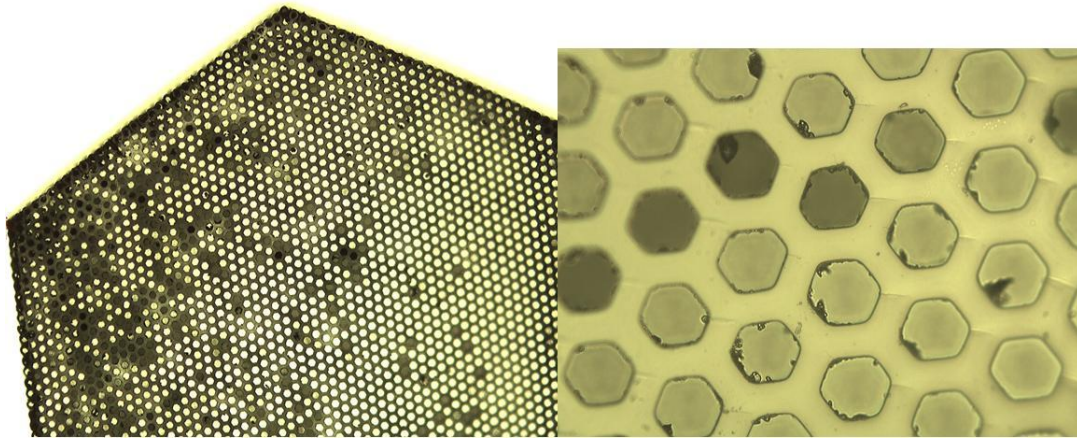
Figure 95: Microscopic view of a structure with hexagonal fibers offering rounded inner edges

In a further simulation, the inner edges of the hexagonal fiber were rounded comparable to the microscopic view in Figure 95. That circumstance leads to decreased stress at the inner corners, what for the maximum stress will be reduced to one third (Figure 96). The occurring compressive stress is slightly decreased and has a value of 42 MPa. The bending stress in the middle of the straight walls is also decreased at about 200MPa and shows a value of about 800MPa.
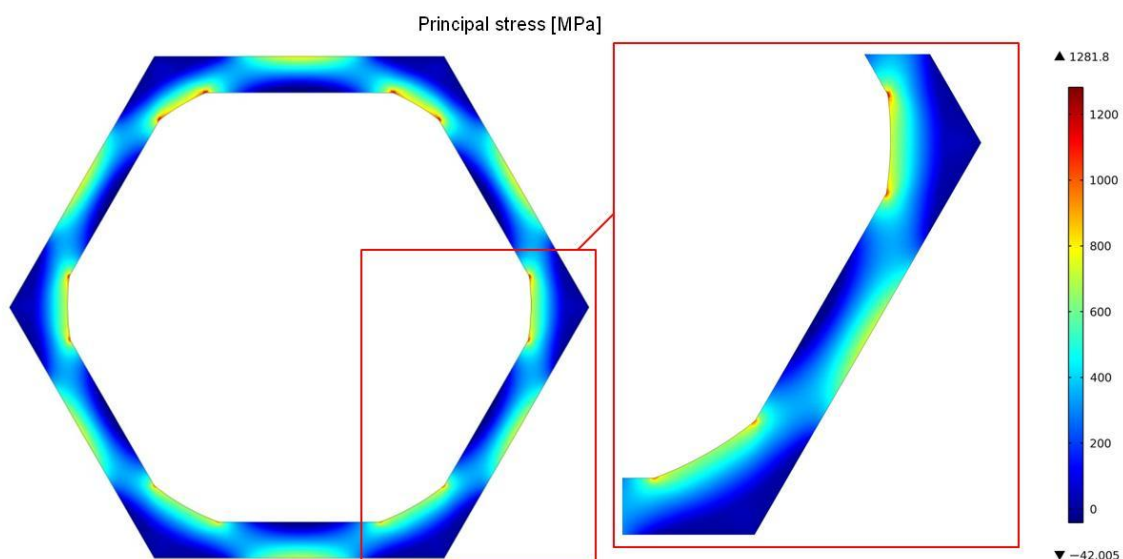
Figure 96: Occurring first principal stress in MPa in a single fiber with hexagonal shape and rounded inner edges with D_o=400µm and an inner diameter D_i=350µm flat-to-flat with 50 MPa applied inner pressure

Contrary to the stress, the expansion of the fiber is not influenced by the rounded corners as shown in Figure 97. Merely, the bending deformation is lower with 1.5µm which results in the lower bending stress value of about 800MPa. The bending deformation is also demonstrated in Figure 97. The position of the wall without applied pressure is displayed by the black line.
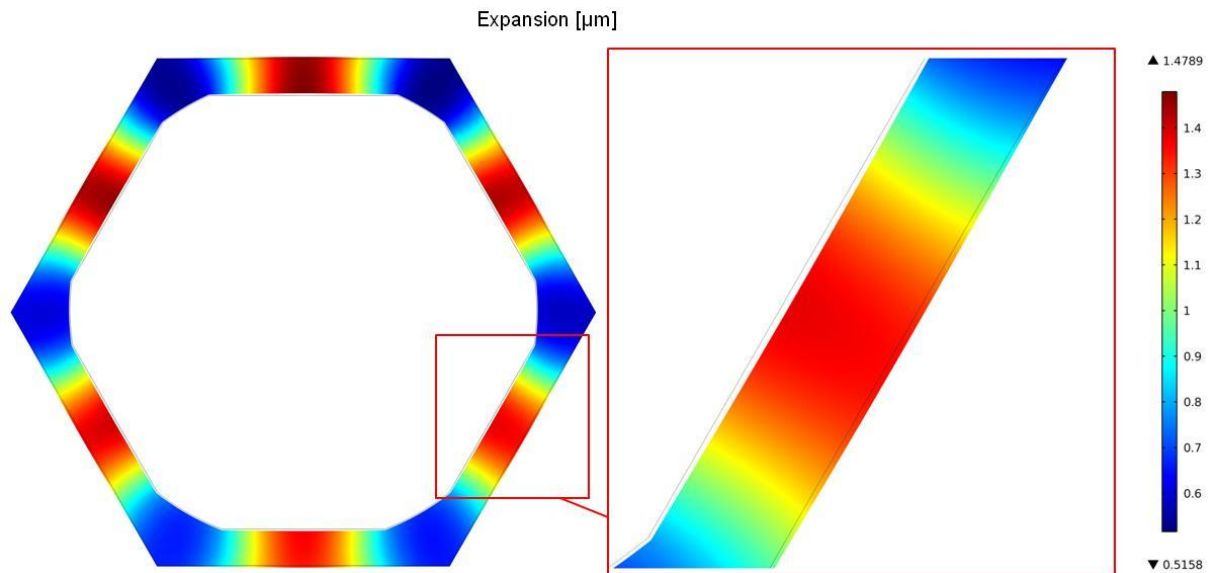
Figure 97: Occurring expansion in µm in a single fiber with hexagonal shape and rounded inner edges with D_o=400µm and an inner diameter D_i=350µm flat-to-flat with 50 MPa applied inner pressure

As further step, a structure consisting 169 hexagonal fibers with D_o=400µm and D_i=350µm flat-to-flat was examined regarding the "rounded inner edges". The general behavior of stress distribution and expansion is not influenced by that variation. The values are similar to the structures without rounded edges shown in Figure 89. The stress at the inner walls between the fibers does not change. Merely, the small stress peaks at the inner corners are vanished. In contrast to the similar stress at the inner walls, the stress at the outer fibers is approximately halved. Due to that fact, the maximum stress at the outer fiber walls without counter pressure is shrunk to barely 1600 MPa.

Principal stress [MPa]
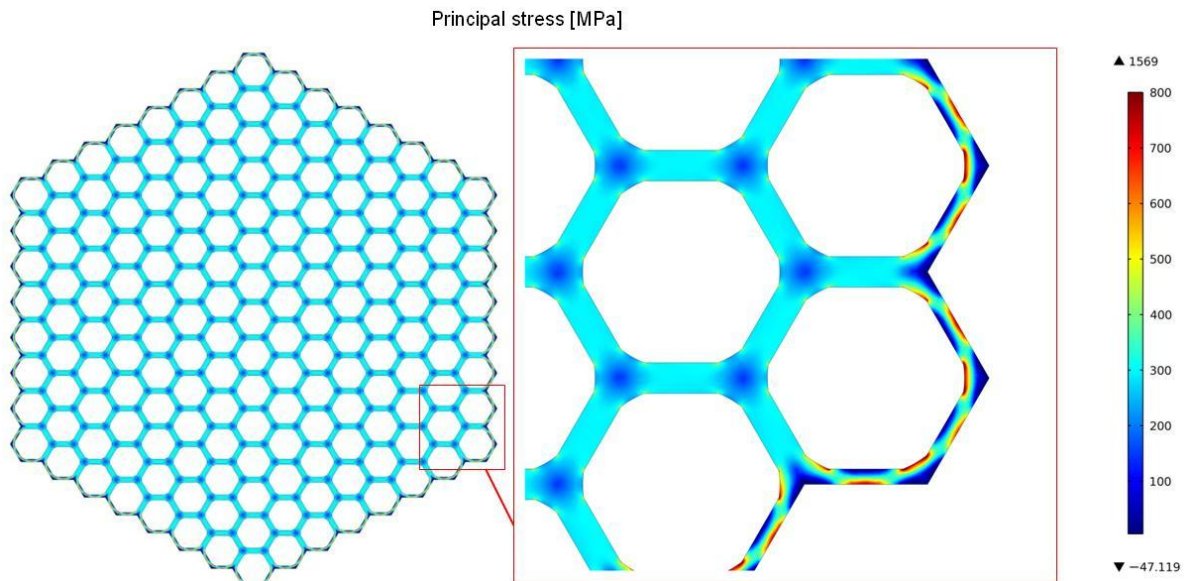
Figure 98: Occurring first principal stress in MPa at a structure made of 169 hexagonal fibers with D_o=400µm and D_i=350µm flat-to-flat bundled in honeycomb way and rounded inner edges with 50 MPa applied inner pressure

The higher the wall thickness between the hexagonal single fibers, the higher is the rounding of the inner corners. The in chapter 5.4.2 "Hexagonal Structures Made Of Hexagonal Hollow Glass Fibers Without Outer Glass Shell" discussed structure 3574a shows higher wall thickness and, correlated to that, more rounded inner edges. The structure shows a maximum burst pressure value of 50.3 MPa.

5.6.11   Influence Of Solid Fibers On The Strength Of Structures Made Of Hexagonal Fibers

In addition to the problem of high stress areas at the outer walls, the structure samples frequently showed broken fibers, especially at the outer corners. Those damages occurred during transportation caused by contact to other glass structures or packing material, if not properly and each structure separately packed. Additionally, many structures which were not visibly damaged failed during minimum pressure treatment by breaking only at these fibers at

the corners. In order to avoid such defects, the hollow fiber at each outer edge of the structure is replaced by a solid fiber, as shown in Figure 99. In this way, the outer hollow edge fibers are protected against external influence. That structural modification results in reduced stress at these outer solid fibers which does not exceed 100 MPa. The stress between the fibers keeps similar to the previous structure without solid fibers. The maximum stress at the outer straight structure wall is 1653 MPa.
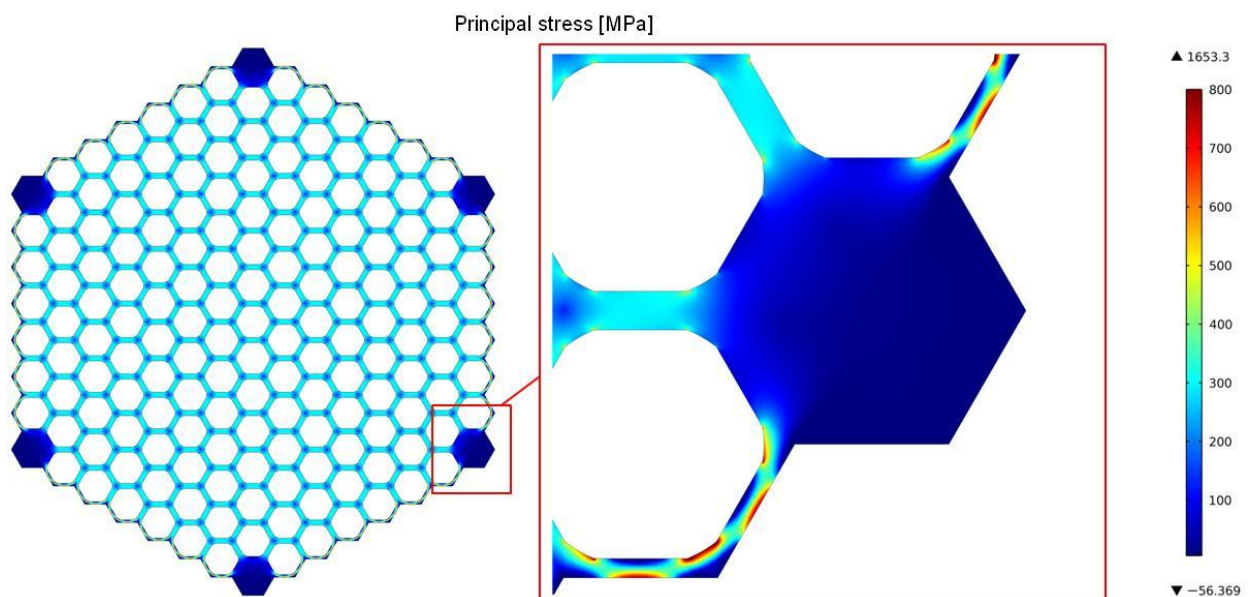
Figure 99: Occurring first principal stress in MPa at a structure made of 169 hexagonal fibers with D_o=400µm and D_i=350µm flat-to-flat bundled in honeycomb way with rounded inner edges and one solid fiber at each corner with 50 MPa applied inner pressure

The exemplary structure 3837 with one solid fiber in the corners was tested and discussed in chapter 5.4.5 "Hexagonal Structures Made Of Hexagonal Single Hollow Glass Fibers And Solid Fibers At The Outer Corners Of The Structure" and is displayed in Figure 100. The maximum burst pressure of structure 3837 with one solid fiber per edge is 89.1MPa.
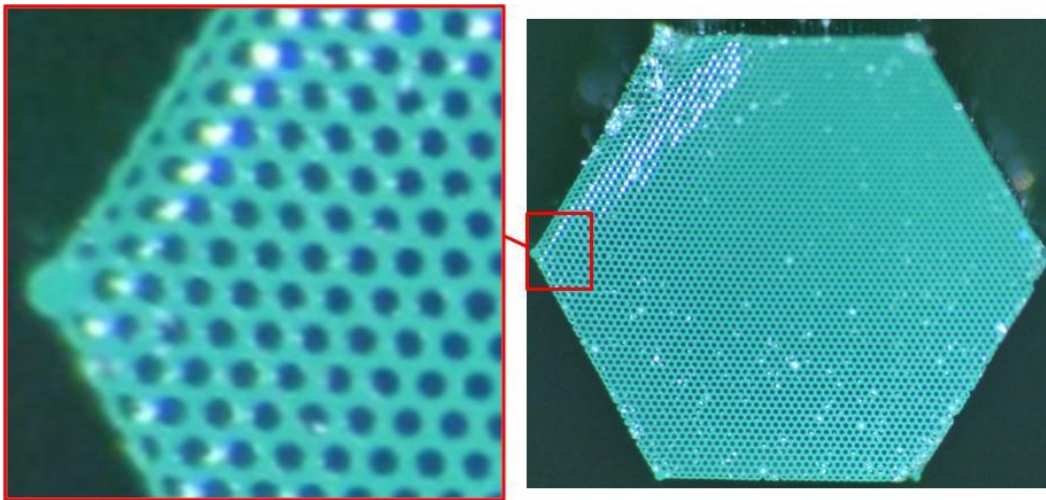
Maximum burst pressure [MPa]
89.1

Figure 100: Microscopic picture of structure 3837 made of 3361 hexagonal fibers bundled in honeycomb way with rounded inner edges and 1 solid fiber at each corner

A similar structure with three solid fibers at each outer corner, shows comparable behavior, as shown in Figure 101. The stress at the solid fibers is lower than 100MPa, whereby the stress at the outer straight walls is slightly increased to about 1860MPa.
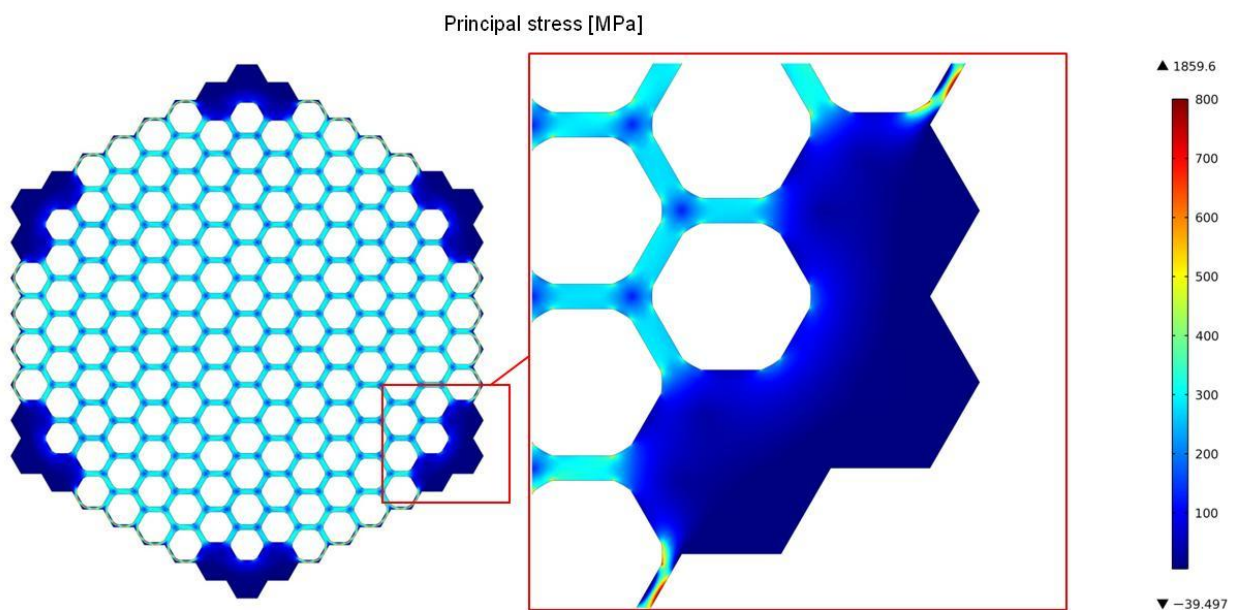
Figure 101: Occurring first principal stress in MPa at a structure made of 169 hexagonal fibers with D_o=400µm and D_i=350µm flat-to-flat bundled in honeycomb way with rounded inner edges and three solid fibers at each corner with 50 MPa applied inner pressure

Structure 3843, which is displayed in Figure 102 and tested and discussed in chapter 5.4.5 "Hexagonal Structures Made Of Hexagonal Single Hollow Glass Fibers And Solid Fibers At The Outer Corners Of The Structure", has eleven solid fibers per edge. The highest measured burst pressure value is with 70.8MPa about 20 MPa lower than at the comparable structure 3837 with only one solid fibers at each corner. This decreased burst pressure conforms to the simulated higher stress in Figure 101, compared to Figure 99.

The step of using solid fibers at the outer edges of the structure reduced the amount of damaged fibers in this area.
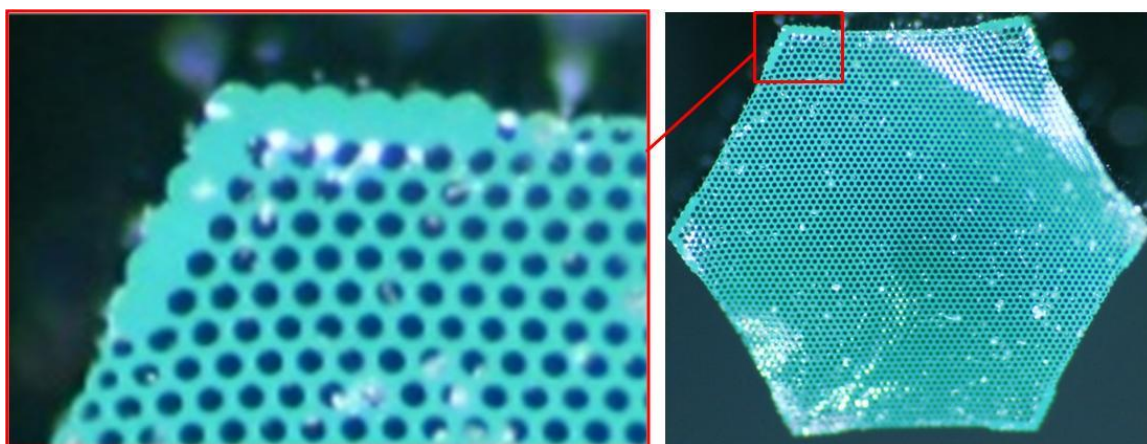
Maximum burst pressure [MPa]
70.8

Figure 102: Microscopic picture of structure 3843 made of 3301 hexagonal hollow glass fibers bundled in honeycomb way with rounded inner edges and eleven solid fibers at each corner

The outer hollow fibers at the straight walls still show peaks of increased stress. The low stress at the corner fibers, resulting from adding solid fibers at the edges, solid fibers as complete outer fiber row were used to protect the inner fibers against exterior influence and for reducing the stress at the outer hollow fibers. The inner fibers keep similar to the previous structure with smooth inner edges. Examining the resulting structure with FEM simulation leads to reduced stress at the outer hollow fibers as displayed in Figure 103. The left picture shows the whole structure and the right picture offers an enlarged view to the most significant part. As a matter of fact, the maximum stress at the outer fibers falls below the

stress between the fibers and shows a maximum of around 100 MPa. The edges show stress peaks and are observable up to 1200 MPa.
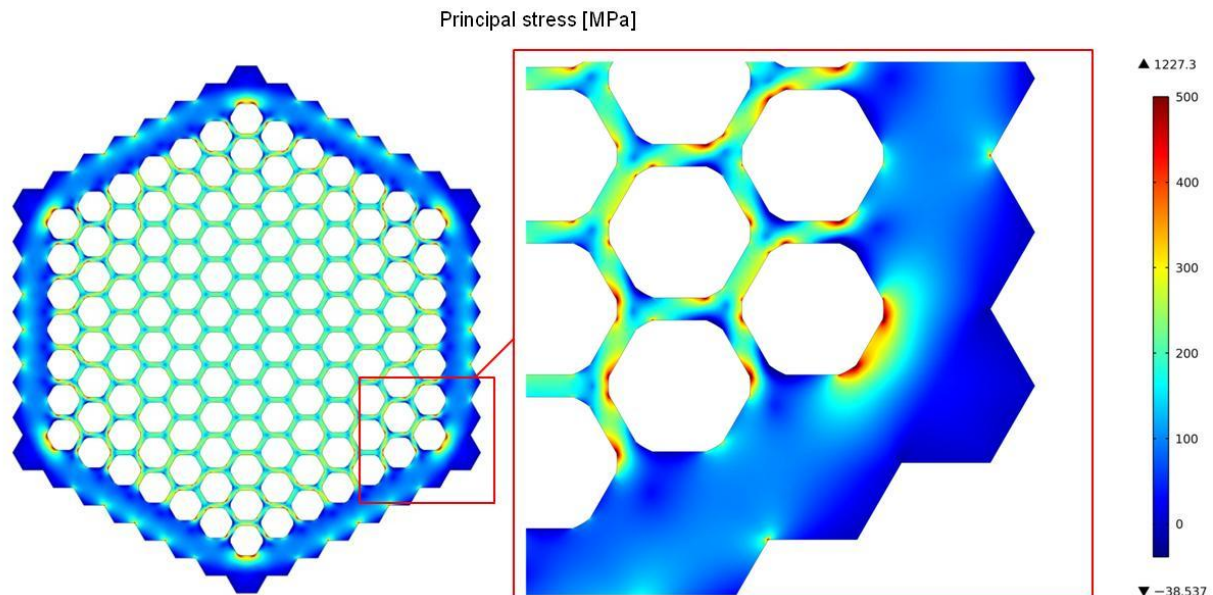
Figure 103: Occurring first principal stress in MPa of a structure made of 169 hexagonal fibers with D_o=400µm and D_i=350µm flat-to-flat bundled in honeycomb way with rounded inner edges and solid fiber as outer row and 50 MPa applied inner pressure

The results of experimental examinations of comparable structures show increased burst pressure values, compared to structures without solid fibers at the outer walls. Several test series were examined and discussed in chapter 5.4.6 "Hexagonal Structures Made Of Hexagonal Single Hollow Glass Fibers And Solid Fibers As Outer Fiber Layer". The highest measured burst pressure values are in a range of about 100MPa, the maximum value is 117.1 MPa at structure 3624, which is demonstrated in Figure 104. That value is about three times higher than at comparable structures without solid fibers. Also, the structures with solid fibers only at the outer corners show lower burst pressure values and therefore lower strength. That experimental result fully corresponds to the results of the executed FEM simulations.
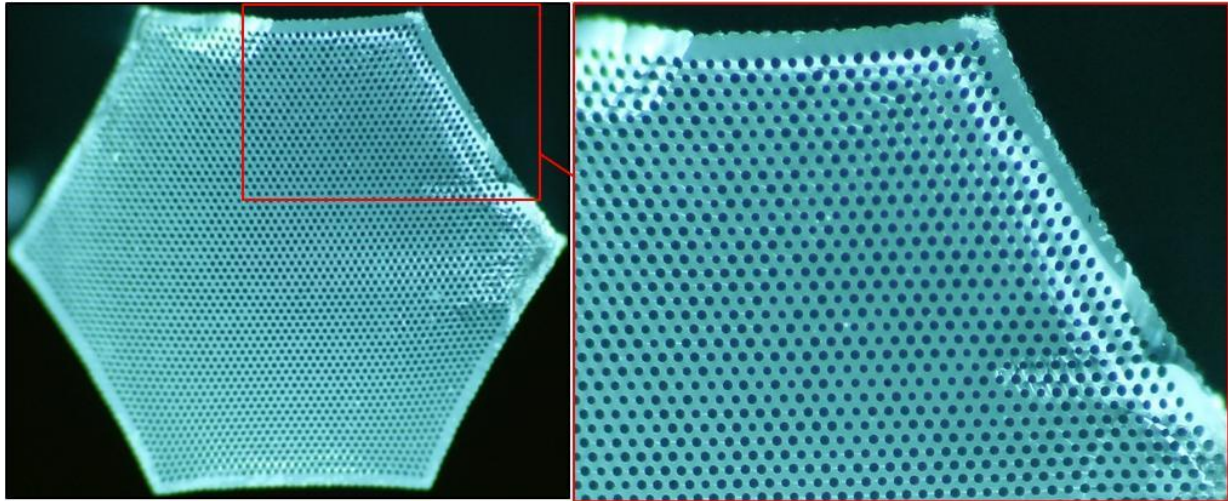
Maximum burst pressure [MPa]
117.1

Figure 104: Microscopic picture of structure 3624-9 made of 3169 hexagonal hollow glass fibers bundled in honeycomb way with rounded inner edges, surrounded from 198 solid fibers

5.6.12 Combination Of Fibers With Round And Hexagonal Shape

A crucial disadvantage of adding solid fibers to a structure is the decreasing gravimetric and volumetric storage capacity. In order to reduce the negative effect of the solid outer fiber row to the storage capacities, the solid fibers were replaced by fibers still being hollow, but having comparably high wall thickness and therefore only small inner diameter. The resulting structure and the occurring stresses of pressure treatment are displayed in Figure 105. The storage capacities are increased caused by additional storage volume. Modeling the stress for this structure leads to maximum stress of about 150 MPa lower than at the same structure with solid fibers, which is shown in Figure 103.

Principal stress [MPa]
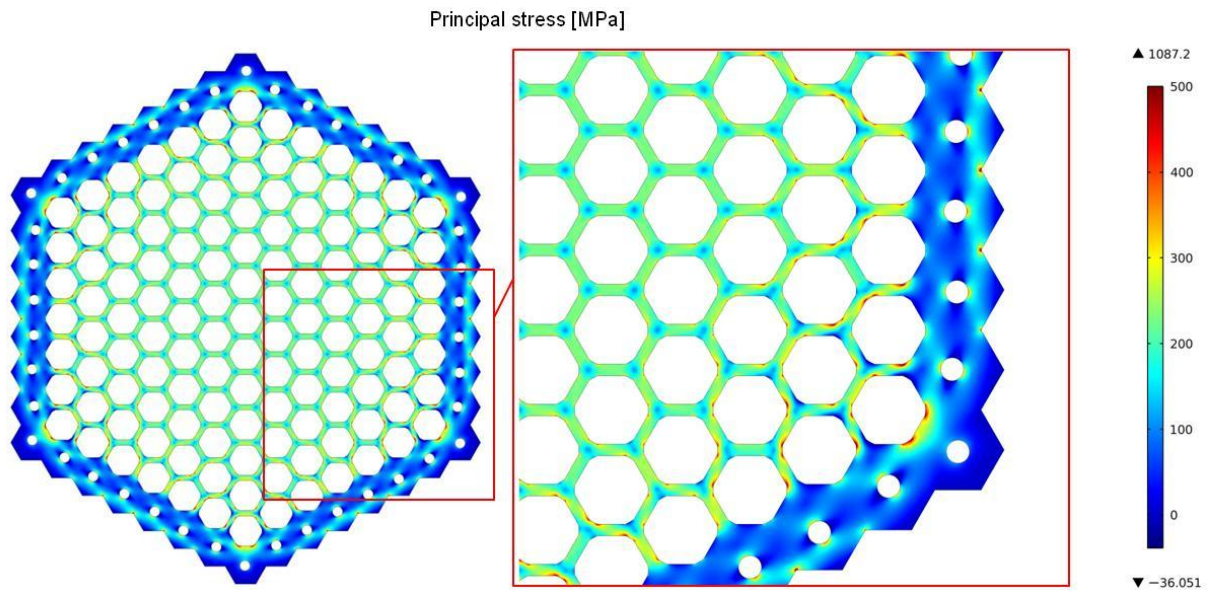
Figure 105: Occurring first principal stress in MPa of a structure made of 169 hexagonal fibers with D_o=400µm and D_i=350µm flat-to-flat bundled in honeycomb way with rounded inner edges and massive fibers with round inner shape and high wall thickness as outer row with 50 MPa applied inner pressure

For increasing the storage capacities, a structure with 19 hexagonal fibers has been surrounded by a row of round fibers which is visualized in Figure 106. Thus, the stress between the hexagonal fibers does not change, compared to a structure with hexagonal fibers only. Similar to the structure made of round fibers, areas of increased stress between the round fibers emerge. Nevertheless, the stress at the outer walls is homogeneous without any stress peaks. The value of the maximum stress at the outer wall does not exceed 200 MPa.
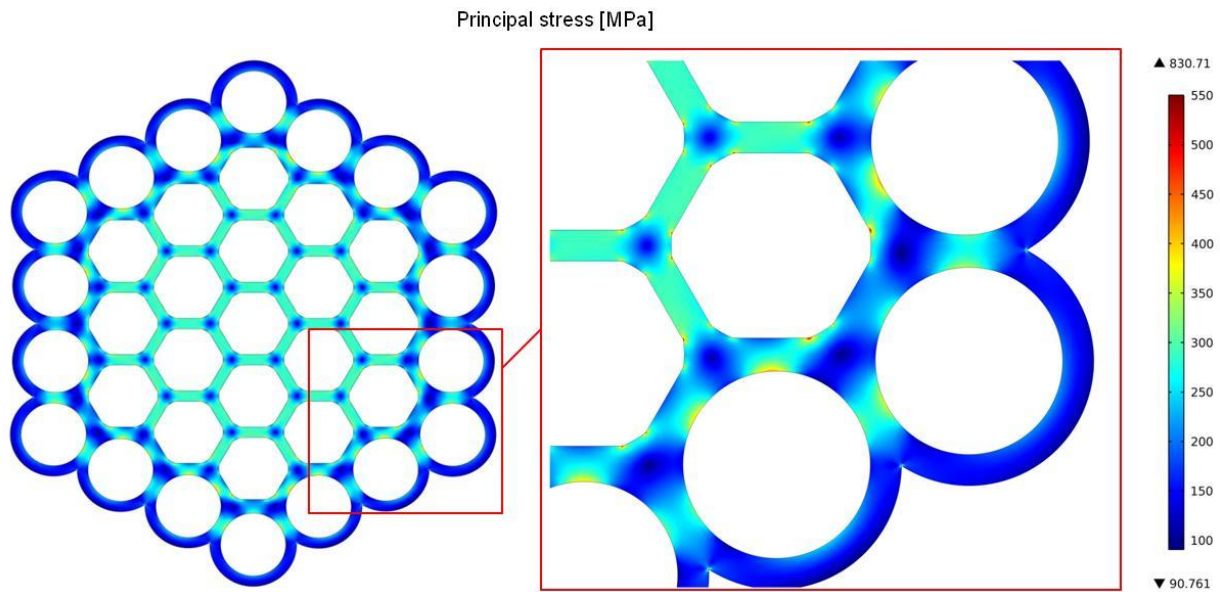
Figure 106: Occurring first principal stress in MPa of a structure made of 19 hexagonal fibers with D_o=400µm and D_i=300µm flat-to-flat bundled in honeycomb way with rounded inner edges and additional round fibers as outer row with 50 MPa applied inner pressure

Determining the burst pressures of the comparable structure 399-3316-A leads to a maximum burst pressure of 71.9 MPa. Due to the comparably high free inner volume of 64%, that structure shows the highest gravimetric storage capacity of all tested structures. That result corresponds to the comparably low calculated stress. The results as well as microscopic pictures of these samples are displayed in Figure 107. At the connection area of the round fibers to the hexagonal ones, deformed fibers and scattered interspaces between the fibers are recognizable. As already mentioned, the presence of those interspaces decreases the strength of a structure, whereby the burst pressure is lowered.
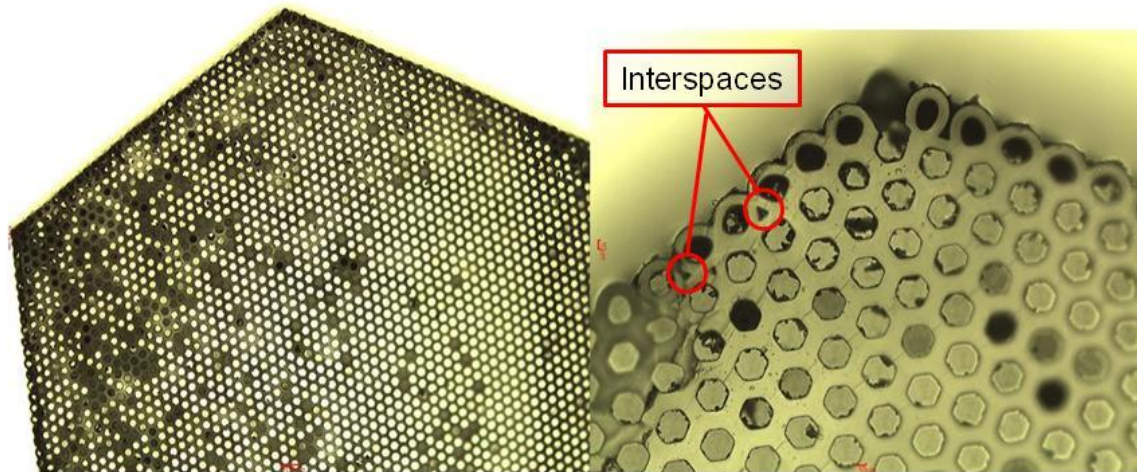
Maximum burst pressure [MPa]
71.9

Figure 107: Microscopic picture of structure 399-3316-A, made of 3367 hexagonal fibers bundled in honeycomb way with rounded inner edges and additional round fibers as outer row with interspaces and a determined maximum burst pressure of 71.9 MPa

So far, surrounding the hexagonal fibers with round fibers leads to the best results for this type of structures. The occurring stress is well distributed without peaks of high stress. Additionally, the abandonment of solid fibers does not influence the storage capacities in a negative way. Nevertheless, the outer fibers need to be protected against external influences, as already pointed out in chapter 5.6.11.

5.6.13   Combination Of Hexagonal Fibers With Varying Free Space

Further research deals with the problem of increasing the storage capacities. Regarding the results so far, it turned out that the wall thickness in the inner area of the structure can be small, but the closer the area gets to the outside (border to atmospheric pressure), a higher wall thickness is required.. If hollow fibers are used as outer fiber layer, they need to have round shape and possibly high wall thickness for withstanding higher inner pressure, although this is counterproductive regarding the storage capacities. Nevertheless, the inner

fibers can be less massive and thereby the storage capacities can be increased. The following FEM simulation which is displayed in Figure 108 shows a combination of two separate previously simulated structures. A structure made of 19 hexagonal fibers with a wall thickness of only 5 µm was surrounded by six structures, made of hexagonal fibers with a wall thickness of 25 µm and rounded inner edges. The thin-walled structure in the middle shows, when separately simulated, stress values of about 47000 MPa, as already presented in Figure 94. The more massive structures around the central structure show a maximum burst pressure value of about 1520 MPa as displayed in Figure 109 (left) which is compared to the thin-walled structure in Figure 109. The combination of these structures in the previously described way leads to decreased stress especially at the outer fibers of the thin-walled structure which show the high stress, if separately simulated. This is caused by the emerged counter pressure from the surrounding fibers. The stress value of the thin inner walls is similar to the thin-walled single structure displayed in Figure 109 (right). The maximum stress at the combined structure is located at the outer fibers similar to the thick-walled single structures and shows comparable values to them.
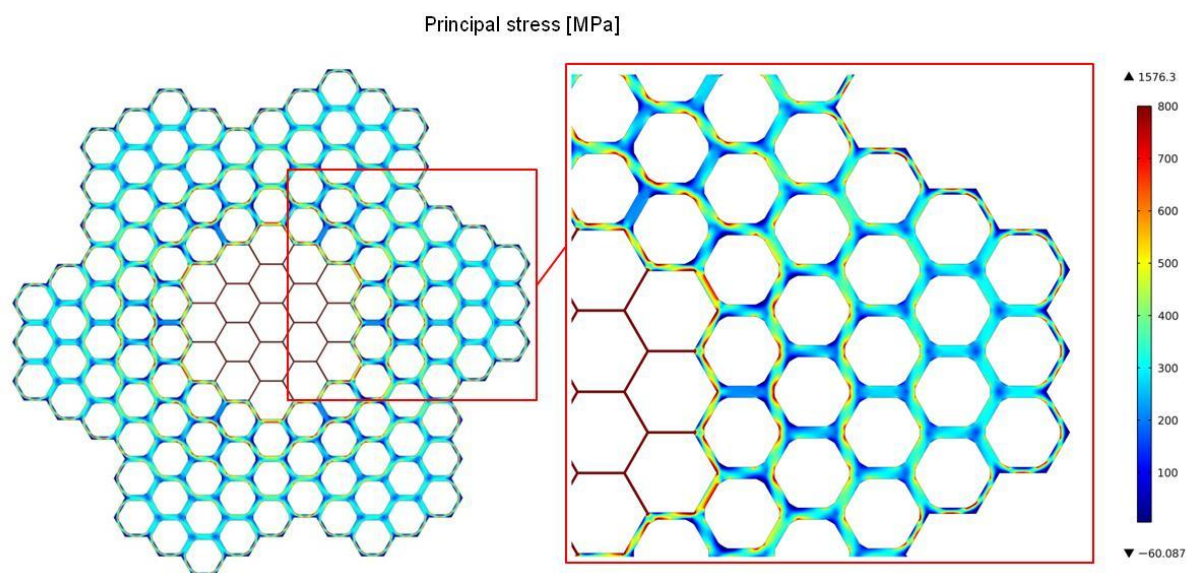
Figure 108: Occurring first principal stress in MPa of a multi-structure made of structures made of 19 hexagonal single fibers with D_o=400µm and D_i=390µm flat-to-flat bundled in honeycomb way surrounded by six structures made of 169 hexagonal fibers with D_o=400µm and D_i=350µm flat-to-flat bundled in honeycomb way and rounded inner edges with 50 MPa applied inner pressure

Figure 109 compares the thin-walled center structure (right) with the surrounding more massive structure (left). The maximum occurring stress differs from 1500 MPa at the left structure to more than 47 GPa at the right one. Caused by the thinner walls and the consequently higher free space, the stress at the right structure is generally much higher than at the left structure. Combining these two structures as demonstrated in Figure 108 leads to decreased stress at the outer fibers of the thin-walled structure displayed in Figure 109 (right) by generating counter pressure to them.
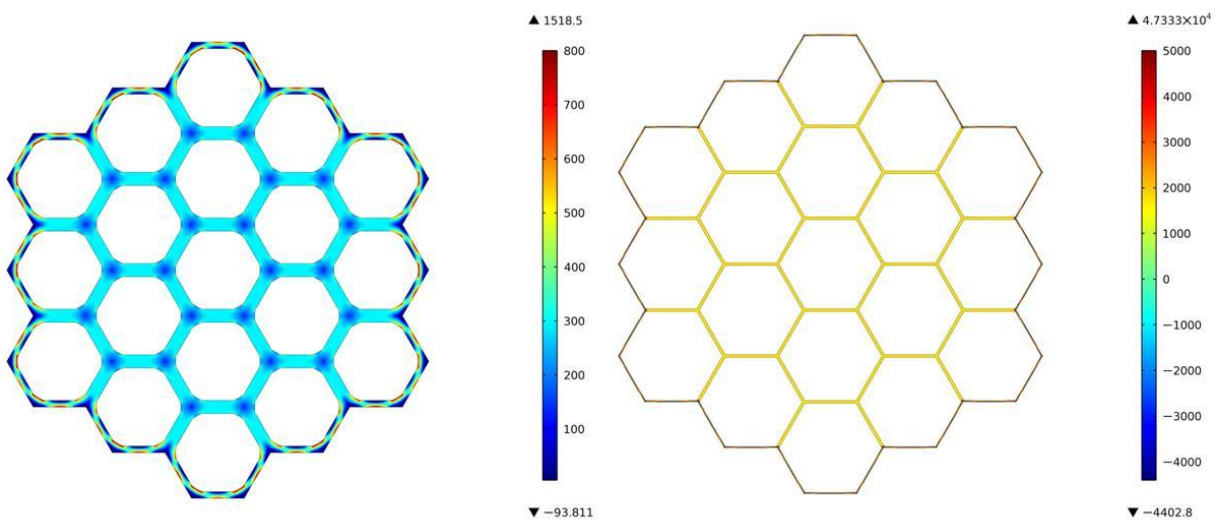
Figure 109: Comparison of the occurring first principal stress in MPa of a structure made of 19 hexagonal fibers with D_o=400µm and D_i=350µm flat-to-flat and rounded inner edges (left) and a structure made of 19 hexagonal fibers with D_o=400µm and D_i=390µm flat-to-flat (right); both bundled in honeycomb way with 50 MPa applied inner pressure

5.6.14 Optimized Structure Based On The Preliminary Findings

For additional augmentation of free space and, correlated to that, augmentation of gravimetric and volumetric storage capacity, the amount of thin-walled fibers has been extended compared to the amount of surrounding more massive fibers. Furthermore, the outer massive fibers became round. The fibers of the second layer show hexagonal shape but with rounded inner edges. The structure is displayed in Figure 110 together with the calculated stress values. Generally, the outer round fibers show comparably low stress with

values from about 200 MPa up to 500 MPa. The stress value at the inner thin walls is still about 1300 MPa to 1500 MPa. The influence of the structure size to the stress value of these thin fibers seems to be low. Nevertheless, the stress in this area is less well distributed. The value fluctuates from 1000 MPa to 1500 MPa. Furthermore, the outer hexagonal fibers, especially at the edges of the structure, show peaks of high stress with values up to 3900 MPa. These sharp edges also need to be rounded to prevent those high stress peaks.
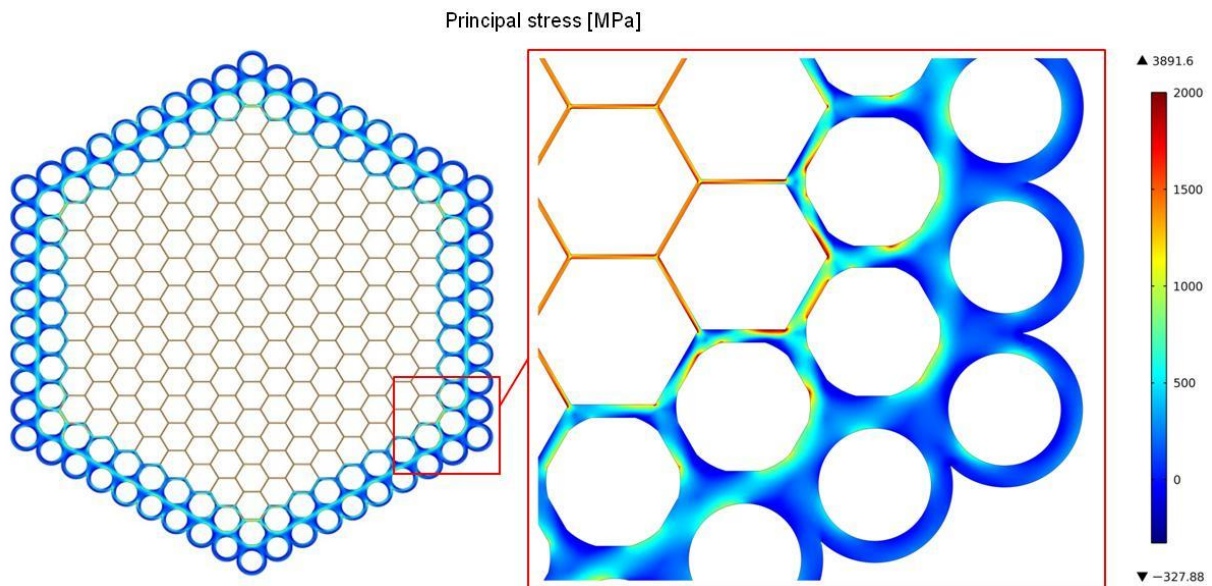
Figure 110: Occurring first principal stress in MPa of a structure made of 169 hexagonal fibers with D_o=400µm and D_i=390µm flat-to-flat bundled in honeycomb way and additional rounder becoming fibers at the two outer rows with D_o=400µm and D_i=350µm with 50 MPa applied inner pressure

These structures are able to be bundled to larger structures, as displayed in Figure 111. To ensure bundling without emerging interspaces, the outer walls of the seven single structures are filled till the outside. The outer walls of the structures show areas of increased stress up to a maximum value of 2900 MPa. Additionally, the area between the round fibers of two neighbored structures shows raised stress. Compared to the single structure (displayed in Figure 110), the bundled multi structure is exposed to lower maximum stress. Additional stress peaks occur at the outer round fibers of every structure. A straight outer surface is necessary for bundling those structures without emerging interspaces. Nevertheless, they increase the occurring stress at the outer walls of the multi structure, which may be caused

by the filled interspaces at the outside. Optimally, only the surfaces of the single structures, which will connect to the next structure and not the outer surfaces of the constructed multi structure, should be straight.

Principal stress [MPa]
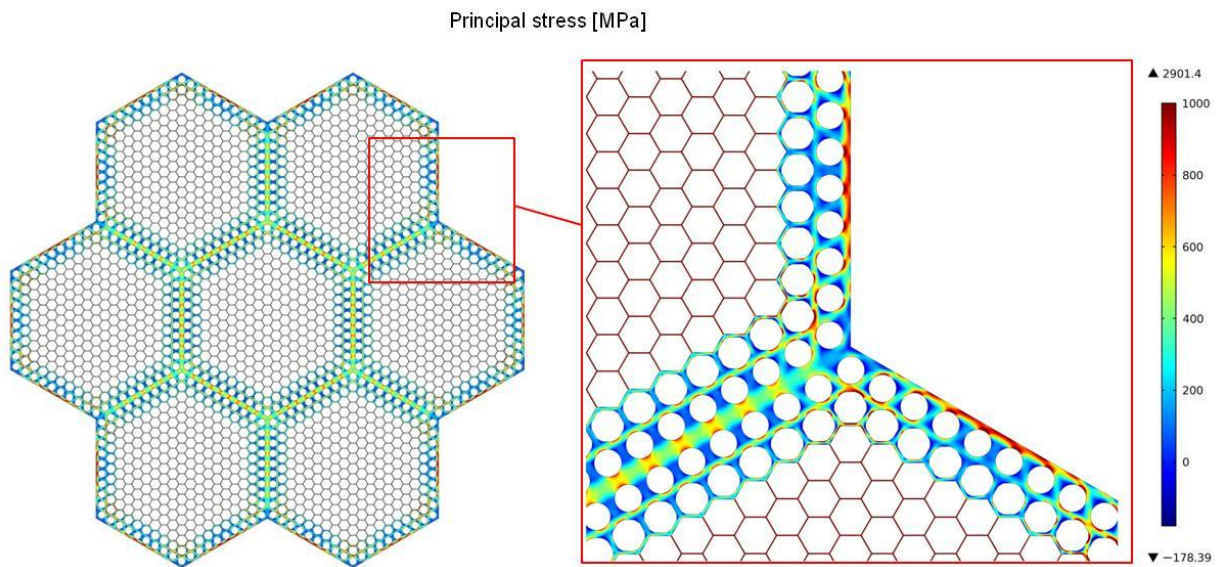
Figure 111: Occurring first principal stress in MPa of a multi-structure made of structures with 169 hexagonal single fibers with D_o=400µm and D_i=390µm flat-to-flat bundled in honeycomb way and additional rounder becoming fibers at the two outer rows with D_o=400µm and D_i=300µm and straight outer surfaces with 50 MPa applied inner pressure

In summary, hexagonal glass fibers are more convenient for becoming bundled to complex structures, for the impending influence of the interspaces which emerge at bundling round fibers is wiped out. The increased stress of single fibers related to the hexagonal shape does not appear after bundling because the applied pressure of the opposed wall surfaces is identical. The influence of the amount of bundles fibers to the inner stress value is quite low. Nevertheless, the increasing total expansion of the structure at increasing structure dimension has to be considered.

Fibers at the center of the structure should have high value of free space for increasing the gravimetric and volumetric storage capacity. At the outer surface of the structure, the fibers should become more massive in order to achieve lower stress values, but this results in lower free space. Optimally, the fibers at the outer surface should be round with low free

space so that the stress, which occurs at the outer surface, will be minimized. And this way the fibers are protected against outer influences.

According to the results of chapter 6.3.1 "Influence of sample dimension to strength", the inner fibers need to be minimized for increasing their strength. The large dimension of bundled structures compared to single fibers facilitates the handling. Using thick-walled fibers or solid fibers at the outer surface of the structure minimizes the strength-decreasing influence of outer defects.

5.7 Examination Of External Influences On The Strength Of Glass Structures

All executed experimental examinations demonstrated the phenomena that the spread of the burst pressure values is quite large. Commonly, the maximum value is more than two times higher than the minimum value of samples with identical parameters. The location of the initial fracture will be a hint of the weakest part of the structure. The circumstance where crack formation occurs with sonic speed necessitates further equipment for visualizing the initial fracture.

5.7.1 Localization Of The Initial Fracture At Pressure Load

In order to determine the location of the initial fracture at critical stress, a test series of 19 structures was executed. The locations of fracture are sectioned in "connection area", "middle part" and "closed end", which are illustrated in Figure 112. The collapse of the samples was recorded with a high speed camera and rate of 44000 frames per second. The displayed pictures show several successive frames with a temporal difference of 1/44000 seconds. The summarized results of this test series with one sample for each failure location containing burst pressure and location of rupture are demonstrated as follows. The results for all samples are displayed in Table 50.
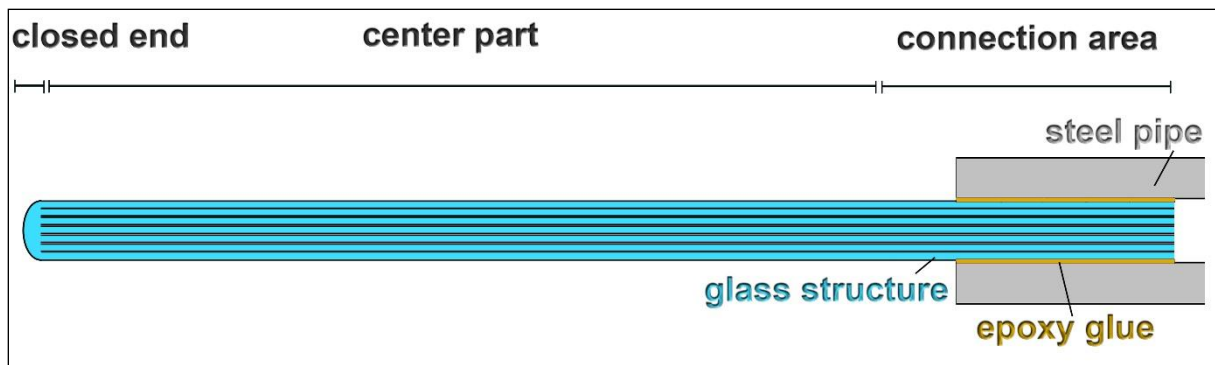
Figure 112: Schematic view of structure connected to high pressure setup
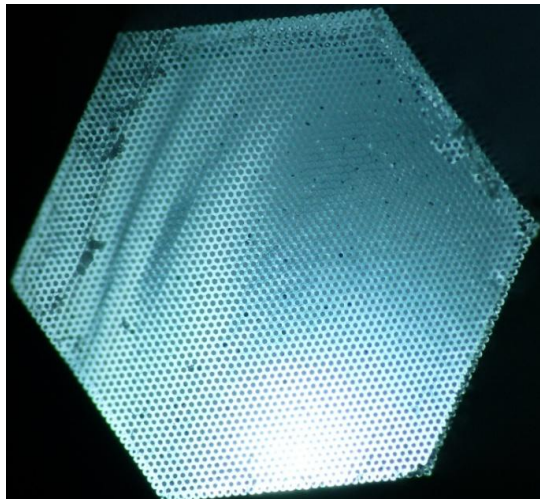
Average burst pressure [MPa]:	38.0
Minimum burst pressure [MPa]:	14.4
Maximum burst pressure [MPa]:	62.0
Rupture at connection area:	5 fibers
Rupture at middle part:	3 fibers
Rupture at closed end:	11 fibers

Figure 113: Microscopic view of tested structure with corresponding burst pressure values and location of the initial fracture

As shown in Figure 114, the first test sample initially broke in the middle part. Starting from this point the crack grows in axial direction to both sides with sonic speed. This sample showed the highest burst pressure of the test series with a value of 62 MPa. The glass fragments, emerging at fracture, are visible as bright powder in Figure 114.
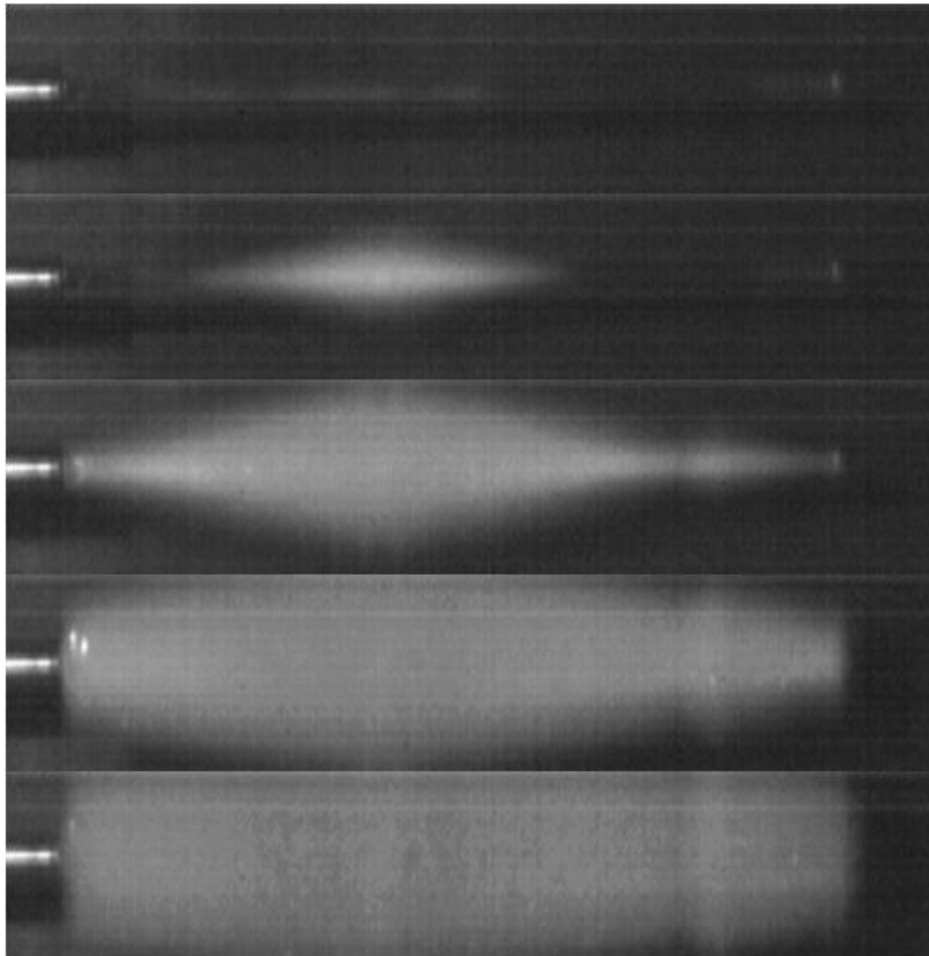
Figure 114: Sequence of bursting structure at 62 MPa with initial fracture at the middle part recorded with high speed camera with a frame rate of 44000 fps

The second example showed the lowest burst pressure of the test series with a value of 14.4 MPa. This sample broke initially at the closed end as demonstrated in Figure 115. The fracture traveled along the glass structure in axial direction. The particles of this sample have much larger dimension than the particles of the previously shown sample in Figure 114 which showed a more than 4 times higher burst pressure. Contrary, the previous sample, the particles of sample 04 are visible as broken bits of glass.
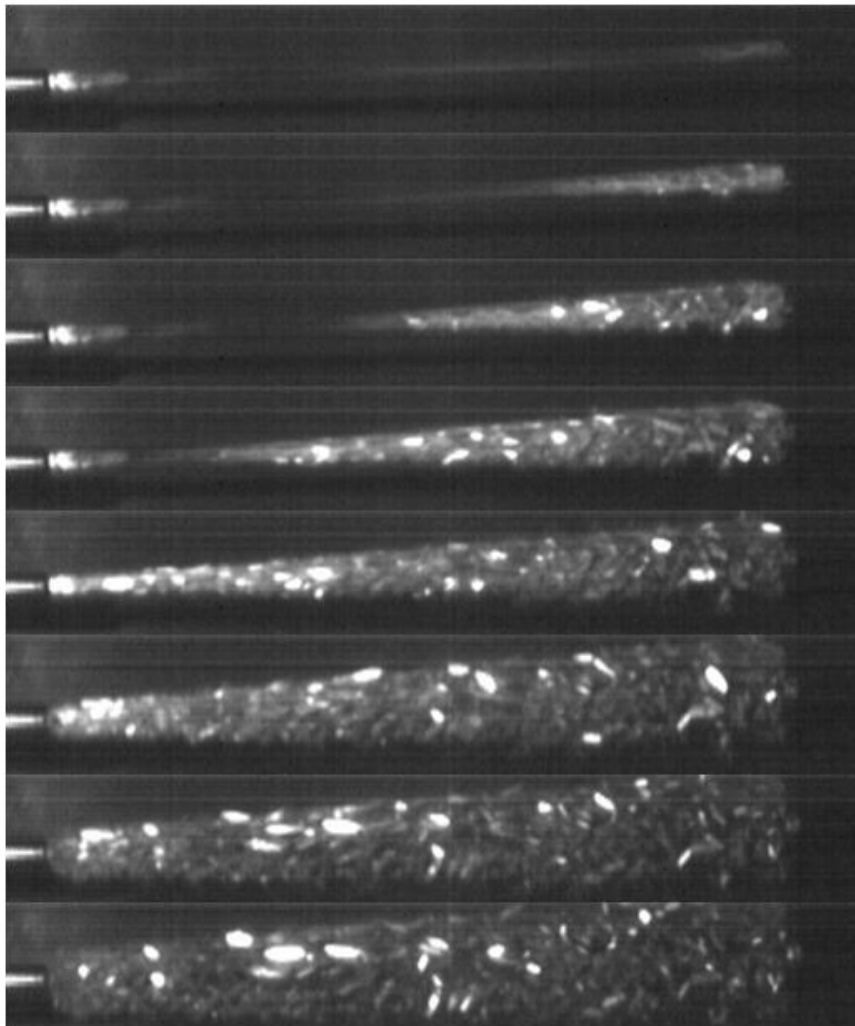
Figure 115: Sequence of bursting structure at 14.4 MPa with initial fracture at the closed end recorded with high speed camera with a frame rate of 44000 fps

The third example is test sample 05 which broke initially at the connection area. The steel pipe is recognizable at the left margin of Figure 116. Even in this case, the fracture grows in axial direction starting from the point of initial fracture. As well as the burst pressure, the particle size is dimensioned between sample 02 and sample 04.
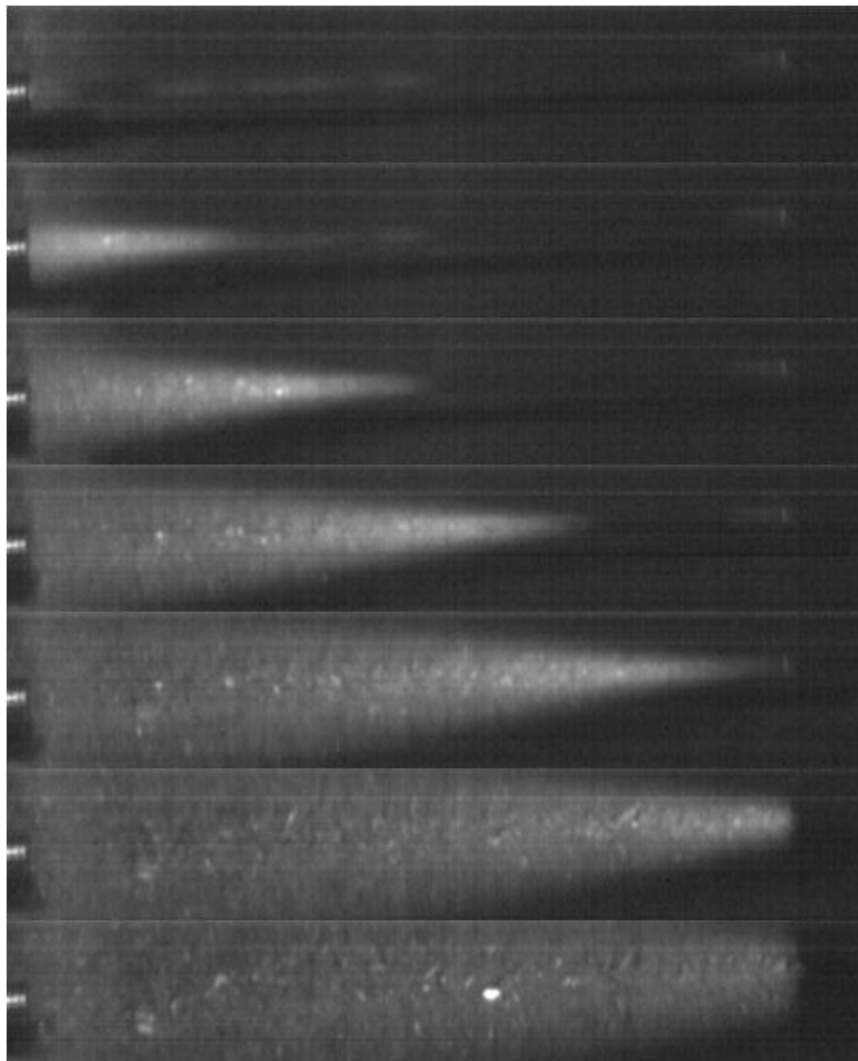
Figure 116: Sequence of bursting structure at 28.8 MPa with initial fracture at the adapter area recorded with high speed camera with a frame rate of 44000 fps

Table 50: Results of high speed recordings of burst pressure tests

Sample	Frame rate [fps]	Burst pressure [MPa]	Failure position	Fragment size
1	44000	52.0	Closed end	Powder
2	44000	62.0	Middle area	Powder
3	44000	33.7	Closed end	small / visible particles
4	44000	14.4	Closed end	large particles
5	44000	28.8	Adapter area	small / visible particles
6	44000	31.6	Closed end	small / visible particles
7	44000	42.0	Closed end	small / visible particles
8	44000	40.9	Middle area	powder / visible particles
9	44000	41.4	Closed end	powder / visible particles
10	44000	34.5	Adapter area	small / visible particles
11	44000	41.5	Closed end	powder / visible particles
12	44000	42.0	Closed end	powder / visible particles
13	44000	31.2	Closed end	small / visible particles
14	44000	41.4	Closed end	powder / visible particles
15	44000	57.2	Adapter area	Powder
16	44000	28.1	Middle area	small / visible particles
17	44000	45.2	Closed end	powder / visible particles
18	44000	45.6	Adapter area	powder / visible particles
19	44000	33.9	Adapter area	powder / visible particles

Summarizing, the initial fracture occurs at various locations despite identical parameters of the test samples. Most frequently, the samples broke at the closed end with 11 of 19 structures, whereby this is the critical location. The amount of fractures in the connection area and at the middle part is less than 50% (connection area) and 30% (middle part). That demonstrates that the glued connection is not the critical part of the system. The elasticity of the glue seems to be high enough for not inhibiting the glasses expanding during pressure treatment. Thus, the occurring stress in the connection area is lower than the stress caused by randomly distributed defects or the stress at the closed end.

Additionally, a relationship of the level of the burst pressure value and the location of initial fracture cannot be detected. The low, as well as, the high burst pressure values of one test series emerge well distributed in the three location areas, whereby the cause of initial fracture must be well distributed.. Micro defects at the surface or inside the material assume to be the main reason for crack initiation.

Likewise, the study of the location of the initial fracture show a coherence of burst pressure and fragment size. The higher the burst pressure the smaller are the particles which emerge at failure. Whereas the particles of test sample 02 show powdery scale at burst pressure of 62 MPa, the fragments become larger at sample 05 which broke at 29 MPa. Sample 04 showed the lowest burst pressure with 14 MPa and at the same time the largest particles.

5.7.2 Influence Of Defects On The Strength Of Structures

To determine the influence of different kinds of defects, several FEM simulations were executed. In the first simulation, different crack types at the surface of a borosilicate glass plate with applied tensile tension were considered. On that account, a crack with a randomly chosen length of 2 μm on the surface of a glass plate with applied tensile tension was simulated. The tip of the crack was designed in a rounded shape as displayed in Figure 117. The occurring stress at the tip of the crack has a maximum value of about 3000 MPa, whereas the stress in the residual material shows a constant value of about 100 MPa. The 15 times higher stress at the crack tip makes this area of the location of the initial failure.

A further conspicuity is the decreased stress at the inner surface of the crack. Caused by the crack, there is no tensile tension in this area and related to that there is no stress inside the material at this surface.
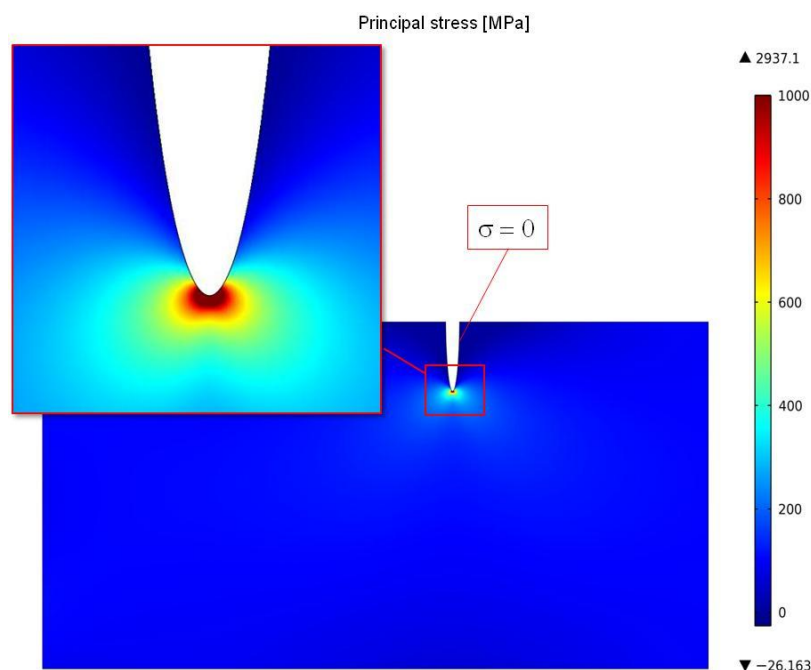
Figure 117: Occurring first principal stress in MPa at a crack in the surface with round tip

Replacing the round crack by one with acuminate tip with equal length of 2 μm, the stress at this sharp tip is raised to more than 5000 MPa. Figure 118 displays that behavior. Contrary to this, the residual stress shows stress values of about 100 MPa which is similar to the sample with rounded crack tip. The distribution of the increased stress area around the crack tip is similar at the two samples, as well as, the non-existent stress at the surface inside the crack.
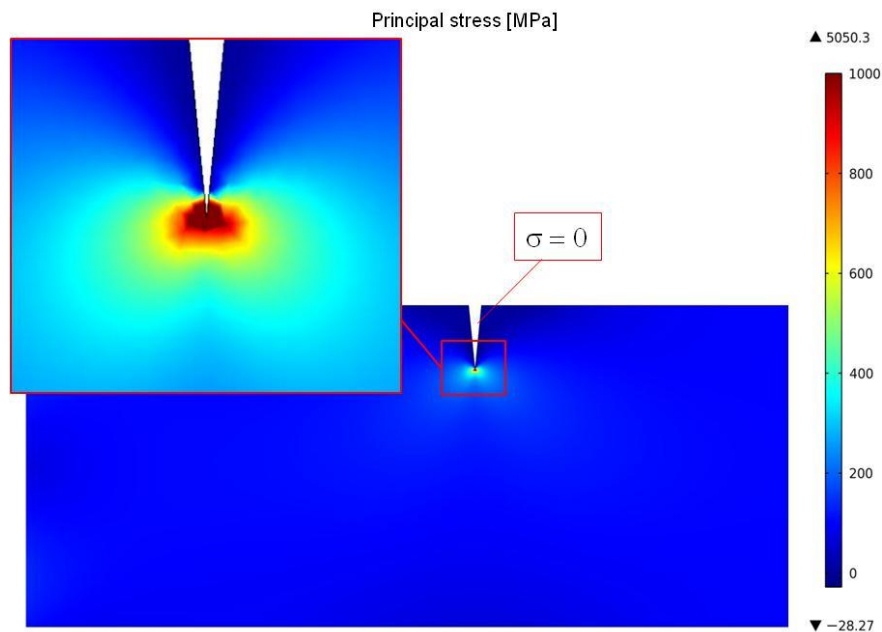
Figure 118: Occurring first principal stress in MPa at a crack in the surface with sharp tip

The following step was to switch from face plate to round fiber. A single fiber with D_o=400μm, D_i=300μm and a resulting wall thickness of 50μm was furnished with a sharp tipped crack with 25 μm length which is illustrated in Figure 119. The round shape of the sample changes the stress determination as compared with the face plate. Just as at the face plate, the maximum stress occurs at the tip of the crack. Also, there is no stress at the inner surface of the crack. As contrasted to the plain sample, the area of increased stress is larger at the hollow fiber. About 50% of the inner surface show nearly doubled stress up to about 250MPa, compared to the residual inner surface. Directly at the crack, the inner surface of the fiber shows compressive stress of about 30 MPa. This is visualized by the minus-sign in front of the stress in this area which is a hint for the presence of bending deformation.
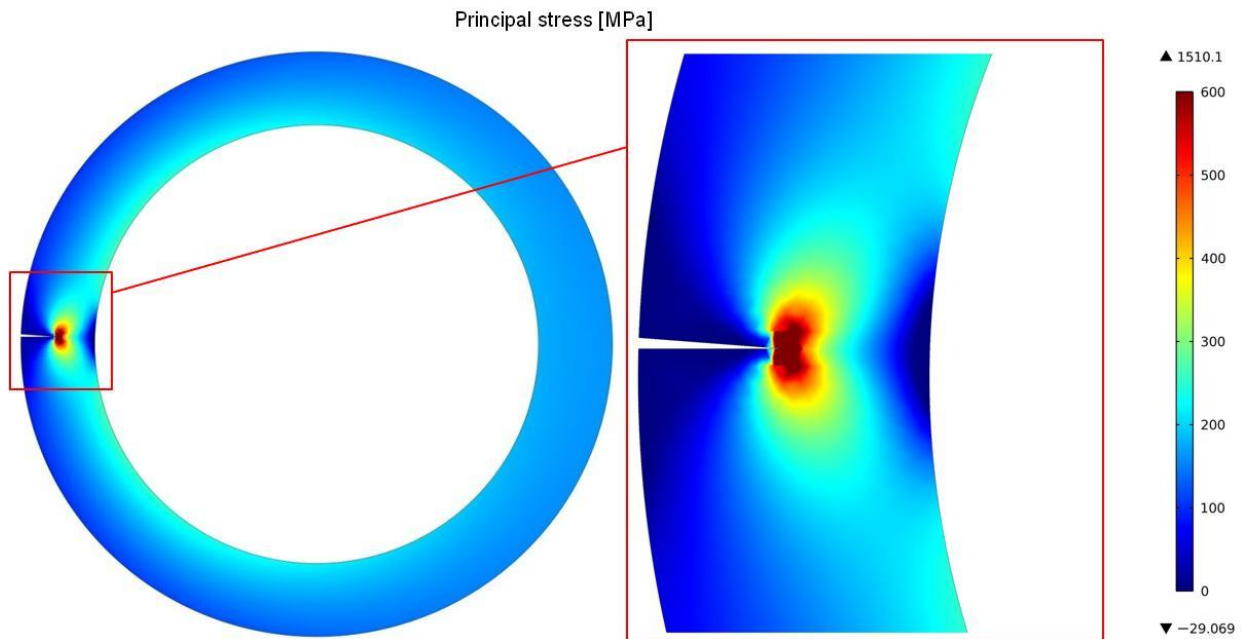
Figure 119: Occurring first principal stress in MPa at a crack with 25 µm length and sharp tip in the outer surface of a round single fiber with D_o=400µm and D_i=300µm with 50 MPa applied inner pressure

Hence, the presence of compressive stress can be explained by having a look to the expansion. The left picture in Figure 120 visualizes the expansion of the fiber at pressure treatment. In contrast to a defect free single fiber, the expansion is imbalanced. The highest expansion occurs in the area around the crack. Also the side opposed the crack shows higher deformations. Related to the whole fiber, the imbalanced expansion leads to uneven deformation. Comparable to the tensile tension, which is caused by the applied pressure, the crack causes bending deformation, which is exaggerative illustrated in Figure 120. The black lines show the initial position of the fiber without pressure inside. The bending deformation leads to enlarging of the crack. Accordingly, the inner surface of the fiber close to the crack will be clinched, whereby the compressive stress emerges.
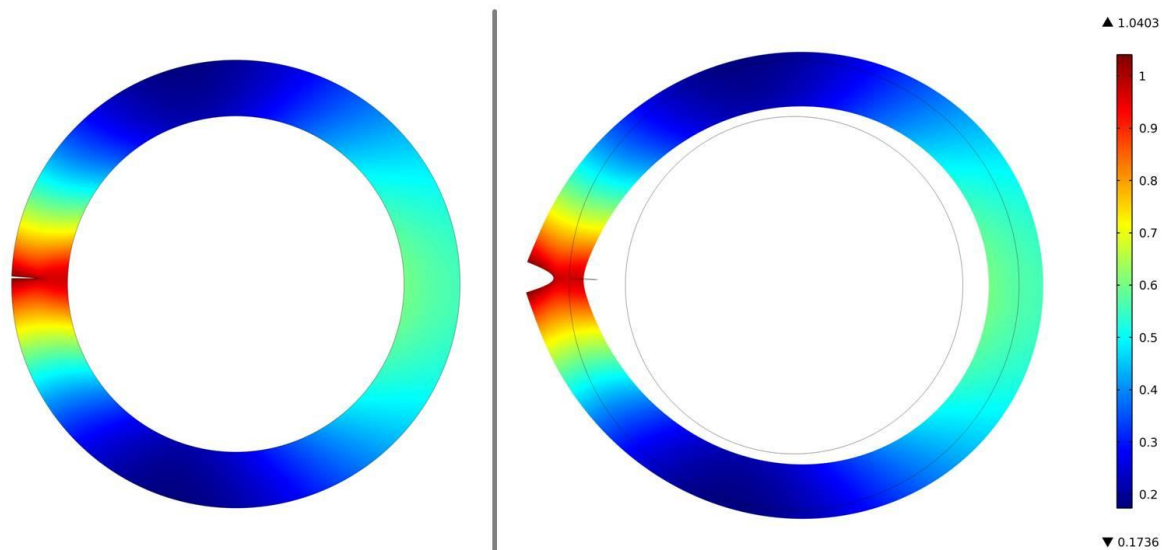
Figure 120: Occurring expansion in µm (left) at a crack with 25 µm length and sharp tip in the outer surface of a round single fiber with D_o=400µm and D_i=300µm and exaggerated displayed deformation with 50 MPa applied pressure

In order to determine the influence of the crack length on the occurring stress and deformation, a series of 5 samples with varying crack length was simulated. Consequently, the crack length was increased from 5 µm to 45 µm in steps of 10 µm. The result of the comparison is displayed in Figure 121. Going on from the left to the right column the crack length is increased stepwise from 5 µm up to 45µm. The pictures above the columns visualize the calculated stress in the fiber at the respective applied pressure. The compressive stress, which is visualized by the negative minimum stress values, increases with growing crack length, as does the maximum stress at the crack tip and the expansion of the fiber. Furthermore, the area of increased stress grows with increasing crack length. Although the crack length was increased with constant rate the increase of maximum and compressive stress as well as expansion follows an exponential increase.
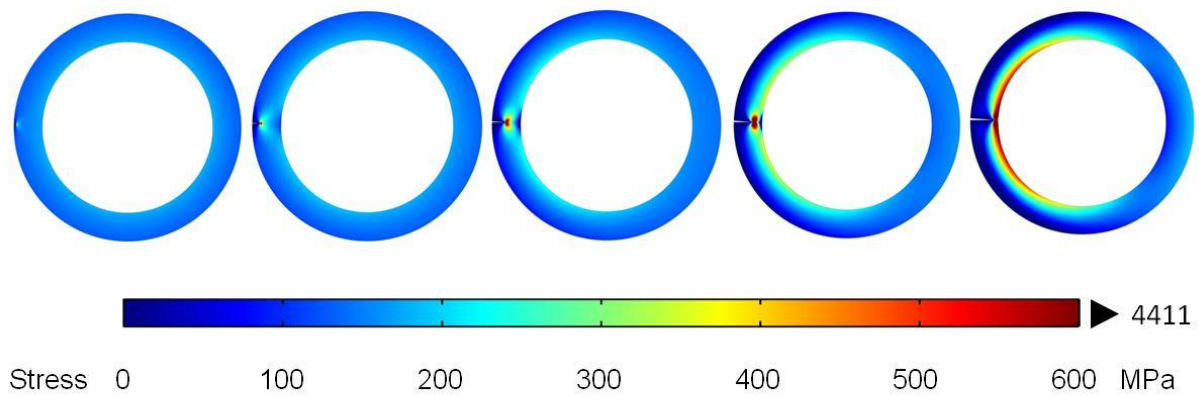
Crack length [µm]				
5	15	25	35	45
Minimum stress [MPa]				
-2	-3	-29	-62	-85
Maximum stress [MPa]				
427	806	1510	2551	4411
Expansion [µm] / [%]				
0.8 / 0.2	1.1 / 0.3	2.1 / 0.5	4.2 / 1.1	8.8 / 2.2

Figure 121: Influence of the crack length on the occurring first principal stress in MPa at a crack with sharp tip in the outer surface of a round single fiber with D_o=400µm and D_i=300µm with 50 MPa applied pressure

The dependence of stress and expansion from the crack length is illustrated in Figure 122. The diagram displays the internal stress in MPa at the primary ordinate (left) and the expansion in µm at the secondary ordinate (right). The abscissa shows the crack length in µm. The graphs showing minimum and maximum stress in MPa as well as the expansion in µm plotted against crack length in µm follow an exponential trend.
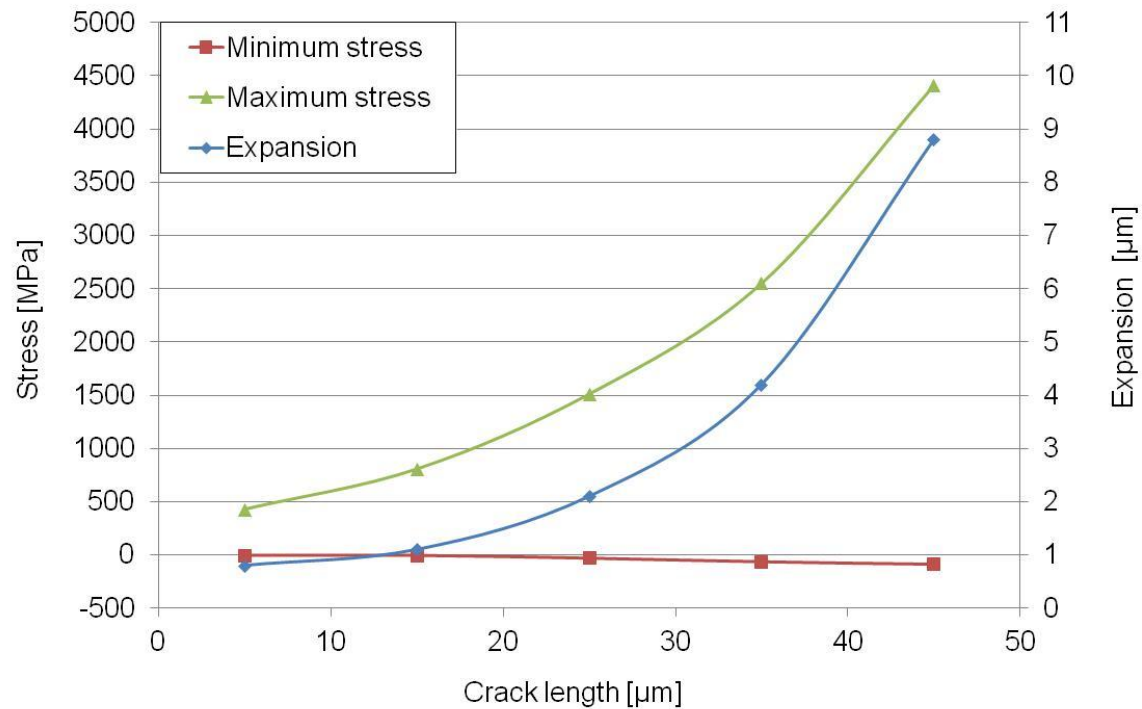
Figure 122: Dependence of the first principal occurring stress, as well as, the expansion on the crack length at a crack with sharp tip in the outer surface of a round single fiber with D_o=400µm and D_i=300µm with 50 MPa applied pressure

Due to the fact that the stress peak is located directly at the tip of the crack, the diameter of that crack does neither have an influence on the occurring stress nor to the expansion, as demonstrated in Figure 123. Going from the left to the right column, the crack diameter is increased from 2µm to 4µm respectively 10µm. The pictures above the columns visualize the calculated stress in the fiber at the respective applied pressure. The length of the crack kept unchanged. All three samples show nearly similar values of minimum and maximum stress as well as expansion.
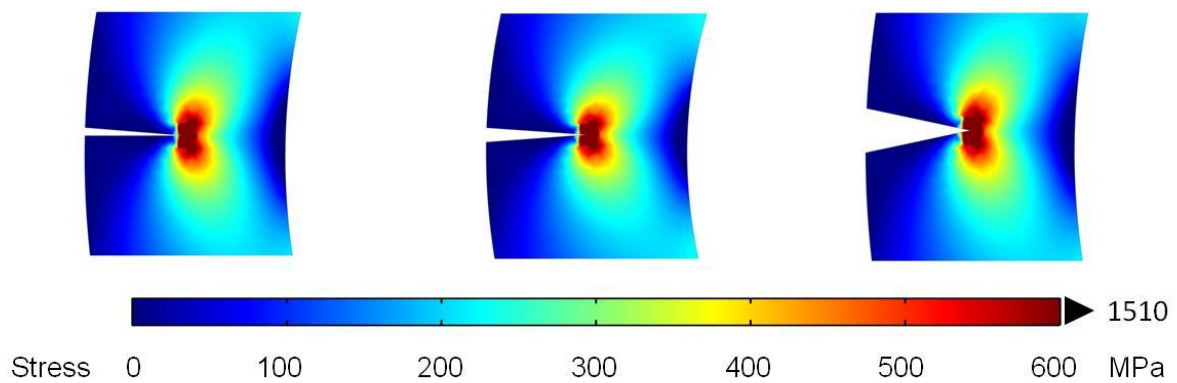
Crack diameter [µm]		
2	4	10
Minimum stress [MPa]		
-29	-29	-29
Maximum stress [MPa]		
1510	1486	1505
Expansion [µm] / [%]		
2.08 / 0.5	2.08 / 0.5	2.08 / 0.5

Figure 123: Influence of the crack diameter on the occurring first principal stress in MPa at a crack with sharp tip in the outer surface of a round single fiber with D_o=400µm and D_i=300µm with 50 MPa applied pressure

As mentioned in chapter 3.4 "Defects", cracks on the surface are not the only possible kinds of defects. Further frequently occurring defects are voids inside the material. Figure 124 shows a single fiber with two different sized voids in the material. In the area of the voids, the material is exposed to high stress with a maximum value of 533 MPa at the larger void, respectively 477 MPa at the smaller void. Additionally, the material close to both voids is exposed to compressive stress with a value of about 8 MPa. The stress inside the residual structure is well distributed from 130 MPa at the outer surface to 180 MPa at the inner surface of the fiber. Comparing the voids inside the material directly with the cracks at the surface leads to the result that the influence of cracks to the strength of a glass structure is larger because of the higher resulting stresses inside the material. Nevertheless, small voids lead to stress which usually exceeds the residual stress inside the structure whereby the initial failure occurs in this area.
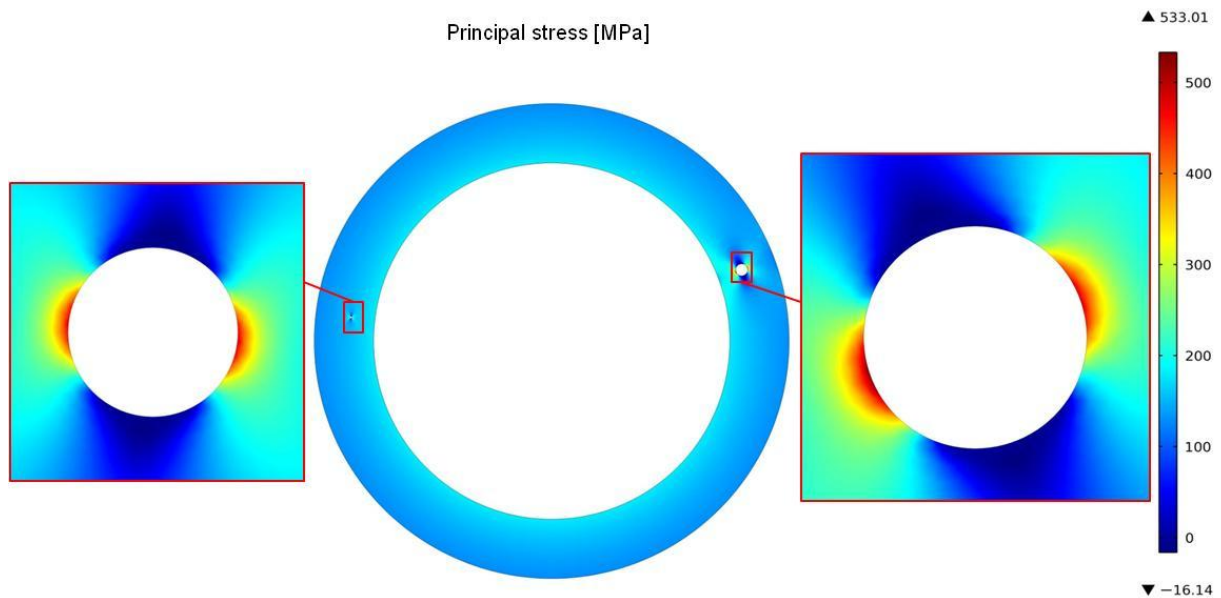
Figure 124: Occurring first principal stress in MPa with differently scaled voids inside the material of a round single fiber with D_o=400µm and D_i=300µm with 50 MPa applied pressure

According to chapter "3.4 Defects", the influence of cracks depends on the temperature. If the critical stress is exceeded at the crack tip, the crack grows with supersonic speed and the sample breaks. Low temperature delays the crack growth, whereby its negative influence on the strength is diminished and the strength of the material is increased.

To determine the influence of cracks experimentally, a test series was executed, whereby the burst pressure of single fibers was determined in liquid nitrogen (-196 °C) and at 40 °C for comparison. The results are displayed in Table 51.

Table 51: Influence of varying ambient temperature on the burst pressure of round single fibers made of borosilicate glass

Test temperature	D_o ["]	Free space [%]	Average burst pressure [MPa]	Minimum burst pressure [MPa]	Maximum burst pressure [MPa]
40 °C	0.015	75	38.9	11.5	49.9
-196 °C	0.015	75	84.6	51.2	122.2

The minimum burst pressure is about 5 times higher at -196 °C than at 40 °C. The average and maximum burst pressure is more than doubled at the lower temperature. Plotting the values of minimum, maximum and average burst pressure into a diagram as shown in Figure 125, demonstrates the increased strength of the samples at low temperature.
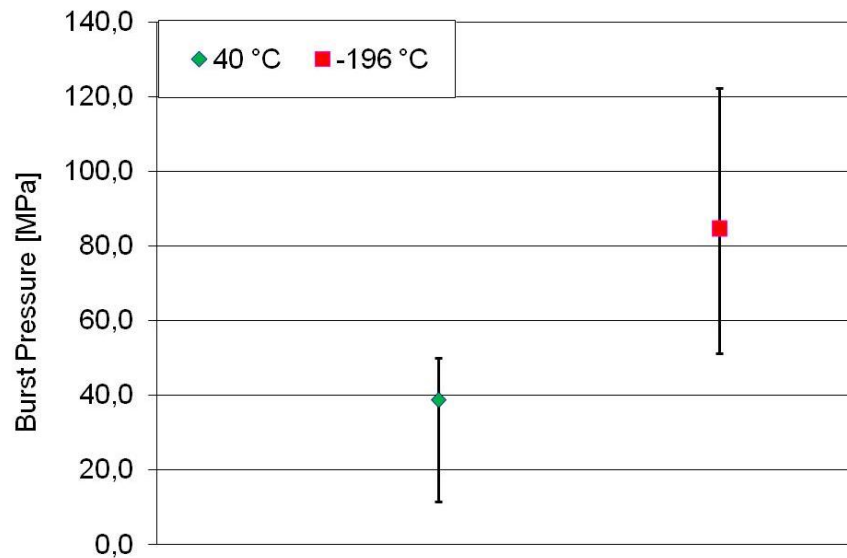
Figure 125: Influence of varying ambient temperature from 40°C to -196°C on the burst pressure of round single fibers made of borosilicate glass

The increased stress at structures with defects, which was calculated in FEM simulation before, fully corresponds to the lower burst pressure of samples tested at 40 °C. Decreasing the ambient temperature from 40 °C to -196 °C the influence of defects could be reduced by slowing down crack growth whereby the average strength of the material could be doubled.

Furthermore, the already tested structure 3624 10 showed a high number of large defects on the outer surface of the structure. The test results are shown and discussed in chapter 5.4.6 "Hexagonal Structures Made Of Hexagonal Single Hollow Glass Fibers And Solid Fibers As Outer Fiber Layer". The measured burst pressure values of these samples are lower than the values of comparable structures.

Regarding the case that single fibers inside a structure will fail, further simulations dealing with that problem were executed. Figure 126 demonstrates the failure of a single fiber and additionally three neighbored fibers in a hexagonal structure. The failure of a single fiber in a

structure does not result in peaks on increased stress. Rather, the walls of the fibers show decreased and well distributed stress values.
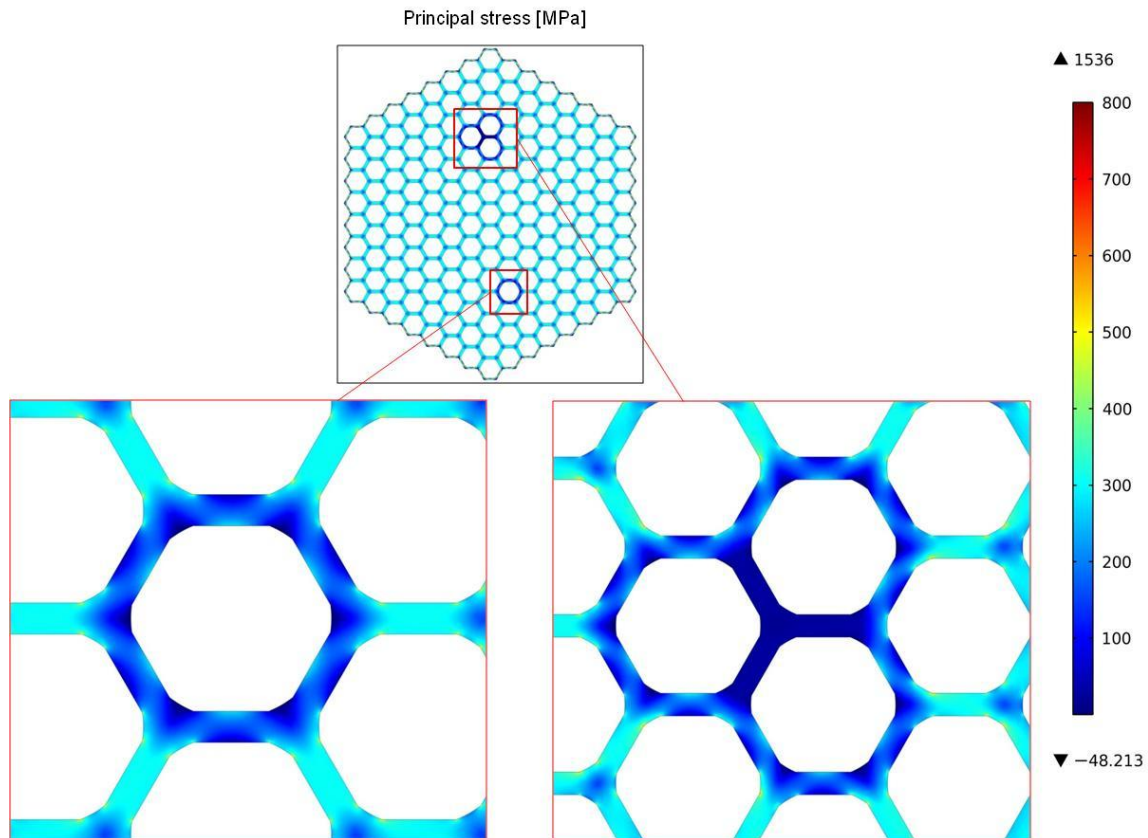
Figure 126: Occurring first principal stress in MPa with failing single fibers inside a structure made of 169 single fibers with D_o=400µm and D_i=300µm flat-to-flat with 50 MPa applied pressure

In summary, all kinds of defects show negative influence to the structure. Any kind of cracks or voids evoke points of high stress. At these points the critical stress will be reached at first, whereby the initial crack occurs at this point. Failing single fibers inside the structure do not evoke stress peaks. On the other hand, leakages may occur or the surface of neighboring fibers may be damaged, whereby the strength of these fibers will be lowered.

Generally, avoiding any kinds of defects should have highest priority for reaching higher strength values which are closer to the theoretical strength of glass. Doing so ensure that the burst pressure of the fibers can be increased and at the same time the spread of the burst pressure values minimized. Appropriate examinations with regard to the protection of the

coating layer of the outer surface of the fibers (applied directly after the production processes) are discussed in the PhD thesis of R. Meyer [169 - 173].

6 Summary And Conclusion

Thin walled glass fibers offer the opportunity to withstand high inner pressure due to their high tensile strength, making stored gases at high pressure in glass fibers, and leading to an optimal storage system with a storage pressure of 70MPa. In order to obtain a high storage volume, high amounts of hollow glass fibers are necessary. The single hollow glass fibers need to be bundled to complex structures in order to keep the outer volume of the storage system as small as possible.

Bundling micro-scale single hollow glass fibers to complex structures provides the advantage of being independent in the outer shape and volume of the system because every single fiber works as an independent pressure vessel.

6.1 Summary

The primary objective of the thesis was the examination of the occurring stress in complex glass structures made of a high number of hollow glass fibers during inner pressure treatment. Therefore, experimental studies as well as FEM simulation were used for examination and evaluation.

The common test methods to determine the tensile strength of a material in experimental way is the tensile test method. In order to ensure that the burst pressure test method, which is used in this thesis, is a suitable method to determine the tensile strength of the samples, the burst pressure method was compared to the tensile test method. The strength of the single hollow glass fibers was determined with the burst pressure test methods and compared to the results of tensile test method with identical fibers. Although the speed of force application differed at the two test methods, both test methods resulted in comparable strength values for the samples. Therefore, the burst pressure method is a further adequate tool to determine the tensile strength of a material.

To examine the influence of varying properties like dimension or amount of single fibers on the strength of a structure, a large number of test series is necessary. Due to the fact that the burst pressure test method is a destructive test method, at least 30 test samples per test series are necessary in order to obtain a valid statistical evaluation. In addition to the strenuous effort and the high costs of such experimental examinations, numerical simulation appeared as a helpful tool. In this thesis, FEM simulation was used to determine the occurring stress and expansion of single hollow glass fibers. as Additionally, complex glass

structures made of bundled glass fibers was determined at applied inner pressure. Therefore, several models of glass structures were simulated concerning the occurring stress and expansion at an applied inner pressure of 50MPa. The critical stress value, at which the glass structure will break, is specific of the material. Increasing the inner pressure constantly in a glass structure will increase the occurring stress in the material. In structures which show higher stress at an applied inner pressure of 50MPa the critical stress value will be reached at lower inner pressure, compared to structures which show lower stress at the same inner pressure. Therefore, high stress at applied inner pressure of 50MPa will lead to lower strength of the structure.

The results of FEM simulation of glass structures in this thesis were compared to the results of burst pressure tests of comparable structures. Both methods, the theoretical and the experimental examination, lead to comparable results. Structures which show in FEM simulation high stress show equally low burst pressure and, corresponding to that, low strength. Calculating the stress in the material with the Barlow's formula, based on the previously examined burst pressure value, leads to comparable results. Therefore, FEM simulation poses an adequate tool for comparing the strength of different complex structures made of hollow glass fibers. Due to the large difference between theoretical strength and practical strength, FEM simulation is not valid to determine the concrete pressure at which the structure will break.

According to FEM simulation results, the glass material has no influence on the occurring stress and expansion of glass fibers. The occurring stress in three single hollow glass fibers made of different materials at an applied inner pressure of 50MPa is nearly identical. Due to the fact that the critical stress value at which the material will break is material specific the glass material with the highest critical stress value will be able to withstand the highest inner pressure. Previously executed burst pressure tests of single hollow glass fibers made of different materials provide borosilicate glass to withstand the highest inner pressure values and thereby to have the highest critical stress value. Respectively, borosilicate glass has been chosen as basic material for the produced glass as well as for the simulated structures in this thesis.

To determine the influence of the dimension of single fibers to their strength, the stress in different scaled single fibers with identical inner diameter but varying wall thickness was calculated at applied inner pressure of 50 MPa. It turned out that the stress increases exponentially at decreasing wall thickness. Related to that, the wall thickness should not undercut a certain value, otherwise the high occurring stress leads to failure at comparable low pressures.

A low wall thickness related to the diameter is necessary for obtaining high gravimetric and volumetric storage capacities. The relation of wall thickness and diameter is defined as free space. Lower wall thickness in relation to the diameter results in a higher free space. Calculating the gravimetric storage capacity of samples with varying free space also leads to an exponential increase of the gravimetric storage capacity at continuously increased free space. Figure 127 [170] illustrates that behavior graphically for an applied pressure of 20MPa, 35MPa and 70MPa. The exponential trend of the graphs leads to high increase of the gravimetric storage capacity from a free space of about 80%.
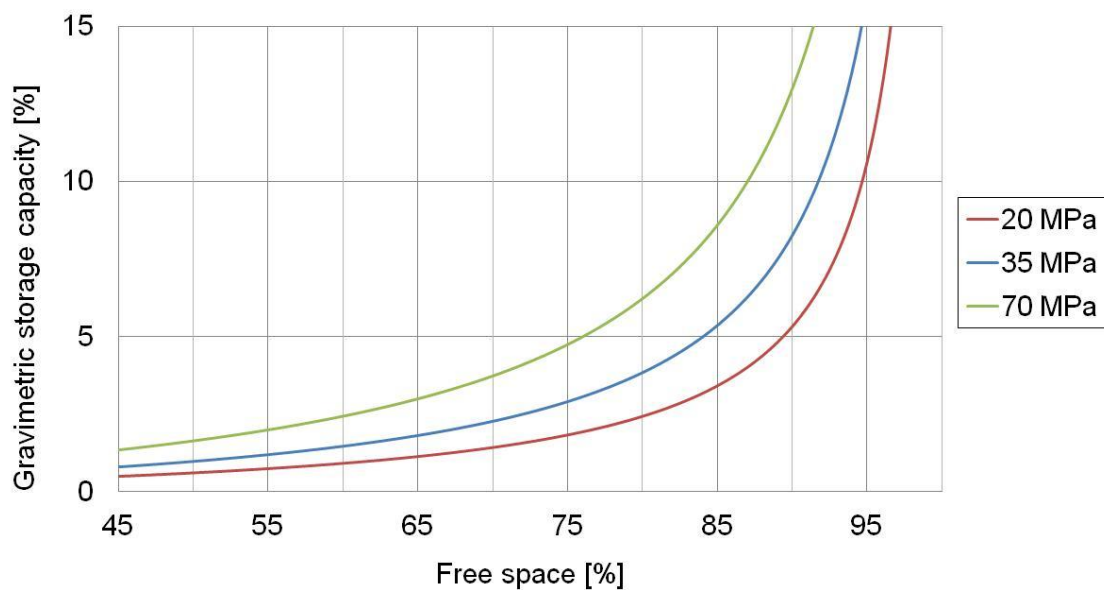
Figure 127: Dependence of the gravimetric storage capacity on the free space at 20 MPa, 35 MPa and 70 MPa

In chapter 5.6.3 an exponentially decreased strength at increasing free space was noticed and discussed. Due to these results, increasing the gravimetric storage capacity by increasing the free space will always lead to equally decreased strength, which are caused by higher occurring stress values. The dependence of the burst pressure on the free space of a structure could be confirmed with experimental tests. Samples with a free space of more than 60% show highly decreased burst pressure values compared to structures with 45% free space. Therefore, an optimal free space value, which poses a good compromise between storage capacities and strength, needs to be found. Caused by the large difference between theoretical and practical strength of glass this value has to be confirmed by

experimental examination. According to Figure 127, a free inner volume of more than 85% is necessary for obtaining a gravimetric storage capacity of 8% at an inner pressure of 70MPa. As shown in Figure 54 in chapter 5.5, structure 399-331-A with a free space of 64% showed the highest gravimetric storage capacity of all tested structures with a value of about 2.5% at its maximum burst pressure value of 71.9MPa.

Further simulations were examined regarding the influence of changing the fiber's size by keeping the ratio of inner and outer diameter constant. That examination led to constant values of stress and expansion in FEM simulation. Contrary to this, practical experiments show increasing strength of smaller scaled fibers. Griffith gave a possible explanation for that phenomenon. According to his theory, the statistical possibility of emerging large-scale defects, which will decrease the strength massively, is higher in larger samples. According to these results, the single fibers have to be preferably small for obtaining higher strength.

In order to obtain higher volume for gas storage bundling single fibers to structures is necessary. According to FEM simulation, bundled hollow glass fibers show different behavior at inner pressure treatment than single fibers. Bundling round hollow glass fibers to structures according to the principle of close packing of spheres always leads to interspaces which are not able to withstand comparably high pressure to the fibers due to their unfavorable geometry. Bundling hexagonal fibers in honeycomb structure prevents this problem but leads to some disadvantages. The behavior of hexagonal single hollow glass fibers differs from that of complex structures made of bundled hexagonal single fibers. This is caused by the fact that the applied pressure at the opposed surfaces of the inner walls is identical. Therefore, any bending deformation, which inevitably leads to areas of increased stress, is prevented within these walls. This stabilizing character of the neighbored fibers makes the inner fibers possible to withstand high pressure although the wall thickness can be lower than that of fibers without neighbored fibers. Conversely, outer fibers of a structure with round shape and at the same time higher wall thickness and with low free space show lower stress at pressure treatment. Any interspaces or voids, which are caused by the round shape of the outer fibers, have to be filled with glass or any other material, which is resistant to the stored gas. Thus, the stress which emerges at the outer structure walls is decreased. Furthermore, the higher wall thickness protects the fibers against outer influences. Such structures can be bundled to multi structures. Therefore, a hexagonal outer shape of the structure is preferable due to the identical advantages of bundling hexagonal single fibers. Similar to the way of bundling single structures, inner structures made of fibers with higher free space, which are surrounded from outer structures with higher wall thickness and round outer fibers show decreased stress at the outer surface of the multi structure.

Further examinations were done to determine the influence of defects such as cracks on the surface or voids inside the material of a fiber. Several FEM simulations were executed. According to these simulations, all kinds of defects in the material or at the surface lead to areas of increased stress. The critical stress, which leads to fracture, will be reached in this area first. An exception of this is the failure of single fibers inside an entire structure. Hence, the stress at the participating walls decreases. Due to the fact that collapsing fibers will break in small pieces the surface of these walls may be damaged by glass fragments, whereby cracks at the surface may occur.

A further problem which was examined in this thesis is the expansion, especially of large structures during pressure treatment. According to FEM simulation, the total expansion of a structure grows with its size. Thereby, a possibly low expansion is necessary when thinking about larger structures, which consist of many thousand single fibers. Accordingly, the construction of a storage system has to compensate the stress, which is caused by the expansion of the glass modules. Furthermore, the expansion has to be considered at the connection parts of the glass structure to other materials. These materials have to be able to compensate the expansion in order to prevent further occurring stress.

6.2 Conclusion

FEM simulation is an adequate tool for the examination of the optimal glass structure for storing gas at high pressure,. It provides the possibility of examining the influence of varying shape or dimension of the single fibers inside a structure. In addition, it is a useful method for the amount of these fibers on the occurring stress during pressure treatment and on the strength of the structure.

The optimal structure with the ability to withstand high inner pressure shows possibly low inner stress during pressure treatment. Therefore, any kind of interspaces between the bundled single fibers has to be avoided. Additionally, the shape of the inner fibers of a structure has to be hexagonal shaped. The wall thickness of the inner fibers has to be low in order to decrease the amount of glass material and thereby increase the volumetric and gravimetric storage capacity. In contrast, the outer fibers of the structure need to be round shaped. Furthermore, the wall thickness of these round outer fibers has to be higher than of the inner fibers to compensate the increased stress at the outer surface, which is caused by the expansion of the thin-walled inner fibers. A model of such a structure is shown in Figure

110 and discussed in chapter 5.6.14 "Optimized Structure Based On The Preliminary Findings".

According to the results of FEM simulation as well as experimental studies, which demonstrate an increasing strength at decreasing sample size and constant free volume, the size of the structures has to be as small as possible to reach higher burst pressure values.

In order to be competitive with existing hydrogen storage systems, a gravimetric storage capacity of at least 8% has to be reached. According to the relationship of the gravimetric storage capacity and the free space of a structure, which is displayed in Figure 127, a free inner volume of 85% and a storage pressure of 70MPa are necessary for obtaining this target. Regarding the inalienable minimum safety-factor of 2, the burst pressure of such a structure has to be at least 140MPa. None of the tested structures was able to reach this value. The highest burst pressure values of about 100MPa were reached at structures with about 45% free inner volume. Structures with higher free inner volume showed much lower burst pressure values. The best tested structure concerning the free inner volume and burst pressure is structure 399-331-A, with a free space of 64% and a maximum burst pressure value of 71.9MPa. The gravimetric storage capacity of this structure is 2.5%.

With regard to the large difference of theoretical and practical strength of glass, such optimized structures are theoretically able to withstand the desired inner pressure of 140MPa. The major cause of the much lower practical strength of glass are defects on the surface and in the material, which are primary related to the production conditions as well as to the handling process. In order to determine the theoretical strength of glass according to Griffith, the atomic distance between Si and O is taken as value for the minimum crack size. The strength directly correlates to the crack dimension. All kinds of cracks which are caused during production or treatment (handling, transport, etc.) have a larger scale and therefore, the strength of the material is decreased. Indeed, this is how the difference of theoretical and practical strength can be explained. In order to induce the practical strength of glass closer to the theoretical strength any kind of defects have to be avoided. Therefore, in order to avoid the discharge with foreign substances sterile manufacturing conditions are necessary

Furthermore, any direct contact to the unprotected surface leads to micro-scale defects and has to be prevented. Therefore, the drawn fiber must not have contact to any part of the machinery to avoid scratches on the surface. Additionally, the drawing conditions must be optimal for preempting the existence defects like knots, bubbles or striations. After the production process, the glass samples are exposed to air humidity and contact during transportation and handling, whereby further defects of the surface are created. An outer

protection, exemplary realized with a directly after final production of the structures applied polymer coating on the surface of the samples, will be necessary.

Neither the defect free production, nor the additional protection against outer influence can be realized with the actually manufacturing process, whereby the desired strength cannot be reached at the actual structures.

7 Future Prospects

In order to prevent the existence of strength decreasing defects the optimization of the production process, as well as the protection of the surface of the glass structures after production is necessary. An examination of protecting single fibers using different kinds of ALD coating (atomic layer deposition) were examined by R. Meyer [169]. The use of polymer coating, which is applied directly after the final production of the structures, is a promising way of protection and needs to be examined in the future.

Structures with optimized design, according to the results of FEM simulation in this thesis should not be produced until the optimization of the production process. Due to the fact that only the theoretical strength can be examined with FEM simulation, the optimal dimension of these optimized structures has to be determined in experimental studies.

Looking at a three-dimensional glass fiber or structure, there are further potential areas of increased stress. These areas also need to be examined and optimized in order to decrease the occurring stress during pressure treatment. One of these areas is the connection area of glass and metal, if the expansion of the glass structure is prevented by the metal tube, as displayed in Figure 128. The picture shows a single fiber which is glued into a stainless steel pipe. According to FEM simulation, the glass shows increased stress, especially in the connection area. The glue prevents the expansion of the glass which occurs during pressure treatment. Beyond the area of connection, this prevention is not given anymore and the glass will expand. Consequently, uneven deformation of the glass occurs by which the mentioned stress peak emerges. The stress, which occurs at the inner surface of the fiber is tensile stress, while the stress at the outer surface in this area is characterized by compressive stress. The main influence on the occurring stress is the hardness of the glue. Using glue with lower hardness may compensate the expansion of the glass, so that the occurring stress will be reduced. The influence of different kinds of glue with varying hardness needs to be determined in the future.
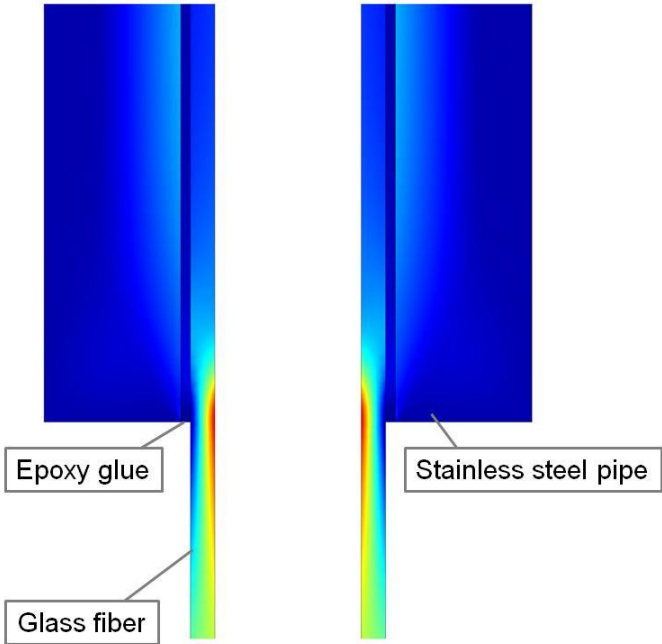
Figure 128: Current connecting method of glass samples to the high pressure setup

8   List Of Figures

9 List Of Tables

10 List of References

1   Ahluwalia, R.K.; Peng, J-K; Hua T.Q.; **Cryo-Compressed Hydrogen Storage: Performance and Cost Review**; *Compressed and Cryo-Compressed Hydrogen Storage Workshop;* Argonne National Laboratory; Crystal City Marriott, Arlington VA; 2011

2   Schlapbach, L.; Züttel, A.; **Hydrogen – storage materials for mobile applications**; *Nature*; Vol. 414; 2001

3   Lide, R.; **CRC Handbook of Chemistry and Physics**; 90th edition; 2010

4   Müller, M.; **Die Entwicklung von Energieversorgungssystemen mit PEM-Brennstoffzellen**; *gwf Gas Erdgas*; 2003

5   Morris, C.; **Brennstoffzelle ist nicht gleich Brennstoffzelle**; *Telepolis*; 2004

6   H. Boetius; **Die Wasserstoffwende**; 2005; p.83

7   Berstad, D. O.; Stang, J. H., et al; **Comparision criteria for large-scale hydrogen liquefaction processes**; *International Journal of Hydrogen Energy;* Vol. 34; 2009

8   Wolf, J.; Linde Gas AG; **Liquid Hydrogen Tank & Filling Systems for Vehicles**; *Workshop Wasserstoff Speicherung*, Günzburg, 2001

9   Garche, J.; Treffinger, P.; Jörissen, L.; **Wasserstoffspeicherung und Verkehr**; *FVS Themen 2001*; 2001

10   Ahluwalia, R. K.; **System Level Analysis of Hydrogen Storage Options**; *DOE Hydrogen Program Review*; 2010

11   Ross, D. K.; **Hydrogen storage: The major technological barrier to the development of hydrogen fuel cell cars**; *Vacuum - Surface Engineering, Surface Instrumentation & Vacuum Technology*; 80; 2006

12   Kampitsch, M.; BMW Group; **BMW – Cryocompressed Hydrogen Refueling**; *WHEC World Hydrogen and Energy Conference 2012*; Canada; 2012

13   U.S. Department of Energy Hydrogen Program; **Technical Assessment: Cryo-Compressed Hydrogen Storage for Vehicle Applications**; 2006

14   Dillon, A. C.; Heben, M. J.; **Hydrogen storage using carbon adsorbents: past, present and future**; *Applied Physics A - Materials Science and Processing*; 72; 2001

15   Zhou, L.; Zhou, Y.; Sun, Y.; **A comparative study of hydrogen adsorption on superactivated carbon versus carbon nanotubes**; *International Journal of Hydrogen Energy*; 29; 2004

16   Niemann, M.U. et al.; **Nanomaterials for Hydrogen Storage Applications: A Review**; *Journal of Nanomaterials*; Volume 2008

17   Anson, A.; Callejas, M. A.; Benito, A.M.; Maser, W. K.; Izquierdo, M. T.; Rubio, B.; Jagiello, J.; Thommes, M.; Parra, J. B.; Martinez, M. T.; **Hydrogen adsorption studies on single wall carbon nanotubes**; *Carbon*; 42; 2004

18   Liu, c.; Fan, Y. Y.; Liu, M.; Cong, H. T.; Cheng, H. M.; Dresselhaus, M. S.; **Hydrogen storage in single-walled carbon nanotubes at room temperature**; *Science*; 286; 1999

19   Teitel, R.J.; **Microcavity Hydrogen Storage - Final Progress Report**; *Brookhaven National Laboratory*; Upton, New York; 1981

20   Kohli, D. K. et al.; **Glass micro-container based hydrogen storage scheme**; *International Journal of Hydrogen Energy*; Vol. 33; 2008

21   Rambach, G.D.; **Hydrogen Transport and Storage in engineered Glass Microstructures**; *Sandia National Laboratory*, Livermore; 1994

22   Herr, M.; Lercher, J. A.; **Hydrogen Storage in Microspheres - Final Report**, *ET Energie Technologie GmbH: ESA Contract No. 16292/02/NL/PA*; 2003

23   Wicks, G.G. et al:; **Microsheres and Microworlds - SRNL'S Porous, Hollow Glass Balls open New Opportunities for Hydrogen Storage, Drug Delivery and National Defense**; *American Ceramic Society Bulletin*; 87, No. 6; 2008

24   Shelby, J.E.; **A Radically New Method for Hydrogen Storage in Hollow Glass Microspheres**; *DOE U.S. Department of Energy Hydrogen Program, 2004 Annual Progress Report*; 2004

25   Shelby, J.E.; **Glass Microspheres for Hydrogen Storage**; *DOE U.S. Department of Energy Hydrogen Program*, 2008 Annual Progress Report; 2008

26   Schmitt, M.L.; Shelby, J.E.; Hall, M.M.; **Preparation of hollow glass microspheres from sol-gel derived glass for application in hydrogen gas storage**; *Journal of Non-Crystalline Solids*; Vol. 352; 2006

27   Budov, V. V.; **Physicochemical processes in producing hollow glass microspheres**; *Glass and Ceramics*, Vol. 47, No. 3; 1990

28   Friedrichs, C.; **H2-Speicherung in Metal-Organic Frameworks**; *Universität Bayreuth*

29   Yan, Y. et al; **Exceptionally high H$_2$ storage by a metal-organic polyhedral framework**; *Chemical Community*; 2009

30   Gedrich, K.; **A Family of Chiral Metal-Organic Frameworks**; *Chemistry – A European Journal*; 2011

31   Rosi, N. L.; Eckert, J.; Eddaoudi, M.; Vodak, D. T.; Kim, J.; O'Keeffe, M.; Yaghi, O. M.; **Hydrogen Storage in Microporous Metal-Organic Frameworks**; *Science*; 300; 2003

32   Zhou, W.; **PHYS 478-Enhanced H2 adsorption in isostructural metal-organic frameworks with open metal sites: Strong dependence of the binding strength on metal ions**; *Abstracts of Papers of the American Chemical Society*

33   Hongwei Yang; **Study of mechanochemical synthesis in the formation of the metal–organic framework Cu$_3$(BTC)$_2$ for hydrogen storage**; *Microporous and Mesoporous Materials*; Volume 143, Issue 1, 2011, 37–45

34   Rowsell, J. L. C.; Yaghi, O. M.; **Metal-organic frameworks: a new class of porous materials**; *Microporous and Mesoporous Materials*; 73; 2004

35   Rowsell, J. L. C.; Yaghi, O. M.; **Strategien für die Wasserstoffspeicherung in metal-organischen Kompositgerüsten**; *Angewandte Chemie*, Wiley-VHC Verlag, Weinheim; 2005

36   Barkhordarian, G.; Klassen, T.; Bormann, R.; **Fast hydrogen sorption kinetics of nanocrystalline Mg using Nb$_2$O$_5$ as catalyst**; *Scripta Materialia*; 49; 2003

37   Wang, Z.**; Tuning Hydrogen Sorption Properties of Metal–Organic Frameworks by Postsynthetic Covalent Modification**; *Chemistry – A European Journal*; Volume 16; Issue 1; 2010; 212-217

38   Friedrichs; O.; Klassen, T.; Sanchez-Lopez, J. C.; Bormann, R.; Fernandez, A.; **Hydrogen sorption improvement of nanocrystalline MgH$_2$ by Nb$_2$O$_5$ nanoparticles**; *Scripta Materialia*; 54; 2006

39   Klassen, T.; Oelerich, W.; Bormann, R.; **Nanocrystalline Mg-based Hydrides: Hydrogen Storage for the Zero-Emission Vehicle**; *Materials Science Forum*; 360-362; 2001

40   Huhn, P.-A.; Dornheim, M.; Klassen, T.; Bormann, R.; **Thermal stability of nanocrystalline magnesium for hydrogen storage**; *Journal of Alloys and Compound*s; 404-406; 2005

41   Murray, L. J.; Dinca, M.; Long, J. R.; **Hydrogen storage in metal-organic-frameworks**; *Chemical Society Reviews*; 38; 2009

42   Güther; V.; Otto; A.; **Recent developments in hydrogen storage applications based on metal hydrides**; *Journal of alloys and Compounds*; 293-295; 1999

43   Sakintuna, B.; Lamari-Darrim, R.; Hirscher, M.; **Metal hydride materials for solid hydrogen storage: A review**; *International Journal of Hydrogen Energy*; 32; 2007

44   Crabtree, R. H.; **Hydrogen storage in liquid organic heterocycles**; *Energy and Environmental Science*; 1; 2008

45   Otto, A.; **Wasserstoffspeicherung in Niedertemperatur-Metallhydriden**; *Forschungsverband Sonnenenergie*; Workshop Wasserstoffspeicherung; 2001

46   Srepusharawoot, P.; **Hydrogen binding in alkali-decorated iso-reticular metal organic framework-16 based on Zn, Mg, and Ca**; *International Journal of Hydrogen Energy*; Volume 36, Issue 1, 2011, 555–562

47   Jain, I. P.; Chhagan, L.; Jain, A.; **Hydrogen storage in Mg: A most promising material**; *International Journal of Hydrogen Energy*; 35; 2010

48   Rosi, N. L.; **Hydrogen Storage in Microporous Metal-Organic Frameworks**; *Science*; 2003; Vol. 300; Issue 5622; 1127-1129

49   Yan, Y.; **Exceptionally high H2 storage by a metal-organic polyhedral framework**; *Chemical Comunity*; 2009

50   Villalonga, S.; **Composite 700 bar-vessel for on-board compressed gaseous hydrogen storage**; *ICCM 17*; Edinburgh; 2009

51   Di Profio, P.; Arca, S.; **Comparision of hydrogen hydrates with existing hydrogen storage technologies: Energetic and economic evaluations**; *International Journal of Hydrogen Energy;* Vol. 34; 2009

52   Rowsell, J. L. C.; **Strategien für die Wasserstoffspeicherung in metall-organischen Kompositgerüsten**; *Angewandte Chemie*, Wiley-VHC Verlag, Weinheim; 2005

53   Mair, G. W.; **Prüfung/wiederkehrende Prüfung von Composite Druckgefäßen**; *6. Fachgespräch Druckgefäße*; Berlin; 2010

54   Bonhoff, K., Jörissen, L., Stadermann, G.; **Forschungsverbund Sonnenenergie - Workshop Wasserstoffspeicherung**; *Zentrum für Sonnenenergie- und Wasserstoff-Forschung*; 2001

55   Metal Mate Corp., **High Pressure Composite Cylinder**

56   Red, C.; **The outlook for composite pressure vessels**; *Composites technologies*; 2009

57   Shapaan, M.; **Structural and electric-dielectric properties of some bismuth - phosphate glasses**; *Journal of Physics and Chemistry of Solids*; Volume 73,   Issue 3, 2012, 407–417

58   Ried, P.; **H$_2$-permeability and burst pressure of glass capillaries**; 2010

59   Zhevago; N.K.; Glebov, V.I.; **Hydrogen storage in capillary arrays**; *Energy Conversion and Management*; Vol. 48; 2007

60   Zhevago, N.K. et al; **Experimental investigation of hydrogen storage in capillary arrays**; *International Journal of Hydrogen Energy*; Vol. 35; 2010

61   Zhevago, N. K. et al; **Storage of cryo-compressed hydrogen in flexible glass capillaries**; *International Journal of Hydrogen*; 2013

62   Beckmann-Kluge, M.; Eliezer, D.; et al.; **Pressure Resistance of Glass Capillary Structures for Gas Storage Purposes**; *1st International Conference on Materials for Energy*, Karlsruhe; 2010

63   Meyer, R.; **A New Technology for Hydrogen Safety: Glass Structures as a Storage System**; *4th International Conference on Hydrogen Safety (ICHS)*; San Francisco, CA, USA; 2011

64   Gröschl, C.; Meyer, R.; Holtappels, K.; Beckmann-Kluge, M.; Eliezer, D.; **A New Technology for Hydrogen Safety: Glass Structures as a Storage System**; *H2-Expo*; Hamburg, Germany; 2011

65   Holtappels, K.; Beckmann-Kluge, M.; Gebauer, M.; Eliezer, D.; **Pressure Resistance of Glass Capillaries for Hydrogen Storage;** *Materials Testing*; Vol. 53;   2011

66   Barton, J. L. and M. Morain; **Hydrogen Diffusion in Silicalite Glass**; *Journal of Non-Crystalline Solids* 3; 1970

67   Tsugawa, R. T., I. Moen, et al.; **Permeation of helium and hydrogen from glass-microsphere laser targets**; *Journal of Applied Physics;* Vol. 47; 1976

68   Rapp, D. B.; Shelby, J. E.; **Photo-induced hydrogen outgassing of glass**; *Journal of Non-Crystalline Solids*; Vol. 349; 2004

69   Shang, L. et al.; **Determination of diffusion coefficients of hydrogen in fused silica between 296 and 523 K by Raman spectroscopy and application of**

fused silica capillaries in studying redox reactions; *Geochimica et Cosmochimica Acta*; Vol. 73; 2009

70 Shelby, J. E.; **Handbook of Gas Diffusion in Solids and Melts**; *ASM International*; 1996

71 Shetty, S.; Hall, M.; **Facile production of optically active hollow glass microspheres for photo-induced outgassing of stored hydrogen**; *International Journal of Hydrogen Energy*; Vol. 36; 2011

72 Kurita, N. et al.; **Measurements of hydrogen permeation through fused silica and borosilicate glass by electrochemical pumping using oxide protonic conductor**; *Solid State Ionics*, Vol. 146; 2002

73 Elsey, H. M.; **The Diffusion of Helium and Hydrogen through Quartz Glass at Room Temperature**; *Journal of the American Ceramic Society*; Vol. 48; 1926

74 Williams, G. A. and Ferguson, J. B.; **The Diffusion of Hydrogen and Helium through Silica Glass and other Glasses**; *Journal of the American Ceramic Society*; Vol. 44; 1922

75 Wagner, W.; **Festigkeitsberechnungen im Apparate- und Rohrleitungsbau**; *Vogel Buchverlag*; 6. Überarbeitete Auflage

76 Issler, L.; Ruoß, H.; Häfele, P.; **Festigkeitslehre – Grundlagen**; *Springer*; 2. Auflage; 1997; 298-299

77 Mutz, A.; **Strukturmechanische Bewertung von Rohrleitungskomponenten und -systemen in Energiewandlungsanlagen unter Berücksichtigung der realen Werkstoffcharakteristik**; *PhD thesis*; Universität Stuttgart; 2011

78 Rankine, W.J.M.; **A Manual of Applied Mechanics**; London; 1861

79 v. Mises, R.; **Mechanik der festen Körper im plastisch deformablen Zustand**; *Nachrichten von der Gesellschaft der Wissenschaften zu Göttingen, Mathematisch-Physikalische Klasse*; 1913; 582-592

80 Tammann; G.; **Der Glaszustand**; Leipzig; 1933

81 Wörner, J.-D.; Schneider, J.; Fink, A.; **Glasbau**; 2001; 55

82 Holzmann, G.; Meyer, H.; Schumpich, G.; **Technische Mechanik Festigkeitslehre**; *Vieweg & Teubner Verlag*; 10th revisededition; Wiesbaden; 2012

83 DIN ISO 7884-1 - Viskosität und viskosimetrische Festpunkte, Teil 1: **Grundlagen für die Bestimmung der Viskosität und der viskosimetrischen Festpunkte (ISO 7884-1 : 1987)**; *Beuth Verlag*, Berlin; 1998

84   DIN ISO 7884-2 - Viskosität und viskosimetrische Festpunkte, Teil 2: **Bestimmung der Viskosität mit Rotationsviskosimetern (ISO 7884-2 : 1987)**; *Beuth Verlag*, Berlin; 1998

85   DIN ISO 7884-3 - Viskosität und viskosimetrische Festpunkte, Teil 3: **Bestimmung der Viskosität mit dem Fadenzieh-Viskosimeter (ISO 7884-3 : 1987)**; *Beuth Verlag*, Berlin; 1998

86   DIN ISO 7884-4 - Viskosität und viskosimetrische Festpunkte, Teil 4: **Bestimmung der Viskosität durch Balkenbiegen (ISO 7884-4 : 1987)**; *Beuth Verlag*, Berlin; 1998

87   DIN ISO 7884-6; Glass — Viscosity and viscometric fixed points — Part 6: **Determination of softening point (ISO 7884-6: 1987)**; *Beuth Verlag*, Berlin; 1998

88   DIN ISO 7884-7; Glass — Viscosity and viscometric fixed points — Part 7: **Determination of annealing point and strain point by beam bending (ISO 7884-7 : 1987)**; *Beuth Verlag*, Berlin; 1998

89   DIN ISO 7884-8; Glass — Viscosity and viscometric fixed points — Part 8: **Determination of (dilatometric) transformation temperature (ISO 7884-8 : 1987)**; *Beuth Verlag*, Berlin; 1998

90   DIN ISO 9385; **Glass and glass-ceramics**; *Knoop hardness lest*; Identical with ISO 9385 : 1990

91   **Prüfbericht zum Laborauftrag Nr. 0579/2011**; *Zentrum für Glas- und Umweltanalytik*; 2011

92   Scholze, H.; **Glas – Natur, Struktur, Eigenschaften**; *Springer – Verlag*; zweite Auflage; 1977; Berlin Heidelberg New York; 6

93   Varshneya, A. K.; **Fundamentals of Inorganic Glasses**, *Society of Glass Technology*; Second Edition; 2006

94   Wörner, J.-D.; Schneider, J. Fink; A.; **Glasbau**; 2001; 53

95   Scholze, H.; **Glas – Natur, Struktur, Eigenschaften**; *Springer – Verlag*; zweite Auflage; 1977; Berlin Heidelberg New York; 7

96   Gebauer, M.; **Untersuchung der Druckfestigkeit von Kapillaren verschiedener Materialien**; *Diploma thesis*; 2009

97   DIN 52296; **Glass and glass ceramics; Hydrolytic resistance of the surface of glass and glass ceramic plates at 98°C**; Method of test and classification

98   Xuenan Gu; **Corrosion of, and cellular responses to Mg–Zn–Ca bulk metallic glasses**; *Biomaterials*; Volume 31; Issue 6; 2010; 1093-1103

99   HVG Hüttentechnische Vereinigung der Deutschen Glasindustrie; **Oberflächenveredelung von Glas**; *Fortbildungskurs 2003*; 8

100   Kitaigorodski, I.I.; **Technologie des Glases**; *R. Oldenbourg Verlag*; 1957; 72

101   HVG Hüttentechnische Vereinigung der Deutschen Glasindustrie; **Veränderung und Veredelung von Glas;** *Fortbildungskurs 1989*; I/11

102   Schillmöller, A.; **Über die physikalisch-chemischen Vorgänge bei der Wasserauslaugung von Glasoberflächen**; *Glastechnische Berichte 33*; 1960; 109-116

103   DIN EN 1748-1: 1998-04; **Glass in building - Special basic products - Borosilicate glasses - Part 1-1: Definitions and general physical and mechanical properties**; German version EN 1748-1-1:2004

104   Kitaigorodski, I.I.; **Technologie des Glases**; *R. Oldenbourg Verlag*; 1957; 75

105   Yuan-Yun Zhao; **Reliability of compressive fracture strength of Mg–Zn–Ca bulk metallic glasses: Flaw sensitivity and Weibull statistics**; *Scripta Materialia*; 2008; 494-499

106   Zberg, B.; **Tensile properties of glassy MgZnCa wires and reliability analysis using Weibull statistics**; *Acta Materialia*; Volume 57; Issue 11; 2009; 3223-   3231

107   Mencik, J.; **Strength and fracture of glass and ceramics**; *Glass science and technology;* Volume 12; 1992

108   Mecholsky Jr., J. J.; S**trength and fracture of glass and ceramics,** *Glass Science and   Technology*; Volume 12; 1992,

109   Rexer, M.; "**Festigkeit gespannter Glasstäbe***"; Z. Tech. Phys.*, Vol. 20; 1939

110   Kitaigorodski, I.I.; **Technologie des Glases**; *R. Oldenbourg Verlag*; 1957; 77

111   Lund, M. D.; **Tensile strength of glass fibres**; *PHD dissertation*; 2010

112   Mencik, J.; **Strength and fracture of glass and ceramics**; 1992

113   Varner, J.; **Festigkeit von Glas – Grundlagen und Messverfahren**; *HVG*; 2001

114   Doremus, R. H.; **Glass Science**; *John Willey & Sons Inc.*; second Edition; New York; 1994

115   Dunken, H. H.; **Physikalische Chemie der Glasoberfläche**; *VEB Deutscher Verlag für Grundstoffindustrie*, Leipzig; 1981

116   Wagner, E.; **Glasschäden - Oberflächenbeschädigungen Glasbrüche in Theorie und Praxis**; *Hofmann Verlag, Fraunhofer IRB Verlag*, 3. Überarbeitete Auflage; 2008; 55

117   Vogel, W.; **Glass Chemistry**; 2nd revised Edition; *Springer Verlag, Berlin Heidelberg*; 1994

118   Gauckler, L.J.; **Grundzüge der Keramik**; *Lecture script*; ETH Zürich

119   Gross, D.; Seelig, T.; **Bruchmechanik**; 2006

120   Griffith, A. A.; **The Phenomena of Rupture and Flow in Solids**; *JSTOR*; 1921

121   Otto, W. H.; **Relationship of Tensile Strength of Glass Fibers to Diameter**; *Journal of The American Ceramic Society*; Vol. 38, No. 3; 1955; 122-125

122   Mould, R. E.; **Crossbending Tests of Glass Fibers and the Limiting Strength of Glass**; *J. Appl. Phys.*; Vol. 29; 1958

123   Thomas, W. F.; **An investigation of the factors likely to affect the strength and properties of glass fibres**; *Phys. Chem. Glass*; Vol. 1; 1960; 4-18

124   Cameron, N. M.; **Relation between melt treatment and glass fiber strength**; *Journal of The American Ceramic Society*; Vol. 49; 1966; 144-148

125   Williams, G. A.; Ferguson, J. B.; **The diffusion of hydrogen and helium through silica glass and other glasses**; *J. Am. Chem. Soc.*, 1922, 2160-2167

126   Elsey, H.M.; **The Diffusion of Helium and Hydrogen through Quartz Glass at Room Temperature;** *J. Am. Chem. Soc.*, 1926, 1600-1601

127   L. Shang et al.; **Determination of diffusion coefficients of hydrogen in fused silica between 296 and 523 K by Raman spectroscopy and application of fused silica capillaries in studying redox reactions**; *Science direct; Geochimica et Cosmochimica Acta* 73; 2009

128   Ried, P. et al.; **H2-permeability and burst pressure of glass capillaries;** *Poster*

129   Ried, P. et al.; **Hydrogen permeability of a barium-aluminoborosilicate glass- A methodical approach;** *Journal of Non-Crystalline Solids*; 394–395; 2014

130   Noriaki, K.; **Measurements of hydrogen permeation through used silica and borosilicate glass by electrochemical pumping using oxide protonic conductor;** *Solid State Ionics*; 146; 2002; 101– 111

131   Merker, L.; Williams, H. P.; Vogel, W.; Krämer, F.; **Glastechnische Fabrikationsfehler**; *Hüttentechnische Vereinigung der Deutschen Glasindustrie*, HVG Fortbildungskurs 1991; 2.Auflage; 1992

132   Jebsen-Marwedel, H.; **Glastechnische Fabrikationsfehler**; 4th Edition; 2011

133   Petrusenko, Y.; **Defects and Plastic-Deformation Modes of Bulk-Metallic Glasses**; *Metallurgical and Materials Transactions A*;, Volume 42; Issue 6;   2011; 1511-1515

134   Wörner; **Glasbau – Grundlagen, Berechnung, Konstruktion**; *Springer-Verlag Berlin Heidelberg New York*; 2001; 63

135   Scholze, H.; **Glas – Natur, Struktur und Eigenschaften**; 2nd Edition; 1977; 209

136   Scholze, H**.; Glas – Natur, Struktur und Eigenschaften**; 2nd Edition; 1977; 213-215

137   Müller-Simon, H.; **Transport und Lagerung in der Glasindustrie**; *HVG*; 2006; 83

138   DIN EN 12150-1; **Glass in building - Thermally toughened soda lime silicate safety glass - Part 1: Definition and discription**

139   DIN EN 12150-2; **Glass in building - Thermally toughened soda lime silicate safety glass - Part 2: Evaluation of conformity/Product standard**; German version EN 12150-2:2004

140   DIN EN 13024-2; **Glass in building - Thermally toughened borosilicate safety glass - Part 2: Evaluation of conformity/Product standard**; German version EN 13024-2:2004

141   Weißmann, R.; **Veränderung und Veredelung von Glasoberflächen**; *HVG*; 1989; III/18 –III/20

142   Wagner, E.; **Glasschäden**; Vol. 3; 2008; 82-83

143   DIN EN 12337-2; **Glass in building - Chemically strengthened soda lime silicate glass - Part 2: Evaluation of conformity/Product standard**; German version EN 12337-2:2004

144   Weißmann, R.; **Veränderung und Veredelung von Glasoberflächen**; *HVG*;   1989; III/20 –III/23

145   Hebel, J.; **Modellierung spröder Rissbildung an Spannungskonzentrationen mit der Bruchmechanik finiter Risse**; 2010

146   Visaria, M.; **Experimental investigation and theoretical modeling of dehydriding process in high-pressure metal hydride hydrogen storage systems**; *International Journal of Hydrogen Energy*; Volume 37, Issue 7, 2012, 5735 – 5749

147   DIN EN ISO 7458; **Glass containers - Internal pressure resistance - Test methods (ISO 7458:2004)**; German version EN ISO 7458:2004

148   DIN EN ISO 10628:2000; **Flow diagrams for process plants – General rules (ISO 10628:1997)**

149   StAA - SG – V13; **Standardarbeitsanweisung für die Kalibrierung von Druckmessgeräten mittels eines Präzisionsdruckmessgerätes**; *Bundesanstalt für Materialforschung und -prüfung*

150   Technical data sheet, **UHU plus endfest 300**, *Suter-Kunststoffe AG*

151   Technical data sheet, **C5 glass; Borosilicate glass**; *Incom*

152   **Formeln und Tabellen**; *Gesellschaft für Bildung und Technik mbH*

153   DIN ISO 7991; **Glass — Determination of coefficient of mean linear thermal expansion (ISO 7991: 1987)**

154   Technical data sheet, **X6CrNiMoTi17-12-2**, *ThyssenKrupp*

155   Technical data sheet, **stainless steel 1.4571 (X6CrNiMoTi17-12-2)**; *Deutsche Edelstahlwerke GmbH*, Witten, Germany; 2008

156   DIN 2413; **Nahtlose Stahlrohre für öl- und wasserhydraulische Anlagen – Berechnungsgrundlage für Rohre und Rohrbögen bei schwellender Beanspruchung**

157   Voorhees, H. R.; **Thick-Walled Pressure Vessels**; *Industrial and Engineering Chemistry*; 1956

158   ASTM D 2343-09; **Standard Test Method for Tensile Properties of Glass Fiber Strands, Yarns, and Rovings Used in Reinforced Plastics**

159   Ted Li;; **Tensile Property and Fractography of Capillary Glass Tube for H_2 Storage**; *Air Liquide*; 03.07.2013; p.4

160   ISO 3585: 1998-07-01; **Borosilicate glass 3.3 – Properties**

161   DIN 1259-1; **Glass – Part 1: Terminology for glass types and groups**

162   Technical data sheet 0500, **Borosilicate glass 3.3,** *Hilgenberg*

163   Technical data sheet 0620, **Quartz glass**, *Hilgenberg*

164   Technical data sheet 0813, **Alumosilicate glass 0813**, *Hilgenberg*

165   Technical data sheet 0812, **Alumosilicate glass 0812**, *Hilgenberg*

166   Technical data sheet, **Soda-Lime glass**, *Hilgenberg*

167   Technical data sheet C1S glass; **Borosilicate glass**; *Incom / Schott*

168   Gröschl, C.; **Steigerung der Druckfestigkeit von Glasstrukturen**; *Master thesis*; 2010

169   Meyer, R.; **An experimental study about the strength of glass capillaries at internal pressure load***; PhD thesis*; 2015

170   Gröschl, C.; **Wasserstoffspeicherung in Glasstrukturen**; *5. Doktorandensymposium PTB Braunschweig;* Braunschweig; 2015

171   Sapers, S.; et all; **Coatings on Glass**; *Technology Roadmap Workshop*; Livermore, California, USA, 2000

172   Jylhä, O.; **Atomic layer deposition to strengthen glass**; *Glass worldwide*; issue thirty   one 2010

173   Jyhlä, O.; **Improved cracking resistance by thin film ALD coatings**; *Glass performance days*; 2011

174   Comsol Multiphysics Documentation

175   Müller, G.; Groth, C.; **FEM für Praktiker: Grundlagen: Basiswissen und Arbeitsbeispiele zur Finite-Elemente-Methode mit dem Programm ANSYS**; *Expert Verlag*; 2007

176   Wandinger; **Höhere Festigkeitslehre - Elstizitätstheorie**; 2014